TECHNISCHE UNIVERSITÄT MÜNCHEN

Department Chemie

Lehrstuhl für Biotechnologie

Global and protein-specific analysis of the heat shock response in *S. cerevisiae*

Moritz Mühlhofer

Vollständiger Abdruck der von der Fakultät für Chemie der Technischen Universität München zur Erlangung des akademischen Grades eines Doktors der Naturwissenschaften (Dr. rer. nat.) genehmigten Dissertation.

Vorsitzender: Prof. Dr. Bernd Reif
Prüfer der Dissertation: 1. Prof. Dr. Johannes Buchner
                              2. Prof. Dr. Matthias Feige
                              3. Prof. Dr. Ralf Zimmer

Die Dissertation wurde am 27.07.2020 bei der Technischen Universität München eingereicht und durch die Fakultät für Chemie am 24.09.2020 angenommen.

Contents

Contents

Summary

Hsp26

Hsp26 is one of two sHsps from *S. cerevisiae*. It has been shown in various proteomic studies that Hsp26 is phosphorylated *in vivo*. However, how phosphorylation affects the activity of the chaperone remained enigmatic. In this thesis, known phosphorylation sites were substituted with glutamate to mimic the phosphorylation of the protein *in vitro*. The insertion of a negative charge, especially in the α-crystallin domain (ACD), destabilized the oligomer and led to dissociation at lower temperatures, which is assumed to be linked to activation. Indeed, distinct phosphomimetic mutations resulted in an activation of Hsp26 at non-stress temperature. The position of the phosphorylation strongly influenced the modulating effect. Substitutions in the middle domain (MD) were activating at non-stress temperature but tended to decrease the chaperoning capacity. Mutations in the ACD and C-terminal region (CTR) were more favorable as they led to activated Hsp26 at 25 °C without an observable loss of the chaperoning capacity. No phosphomimetic substitution resulted in a robust additional activation under heat stress compared to the heat-activated wild type (WT). Cell growth and the formation of aggregates *in vivo* was not affected by the expression of the mutants. For the WT protein, a 40-mer cryo-EM structure was resolved to 6.3 Å. The oligomer forms a hollow sphere whereas several flexible NTRs meet in the inside of the sphere. According to the structure, the basic building blocks of Hsp26 are β6-swapped dimers. Furthermore, the IEV binding site could be well resolved and HDX measurements indicate an interaction of the N-terminal part of the MD with an expanded loop of the ACD.

Global analysis of the Heat Shock Response

The Heat Shock Response (HSR) is essential for life as it allows cells to appropriately react to a changing environment. In this work, the yeast HSR to mild (37 °C), severe (42 °C) and sublethal (46 °C) heat stress was analyzed at the level of the transcriptome, translatome and proteome. It could be shown that the stress-responsive program initiated at 37 °C and 42 °C allows continuing growth. Hence, it was called the *productive HSR*. The transcriptome and the translatome correlated very well with more than 1,000 genes that were changed in their expression. At 42 °C, only prolonged stress resulted in a translational arrest. Despite the big changes at the mRNA level, the proteomic changes at those temperatures were mostly limited to chaperones and trehalose biosynthesis enzymes. Analysis of aggregation and degradation under stress implied that the biggest part of the transcriptional HSR serves to maintain the pool of active soluble proteins by replenishing stress-dependent protein turnover. At 46 °C, translation and cell growth were stopped by extensive phase separation and aggregation processes. Therefore, this response is referred to as the *dormant HSR*. In summary, the

analysis of the HSR at various temperatures allowed to define different programs that are specific to the severity of the stress. Thus, the HSR exhibits a *modular* character.

Transcriptional regulation of the HSR

Hsf1 is known to be the key regulator of the HSR, whereas Msn2/4 have been shown to orchestrate a more general response to environmental stresses. To understand the transcriptional regulation of the stress response und the interplay of the transcription factors in detail, the HSR of cells lacking all three transcription factors was investigated. In agreement with previous studies, the effect of Hsf1 depletion alone was small and comprised mostly chaperones. In contrast to WT cells, which usually adapt to mild heat stress with time, Hsf1 depleted cells showed no adaption within 30 min of mild heat stress. Deletion of Msn2/4 negatively affected more genes including those linked to carbohydrate metabolism. Thus, for both strains, a dulled response was observed but still there was a HSR observable. As the absence of either Hsf1 or Msn2/4 hardly affected the transcriptomes of heat stressed cells, a combination of both was analyzed in addition. The strain that lacked all three transcription factors did not exhibit the common HSR program. Those cells completely shifted their transcriptional program to sporulation and thus tried to rescue themselves into this stress-resistant stage. Overall, this analysis revealed two key findings: 1) The absence of Hsf1 and Msn2/4 turns off the *productive* stress response. 2) The targets of Hsf1 and Msn2/4 are at least ~50 % overlapping.

Zusammenfassung
Hsp26

Hsp26 ist eines von zwei kleinen Hitzeschockproteinen (sHsps) aus *S. cerevisiae*. Im Rahmen einiger Phosphoproteomstudien wurde gezeigt, dass Hsp26 *in vivo* phosphoryliert wird. Es war jedoch unklar, wie genau Phosphorylierung die Aktivität des Chaperons beeinflusst. In dieser Arbeit wurden bekannte Phosphorylierungsstellen einzeln durch Glutamat ersetzt, um die Proteinphosphorylierung *in vitro* nachzuahmen. Es konnte gezeigt werden, dass das Hsp26 Oligomer durch das Einfügen einer negativen Ladung, insbesondere in der α-crystallin Domäne (ACD), destabilisiert wird. Im Vergleich zum Wildtyp (WT) Hsp26 führte dies zu einer Dissoziation des Oligomers bereits bei niedrigeren Temperaturen. Da davon ausgegangen wird, dass Oligomer-Dissoziation eng mit der Aktivierung von sHsps verbunden ist, war zu vermuten, dass die Mutationen einen aktivierenden Effekt auf das Chaperon zu haben. Dies traf auf einige der Hsp26-Mutanten unter normalen (25 °C) Wachstumsbedingungen zu. Die Position der Mutation war dabei entscheidend für den modulierenden Effekt. Mutationen in der Mitteldomäne (MD) aktivierten das Chaperon zwar bereits bei 25 °C, senkten allerdings die Kapazität des Chaperons, was sich in Coaggregationsprozessen widerspiegelte.

Substitutionen in der ACD oder in der C-terminalen Region (CTR) aktivierten Hsp26 ebenfalls bereits bei 25 °C, ohne sichtbare Reduktion der Bindekapazität. Phosphorylierung brachte keinen weiteren Vorteil unter Hitzestress im Vergleich zum hitzeaktivierten WT. Unter den getesteten Bedingungen verhielt sich auch *in vivo* kein mutiertes Protein besser als der WT. Mittels Cryo-EM wurde eine hochaufgelöste Struktur (bis zu 6.3 Å) des Hsp26 40-mers erhalten. Das 40-mer bildet einen Hohlraum, in welchem sich die flexiblen N-terminalen Regionen (NTRs) einiger Untereinheiten treffen. Der Struktur zufolge bildet Hsp26 sogenannte „β6 invertierte Dimere", welche typisch für alle Nicht-Metazoen sind. Diese Beobachtung ist im Einklang mit dem Modell, welches für die frühere, weniger gut aufgelöste, Hsp26 Struktur ermittelt wurde. Des Weiteren konnte die Bindetasche des IEV Motivs aufgelöst werden und Wasserstoff/Deuterium Austausch (HDX) Messungen deuteten auf eine Interaktion zwischen dem N-terminalen Teil der MD und einer ausgedehnten Schleife in der ACD hin.

Globale Analyse der Hitzeschockantwort

Die Hitzeschockantwort (HSR) ist essenziell für Leben, da sie es den Zellen erlaubt, auf eine sich verändernde Umwelt zu reagieren. Im Rahmen dieser Arbeit wurde die HSR von *S. cerevisiae* als Reaktion auf unterschiedlich starke Hitzestresse (37 °C, 42 °C und 46 °C) auf der Ebene des Transkriptoms, des Translatoms und des Proteoms untersucht. Es konnte gezeigt werden, dass das Programm, das bei 37 °C und 42 °C initiiert wird, Wachstum weiterhin ermöglicht. Folglich wurde diese Antwort *produktive HSR* genannt. Unter Stress war die Expression von über 1000 Genen verändert, wobei das Transkriptom und das Translatom eine hohe Korrelation aufwiesen. Stress, der über 30 min bei 42 °C hinausging, führte zum Aussetzen der Translation. Trotz der großen Veränderungen auf mRNA Ebene waren die Veränderungen auf Proteinebene zum Großteil auf Chaperone, sowie Enzyme, die im Kohlenhydratstoffwechsel, speziell in der Trehalosebiosynthese, involviert sind, beschränkt. Auf Proteinebene wurde also ausschließlich die generelle Hitzestressantwort hochreguliert. Analysen von Aggregations- und Degradationsprozessen unter Hitzestress legten nahe, dass der überwiegende Teil der transkriptionellen HSR dazu dient, den Pool von aktiven, löslichen Proteinen aufrechtzuerhalten. Dies wird dadurch gewährleistet, dass der Proteinumsatz unter Stress durch Neusynthese ausgeglichen wird. Bei 46 °C jedoch werden Zellwachstum und Translation durch starke Aggregationsprozesse gestoppt. Deshalb wird diese Antwort im Folgenden als die *ruhende HSR* bezeichnet werden. Diese Analyse der HSR führte zu der Erkenntnis, dass abhängig von der Stärke des Stresses, unterschiedliche Programme angesteuert werden und die HSR in Stress-spezifischen Modulen organisiert ist.

Transkriptionelle Regulation der HSR

Es ist bekannt, dass Hsf1 der Schlüsselregulator der HSR ist, wohingegen Msn2/4 die transkriptionelle Antwort auf allgemeinen, umweltbedingten Stress steuern. Um die Regulation der Stressantwort genauer zu verstehen, wurden Zellen untersucht, denen alle drei Transkriptionsfaktoren fehlten. Wie erwartet, hatte die Depletion von Hsf1 insgesamt nur kleine Effekte, welche überwiegend auf Hitzeschockproteine beschränkt waren. Es konnte allerdings gezeigt werden, dass Zellen ohne Hsf1 nicht in der Lage sind, sich, wie der WT, mildem Hitzestress anzupassen. Somit wurde das transkriptionelle Programm dieser Zellen nicht innerhalb von 30 min wieder zurückgefahren. Die Deletion von Msn2/4 beeinflusste die Expression von mehr Genen. Betroffen waren vorwiegend Enzyme, die im Kohlenhydratstoffwechsel involviert sind. Beide Stämme, denen entweder Hsf1 oder Msn2/4 fehlte, zeigten somit eine gedämpfte HSR, es war jedoch eindeutig noch ein Restprogramm erkennbar. Aus diesem Grund wurde in dieser Arbeit die Kombination von beiden getestet und analysiert. Der Stamm, dem alle drei Transkriptionsfaktoren fehlten, war nicht mehr in der Lage, die gewöhnliche HSR einzuleiten. Diese Zellen veränderten ihr transkriptionelles Programm in Richtung Sporulation, um sich in dieses stressresistente Stadium zu retten. Insgesamt lieferte diese Analyse zwei wichtige Erkenntnisse: 1) Das Fehlen von Hsf1 und Msn2/4 führt zur vollständigen Abschaltung der *produktiven HSR*. 2) Die Zielgene von Hsf1 und Msn2/4 überlappen zu ca. 50 %.

1 Introduction

Living organisms have to deal constantly with changes in the environment. Even though the temperatures, at which living organisms can be found range from -20 °C to 120 °C (Clarke, 2014), only a few degrees above the physiological conditions are a challenge for life. To fulfill their biological function, proteins usually exhibit dynamic structures with the consequence that many proteins are only stable within a relatively small temperature range (Verghese et al., 2012, Shoichet et al., 1995). To understand this important characteristic of proteins in more detail, I will first focus on the biophysics of protein folding.

1.1 Biophysical examination of protein folding

Around 60 years ago, Christian Anfinson concluded from his refolding experiments with Ribonuclease A that the biological information of a protein, namely the structure, is encoded in its amino acid sequence (Anfinsen et al., 1961, Anfinsen, 1973), more specifically in the energy landscape of the polypeptide sequence (Anfinsen and Scheraga, 1975). Even though this finding is relatively old, the prediction of the native structure from the polypeptide chain is still a matter of research (Kuhlman and Bradley, 2019). It was calculated for an exemplary polypeptide with 100 residues that it would take around 10^{52} years to fold if every single conformation had to be tested at a rate of 10^{11} s^{-1} (Karplus, 1997, Levinthal, 1969). As protein folding takes place in milliseconds to seconds, the folding process has to be guided (Bryngelson et al., 1995, Dill et al., 2008, Kuhlman and Bradley, 2019). Some main principles have emerged to explain the fast folding process, which all assume the formation of secondary structure elements, which were first described by Linus Pauling (Pauling et al., 1951), before the tertiary structure is adopted (Dill et al., 2008). According to the diffusion-collision model, folding of larger structures is preceded by the formation of secondary structure elements, which subsequently meet and assemble due to diffusion processes (Karplus and Weaver, 1979). For helical bundles, this assembly was shown to occur in a hierarchical manner (Myers and Oas, 2001). In the nucleation-condensation model, specific secondary structure elements are formed, which induce tertiary contacts (Fersht, 1997). Another alternative is that hierarchic condensation is taking place whereat parts of the proteins are first structured and compacted. Subsequently, they assemble to the correctly folded protein (Lesk and Rose, 1981). The fact that native proteins are only 5-10 kcal/mol more stable than the unfolded state, makes *in silico* prediction of the protein structure even more difficult (Yang et al., 2007). Structure prediction algorithms can be based on protein structure templates, with which the structure of the target protein is predicted using the known structure of a similar protein (Bowie et al., 1991, Jones et al., 1992). Alternatively, *ab initio* structure prediction algorithms such as ROSETTA were developed (Simons et al., 1999). In the template-free approaches, the structure is calculated on the basis of energy functions (Kuhlman and Bradley, 2019). Nowadays both approaches are combined and machine learning is integrated into structure prediction but nevertheless a

correct prediction remains very challenging and demands much time as well as processing units (Jones and Kandathil, 2018, Kuhlman and Bradley, 2019). Despite their differences, all models for protein folding share the assumption that the folding process is stepwise and that the polypeptide passes through intermediate conformations on its way to the stable, native structure, which is depicted in the so-called *folding funnel* (Figure 1). The folding process can be supported by molecular chaperones. Especially proteins with complex and large topologies seem to be dependent on chaperones to obtain and maintain their structure (Hartl et al., 2011, Hipp et al., 2019). Two main factors determine the conversion of the native into the aggregated form, which would be another minimum in the folding funnel. On the one hand thermodynamic stability and on the other hand the kinetic accessibility of the aggregated state whereas higher concentrations favor the formation of aggregates (Vecchi et al., 2020, Knowles et al., 2014, Kiefhaber et al., 1991). In this context, the term supersaturation was introduced as it was shown that the protein concentrations in the cell come close to their critical concentrations above which they become metastable and tend to aggregate (Tartaglia et al., 2007, Ciryam et al., 2015).
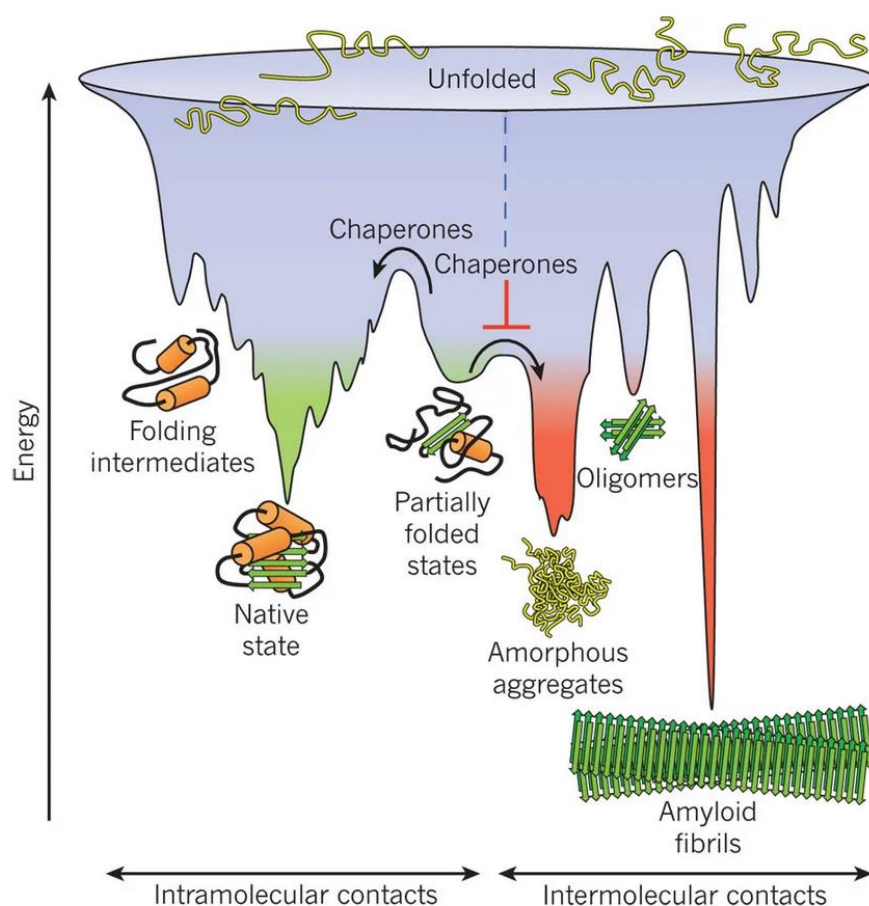
Figure 1: Protein folding funnel. *Protein folding is supposed to take place guided along the energy landscape towards the stable native conformation. Chaperones help to overcome energetic barriers and prevent aggregation of partially folded proteins. The figure was reprinted with the permission of Springer Nature: Molecular chaperones in folding and proteostasis (Hartl et al., 2011).*

1.2 Protein folding in the cell

To prevent aggregation of proteins within the crowded environment of the cell with a protein concentration of around 280 mg/ml (Brown, 1991), sophisticated pathways have evolved. In the cell, many unspecific interactions can occur and the proteins cannot diffuse freely, which stands in contrast to the *in vitro* refolding assays performed in diluted solutions (Gershenson and Gierasch, 2011). It was shown that cellular proteins are often folded co-translationally, spontaneously, as well as assisted by ribosome-associated chaperones (Kramer et al., 2009, Waudby et al., 2019). Chaperones also fold, stabilize and prevent aggregation of proteins independent of the ribosome (Fujiwara et al., 2010, McClellan et al., 2007, Apetri and Horwich, 2008). Another mechanism that supports folding is the spatial organization within the cell, which allows providing different redox potentials or pH values (Tapley et al., 2010, Feige et al., 2009, Gershenson and Gierasch, 2011).

1.3 The Heat Shock Response
1.3.1 Discovery of the Heat Shock Response and Heat Shock Proteins

As already mentioned in the preceding paragraph, chaperones fulfill important functions for protein homeostasis. Especially under stress conditions, which can for example be induced by heat, oxidizing agents, hypoxia, high salt concentration, DNA damage, fast growth or heavy metals, the proteostatic system becomes fragile and chaperones gain importance as proteins unfold and become aggregation prone (Simmons et al., 2009). Different kinds of stresses induce different signaling pathways. In yeast, osmotic stress activates a MAP kinase pathway, the so-called high-osmolarity glycerol (HOG) pathway, whereas oxidative stress is also sensed via the HOG pathway as well as Skn7 and the AP-1-like transcription factor (Yap1) in *S. cerevisiae* (Figure 2) (Hohmann, 2002, Ikner and Shiozaki, 2005, He et al., 2009). All these stress responsive pathways have in common that in the end specific transcription factors are activated which initiate a stress protective transcriptional program mostly including chaperones (Hohmann, 2002, Ikner and Shiozaki, 2005, Lindquist, 1986). As the outcomes of the different stress responses are overlapping, submitting cells to one stress condition can lead to cross-protection against a second stress (Lindquist, 1986). Exposure to mild heat stress makes yeast cells more resistant against ethanol stress (also the other way round), a phenomenon called thermotolerance (Lindquist, 1986, Plesset et al., 1982, Watson and Cavicchioli, 1983). First experimental findings implying the existence of heat shock proteins were obtained with heat shocked *Drosophila* (Ritossa, 1962). Ritossa observed chromosomal puffs after exposure to heat, which indicate extraordinary strong and local transcriptional activity (Ritossa, 1962). Radioactive labelling of newly synthesized proteins confirmed that several specific proteins are translated during stress. This set of proteins was then named *heat shock proteins*, even though they are also upregulated under other kinds of stresses (Tissiéres et al., 1974, Lindquist, 1986, Ashburner and Bonner, 1979). Soon, it was shown that the heat shock response is not specific

for *Drosophila* but rather ubiquitously found in almost all organisms (Lemaux et al., 1978, McAlister and Finkelstein, 1980, Kelley and Schlesinger, 1978). Known exceptions that seemingly do not have a heat stress protective program and thus fail to respond to elevated temperatures are *Hydra oligactis*, *Mycobacterium leprae* and several antarctic marine organisms (Bosch et al., 1988, Williams et al., 2007, Clark and Peck, 2009). Those organisms tolerate only short periods of heat stress and do not show thermotolerance (Williams et al., 2007, Bosch et al., 1988).
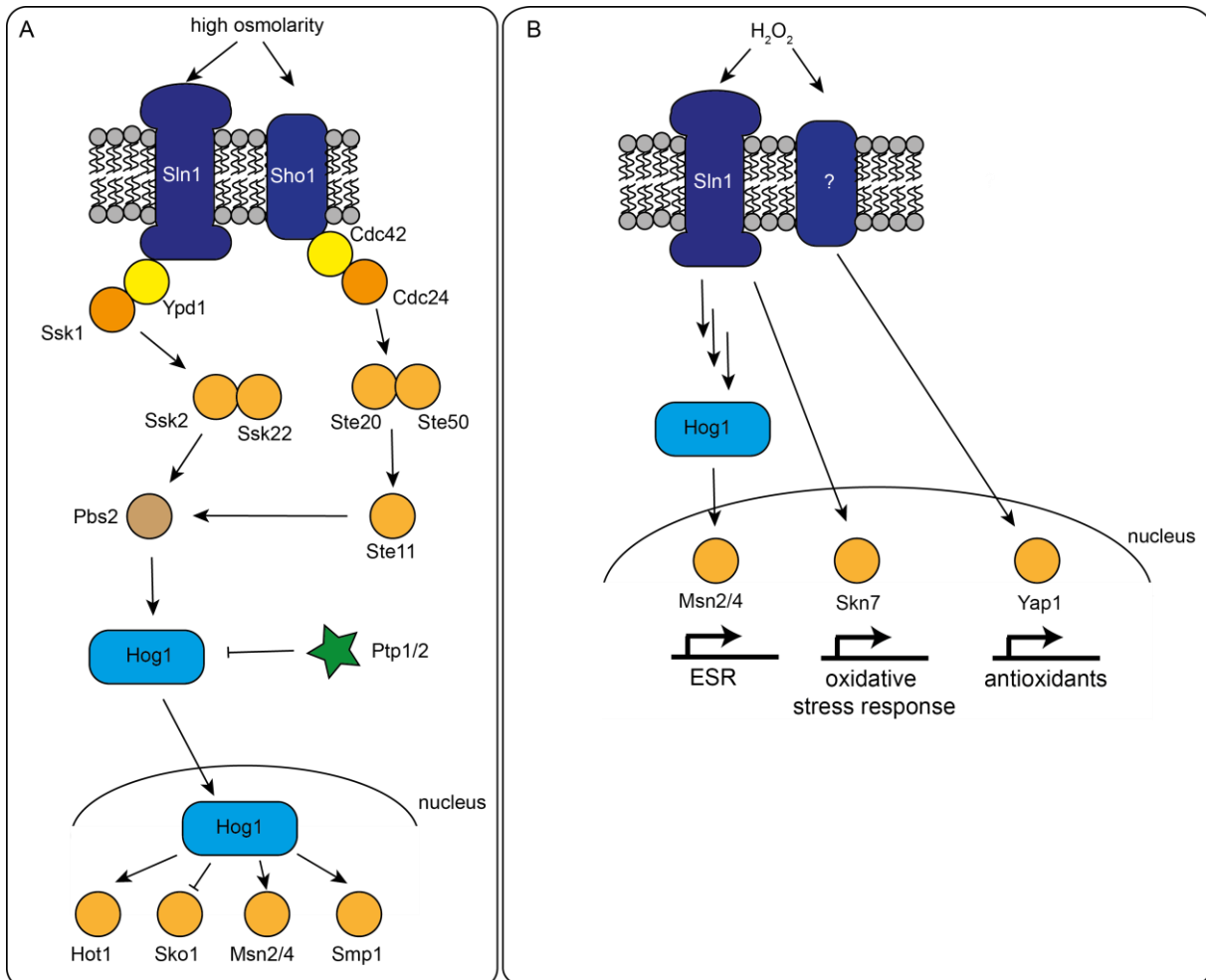
Figure 2: Schematic overview of the signaling pathways initiated by osmotic (A) and oxidative (B) stress. *A) MAP kinase pathway initiated by high osmolarity results in activation of Hot1, Msn2/4 and Smp1 and inhibition of Sko1. The signaling pathway is shown equally in Hohmann, 2002. B) Oxidative stress induces the activation of Msn2/4 via Sln1/Ypd1 as well as Skn7 and Yap1. The signaling pathways were designed based on the cited publications (He et al., 2009, Ikner and Shiozaki, 2005).*

1.3.2 Effects of heat stress

Proteins are optimized for the growth temperature of the respective organism and are only stable in a small temperature range (Verghese et al., 2012, Richter et al., 2010). Molecular chaperones help to maintain protein homeostasis under stress by keeping them soluble and promoting the native state. If the burden of misfolded proteins exceeds the chaperone capacity,

unfolded protein can be sequestered into cellular deposit sites, such as IPOD, CytoQ or INQ, which will be described later in more detail (Miller et al., 2015b, Kaganovich et al., 2008). Heat stress also affects the cell morphology as stress fibers are formed under mild heat stress and severe heat stress even leads to aggregation of cytoskeleton proteins (Karpova et al., 1998, Toivola et al., 2010). This results in disrupted cellular transport processes and finally leads to the fragmentation of the endoplasmic reticulum and the Golgi apparatus. Furthermore, the amount of mitochondria and lysosomes decreases under stress (Welch and Suhan, 1985). The loss of mitochondria together with uncoupled oxidative phosphorylation under stress leads to a drop of the ATP levels (Patriarca and Maresca, 1990, Richter et al., 2010). Furthermore, heat affects the membrane composition and increases its fluidity (Vigh et al., 2007, Richter et al., 2010). This effect could be linked to an activation pathway for the heat stress response, the so-called cell wall integrity pathway (Verna et al., 1997, Zu et al., 2001).

In addition, the trehalose biosynthesis machinery is upregulated under stress (De Virgilio et al., 1994, Verghese et al., 2012). Trehalose is a disaccharide consisting of two glucose molecules linked via an α-1,1´ glycoside bond, which is known to be able to replace water molecules around proteins and therefore helps to overcome desiccation (Crowe, 2007, Tapia et al., 2015). Hence, it effectively stabilizes proteins and prevents aggregation of unfolded proteins *in vivo* (Hottiger et al., 1994, Singer and Lindquist, 1998, Verghese et al., 2012). High trehalose levels consequently impede protein refolding and therefore the trehalase Nth1 becomes important during recovery (Singer and Lindquist, 1998, Wera et al., 1999).

Furthermore, translation is strongly affected by heat stress and RNA splicing is disrupted under heat stress (Yost and Lindquist, 1991, Vogel et al., 1995). Translational regulation under stress is closely linked to the integrated stress response (ISR). In metazoans, various proteotoxic stresses are sensed by the four kinases PERK, GCN2, PKR and HRI which phosphorylate Ser51 of eIF2 (Costa-Mattioli and Walter, 2020). Thus, the stress sensors are located in the ER and in the cytosol. Furthermore, PERK connects the unfolded protein response (UPR) with the ISR (Costa-Mattioli and Walter, 2020). In yeast, only Gcn2 is known as an ISR sensor kinase (Costa-Mattioli and Walter, 2020). Phosphorylation of eIF2 leads to an inhibition of cap-dependent translation initiation (Buchan and Parker, 2009, Stoecklin and Kedersha, 2013, Crawford and Pavitt, 2019, Dever et al., 1992) as phosphorylated eIF2α cannot dissociate from eIF2B (GTP exchange factor) anymore. Therefore, the initiation tRNA[i] is not transferred to the 40S ribosomal subunit (Stoecklin and Kedersha, 2013, Holcik and Sonenberg, 2005). As a result, stress granules (SG) are formed in the cytosol where translation initiation factors, RNA binding proteins, such as Pab1 and Pub1 and non-translated mRNAs are deposited (Stoecklin and Kedersha, 2013, Buchan and Parker, 2009, Cherkasov et al., 2015, Buchan et al., 2011). In yeast, SG formation is mostly observed under heat stress, glucose deprivation, sodium azide

stress and hydrogen peroxide stress. Interestingly, there is only slight evidence that yeast SGs contain small ribosomal subunits and the composition of yeast SGs is dependent on the type of stress (Buchan and Parker, 2009, Buchan et al., 2011, Hoyle et al., 2007, Stoecklin and Kedersha, 2013, Grousl et al., 2009). SGs are thought to be a reservoir for translation-potent, but (temporary) stalled mRNAs. As those mRNAs might be needed subsequent to the stress, SGs allow to prepare for different needs depending on the SG trigger (Crawford and Pavitt, 2019, Buchan et al., 2011). The composition of processing bodies (PB) and SGs is overlapping in yeast. They are dynamic and can be converted into each other (Buchan and Parker, 2009, Hoyle et al., 2007). Nevertheless, PBs are generally assumed to be sites of RNA degradation as the deposited mRNA usually lacks the poly(A) tail, is decapped and RNA degradation enzymes co-localize (Franks and Lykke-Andersen, 2007, van Dijk et al., 2002, Kedersha et al., 2005, Ozgur et al., 2010). It was hypothesized that SGs might work as a sorting compartment from which PBs that harbor mRNAs which should be degraded could evolve (Kedersha et al., 2005).

Finally, cell growth is stopped under heat stress (Zeuthen, 1971, Lindquist, 1980, Morano et al., 1999). The cell cycle arrest is due to a decrease of Cln1/2 transcripts, which induce cell cycle progression from G1 to the S phase (Rowley et al., 1993). Therefore, heat stressed cells are arrested in a phase where the chromosome has not been duplicated yet, most likely as the cell tries to avoid replicating its genetic material during proteotoxic stress (Verghese et al., 2012). Taken together, those are the main effects of heat shock on the cell. In the following it will be discussed how yeast cells respond to it.

1.3.3 Transcriptional Heat Shock Response in *S. cerevisiae*

Until the invention of RNA microarrays and RNA sequencing, the transcriptional analysis of the heat stress response was limited to single genes. The first global microarray approaches showed that during heat stress extensive transcriptomic changes are taking place, with 300 genes that were upregulated and 600 genes being repressed (Eisen et al., 1998, Gasch et al., 2000). Moreover, it was shown by time resolved analysis that the response is rapid but kinetics seem to differ for different genes (Gasch et al., 2000). Genes coding for chaperones peaked after 10-15 min (Gasch et al., 2000). The analysis of the transcriptomic heat shock response in mammalian cells also indicated groups of genes that differed in the kinetics of their regulation (Mahat et al., 2016). As protein unfolding by heat is a very fast process, it is important that the reaction of the cell is fast, as well. A core set of approximately 10 % of the changed genes was identified under all stress conditions. This group of genes was termed "environmental stress response" (ESR) (Causton et al., 2001). *Carbohydrate metabolism*, *stress response*, *energy generation* were the most enriched categories within this common response and the two transcription factors Msn2 and Msn4 were identified as the main regulators of the ESR

(Causton et al., 2001). In contrast, the ESR represses the expression of *ribosomal subunit* and *ribosome biogenesis* genes (Causton et al., 2001, Gasch et al., 2000). Besides Msn2/4, Hsf1 is the most important regulator of the heat shock response (HSR) (Morano et al., 2012, Richter et al., 2010). Additionally, the before mentioned cell wall integrity pathway (CWI) plays a role in regulating the transcriptional HSR in yeast (Verghese et al., 2012).

1.3.3.1 Cell wall integrity pathway

Changes in the cell wall or membrane can be perceived by transmembrane proteins of the outer membrane, which subsequently activate a MAP kinase pathway to counteract the stress (Levin, 2011, Sanz et al., 2017). In detail, cell wall aberrations are sensed by Wsc1-3, Mid2 and Hkr1, respectively. Wsc1 or Mid2 interact with the GTP exchange factor Rom2 that activates the GTPase Rho1. Rho1 then activates Pkc1, which phosphorylates Bck1 (MAPKKK) followed by Mkk1/2 (MAPKK), which finally phosphorylate the MAP kinase Slt2 (Sanz et al., 2017). Slt2 mediates the activity of two transcription factors, Rlm1 and Swi4/6 (Sanz et al., 2017) (Figure 3). Rlm1 induces the transcription of mostly stress responsive genes, e.g. HSP12 or cell wall remodeling enzymes whereas Swi4/6 play a role in cell cycle progression (Sanz et al., 2017, Watanabe et al., 1997, Baetz et al., 2001). How heat activates this pathway is still not understood completely (Verghese et al., 2012). It was observed that cells that are defective in the CWI induce a normal HSR, but are very sensitive to heat shock and induce an autolytic program (Zu et al., 2001, Verna et al., 1997).
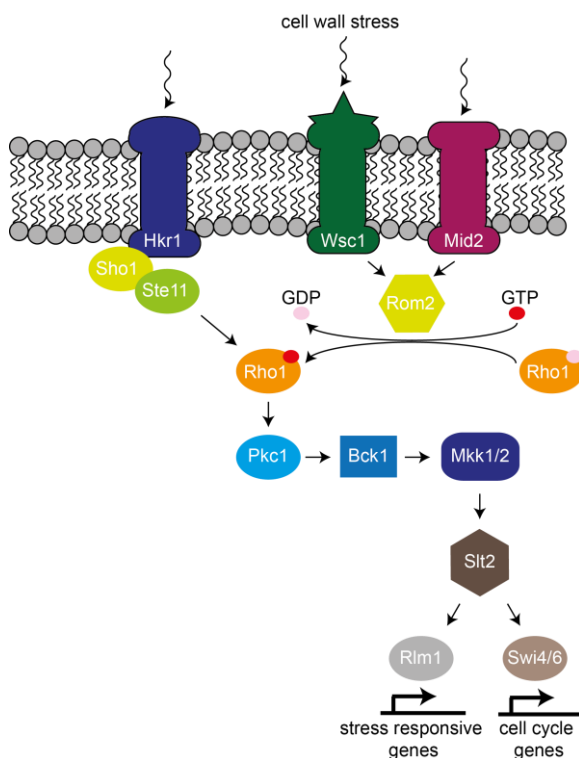
Figure 3: Scheme of the cell wall integrity (MAP kinase) pathway after cell wall stress. *The figure is inspired by a scheme shown by Sanz et al., 2017.*

1.3.3.2 Heat shock transcription factor 1 (Hsf1)

In eukaryotes, heat shock factors (Hsf) are the key regulators of the transcription of heat shock proteins (Hsp) (Morimoto, 1998, Lis and Wu, 1993, Morimoto, 1993). Whereas vertebrates usually express four heat shock factors, yeast only expresses Hsf1, which, importantly, is an essential gene (Akerfelt et al., 2010, McDaniel et al., 1989, Solís et al., 2016). Yeast Hsf1 consists of five domains. Comparable to all other Hsfs, Hsf1 has a DNA binding domain (DBD), a leucine zipper domain with three leucine zipper repeats, which is essential for trimerization and a C-terminal transactivation domain (CTA) (Trott and Morano, 2003, Verghese et al., 2012). Furthermore, yeast Hsf1 carries a control element (CE2) and a second N-terminal transactivation domain (Figure 4A) (Nieto-Sotelo et al., 1990). It was shown for the *K. lactis* Hsf1 that the DBD is organized as a winged helix turn helix whereas one helix is binding into the major groove of the DNA and the turns interact with adjacent Hsf1 DBD turns (Littlefield and Nelson, 1999). Recent crystal structures of the human Hsf1 DBD with the coiled coil oligomerization domain bound to DNA revealed that the transcription factor subunits do not bind to the same side of the strand and seem to embrace the DNA (Figure 4B) (Neudegger et al., 2016). The DBD of Hsf recognizes so-called pentameric heat shock elements (HSEs), NGAAN in the promoter region (Sorger and Pelham, 1987). A perfect HSE comprises three inverted repeats of the HSE without gap (NTTCNNGAANNTTC) (Sorger and Pelham, 1987). The repeats can also be discontinuous if short 5 bp gaps are present. This lowers the affinity of human Hsf1 but does not seem to impair DNA binding of yeast Hsf1, as long as three pentameric repeats are present, so that each subunit can bind to the DNA (Hashikawa et al., 2007, Sakurai and Takemori, 2007, Yamamoto et al., 2009). The trimerization mediated by the leucine zipper is important to increase the affinity of Hsf1 to DNA (Drees et al., 1997). Trimer formation is known to be an important regulation point in higher eukaryotes whereas in yeast, Hsf1 is constitutively localized to the nucleus and bound to the DNA as a trimer (Bonner et al., 1994, Solís et al., 2016, Baler et al., 1992, Rabindran et al., 1993). It was reported that heat stress increases the affinity of Hsf1 for non-perfect HSEs (Giardina and Lis, 1995). Specifically, the CTA that can be modulated by different external stimuli, such as heat, pH or trehalose, confers sustained transactivation (Pattaramanon et al., 2007, Bulman and Nelson, 2005). Thus, trehalose augments the heat activation of Hsf1 (Bulman and Nelson, 2005). It was also reported that the CTA is essential for heat or oxidative stress induced *CUP1* expression but seems to be less important for *SSA1* or *SSA3* induction (Tamai et al., 1994). Thus it was suggested that the CTA is especially needed for the regulation of the expression of genes with gapped HSEs (Santoro et al., 1998). Deletion of the NTA leads to a constitutively active Hsf1, which indicates that the NTA is a negative regulator of Hsf1 masking the CTA in the non-activated state (Bonner et al., 1992, Zheng et al., 2016). Moreover it was observed that the NTA negatively interferes with DNA binding of Hsf1 (Krakowiak et al., 2018). Besides the

negative regulation by the NTA, the CTA is repressed by the CE2 (Sorger, 1990, Jakobsen and Pelham, 1991). The activity of Hsf1 is also modulated by post translational modifications with phosphorylation as the best studied one (Sorger et al., 1987, Sorger and Pelham, 1988). In general, it seems that phosphorylation of Hsf1 leads to its activation, but also other cases were observed in which phosphorylation had opposite effects (Sorger, 1990). Especially a serine-rich patch close to the CE2 leads to repression if the serine residues are phosphorylated (Høj and Jakobsen, 1994). The phosphorylation pattern under heat shock pinpoints towards serine-threonine kinases. Nevertheless, in an RNAi-based screen no kinases could be identified as regulators of Hsf1 (Sorger, 1990, Verghese et al., 2012, Raychaudhuri et al., 2014). Recent investigations of the kinome under heat stress revealed that 14 kinases are important for the regulation of the HSR in yeast (Rim11, Pkc1, Snf1, Mrk1, Pho85, Ypk1, Sch9, Ssn3, Pbs2, Ste11, Cdc15, Ypk3, Yak1 and Ire1) (Mace et al., 2020). Nevertheless, only the inhibition of Snf1 and Cdc15 affected the expression of Hsf1 targets (Mace et al., 2020, Hahn and Thiele, 2004). It was shown that phosphorylation is not necessary for the activation of Hsf1 but helps to strengthen the transcriptional outcome (Zheng et al., 2016, Budzynski et al., 2015). Another regulation mechanism of Hsf1 is the chaperone titration model (Figure 4C) (Voellmy and Boellmann, 2007). In this model, Hsf1 is bound by Hsp70s and/or Hsp90 and kept inactive (Craig and Gross, 1991, Voellmy and Boellmann, 2007). When proteins unfold under stress, the chaperones are recruited towards the misfolded proteins, Hsf1 becomes free and activates the transcription of Hsps. This allows a fast response and additionally includes a negative feedback loop, as the upregulated chaperones repress Hsf1 as soon as enough Hsps are present (Voellmy and Boellmann, 2007, Richter et al., 2010). Biochemical evidence supports the Hsp70 family as the main regulator. It was shown that Hsp70 (Ssa1) binds the NTA, as well as the CE2 of Hsf1 with its substrate binding domain (SBD) (Krakowiak et al., 2018, Zheng et al., 2016, Peffer et al., 2019). Consequently, the deletion of CE2 leads to a higher basal activity of Hsf1 and much slower deactivation after the stress (Zheng et al., 2016, Krakowiak et al., 2018). Multiple CE2s however, lead to a stronger repression of Hsf1 (Krakowiak et al., 2018). Besides the substrate binding domain of Hsp70, also the ATPase activity of Hsp70 plays are role in the repression of Hsf1 as the deletion of nucleotide exchange factors also led to an active transcription factor (Verghese et al., 2012). Overall the regulation by chaperones (Hsp70s) seems to be the main switch for Hsf1 in *S. cerevisiae* (Zheng et al., 2016). Even though Hsf1 is thought to be the key player in regulating the HSR, only 45 Hsf1 targets were identified with ChIP-seq (Solís et al., 2016). In experiments in which Hsf1 was depleted from the nucleus only 18 Hsf1-dependent genes were identified under stress (Solís et al., 2016). Before, it was assumed that Hsf1 targets much more genes. According to Hahn and coworkers it has been thought that up to 3 % of the genes in yeast were under the control of Hsf1 (Hahn et al., 2004). Furthermore, Hsf1 depletion could be completely rescued by the Hsf1

independent expression of Hsp70 and Hsp90, showing that these two Hsps fulfill the functions that make Hsf1 essential under physiological conditions (Solís et al., 2016).
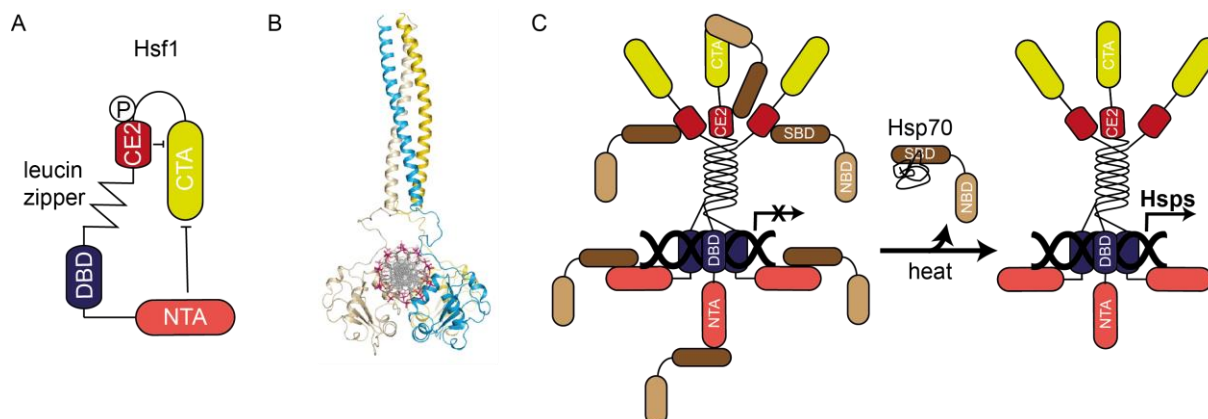
Figure 4: Structure and regulation of Hsf1. *A) Yeast Hsf1 consists of an N-terminal transactivation domain (NTA), a DNA binding domain (DBD), a leucine zipper, a control element (CE2) and a C-terminal transactivation domain (CTA). Close to the CE2, a repressive phosphorylation site is indicated. B) Structural model of human Hsf1 (residues 13-182) bound to DNA. C) Activation of Hsf1 according to the chaperone titration model. Under non-stress conditions, Hsp70 binds the CE2 and NTA with its substrate binding domain (SBD). When proteins unfold under stress, Hsp70 is recruited away from Hsf1 and the transcription of Hsps is initiated. The figure was designed based on the cited publications in the text (Verghese et al., 2012, Voellmy and Boellmann, 2007, Zheng et al., 2016, Peffer et al., 2019, Krakowiak et al., 2018, Høj and Jakobsen, 1994). The structure of the human Hsf1 (figure part B) was taken from Neudegger et al., 2016 and reprinted with the permission of Springer Nature.*

1.3.3.3 Msn2 and Msn4

It was observed long ago, that also an Hsf1-independent stress response exists (Wieser et al., 1991, Kobayashi and McEntee, 1990). The two responsible factors were named multi copy suppressor of Snf1 mutation 2/4 (Msn2 and Msn4). They also recognize a pentameric DNA sequence, called stress-response elements (STRE; CCCCT or AGGGG) (Schmitt and McEntee, 1996). Msn2 contains two zinc finger domains close to the C-terminus and is highly homologous to Msn4 (Estruch and Carlson, 1993). The transactivation domain of Msn2/4 is supposed to be in the N-terminal domain (Boy-Marcotte et al., 2006). One STRE element is sufficient to induce gene expression but multiple copies amplify gene expression more than additive (Kobayashi and McEntee, 1993, Estruch, 2000). Expression of genes under the STRE promoter is dependent on Msn2 or Msn4 and is induced by a variety of different stresses, such as low pH, high ethanol concentration or heat (Martínez-Pastor et al., 1996). Msn2 and Msn4 exhibit functional redundancy (Estruch and Carlson, 1993). Nevertheless, there are examples of genes that are dependent on Msn2 under heat stress (Treger et al., 1998, Estruch, 2000) and for a full activation of many targets both have to be present (Berry and Gasch, 2008). Most of the other genes with STREs are still regulated if one factor is missing, but to a smaller extent (Treger et al., 1998). Across diverse stress conditions it was shown that Msn2/4 control the expression of hundreds of genes (Boy-Marcotte et al., 1998, Hasan et al., 2002, Kandror et

al., 2004, Sadeh et al., 2011). Genomic analyses revealed that several stress-related genes have HSE and STRE elements in their promoter regions, which ends up in the before mentioned redundant regulation by Hsf1 or Msn2/4 (Treger et al., 1998). In another study it was shown that the redundancy appeared to be rather small and that Msn2/4 mostly target genes that can be categorized into antioxidants and carbon metabolism whereas Hsf1 controls the expression of chaperones (Boy-Marcotte et al., 1999). There are also indications that the need of the transcription factor is dependent on the stress condition, as it was shown for Hsp26 that it is dependent on Hsf1 under heat stress and on Msn2/4 under oxidative, osmotic or carbon source stress (Amorós and Estruch, 2001). Nevertheless, this regulation model for genes having both regulatory elements, HSE and STRE, is not universal as it was shown for Hsp104 that it is dependent on Hsf1 also under the other stress conditions (Amorós and Estruch, 2001). An elaborated phosphorylation cascade, which possibly is still to be completed, regulates Msn2/4 (Figure 5). Msn2/4 is repressed by PKA, whereas S288 is thought to be an important phosphorylation site to prevent nuclear localization of Msn2/4 (Gorner et al., 1998). Thus, low PKA activity induced by low glucose levels or heat leads to nuclear import of Msn2/4 (Görner et al., 2002, Görner et al., 1999). In consequence, the regulatory subunit Bcy1 of PKA positively influences Msn2/4 activation by suppressing PKA mediated phosphorylation (Görner et al., 2002). Recently, it was suggested that the PKA pathway is under the control of the HOG pathway, which links osmotic stress signalling to Msn2/4 (Mace et al., 2020). There are also reports for Msn2/4 dephosphorylation by protein phosphatase1 (PP1) and PP2A, which leads to nuclear localization of the transcription factors (Lenssen et al., 2005, De Wever et al., 2005, Santhanam et al., 2004). PP1 itself is repressed by the TOR kinase, thus TOR signalling also leads to Msn2/4 repression (Santhanam et al., 2004, Beck and Hall, 1999). If PKA is repressed, Yak1 becomes activated and phosphorylates Msn2/4 as well as Hsf1. In this case phosphorylation results in activation (Lee et al., 2008). Additionally, CK2 activates Msn2/4 under stress by the phosphorylation of S638 (Cho and Hahn, 2017). Upon prolonged glucose starvation Msn2/4 is phosphorylated and depleted from the nucleus by Snf1, which might be an adaptive mechanism (De Wever et al., 2005). Besides localization, there are indications that Gsk3 indirectly affects DNA binding of Msn2/4, which might be another point of regulation (Hirata et al., 2003). A third important regulatory mechanism of Msn2/4 is degradation, which depends on the intracellular localization, a kinase (Srb10) and possibly on hyperphosphorylation (Durchschlag et al., 2004, Lallet et al., 2004, Bose et al., 2005, Garreau et al., 2000, Boy-Marcotte et al., 2006).
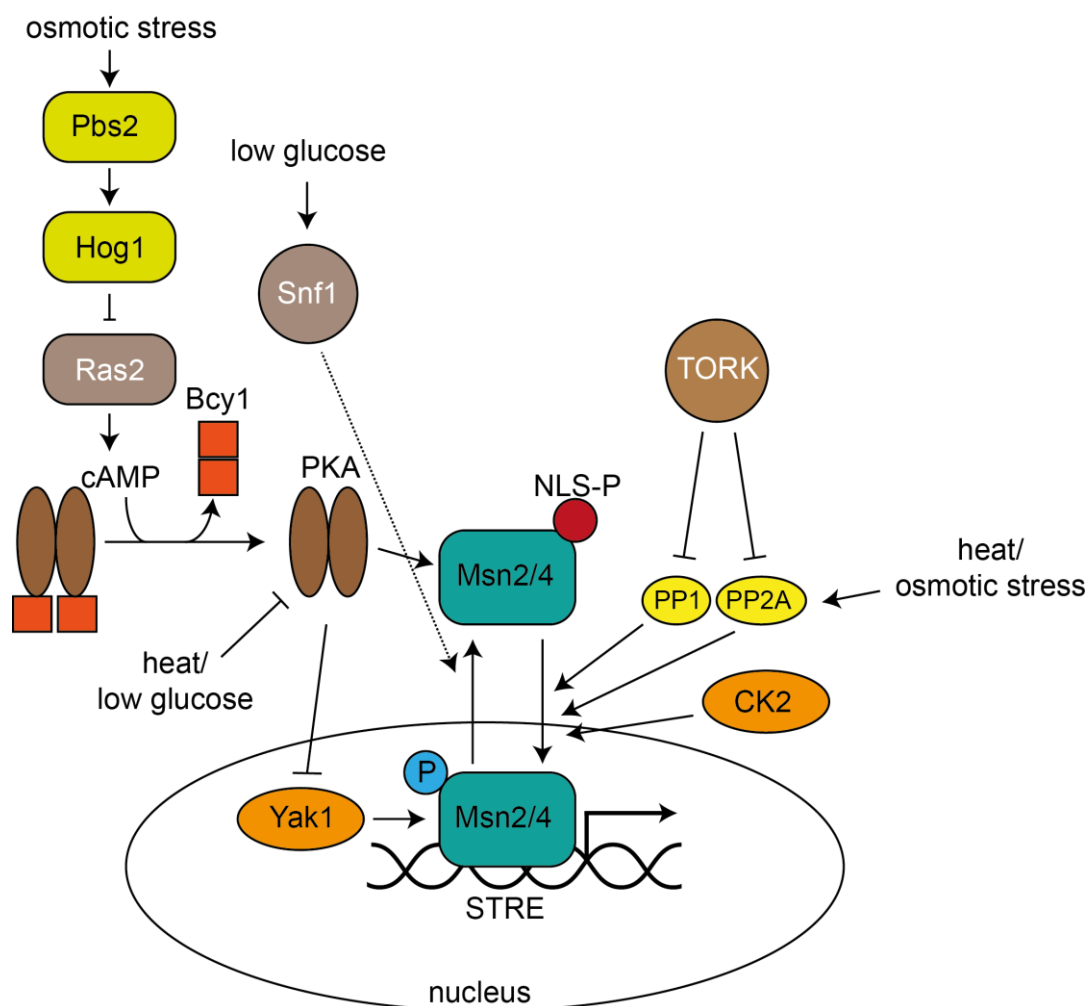
Figure 5: Regulation of Msn2/4 by phosphorylation. *Heat, osmotic stress and low glucose levels lead to the repression of PKA and therefore less Msn2/4 phosphorylation in the NLS. PKA phosphorylation of the NLS leads to nuclear export of the transcription factors. PKA phosphorylation can be reverted under stress by PP1 and PP2A. The phosphatases in turn are inhibited by the TOR kinase under high glucose concentrations. YAK1 phosphorylation as well as phosphorylation by CK2 activate Msn2/4. SNF1 phosphorylates Msn2/4 and induces its export after prolonged glucose starvation (De Wever et al., 2005, Görner et al., 2002, Lenssen et al., 2005, Santhanam et al., 2004, Cho and Hahn, 2017, Lee et al., 2008, Beck and Hall, 1999, Mace et al., 2020).*

1.3.4 Effects of heat stress on translation

It was shown with radio-labelled amino acids that exposure to heat stress leads to a change in protein synthesis (Lindquist, 1980, Miller et al., 1979). In contrast to non-stress conditions where a broad variety of proteins was synthesized, heat stress led to an overall decrease of proteins synthesis and a shift towards the synthesis of heat shock proteins as mentioned above (Lindquist, 1980). The transcriptomic and translatomic changes were found to correlate well in cells stressed at 37 °C for 30 min (Preiss et al., 2003). In fact, there was even potentiation observed due to adapted translation rates even though this effect seemed to be dependent on the stress and its severity (Preiss et al., 2003, Gerashchenko et al., 2012). Translation can be divided into three main steps: initiation, elongation and termination (Dever et al., 2016). Heat

stress induced inhibition of the initiation step by phosphorylation of eIF2α is a very important regulatory switch and was already discussed in the section of general heat shock effects on the cell (Hinnebusch, 2005, Costa-Mattioli and Walter, 2020). Another factor that influences translation under stress is the dependence of many transcripts on the RNA helicases eIF4A and Ded1 for translation (Gao et al., 2016, Sen et al., 2015). Importantly, both are known to localize to SG under heat stress and therefore are not available anymore (Hondele et al., 2019, Wallace et al., 2015). Furthermore, it is known that translationally active mRNA is often arranged as a circle whereupon the cap binding eIF4E is connected to the poly(A) binding protein (Pab1) via eIF4G (Preiss and Hentze, 1998). This allows efficient re-initiation of the ribosome (Prévôt et al., 2003) (Figure 6). As Pab1 phase separates under heat stress, this circulation is impeded under stress (Riback et al., 2017, Wallace et al., 2015). Those effects lead to suppression of cap- and helicase-dependent translation under heat shock conditions (Wallace et al., 2015). In contrast, translation of several genes such as the ISR effector *GCN4* transcript is activated after the phosphorylation of eIF2 (Costa-Mattioli and Walter, 2020). Interestingly, transcripts coding for stress-protective proteins often carry a poly(A) leader in their 5´upstream sequence which enables cap-independent translation for which eIF3 and eIF4F are dispensable (Rhoads and Lamphear, 1995, Shirokikh and Spirin, 2008). Of note, the protein synthesis rate increases with the length of the poly(A) stretch. If the poly(A) stretch is 12 bp or longer, Pab1 binds and suppresses translation under non stress conditions whereas under heat stress the mRNA becomes accessible due to the phase transition of Pab1 (Xia et al., 2011). Less is known about effects of heat stress on translation elongation (Crawford and Pavitt, 2019). It was observed under several stress conditions that uncharged tRNAs accumulate and lead to ribosomal stalling (Zaborske et al., 2009, Pelechano et al., 2015, Shenton et al., 2006). Furthermore, upon severe heat stress stalling after hydrophobic stretches was reported for mammalian cells (Shalgi et al., 2013). Folding of nascent peptides is assisted by ribosome-associated chaperones, such as Hsp70 (Ssb in yeast) (Peisker et al., 2010, Kramer et al., 2009). Especially folding of hydrophobic peptide sequences is dependent on Hsp70 (Hartl et al., 2011). Thus, stalling under stress is probably due to the recruitment of Hsp70 away from the ribosome towards unfolded cellular proteins (Shalgi et al., 2013). Those stalling effects should not be over-interpreted, as the observations that ribosomes pause towards the 5´-end during stress were challenged by another study in yeast (Gerashchenko and Gladyshev, 2014). It was shown that the ribosome accumulation under stress depends on the treatment with cycloheximide (CHX) and that the treatment time influences the pausing point (Gerashchenko and Gladyshev, 2014, Hussmann et al., 2015). In stressed cells that were not treated with CHX no enrichment towards the 5´ end of translated mRNAs was observed (Gerashchenko and Gladyshev, 2014). In conclusion, translation initiation seems to be the major point of translational regulation under stress (Crawford and Pavitt, 2019).
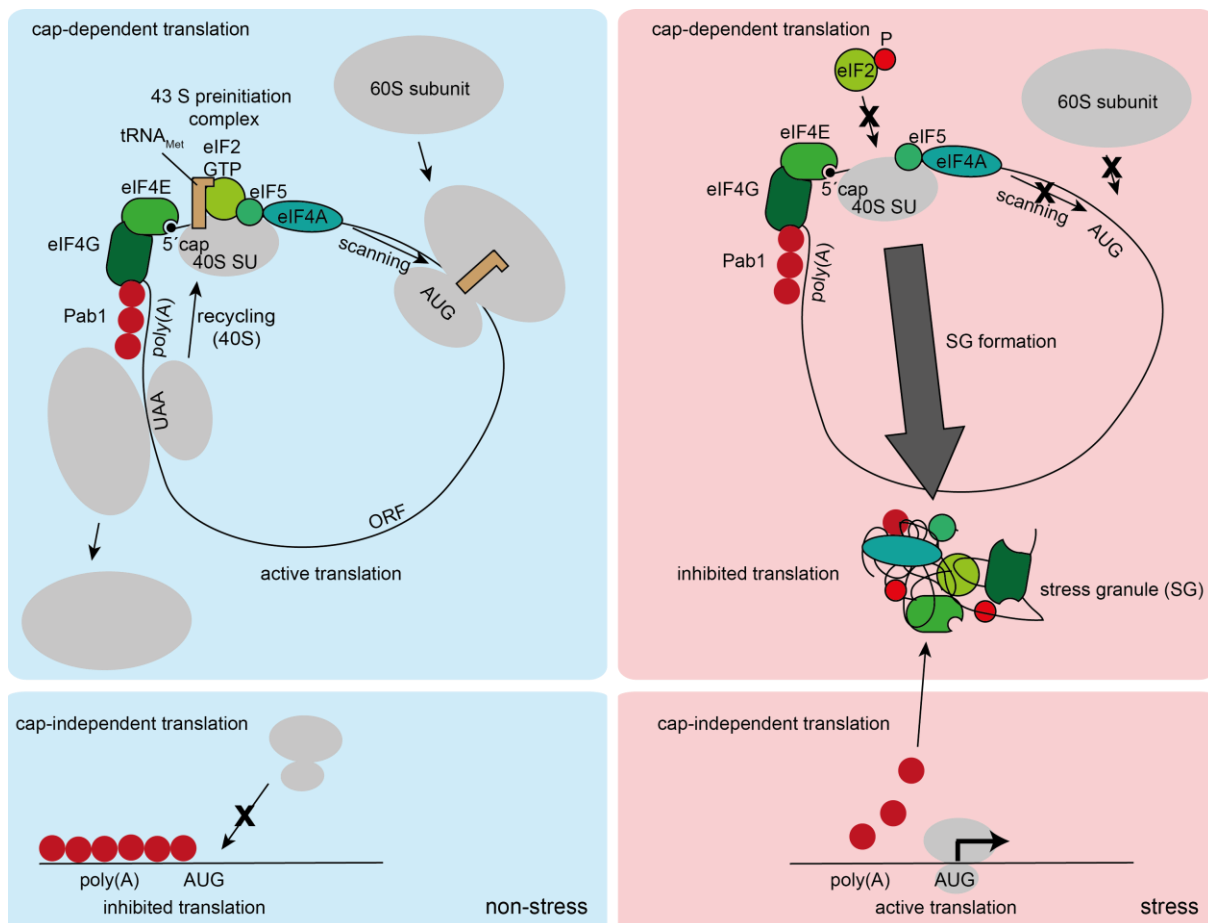
Figure 6: Regulation of translation initiation under non-stress (blue box) and stress conditions (red box) in yeast. Under non-stress conditions, the 43S preinitiation complex scans until the start codon. At the start codon, the initiation factors are released and the 60S ribosomal subunit joins the 40S subunit. At the stop codon, the ribosome dissociates from the mRNA. Due to the ring formation mediated by Pab1, eIF4G and the cap binding protein eIF4E the 40S subunit can rebind efficiently in the 5´ UTR. In contrast, cap independent translation is blocked by Pab1, which binds the poly(A) stretch in the 5´ UTR and inhibits binding of the ribosome under non-stress conditions. Under stress eIF2 is phosphorylated and cannot transfer the initiation tRNA anymore. Subsequent phase transition of the initiation factors, RNA helicases eIF4A and Ded1 as well as Pab1 leads to the formation of stress granules and thus inhibition of cap-dependent translation. Cap-independent translation (of stress protective factors) however is now possible due to phase transition of Pab1, which makes the start codon accessible. The figure was designed based on the cited publications in the text (Crawford and Pavitt, 2019, Hondele et al., 2019, Preiss and Hentze, 1998, Wallace et al., 2015, Xia et al., 2011, Hinnebusch, 2005, Shirokikh and Spirin, 2008).

1.3.5 Effects of heat stress on the proteome

The clearest effect of heat shock on the proteome was already described above: The upregulation of heat shock proteins (Lindquist and Craig, 1988). Even though transcription and translation correlate well, at least under mild stress, overall proteomic changes turned out to be only weakly correlating with changes at the mRNA level in yeast (Fournier et al., 2010, Soufi et al., 2009, Gerashchenko et al., 2012). Especially downregulation at the mRNA level is almost not reflected at the protein level. This was exemplary shown in fission yeast. However, the correlation of upregulated genes and the corresponding proteins tended to be better

(Lackner et al., 2012). Thus, it was hypothesized that the main reason for downregulating mRNAs is to prevent competition of these mRNAs with the upregulated mRNAs at the ribosome (Lee et al., 2011). As translation follows transcription, another experimental problem can be that transition states but not steady states are compared, which leads to bad correlations (Liu et al., 2016). A time-resolved heat stress proteome study over 4 h in yeast revealed that the response at the proteomic level is delayed and that the correlation between the transcriptome and the proteome improves with time (Jarnuczak et al., 2018). Nevertheless, the significant changes were still limited to chaperones and the trehalose biosynthesis pathway (Jarnuczak et al., 2018). Under heat shock, phase separation, phase transition and aggregation processes severely shape the yeast proteome (Wallace et al., 2015). Temperature-induced phase transition of specific thermosensors, such as Pab1 or Pub1, induces an immediate stress response with the before described effects, mainly on translation (Kroschwald et al., 2018, Riback et al., 2017, Wallace et al., 2015, Yoo et al., 2019). Importantly, foci and stress granule formation was shown to set in at temperatures around 46 °C *in vivo*, thus significantly above 37 °C, which is already considered to be heat stress for *S. cerevisiae* (Cherkasov et al., 2015, Gasch et al., 2000, Morano et al., 2012). As chaperones are essential to maintain proteostasis and many of them are strongly upregulated under stress, they will be grouped and characterized in the following section.

1.4 Molecular chaperones

In yeast, five different classes of chaperones have been described, Hsp104, Hsp90 (+ cochaperones), Hsp70s (+cochaperones), chaperonins and sHsps (Verghese et al., 2012, Richter et al., 2010). Chaperones are constantly needed to prevent aggregation and assist in protein (re-)folding (Gragerov et al., 1991, Mayer, 2010). They recognize and bind exposed hydrophobic residues, which are usually found in non-native proteins. Thus, chaperones work very promiscuously and have broad substrate spectra (Bukau et al., 1996, Viitanen et al., 1992). Refolding of substrates is achieved by preventing unwanted interactions and the cycling between at least two affinity states by ATP hydrolysis, which leads to controlled binding and release events (Sharma et al., 2008, Walter and Buchner, 2002, Richter et al., 2010). In the following, the different chaperone classes will be introduced in detail.

1.4.1 Hsp104

Hsp104 forms hexameric complexes and belongs to the group of AAA+ translocases (Sweeny et al., 2019, Wendler et al., 2009). AAA+ ATPases are able to move substrate under ATP hydrolysis, which allows Hsp104 to work as a disaggregase (Schirmer et al., 1996, Shorter and Southworth, 2019). Notably, the Hsp100s are the only chaperones that are able to disassemble aggregates, amyloids or prions and metazoans do not have such chaperones (Schirmer et al., 1996, Doyle and Wickner, 2009, Shorter and Southworth, 2019). ATP hydrolysis leads to small

changes, whereas the ADP bound state is more solvated (*open spiral*) than the ATP bound state (*closed ring*) (Sweeny et al., 2019). Transition between those states allows the stepwise translocation of the substrate by the chaperone whereby the substrate interaction is mostly mediated by conserved tyrosine residues of the AAA+ nucleotide-binding domain (NBD) loops (Shorter and Southworth, 2019, Gates et al., 2017). Each monomer has two, an N-terminal and a C-terminal, AAA+ NBD (Shorter and Southworth, 2019). The C-terminal domain is necessary for hexamerization and the N-terminal NBD for disaggregation (Hattendorf and Lindquist, 2002, Schirmer et al., 1998, Mackay et al., 2008). After Hsp70 was recruited to the aggregated proteins by Hsp40s, ADP bound Hsp70 recruits Hsp104 and hands over the substrate to the disaggregase (Kaimal et al., 2017). In yeast, the interaction of Hsp104 and Hsp70 is mediated by Hsp110s (Sse1/2) (Kaimal et al., 2017). In the absence of Sse1/2, Hsp104 cannot fulfill its function as a disaggregase anymore, which indicates that Hsp70 stimulates the translocation reaction (Gates et al., 2017, Kaimal et al., 2017). The aggregated protein enters Hsp104 at the N terminal domain and is released at the C terminal domain (Shorter and Southworth, 2019). Besides the interaction with Hsp70, Hsp104 was shown to take over substrates from Hsp26 (Haslbeck et al., 2005b). Additionally, interactions with several Hsp90 cochaperones were reported whereas these interactions are thought to be much less relevant (Abbas-Terki et al., 2001). If refolding is not feasible, Hsp104 can hand over its substrate to the proteasome for degradation (Lee and Goldberg, 2010). Hsp104 also plays an important role during sublethal heat shock and for thermotolerance but is not an essential gene and cell growth is not affected by Hsp104 deletion under non-stress conditions (Lindquist and Kim, 1996, Sanchez and Lindquist, 1990).

1.4.2 The Hsp90 system

In yeast, two Hsp90 homologues are expressed, the constitutive Hsc82 and the stress inducible Hsp82 (Borkovich et al., 1989). Hsc82 is highly abundant under non-stress conditions whereas Hsp82 is strongly upregulated under stress (Borkovich et al., 1989, Ghaemmaghami et al., 2003). Hsp90 is essential in yeast even though its substrate spectrum seems to be much smaller than of the other chaperones and only native-like proteins are bound and maturated (Picard, 2002, Pratt and Toft, 2003, Borkovich et al., 1989). Nevertheless, several hundred clients are known, including many kinases and transcription factors (Schopf et al., 2017). Hsp90 consists of three domains (Schopf et al., 2017). The C terminal domain (CTD) allows dimerization, which is essential for its functionality and carries an unfolded segment including the EEVD motif, which is recognized by the tetratricopeptide (TPR) repeats of certain cochaperones (Wayne and Bolon, 2007, Harris et al., 2004, Buchner, 1999). The ATP binding pocket is located in the NTD, which is connected to the middle domain (MD) via a charged, flexible linker (Hainzl et al., 2009, Prodromou et al., 1997). The MD provides a client binding site and is important for ATP hydrolysis (Schopf et al., 2017). Throughout ATP hydrolysis,

Hsp90 passes through distinct conformations (Hessling et al., 2009). In the *apo* state without ATP, Hsp90 adopts a V-like structure (open conformation). After binding ATP, there are some rearrangements in the NTD, a lid closes the ATP binding pocket ("intermediate" state), the NTDs of both subunits dimerize and form the "closed 1" state. In the "closed 2" state, the monomers twist and ATP is hydrolyzed. After release of ADP, Hsp90 adopts the open conformation again (Hessling et al., 2009, Schopf et al., 2017). ATP hydrolysis, as well as substrate specificity of Hsp90 are strongly affected by numerous known cochaperones (Schopf et al., 2017, Verghese et al., 2012). Notably, only Sti1 and Cpr6 were found to be upregulated under stress (Eisen et al., 1998). As Sti1 is known to suppress the ATPase activity of Hsp90 and thus prevents further processing of the substrate, this observation indicates that under stress, the holdase function of Hsp90 is favored (Richter et al., 2003, Hessling et al., 2009, Richter et al., 2010). Three essential Hsp90 cochaperones have been identified (Schopf et al., 2017). First, Cdc37, which is important for kinase maturation (Schopf et al., 2017). Second, Cns1, which was shown to link Hsp90 to translation elongation by chaperoning eEF2 (Schopf et al., 2019). The function of the third essential cochaperone Sgt1 remains to be elucidated (Schopf et al., 2017).

1.4.3 The Hsp70 family

Hsp70s are involved in *de novo* protein folding as well as in aggregation prevention and the dissolution of aggregates. Furthermore, they represent the most conserved group of chaperones (Mayer and Bukau, 2005). In yeast, there are nine cytosolic Hsp70 isoforms (Ssa1-4, Ssb1/2, Sse1/2, Ssz1), two Hsp70s located in the ER (Kar2 and Lhs19) and three mitochondrial Hsp70s (Ssc1/3, Ssq1) (Morano et al., 2012). Hsp70 consists of an N-terminal nucleotide-binding domain (NBD) and a C-terminal substrate-binding domain (SBD), which are connected by a flexible linker. The SBD alone can bind substrate, but the NBD and the linker are essential for folding (Vogel et al., 2006b, Vogel et al., 2006a). When ATP is bound to the NBD, the substrate affinity of the SBD is low. By the hydrolysis of ATP structural changes are transferred from the NBD to the SBD, which now adopts a higher affinity state. After ADP has been replaced by ATP, the substrate is released again (Verghese et al., 2012, Mayer, 2013). A seven amino acid stretch of hydrophobic peptides seems to be important for the interaction with exposed hydrophobic patches of the substrate protein (Zhu et al., 1996). Furthermore, the SBD also provides the binding site for J-protein cochaperones (Freeman et al., 1995). In eukaryotes, a constitutive Hsc70 and a stress-inducible Hsp70 homologue are present (Craig and Jacobsen, 1985). In *S. cerevisiae*, Ssa1 and Ssa2 are constitutively expressed, whereas Ssa3 and Ssa4 are induced by stress (Nelson et al., 1992, Verghese et al., 2012). Cells expressing only one Ssa isoform constitutively are viable but thermosensitive, which indicates complementary function to some extent (Werner-Washburne et al., 1987). Besides the general folding activity of the Ssa type chaperones, which fold proteins post-translationally, Ssb1/2 are

associated to the ribosome and support co-translational protein folding together with Ssz1 and Zuo1 (Gautschi et al., 2001, Kim et al., 1998b, James et al., 1997). In the absence of the SSB genes, Ssa can also associate with the ribosome but the deletion phenotype cannot be completely reversed. The same was observed the other way around, as Ssb cannot reverse SSA deletion completely. Obviously, Ssa and Ssb have evolved unique functions whereupon Ssbs seem to be more specific and Ssas are the general chaperones (James et al., 1997, Pfund et al., 2001, Verghese et al., 2012). Besides, their involvement in protein folding, Ssas are involved in protein translocation processes as well as degradation (Satyanarayana et al., 2000, Shulga et al., 1996, McClellan and Brodsky, 2000, Juretschke et al., 2010, Sharma and Masison, 2011). Hsp70s interact with two main classes of cochaperones: J-proteins (Hsp40s) and nucleotide exchange factors (NEFs) (Mayer, 2013). The main function of J-proteins is to bind unfolded substrate and to deliver it to Hsp70 (Kampinga and Craig, 2010). In combination with the substrate, they are also able to strongly stimulate the ATPase activity of Hsp70 (Silberg et al., 2004, Misselwitz et al., 1998). In yeast, 22 J-proteins are known (Kampinga and Craig, 2010). Four classes of NEFs have been identified in yeast, which replace ADP with ATP and therefore modulate substrate release (Kampinga and Craig, 2010, Morano et al., 2012).

1.4.4 Chaperonins

The class of chaperonins is divided into group 1 and group 2 chaperonins. The bacterial GroEL/ES complex belongs to class 1 and forms cylinders of two hexameric GroEL rings, which are covered stoichiometric by GroES (Grallert and Buchner, 2001). GroE is a very promiscuous chaperone and supports protein folding in isolation by providing a cavity (Horwich et al., 2006, Hartl and Hayer-Hartl, 2002, Viitanen et al., 1992). The yeast mitochondrial Hsp60 is homologous to the bacterial GroEL and interacts with Hsp10 to fold proteins that were imported into mitochondria (Meng et al., 2018). Additionally, yeast expresses Tcp1 ring complex (CCT/TRiC) in the cytosol, which belongs to the second class of chaperonins and forms a double ring structure. Each ring is composed of octamers (Valpuesta et al., 2002, Frydman et al., 1992). Notably, the eukaryotic chaperonins seem to be less promiscuous and are thought to be involved in the folding of 5 - 10 % of newly synthesized proteins with components of the cytoskeleton as major clients (Siegers et al., 1999, Kabir et al., 2011). More detailed analysis of the substrate spectra revealed that especially proteins with complex folds and therefore lower folding kinetics are substrates of the CCT/TRiC chaperonin (Yam et al., 2008). Prefoldin acts as a cochaperone, which delivers substrate to the CCT/TRiC complex (Vainberg et al., 1998). Especially for the maturation of cytoskeleton components prefoldin seems to be needed (Kabir et al., 2011, Vainberg et al., 1998). Interestingly, CCT/TRiC is not upregulated under heat shock and therefore this class of chaperones will be less important in this study (Eisen et al., 1998).

1.4.5 Small Heat Shock Proteins

The last group of molecular chaperones found in yeast are small Heat Shock Proteins (sHsps). sHsps are present in archaea, bacteria, eukaryotes and viruses. Hence, they are assumed to be evolutionary old (Bult et al., 1996, Caspers et al., 1995, Kriehuber et al., 2010, Carra et al., 2017, Kappé et al., 2002). Throughout evolution they diverged strongly, which made them the least conserved chaperone class (Kriehuber et al., 2010, de Jong et al., 1993, Kappé et al., 2002). Unicellular organisms normally express one or two sHsps, whereas higher eukaryotes tend to express multiple sHsps. For example, 10 human sHsps are known (Haslbeck et al., 2005a, Kriehuber et al., 2010, Kappé et al., 2003). Exceptions are found amongst pathogenic bacteria, which often do not express sHsps whereas in symbiotic bacteria more than two sHsps are common (Narberhaus, 2002, Kriehuber et al., 2010, Haslbeck and Vierling, 2015). Despite their low conservation, specific features have been defined for the classification of sHsps. sHsps usually form large and dynamic oligomers whereas the single subunits are rather small (12 - 43 kDa). They should be (heat) stress-inducible and they encode an α-crystallin domain (ACD) (Haslbeck et al., 2005a). The best-studied members of the sHsp family are αA-crystallin and αB-crystallin, which are highly identical and essential to maintain proteostasis in the eye lens where protein concentrations of 450 mg/ml are present (Horwitz, 1992, Horwitz, 2003, Slingsby et al., 2013). About one third of the eye lens proteins are α-crystallins, whereupon αA is an eye specific chaperone and αB is expressed ubiquitously and linked to several protein misfolding diseases such as myopathies or Alzheimer´s disease (Arrigo, 2013, Sun and MacRae, 2005). sHsps generally consist of three domains, the well conserved and already mentioned ACD, a non-conserved and variable N-terminal region (NTR) and a shorter but still non-conserved C-terminal region (CTR) (Figure 7A) (Caspers et al., 1995, Kriehuber et al., 2010). Disregarding a few exceptions, the CTR encodes the conserved IXI motif, which was shown to interact with the ACD and thus is involved in the formation of higher order oligomers (Delbecq et al., 2012, Basha et al., 2012, Bukach et al., 2004, Kappé et al., 2004). There are also examples for IXI motifs in the NTR (Stamler et al., 2005, Sluchanko et al., 2017). In the NTR, the amount of phenylalanine residues is relatively high and several phosphorylation sites were identified there in mammalian sHsps (Kriehuber et al., 2010, Heirbaut et al., 2015, Arrigo and Gibert, 2012, Kato et al., 1998, Ito et al., 1997). Interestingly, sHsps are not only found in the cytosol. There are reports of sHsps in principally every organelle (Waters, 2013, Waters and Vierling, 1999, Ma et al., 2006, Siddique et al., 2008, Morrow et al., 2000). As already mentioned in the classification criteria, sHsps usually form oligomers. Those complexes can be very variable in size (12 - >32-mer), but also dimeric sHsps have been found (Basha et al., 2013, Bepperling et al., 2012, Delbecq and Klevit, 2013, Benesch et al., 2010). Of note, dimers are the main building blocks of the oligomers (Delbecq and Klevit, 2013, Haslbeck and Vierling, 2015). The ACDs provide the dimerization surface but, generally, the ACD alone is not

sufficient to form oligomers (Bagneris et al., 2009, Baranova et al., 2011). It is approximately 94 amino acids long and forms a β-sandwich whereas the single β-sheets are connected by short linkers (Figure 7B) (van Montfort et al., 2001a, van Montfort et al., 2001b). The dimerization mode of the ACD is different in metazoans and non-metazoans (Figure 7C) (Haslbeck and Vierling, 2015). According to the solved structures of bacterial, yeast and plant sHsps, dimerization occurs via a swapped β6 strand of the second ACD that interacts with the β2 strand of the first ACD and thus is referred to as "β6 swapped dimer" (Bepperling et al., 2012, van Montfort et al., 2001b, Kim et al., 1998a, Hanazono et al., 2013). In the "metazoan type" however, the dimer interface is formed by antiparallel fused β6/7 strands (Jehle et al., 2009, Delbecq and Klevit, 2013). For oligomerization, the sequences N- and C-terminal of the ACD are necessary (Haslbeck and Vierling, 2015). How oligomerization works in detail is still under investigation. It was shown that the IXI motif binds a groove formed by the β4 and β8 strand of the neighboring monomer supporting the formation of higher order oligomers (Haslbeck et al., 2019). Nevertheless, the IXI motif is not essential for oligomerization (Pasta et al., 2004, Treweek et al., 2007). NTR contacts are also supposed to lead to the formation of oligomers (Delbecq and Klevit, 2013, Hanazono et al., 2013, Kim et al., 1998a, van Montfort et al., 2001a, van Montfort et al., 2001b, Braun et al., 2011). Due to the oligomer dynamics, the amount of atomic sHsp structures with full length proteins is small (Braun et al., 2011, Hanazono et al., 2013, Kim et al., 1998a, van Montfort et al., 2001b, Fleckenstein et al., 2015). Another characteristic of sHsps is that they are ATP independent chaperones, which prevent aggregation of unfolded substrate proteins (Jakob et al., 1993, Horwitz, 1992, McHaourab et al., 2002, Lee et al., 1995). Therefore, they have been termed holdases (Haslbeck et al., 2019). Their activity can be modulated by the temperature, the pH, the redox state, the presence of unfolded substrate, hetero-oligomer formation or post-translational modifications such as phosphorylation (Haslbeck et al., 1999, Ito et al., 1997, Kato et al., 1998, Fleckenstein et al., 2015, Kaiser et al., 2019, Mymrikov et al., 2019, Ratajczak et al., 2009, Haslbeck et al., 2015). Dependent on the sHsp/substrate ratio, different complexes are formed. If the chaperone is present in excess, the substrate complexes are usually polydisperse and soluble (Haslbeck et al., 1999, Basha et al., 2004). If the amount of substrates exceeds the sHsp, generally the formation of amorphous aggregates, including sHsps, is observed (Basha et al., 2004, Haslbeck et al., 2005b, Haslbeck et al., 2019). For substrate release and refolding, cooperation with ATP-dependent chaperones is inevitable (Figure 7D). If the substrate complexes are soluble Hsp70/40s are sufficient for refolding, insoluble complexes additionally rely on Hsp104 in yeast (Veinger et al., 1998, Lee et al., 1997, Mogk et al., 2003, Haslbeck et al., 2005b, Cashikar et al., 2005). In metazoans, a more sophisticated Hsp70 machinery evolved that also allows dissolving such aggregates (Nillegoda et al., 2018, Nillegoda et al., 2015). Thus, sHsp-controlled formation of aggregates is not harmful to the cell. It is most likely a protective

strategy under severe proteotoxic stress (Escusa-Toret et al., 2013, Specht et al., 2011). The detailed mechanism of substrate transfer to ATP-dependent chaperones has not been solved yet and a direct physical association of sHsps and Hsp70 has also not been shown (Haslbeck et al., 2019, Bepperling et al., 2012, Mogk et al., 2003, Friedrich et al., 2004, Rauch et al., 2017).
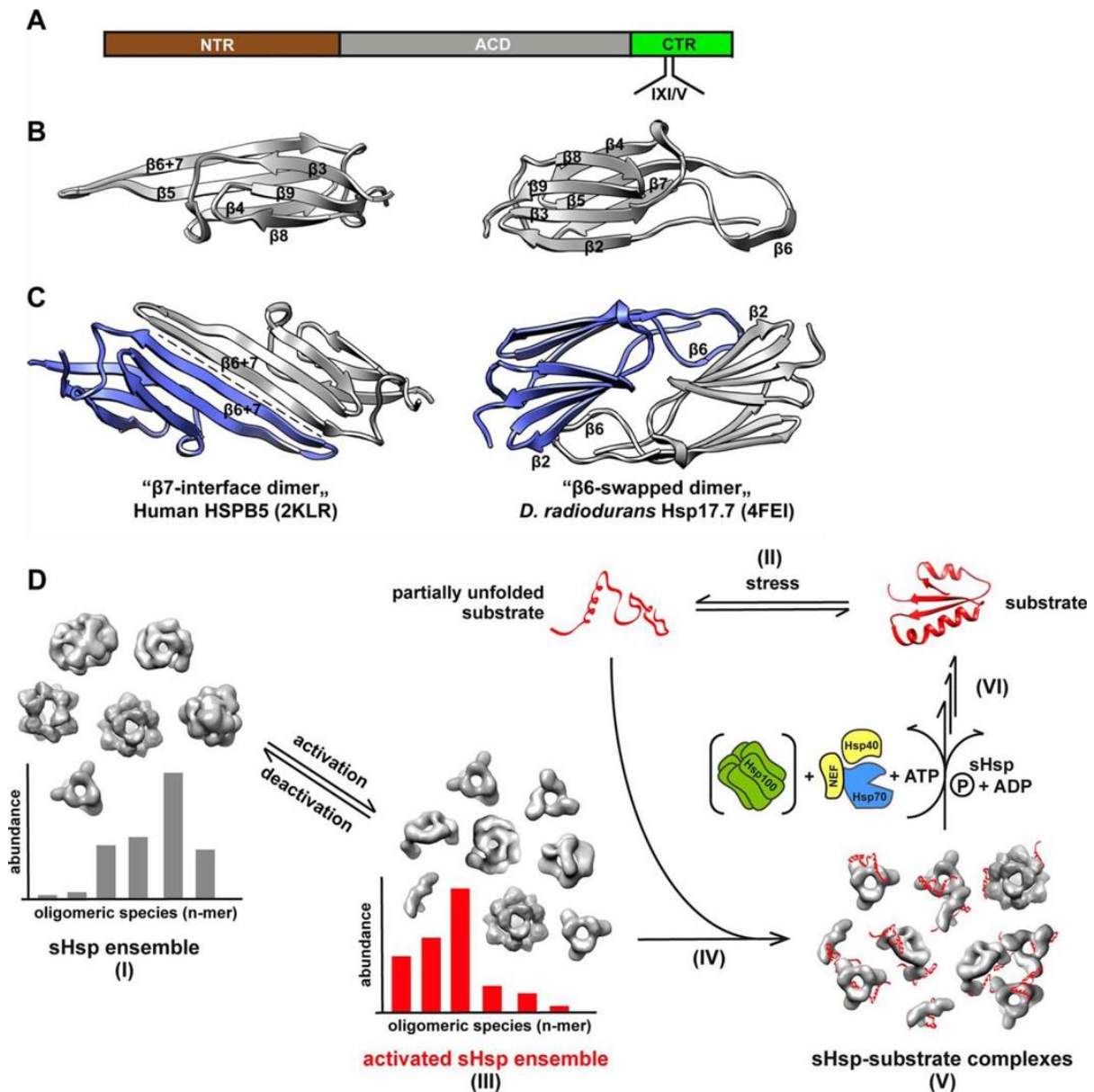
Figure 7: Structure and regulation of small Heat Shock Proteins (sHsps). *A) Schematic structure of sHsps. B) Structures of ACD monomers (left: human HspB5; PDB 2KLR, right: Hsp17.7 from D. radiodurans; PDB 4FEI). C) Structures of ACD dimers (left: metazoan type, right: β6 swapped dimer). D) Activation of sHsps. Under stress conditions, proteins unfold (II). Upon activation, the large oligomers (I) dissociate (III) and bind the unfolded substrate (IV). The sHsp-substrate complexes (V) are dissolved with the help of ATP dependent chaperones, which also refold the substrate proteins (VI). The figure is a combination of two figures from (Haslbeck et al., 2019). The reprint was permitted by the American Society for Biochemistry and Molecular Biology.*

In summary, sHsps are holdases and sequestrases (Haslbeck et al., 2019). Activation of sHsps usually leads to oligomer decomposition with the result that substrate binding sites that were buried in the oligomer become exposed (Peschek et al., 2013, Mchaourab et al., 2009, Giese and Vierling, 2002). Especially the NTR is described to mainly interact with the substrate (Delbecq and Klevit, 2013, Basha et al., 2012, Wu et al., 2019). However, for Aβ40 peptides, which form fibrils, the ACD was identified as the main substrate interaction site (Mainz et al., 2015). Overall, sHsps are extraordinarily promiscuous chaperones with hundreds of possible substrate proteins (Bepperling et al., 2012, Fleckenstein et al., 2015, Mymrikov et al., 2017, Peschek et al., 2013, Haslbeck et al., 2004a). Even though, sHsps are mostly not essential for viability, malfunction or deregulation of sHsps is connected to multiple protein misfolding diseases, such as cataract, multiple sclerosis, neuropathies or cancer, which highlights the importance of understanding their cellular functions in detail (Haslbeck et al., 2019, Haslbeck et al., 2005a). As this study focuses on the heat stress response in yeast, the yeast sHsps, Hsp26 and Hsp42, will be introduced in detail.

1.4.5.1 Yeast Hsp12

Hsp12 was originally classified as a sHsp because of its small size and its regulation under stress (Orlandi et al., 1996). As the sequence homology with the other sHsps is very low, it is usually not listed as a sHsp anymore (Welker et al., 2010). Hsp12 is a monomer, that is 100-fold upregulated under stress (Praekelt and Meacock, 1990). It is unfolded in solution but forms a helical structure in association with the membrane (Welker et al., 2010). Hence, Hsp12 can modulate the fluidity of membranes and its main function under stress is presumably to stabilize cell and organelle membranes (Welker et al., 2010).

1.4.5.2 Yeast Hsp26

Early *in vivo* studies with *HSP26* deletion mutants showed that the chaperone is not essential and deletion does not lead to growth defects neither at non-stress nor under several tested stress conditions (Petko and Lindquist, 1986). It was classified as a sHsp but the function of this 23.7 kDa protein remained enigmatic (Susek and Lindquist, 1989). Later, it was shown *in vitro* that Hsp26 forms big oligomers (24-mers, or even bigger) and that it is able to suppress heat-induced aggregation of citrate synthase, insulin or β glucosidase in a concentration-dependent manner (Haslbeck et al., 1999, Benesch et al., 2010, White et al., 2006). Importantly, chemically-induced aggregation of insulin at 25 °C cannot be suppressed efficiently by Hsp26 (Haslbeck et al., 1999). Thus, Hsp26 needs to be heat-activated, which leads to the dissociation of the big oligomeric complexes into dimeric species (Haslbeck et al., 1999, Benesch et al., 2010). The 24-mer is arranged as a hollow sphere for which two states could be resolved with cryo-EM at a resolution of 11 Å: An expanded and a compact conformation (White et al., 2006).The primary building block of the oligomer is the Hsp26 dimer

(White et al., 2006). Interestingly, the ACD of Hsp26 alone does not form a dimer, as it was observed for many other sHsps (Chen et al., 2010a). In the case of Hsp26, the ACD has to be either N-terminally flanked by the so-called middle domain (MD; amino acids 31-95) or by the C-terminal sequence including the IXI motif and a small part of the MD (Chen et al., 2010a, Baranova et al., 2011). The NTR is not only important for oligomer formation, it also is essential for the chaperone activity of Hsp26 (Stromer et al., 2004). As described for other sHsps, the NTR exhibits a high content of aromatic residues (12.6 %) (Kriehuber et al., 2010). Analysis of different truncation mutants revealed that the NTR can be spilt into a 30 amino acid N-terminal sequence (NTS) and the MD (Figure 8) (Haslbeck et al., 2004b). Lack of the NTS did neither effect the size of the oligomer nor the activity. Nevertheless, the oligomers dissociated earlier and the substrate complexes with the mutant seemed to be less stable than the complexes between wild type Hsp26 and substrate (Haslbeck et al., 2004b). Hence, the MD is the essential part of the NTR (Haslbeck et al., 2004b). Further studies on the heat activation of Hsp26 revealed that oligomer dissociation is not a prerequisite for the activation of the chaperone. A mutant in which the single subunits were cross-linked via disulfide bonds, retained its activity even though heat-induced dissociation was not possible anymore (Franzmann et al., 2005). The necessary rearrangements of the oligomer to obtain an activated Hsp26 could be tracked down to the MD, which was identified to work as a thermosensor (Franzmann et al., 2008). Besides heat, Hsp26 might also be activated by phosphorylation. In phospho-proteomic studies, several phosphorylation sites of Hsp26 have been reported under various (stress) conditions such as DNA damage, inhibition of single kinases/phosphatases, heat stress or perturbation of N-acetyl transferases (Albuquerque et al., 2008, Bodenmiller et al., 2010, Ficarro et al., 2002, Holt et al., 2009, Smolka et al., 2007, Helbig et al., 2010, Chen et al., 2010b, Huber et al., 2009, Schreiber et al., 2012, Kanshin et al., 2015). Recently, Hsp26 was shown to bind and hold substrate in a near native state and to cooperate with the Hsp70/100 refolding machinery subsequent to the stress (Ungelenk et al., 2016). In contrast to its yeast counterpart Hsp42, Hsp26 does not exhibit a sequestrase activity (Ungelenk et al., 2016).
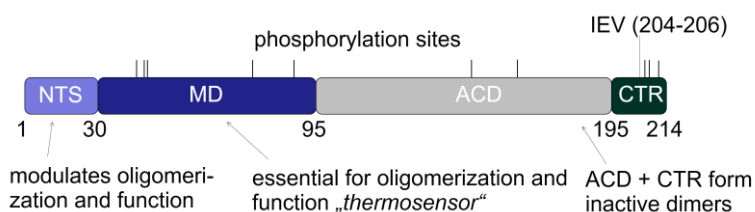
Figure 8: Schematic structure of Hsp26 from S. cerevisiae. *The NTR can be separated in a short NTS, which only modulates the oligomer size and the activity but is not essential for the activity. The second part of the NTR (MD) is essential for the activity of the chaperone. The ACD is 100 amino acids long and does not form dimers alone. The short CTR contains the IEV ("IXI") motif. Several phosphorylation sites (black lines) have been reported all over the primary sequence.*

27

1.4.5.3 Yeast Hsp42

Hsp42 was first described in a two-hybrid screen with the transcriptional regulator Rap1. In this study, it was already identified as a sHsp as it shares some identity with Hsp26 (Wotton et al., 1996). Hsp42 has a mass of 42.8 kDa and is stress-inducible comparable to Hsp26 (Wotton et al., 1996, DeRisi et al., 1997, Gasch et al., 2000). It forms oligomers in a concentration-dependent manner, whereas at higher concentration up to 26-mers were observed (Haslbeck et al., 2004a, Wotton et al., 1996). Negative stain EM revealed a barrel-shaped oligomer. The single rings consist of three Hsp42 dimers and have an outer diameter of 16.5 nm and an inner diameter of 4 nm (Haslbeck et al., 2004a). Interestingly, the Hsp42 oligomer does not dissociate at elevated temperatures (Haslbeck et al., 2004a). Hsp42 exhibits chaperone activity as it is able to prevent aggregation of heat denatured citrate synthase *in vitro* in a concentration-dependent manner (Haslbeck et al., 2004a). At non-stress conditions, the copy number per cell (cpc) of Hsp26 was described to be comparable or higher than the cpc of Hsp42 (Ghaemmaghami et al., 2003, Kulak et al., 2014, Mackenzie et al., 2016). However, Hsp42 seems to be constitutively active and does not need to be heat-activated as it suppresses the aggregation of chemically denatured insulin at 25 °C (Haslbeck et al., 2004a). The substrate spectra of Hsp26 and Hsp42 *in vivo* are highly overlapping. Thus at 25 °C, single deletions of the sHsps can be counterbalanced well by the other chaperone. When both sHsps are deleted the amount of insoluble proteins increases significantly. Under heat stress however, the insoluble fraction is also strongly increased in the single mutants (Haslbeck et al., 2004a). Furthermore, heat stress has effects on the phenotype of *HSP26Δ* or *HSP42Δ* strains, which seemed to be shrunk or desiccated in pictures obtained with SEM (Haslbeck et al., 2004a). Importantly, cell growth is not impaired by the deletion of *HSP42* (Haslbeck et al., 2004a). As already mentioned before, another important protective mechanism against proteotoxic stress is the controlled formation of aggregates. This branch gains special importance when aggregation suppression, refolding and degradation, i.e. the general quality control, fail under severe or prolonged stress conditions (Cohen et al., 2006, Douglas et al., 2009, Ho et al., 2019). In yeast, four main deposit sites have been described: The juxtanuclear quality control compartment (JUNQ), the intranuclear quality control compartment (INQ), insoluble protein deposit sites (IPOD) and CytoQs, whereas the latter include stress foci, peripheral aggregates and Q bodies (Figure 9) (Kaganovich et al., 2008, Gallina et al., 2015, Miller et al., 2015a, Specht et al., 2011, Malinovska et al., 2012, Escusa-Toret et al., 2013). JUNQ and INQ can be combined in one group as they are formed under quite similar conditions and only differ in their location (Miller et al., 2015b, Hill et al., 2017, Sontag et al., 2017). JUNQ, INQ and CytoQ are mostly stress-induced and represent relatively dynamic structures with high protein exchange rates (Rothe et al., 2018). IPOD in contrast contains terminally aggregated proteins and can form under non-stress conditions, as well (Rothe et al., 2018,

Sontag et al., 2014, Kaganovich et al., 2008). The mechanisms of the sequestration processes is still under investigation. It is known that under proteotoxic stress, Hsp42 controls CytoQ formation whereas Btn2 controls formation of INQ/JUNQ (Ho et al., 2019, Malinovska et al., 2012, Specht et al., 2011). For Btn2, no structure has been resolved up to date (Ho et al., 2019). It was predicted to carry an ACD like domain (117 aa), which consists of seven β sheets (Ho et al., 2019). For the NTR (101 aa) and the long CTR (192 aa), no structure could be predicted (Ho et al., 2019). To fulfil its sequestrase function in the nucleus, Btn2 carries a nuclear localization sequence (NLS) in its NTR (Ho et al., 2019). If an NLS is fused to Hsp42, it can complement the deletion of Btn2 (Ho et al., 2019). Both sequestrases (Hsp42 and Btn2) can act under non-stress conditions, as well. Furthermore, Hsp42 is essential for the ageing-related formation of stationary phase granules or granules that harbour inactive proteasomal subunits (Liu et al., 2012, Peters et al., 2015, Marshall et al., 2016). For its sequestration activity, the extraordinary long NTD (247 aa) of Hsp42 is needed (Specht et al., 2011). Specifically, a prion-like domain and a second intrinsically disordered region of the NTR were shown to be inevitable for its sequestrase activity (Grousl et al., 2018).
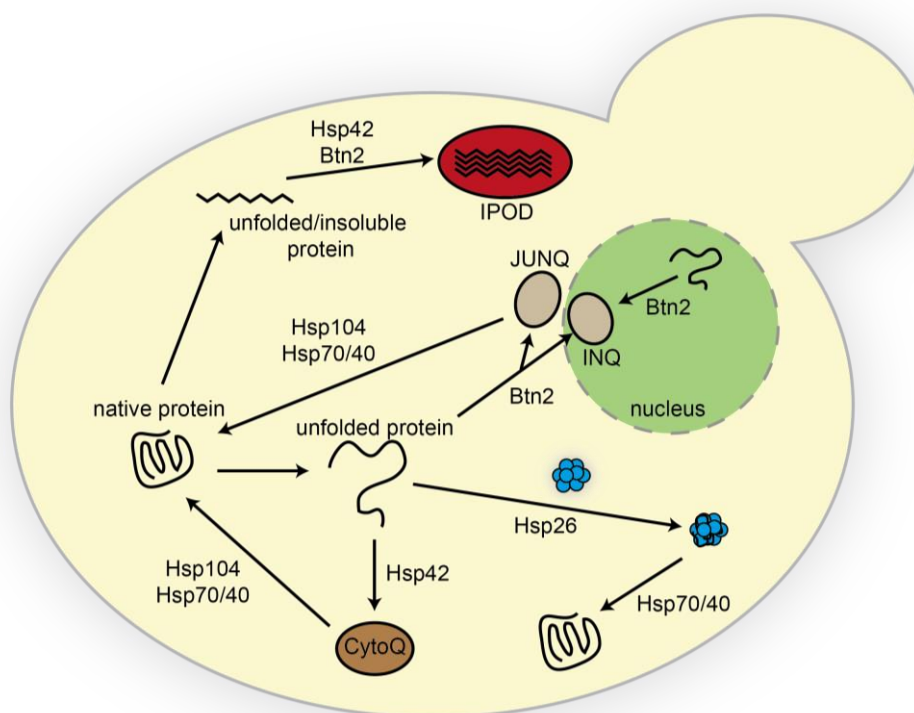
Figure 9: Overview over protein sequestration processes in S. cerevisiae. Native proteins unfold under stress and those unfolded proteins can either be held by sHsps in soluble complexes or sequestered into cellular deposit sites under severe proteotoxic stress. For sequestration in peripheral CytoQ deposits, Hsp42 is required, for protein sequestration in JUNQ or INQ, Btn2 is needed. After the stress, the proteins can be refolded from the deposits with the help of Hsp70/40 and Hsp104. Irreversibly unfolded proteins, such as amyloids are deposited in IPOD. The figure was designed based on the cited studies in the text.

1.5 Objectives of the thesis

In this work, Hsp26 from *S. cerevisiae* was studied in detail. Furthermore, the HSR from yeast was analysed globally by combining transcriptomics, translatomics and proteomics. In the third part of the project, the transcription factors that orchestrate the transcriptional HSR were studied by stepwise depleting and deleting them.

Hsp26

As phosphorylation is known to modulate the activity of sHsps and several Hsp26 phosphorylations were found in different phospho-proteomic studies (Albuquerque et al., 2008, Bodenmiller et al., 2010, Ficarro et al., 2002, Holt et al., 2009, Smolka et al., 2007, Helbig et al., 2010, Chen et al., 2010b, Huber et al., 2009, Schreiber et al., 2012, Kanshin et al., 2015), Hsp26 was analysed with a special interest on the effects of phosphorylation. Up to date, it was not known if and how phosphorylation affects the activity and the structure of Hsp26. For the analysis, single phosphomimetic mutant proteins were studied *in vitro* and *in vivo*. The analyses comprised structural (TEM; H/DX-MS) and functional investigations (activity assays) with the aim to link phosphorylation to a certain structural phenotype with specific functional consequences. The wild type protein was included in the analysis to reproduce and refine recent results. Furthermore, a better resolved cryo-EM structure of Hsp26 was obtained in this study.

Global analysis of the Heat Shock Response

For the global analysis of the HSR, a major goal was to analyse the transcriptomic, translatomic and proteomic response in the same strain and under the same conditions. Transcriptomic and proteomic studies, which had been performed before exhibited strong discrepancies, as the transcriptomic response was much more pronounced than the proteomic response (see 1.3). The transcriptome analysis built up on the work of Dr. Christopher Stratil who already investigated the kinetics of the responses to 37 °C and 42 °C. Those data were completed with the transcriptomes of cells stressed at 46 °C. Translatomic investigations (ribosome profiling) were performed to check to what extent the transcriptional regulation was reflected in the translatome. In addition, *de novo* protein biosynthesis was measured during heat stress. With mass spectrometry, I set out to determine the fate of the proteins during stress. Specifically, besides the changes in the soluble proteome, aggregation and degradation processes were analysed under heat stress. Furthermore, the proteome of recovered cells was studied.

Regulation of the transcriptional Heat Shock Response

In the third part of the thesis, I wanted to shed light on the regulation of the transcriptomic HSR. For this, transcriptome analyses of the heat stress response in cells depleted of Hsf1 and deleted *MSN2/4* were performed. Additionally to transcriptomics, a relatively new method called <u>a</u>ssay for <u>t</u>ransposase <u>a</u>ccessible <u>c</u>hromatin (ATAC-seq) was established in the lab to identify active transcription factor binding sites under stress. This should allow identifying additional heat shock transcription factors.

2.1 Material

2.1.1 General equipment and expendable items

All expendable items, such as falcon tubes, reagent tubes, pipette tips, petri dishes, centrifugal filters etc. were purchased from Roth, Sigma, Merck, VWR or Eppendorf unless otherwise stated.

Table 1: List of general equipment.

Apparatus	Manufacturer
Gel Documentation	
BioDocII	Biometra
Image Scanner III	GE
ImageQuant 300	GE
ImageQuant LAS4000	GE
Scanner Powerlook1120	Umax
Typhoon Scanner	GE
Centrifuges	
Avanti J25 and J26 XP (Rotors JA-10, JA25.50)	Beckman Coulter
Benchtop centrifuge 5418R (Rotor FA-45-18-11)	Eppendorf
Optima Max-E Ultracentrifuge	Beckman Coulter
ProteomLab XL-I	Beckman Coulter
Rotina 420R	Hettich
Speed vacuum concentrator	Eppendorf
PCR Equipment	
Agarose Gel Running Chamber HU10	AlphaMetrix Biotech
Mx3000P System	Agilent
CFX Connect Real-Time PCR detection system	BioRad
Power Supply EPS 601	GE
Thermal Cycler MJ Mini	BioRad
Thermal Cycler Primus, Primus25	Peqlab
Thermal Cycler T100	BioRad

Apparatus	Manufacturer
Chromatography Systems	
ÄKTA PURE	GE
ÄKTA Prime	GE
Fraction collector F9-R	GE
HPLC System	Shimadzu
MALS detector Dawn Heleos II MALS detector	Wyatt
RID-10A	Shimadzu
Superloop (150 ml)	GE
Sterilization Equipment	
Autoclav Varioclav EP-Z	H+P
Autoclav La-MCS-203	Sanoclav
Sterilization Incubator BM 500	Memmert
UV Spectrometers	
Cary50	Agilent
NanoDrop2000	ThermoFisher Scientific
Pherastar plate reader	BMG Labtech
Ultrospec 1100pro, - 3100pro	Amershan Biosciences
Scales	
Scale BL1500S	Sartorius
Precision scale SI-234	Denver Instruments
Microscopes & Equipment	
Axiovert 200 inverted microscope	Carl Zeiss
C4742-95 camera	Hamatsu
Cover glass	ThermoFisher Scientific
Glass slides	Marienfeld
JEM 1400 Plus	JEOL
JEOL 5900 LV microscope	JEOL
Superfrost microscope slides	ThermoFisher Scientific
Titan Krios	ThermoFisher Scientific

Apparatus	Manufacturer
Mass spectrometers	
ACQUITY M-Class UPLC	Waters
Orbitrap Fusion Mass Spectrometer	ThermoFisher Scientific
Orbitrap Q Exactive Mass Spectrometer	ThermoFisher Scientific
PAL RTC	LEAP
Synapt G2-S ESI-TOF mass spectrometer	Waters
Diverse Equipment	
9 mm stainless steel balls	Cole-Parmer
Agilent Bioanalyzer 2100 expert	Agilent
Bandelin sonoplus hd 2200	Bandelin
Bead Mill MM-400	Retsch
Cell disruption apparatus BasicZ	Constant Systems
Chirascan™ - Circular Dichroism Spectrometer	Applied PhotoPhysics
CW3000 industrial chiller	Vevor
Gel electrophoresis devices	Hoefer
GenePulser Xcell	BioRad
Ice machine	Ziegra
Incubator	New Brunswick Scientific
Incubator WB120	Mytron
Magnetic Stirrer MR3001	Heidolph
MagRack 6	GE
TC1 temperature controller	Quantum Northwest
Pipettes (2.5, 10, 20, 200, 1000, 5000 µl)	Eppendorf/ Rainin
Rotator SB3	Stuart
SDS-PAGE Running Chamber	Serva
Silent Crusher	Heidolph
Temp.-Gradient Unit TGGE MAXI System	Biometra
Thermomixer compact,- comfort	Eppendorf
Ultrasonic cleaner USC-T	VWR
Vortexer REOX control	Heidolph

Apparatus	Manufacturer
Waterbath SW22	Julabo
Western Blotting Apparatus Fasblot B34	Biometra

2.1.2 Chemicals

Table 2: List of chemicals.

Chemical	Distributor
2-Mercaptoethanol (β-ME)	Sigma
3-(2-Iodoacetamido)-PROXYL	Sigma
^{35}S-methionine	Hartmann Analytics
^{15}N-Ammoniumchloride	Sigma
Acetic acid	Roth
Acetonitrile	Sigma
Acrylamide/Bis solution 38:2 (40% w:v)	Serva
Agar Agar	Serva
Agarose	Serva
Amino acids	Sigma
Ammonium acetate	Merck
Ammonium bicarbonate	Merck
Ammonium persulfate (APS)	Roth
Ampicillin sodium salt	Roth
BAL wash buffer (2,3 Dimercapto-propan-1-ol)	Invitrogen
Biotin	Sigma
Boric acid	Roth
Bortezomib	LC Laboratories
Calcium chloride	Merck
Chloroform	Sigma
Cobalt(II) chloride hydrate	Sigma
Coomassie Brilliant Blue R-250	Serva
Coomassie Quick Stain	Serva
Copper(II) chloride dihydrate	Merck

Chemical	Distributor
Cycloheximide	Sigma
Deoxynucleoside triphosphates (dNTPs)	Roche
Difco Nutrient Broth	BD Bioscience
Dimethyl sulfoxide (DMSO)	Sigma
Disodium phosphate	Roth
Dithiothreitol (DTT)	Roth
Doxycycline	Sigma
Ethanol	Merck
Ethylenediaminetetraacetic acid (EDTA)	Merck
Formaldehyde	Roth
Formic acid	Sigma
Geneticin G418	Roth
Glucose	Merck
Glutaraldehyde	Merck
Glycerol	Roth
Guanidine hydrochloride	Roth
Hygromycin	Sigma
Imidazole	Sigma
Immersion oil	various sources
Iodoacetamide	Merck
Iron(III) chloride hexahydrate	Merck
Isopropanol	Roth
Isopropyl β-d-1-thiogalactopyranoside (IPTG)	Serva
Kanamycin sulfate	Roth
LB_0 medium (10g/l tryptone, 5 g/l yeast extract, 5 g/l NaCl)	Serva
Lithium chloride	Sigma
Manganese(II) chloride tetrahydrate	Merck
Magnesium chloride	Merck
Magnesium sulfate	Sigma

Chemical	Distributor
Methanol	Sigma
MG-132	Merck
Milk powder	Roth
N-(2-Hydroxyethyl) -piperazine-N'-2 ethane-sulfonic acid (HEPES)	Roth
N,N,N',N'-Tetramethylethylendiamine (TEMED)	Roth
Nonidet P-40 substitute	Sigma
Nourseothricin	Sigma
Phenylmethanesulfonyl fluoride (PMSF)	Sigma
Phenol	Sigma
Polyethylene glycol 4000 (PEG-4000)	Sigma
Potassium chloride	Roth
Monopotassium phosphate	Merck
Phosphatase Mix 2/3	Sigma
PR619	Merck
Protease inhibitor Mix HP/G/FY	Serva
Rapamycin	Sigma
Single Stranded DNA (Salmon testis)	Sigma
Sodium acetate	Roth
Sodium chloride	Roth
Sodium deoxycholate	Merck
Sodium dodecylsulfate (SDS)	Serva
Sodium hydroxide	Roth
Sorbitol	Sigma
Stain G	Sigma
SYBR Gold	ThermoFisher Scientific
Thiamine	Sigma
Trifluoroacetic acid	Sigma
Tris(2-carboxyethyl)phosphine (TCEP)	Sigma
Tris-(hydroxylethyl)-aminomethane (TRIS)	Roth

Chemical	Distributor
Triton X-100	Merck
Tween-20	Merck
Urea	Merck
Water (MS grade)	Merck
WesternBright™ ECL-Spray	Advansta
Yeast Nitrogen Base (YNB) w/o aa	BD Bioscience
YPD (20 g/l peptone, 10 g/l yeast extract, 20 g/l glucose)	Roth
Zinc chloride	Merck

2.1.3 Enzymes, standards and kits

Table 3: List of enzymes, standards and kits.

Product	Distributor
Enzymes	
Dpn1	NEB
Hexokinase	Roche
Hot start GoTaq polymerase	Promega
Insulin	Sigma
Lysozyme	Sigma
Lyticase	Sigma
MDH (pig heart)	Roche
Phusion HiFi DNA polymerase	NEB
Q5 HiFi DNA polymerase	NEB
Restriction enzymes	NEB
RNAseI	Ambion
T4 DNA ligase	NEB
T4 PNK	NEB
Trypsin sequencing grade	Promega

Product	Distributor
Standards	
20 bp DNA ladder	ThermoFisher Scientific
Fast load 1 kb DNA ladder	Serva
Gel Filtration Standard	BioRad
LMW SDS PAGE standard (test mixture 6)	Serva
Serva Dual color protein standard	Serva
Kits	
Brilliant III Ultra-Fast SYBR Green QRT-PCR Master Mix	Agilent
DNA 1,000 Kit	Agilent
K-48 TUBE HF	ThermoFisher Scientific
MinElute PCR Purification Kit	Qiagen
mRNA-seq Library Prep Kit V2	Lexogen
Nextera DNA Library Prep Kit 2017	Illumina
Pierce BCA Assay Kit	ThermoFisher Scientific
Ribo-Zero Kit	Illumina
RNA 6,000 Nano Kit	Agilent
RNA Clean and Concentrator Kit 5/25	Zymo Research
TruSeq RiboProfile (Yeast) Kit	Illumina
Wizard Plus SV Minipreps DNA Purification System	Promega
Wizard SV Gel and PCR clean-up system	Promega
Wizard SV Total RNA Isolation System	Promega

2.1.4 Consumables

Table 4: List of consumables.

Consumables	Distributor
1.5 ml microfuge tubes	Beckman Coulter
15 % urea polyacrylamide gels	ThermoFisher Scientific
200-mesh copper grids	Merck
50 mg SEP PAK (tC18) columns	Waters

Consumables	Distributor
Amicon Ultra-15 centrifugal filter uUnits	Merck
Blotting paper	Whatman
Cellstar®, 15 and 50 mL	Greiner BioOne
Centrifuge Filter, 0.22 µm	Merck
Chromacol Closures, 9 mm, white Silicone/Red PTFE	ThermoFisher Scientific
Chromacol Vials, 9 mm, Polypropylene, 300 µl	ThermoFisher Scientific
Cuvettes (plastic)	Brand
Dialysis membranes Spectra/Por (MWCOs 6 - 8,000)	Spectrum Laboratories
Empore C18 extraction discs	ThermoFisher Scientific
Eppendorf tubes (0.5, 1.5, 2 ml)	Eppendorf/Sarstedt
Glass pasteur pipettes	Labsolute
Microcon – 30 kDa centrifugal filters	Merck
Nitrocellulose Membrane Roti® NC	Roth
Parafilm	Roth
PCR tubes	BioRad
Petri dishes	Greiner BioOne
Plastic tips	Brand/Eppendorf
Q Sepharose Fast Flow	GE
SERVAGel TG PRiME 4-20%, 15 sample wells	Serva
Sterile filter (0.2 µm)	Zefa
Ultracel ultrafiltration disc 3 kDa NMWL ,76 mm	EMD Millipore

2.1.5 Software, databases & web-based tools

Table 5: Software, databases and web-based tools.

Program/Database	Source
2100 Expert Software	Agilent
BeStSel	(Micsonai et al., 2018)
Bioinformatics&Evolutionary Genomics	https://bioinformatics.psb.ugent.be/webtools/Venn/
BioGrid	https://thebiogrid.org/

Program/Database	Source
Blast	https://blast.ncbi.nlm.nih.gov/Blast.cgi
DAVID Bioinformatics	https://david.abcc.ncifcrf.gov/
EndoteX9	Alfasoft GmbH
Expasy	https://www.expasy.org
Expasy ProtParam	https://web.expasy.org/protparam/
GOrilla	(Eden et al., 2009)
GO Slim Mapper	https://www.yeastgenome.org/
GO Term Finder	https://www.yeastgenome.org/
ImageQuant TL	GE
NEB Interactive tools	NEB
Origin	Version 8.1, © OriginLab Corporation
PHYRE^2	(Kelley et al., 2015)
Saccharomyces genome database	https://www.yeastgenome.org/
Saccharomyces regulator database	https://www.yeastgenome.org/
SPELL database	https://spell.yeastgenome.org/
Uniprot	https://www.uniprot.org/
Word; Excel; Power Point	Microsoft Office Package 2016
Yeastract database	https://www.yeastract.com/
SEC-MALS Software	
Astra	Wyatt
Image Processing Software	
Illustrator CS4	Adobe 14.0.0. © 2008
ImageJ	(Schindelin et al., 2012)
MS Analysis Software	
MaxQuant	(Cox and Mann, 2008)
Perseus	(Tyanova et al., 2016)
Xcalibur	ThermoFisher Scientific

2.1.6 Oligonucleotides and plasmids

2.1.6.1 Oligonucleotides

Table 6: Oligonucleotides for library preparation and qRT PCRs.

Name	Sequence	Distributor
RNA Control Oligo I	NNGUACACGGAGUCGACCCGCAACGCNN	Illumina
RNA Control Oligo II	NNGUACACGGAGUCAAGACCCGCAACGCNN	Illumina
TruSeq Ribo Profile 3´Adapter	AGATCGGAAGAGCACACGTCT	Illumina
TruSeq Ribo Profile Forward PCR Primer	ATGATACGGCGACCACCGAGATCTACACGTTC AGAGTTCTACAGTCCGACG	Illumina
Variable index primer	CAAGCAGAAGACGGCATACGAGAT NNNNNN GTGACTGGAGTTCAGACGTGTGCTCTTCCGATC	Illumina
RDN5-1 fw (qRT-PCR)	GGTTGCGGCCA	Eurofins
RDN5-1 rev (qRT-PCR)	AGATTGCAGCACCT	Eurofins
RDN18-1 fw (qRT-PCR)	GGTGAAATTCTTGGATTTATTG	Eurofins
RDN18-1 rev (qRT-PCR)	TAATGATCCTTCCGCA	Eurofins
Hsp42delta69 fw (qRT-PCR)	CTAGGATCCATGTACTACCAGTTCCCTG	Eurofins
Hsp42 rev (qRT-PCR)	CTACTAGCGGCCGCTCAATTTTCTACCGTAGG	Eurofins
Hsp12 fw (qRT-PCR)	ATGTCTGACGCAGG	Eurofins
Hsp12 rev (qRT-PCR)	TTACTTCTTGGTTGGGT	Eurofins

2.1.6.2 Plasmids

Table 7: List of plasmids.

Plasmid	Comment	Origin
p416GPD::*hsp26* and phosphomutants (S42, S47, T48, T69, S90, S144, T163, S207, S208, S211E)	p416 GPDUra with Hsp26 sequence inserted using restriction sites *Spe*I and *Hind*III	This work
p416GPDUra		ATCC
p425GPDLeu		ATCC
p425GPDLeu::*flucDM* p425GPDLeu::*flucDM-EGFP*	p425GPDLeu with FlucDM or FlucDM-EGFP inserted using restriction sites *Spe*I and *Hind*III	(Gupta et al., 2011)
p425GPDLeu::*flucSM* p425GPDLeu::*flucSM-EGFP*	p425GPDLeu with FlucSM or FlucSM-EGFP inserted using restriction sites *Spe*I and *Hind*III	(Gupta et al., 2011)
p425GPDLeu::*flucWT* p425GPDLeu::*flucWT-EGFP*	p425GPDLeu with FlucWT or FlucWT-EGFP inserted using restriction sites *Spe*I and *Hind*III	(Gupta et al., 2011)
p426GPDUra::*hsp42*	p416GPDUra with inserted using restriction sites *Sac*I and *Hind*III	M. Haslbeck
pE-SUMO		LifeSensors
pESUMO::*hsp26allphospho*	pESUMO with the Hsp26 sequence where all known phosphorylation sites were	This work
pQE60::*hsp26*	pQE60 with Hsp26 sequence inserted using restriction sites *Nco*I and *Hind*III	M. Haslbeck
pQE60::*hsp26XE* (X = S42, S47, T48, S47/T48, S207, S208, S211, T69, S90)	pQE60 with Hsp26 phosphomimetic mutant sequences inserted using restriction sites *Nco*I and *Hind*III	This work
pYM15		(Janke et al., 2004)
pYM19		(Janke et al., 2004)

Plasmid	Comment	Origin
pYM24		(Janke et al., 2004)
pYM45		(Janke et al., 2004)

2.1.7 Antibodies

Table 8: List of used antibodies.

Antibody	Source	Identifier
Anti-mouse-IgG	Sigma	Cat# A4789; RRID: AB_258201
Anti-rabbit-IgG	Sigma	Cat# A0545; RRID: AB_257896
Mouse monoclonal anti-HA Tag antibody	Invitrogen	Cat# 26183-1MG
Mouse monoclonal anti-Pab1 antibody	antikoerper-online.de	ABIN1580454
Mouse monoclonal anti-Pgk1	Invitrogen	Cat# PAS-286212
Rabbit polyclonal anti-Cnb1 antibody serum	Pineda	N/A
Rabbit polyclonal anti-GAPDH antibody	OriGene	Cat# AP21309AF-N
Rabbit polyclonal anti-Hch1 antibody serum	Pineda	N/A
Rabbit polyclonal anti-Hsp104 antibody serum	Pineda	N/A
Rabbit polyclonal anti-Hsp26 antibody serum	Pineda	N/A
Rabbit polyclonal anti-Hsp42 antibody serum	Pineda	N/A
Rabbit polyclonal anti-Ubiquitin	Enzo	Cat# ADI-SPA-200-F

2.1.8 *S. cerevisiae* and *E.coli* strains
Table 9: Yeast strains used in this work.

Yeast strain	Comment	Origin
BY4741 DED1-GFP-His	GFP fused to Ded1; Histidine prototroph	Simon Alberti
BY4741 HSP26::KanMX HSP42::Nat	Yeast strain with deleted hsp26 and hsp42; G418 and Nourseothricin resistance cassette	Chris Stratil
BY4741 HSP26::KanMX4	Yeast strain with deleted hsp26; G418 resistance cassette	Euroscarf
BY4741 HSP42::KanMX4	Yeast strain with deleted hsp42; G418 resistance cassette	Euroscarf
BY4741 PAB1-GFP-His3Mx6	GFP fused to Pab1; Histidine prototroph	ThermoFisher Scientific
BY4741; MATa; ura3D0; leu2D0; his3D1; met15D0	WT strain	Euroscarf
DBY 7286	Laboratory WT strain	(Eisen et al., 1998)
DBY 9434	Laboratory WT strain	(Eisen et al., 1998)
*MAT*α leu2-3,112 trp1-1 can1-100 ura3-1 ade2-1 his3-11,15	W303 WT	Susan Lindquist
R1158 PAB1::kanR-tet07-TATA	Pab1 tet off system	Florian Schopf
W303 Mat α tpk1-as tpk2-as tpk3 as TOR1-1(S1972I) fprΔ::NatMX RPL13A-2xFKBP12-TRP1 Hsf1-GFP-FRB-HISMX6	Hsf1-anchor away system; Hsf1 GFP tagged	(Solís et al., 2016)
W303 Mat α tpk1-as tpk2-as tpk3 as TOR1-1(S1972I) fprΔ::NatMX TEF2pr-mKATE2-URA3-4HSE-EmGFP RPL13A-2xFKBP12-TRP1 Hsf1-FRB-HISMX6	Hsf1-anchor away system	(Solís et al., 2016)
W303 Mat α tpk1-as tpk2-as tpk3 as TOR1-1(S1972I) fprΔ::NatMX RPL13A-2xFKBP12-TRP1 Hsf1-GFP-FRB-HISMX6 msn4::hphNT1	Hsf1-anchor away system; Hsf1 GFP tagged; Msn4 knock-out; Hygromycin resistance cassette	This work

Yeast strain	Comment	Origin
W303 Mat α tpk1-as tpk2-as tpk3 as TOR1-1(S1972I) fprΔ::NatMX TEF2pr-mKATE2-URA3-4HSE-EmGFP RPL13A-2xFKBP12-TRP1 Hsf1-FRB-HISMX6 msn4::hphNT1	Hsf1-anchor away system; Msn4 knock-out; Hygromycin resistance cassette	This work
W303 Mat α tpk1-as tpk2-as tpk3 as TOR1-1(S1972I) fprΔ::NatMX TEF2pr-mKATE2-URA3-4HSE-EmGFP RPL13A-2xFKBP12-TRP1 Hsf1-FRB-HISMX6 msn4::hphNT1 msn2::KanMx	Hsf1-anchor away system; Msn4 and Msn2 knock-out; Hygromycin and G418 resistance cassettes	This work

Table 10: E. coli strains used in this work.

E. coli strains	Comment	Origin
BL21 (DE3) B F⁻ *ompT gal dcm lon hsdS$_B$(r$_B$⁻ m$_B$⁻)* λ(DE3 [*lacI lacUV5-T7p07 ind1 sam7 nin5*]) [*malB⁺*]$_{K-12}$(λ^S)	T7 Expression system	Stratagen
HB101 F⁻ mcrB mrr hsdS20(r$_B$⁻ m$_B$⁻) recA13 leuB6 ara-14 proA2 lacY1 galK2 xyl-5 mtl-1 rpsL20(Sm^R) glnV44 λ	T4 expression system	Promega
XL1 Blue endA1 gyrA96(nal^R) thi-1 recA1 relA1 lac glnV44 F'[::Tn10 proAB⁺ lacI^q Δ(lacZ)M15] hsdR17(r$_K$⁻ m$_K$⁺)	Used for cloning	Stratagen

2.2 Methods

Several of the experimental procedures can be found similarly in the associated publication (Mühlhofer et al., 2019).

2.2.1 Molecular Biology

2.2.1.1 Polymerase chain reaction

Polymerase chain reaction (PCR) allows the amplification of DNA *in vitro*. Besides the template DNA (e.g. plasmids or genomic DNA), two primers complementary to the start and the end of the target sequence, dNTPs and a DNA polymerase are needed. At first, the double stranded template DNA is melted by heating, so that the single stranded forward and reverse primers can bind. Subsequently, the DNA is duplicated by the polymerase. The synthesis time is dependent on the length of the amplified sequence as well as the used polymerase. Primers were ordered from MWG Eurofins. The annealing temperature was calculated with the NEB T_M Calculator (NEB). Primers for cloning genes into plasmids additionally encoded suitable restriction enzyme sites. Pipetting schemes for general PCR approaches are shown in table 11, a more specific scheme according to Janke et al., 2004 for genomic manipulation of *S. cerevisiae* is presented in table 12. The DNA was amplified in a thermal cycler according to the schemes below (Tables 13, 14).

Table 11: General PCR pipetting scheme.

	Analytical PCR	Preparative PCR	Colony PCR
	V [µl]	V [µl]	V [µl]
Template DNA (ca. 100 ng/µl)	1	1	2 (cell suspension)
Forward Primer (100 pmol/µl)	0.1	1	0.5
Reverse Primer (100 pmol/µl)	0.1	1	0.5
Polymerase (GoTaq)	0.1	0.5	0.5
dNTP-Mix (10 mM)	0.2	1	0.5
Reaction buffer (10x)	2	20	2
H₂O nuclease-free	16.5	74.5	14

Table 12: Pipetting scheme for "Knop PCR" according to Janke et al. (Janke et al., 2004).

	V [µl]
Knop buffer 1/2	5
Template DNA/cassette plasmid (ca. 100 ng/µl)	1
dNTPs (10 mM)	1
Forward Primer S3 (10 µM)	2.5
Reverse Primer S2 (10 µM)	2.5
H$_2$O nuclease-free	37.3
GoTaq Polymerase	0.5
Q5 HiFi Polymerase	0.2

Table 13: PCR cycling scheme.

	temperature [°C]		time	
	Q5	GoTaq	Q5	GoTaq
Melting	98	95	30 s	3 min
35 cycles				
Melting	98	95	7 s	15 s
Annealing	Depending on the primers		15 s	20 s
Elongation	72		30 s/kb	60 s/kb
Final Extension	72		3 min	5 min
Hold	4		∞	

Table 14: PCR cycling scheme for genomic modification of S. cerevisiae (Janke et al., 2004).

	temperature [°C]	time
Melting	95	3 min
10 cycles		
Melting	95	15 s
Annealing	54	30 s
Elongation	68	2 min 40 s
20 cycles		
Melting	95	15 s

Annealing	54	30 s
Elongation	68	2 min 40 s + 20 s/cycle
Hold	4	∞

2.2.1.2 Agarose gel electrophoresis

DNA was separated by agarose gel electrophoresis for analytical and preparative reasons. 1 g agarose was dissolved in 100 ml 1x TAE buffer (40 mM Tris/Acetate pH 8.0, 50 mM EDTA) by boiling. After cooling the solution, 2.7 µl of Stain G (Serva) were added. Stain G fluoresces in complex with DNA upon irradiation with UV light. Before loading the DNA onto the gel, 5x DNA loading dye (50 % (v/v) glycerol, 10 mM EDTA, pH 8.0, 0.2 % (v/v) bromophenol blue) was added to a final concentration of 1x. As a standard, 1 kB or 100 bp ladders were loaded. 1xTAE was used as running buffer and the DNA was separated for 20 min at 120 V. The bands were visualized under UV-light in an ImageQuant 300 Imager (GE).

2.2.1.3 Purification of the PCR product

PCR products were purified with the Promega PCR purification kit (Wizard® SV Gel and PCR Clean-Up System). First, the PCR product was diluted in the same volume of column binding solution, pipetted onto centrifuge columns and centrifuged for 1 min at 16,000 x g. Then, it was washed with 700 and 500 µl membrane wash solution (1 min at 16,000 x g). Subsequently, the column was centrifuged dry for 2 min at 16,000 x g. The DNA was eluted with 50 µl nuclease-free water (1 min at RT and then centrifugation for 1 min at 16,000 x g) into a new 1.5 ml tube. Alternatively, linear DNA was purified with the Min Elute kit provided by Qiagen according to the manufacturer´s instructions.

2.2.1.4 Restriction digest of DNA

To be able to ligate a linear PCR product into a vector, both have to be treated with specific restriction enzymes to generate fitting overhangs. If possible, high fidelity (HF) variants of the respective enzymes (NEB) were used. The reaction was incubated for 60 min at 37 °C in the respective buffer (see NEB datasheets). The general pipetting scheme is shown in table 15.

Table 15: Pipetting scheme for restriction digest with SpeI and HindIII.

Reagent	Volume [µl]
DNA [1µg]	x
***Spe*I HF (NEB)**	1
***HindIII* HF (NEB)**	1
10x Cut Smart buffer (NEB)	5
water	43-x

To stop the reaction, the enzymes were heat-inactivated for 20 min at 80 °C or the DNA purified.

2.2.1.5 Ligation of DNA

To ligate the digested PCR product into the digested plasmid, both were mixed whereat the PCR product was added in 3- to 5-fold molar excess. To this mixture 10 µl 2x reaction buffer, 1 µl T4 DNA Ligase (NEB) were added and the reaction was filled with water to 20 µl. Ligation took place over night at 16 °C.

2.2.1.6 Q5 site directed mutagenesis

Point mutation primers for amplification of the original vector were designed using the NEBase changer (NEB). The PCR was conducted using Q5 HiFi Polymerase (NEB), 10 µM of each primer and 20 ng/µl template DNA. 25 amplification cycles were applied. After purification of the PCR product as described above, 50-100 ng amplified DNA were treated with 1 µl T4 polynucleotide kinase (PNK; NEB), 1 µl T4 DNA ligase (NEB), 1 µl Dpn1 (NEB) and 1 µl T4 DNA ligase buffer (NEB). The reaction was filled to 10 µl with sterile H_2O and incubated for 60 min at room temperature. Afterwards, the reaction mixture was transformed into chemo-competent *E. coli* cells as described below (2.2.2.5.1).

2.2.2 Cultivation and manipulation of microorganisms

2.2.2.1 Inoculation of cells

Single colonies were picked and inoculated into liquid media with the respective selection marker.

2.2.2.2 Cultivation of *E. coli*

E. coli cultures were grown at 37 °C in LB on plates or in liquid medium supplemented with respective antibiotics. For NMR labelling, the cells were grown in M9 medium supplemented with $^{15}NH_4Cl$.

2.2.2.3 Cultivation of *S. cerevisiae*

Yeast cultures were grown at 25 °C or 30 °C in liquid medium or on plates (YPD/CSM; with antibiotic if necessary).

2.2.2.4 Cryopreservation of cells

2.2.2.4.1 *E. coli*

900 µl of an *E. coli* cell suspension were added to 600 µl 50 % glycerol solution (final 20 % glycerol), frozen in liquid nitrogen and stored at -80 °C.

2.2.2.4.2 *S. cerevisiae*

1.05 ml of a yeast cell suspension were added to 450 µl 50 % glycerol (final 15 % glycerol), frozen in liquid nitrogen and stored at -80 °C.

2.2.2.4.3 Heat shock experiments with *S. cerevisiae*

BY4741 were grown over night, diluted to an OD_{595} of 0.2 in YPD and grown at 25°C while shaking until an OD_{595} of 0.8 was reached (usually 50 ml cultures; except for ribosome profiling experiments which had to be performed in 500 ml cultures). Then, the cells were stressed at 37 °C or 42 °C in a water bath (Julabo) for 10 and 30 min, respectively. For ATAC-seq experiments, the heat shock was conducted in 2 ml Eppendorf tubes in a thermoblock (Eppendorf).

2.2.2.4.4 Spot assays

BY4741 overnight cultures were diluted to an OD_{595} of 1.0 with YPD. Four further 1/5 dilutions were prepared. Of each dilution (5^0 - 5^{-4}), 5 µl were spotted onto an agar plate with the respective selection marker and/or stressor. The plates were incubated for 24 - 72 h at 25 °C, 37 °C or 42 °C, respectively. For temperature gradient spot assays, 5 µl of cells at OD_{595} 1.0 were spotted onto agar plates and incubated for 24 h on a temperature gradient plate (25 °C – 48 °C).

2.2.2.5 Transformation of cells

2.2.2.5.1 Transformation of chemo-competent *E. coli*

200 µl of chemo-competent bacteria were thawed on ice and 1 µl plasmid DNA (optionally the whole ligation approach) was added. The suspension was incubated for 15 min on ice, then the cells were heat-shocked for 90 s at 42 °C and incubated for another two minutes on ice. Subsequently, 500 µl LB_0 medium were added and the cells were incubated for further 30 min at 37 °C while shaking (400 rpm) in a thermomixer (Eppendorf). The cells were pelleted (2 min, 7,000 x g) and the supernatant decanted. Finally, the cells were resuspended 50 µl LB_0 medium, plated on medium supplemented with the respective antibiotic and grown at 37 °C over night.

2.2.2.5.2 Transformation of *S. cerevisiae*

2.2.2.5.2.1 Plasmid transformation into stationary cells

200 µl of an overnight yeast culture were harvested for 30 s at 4,200 g. The supernatant was decanted and the cells were resuspended by a short vortexing step. Subsequently, 150 µl plate mix (40.5 % (w/v) PEG-4000, 0.1 M lithium acetate, 10 mM Tris, 1 mM EDTA) were added, as well as 1.0 µl ssDNA (salmon sperm, Sigma), 6 µl 1 M DTT and 200 - 700 ng plasmid DNA. The suspension was vortexed and incubated over night at room temperature. Then, the cells were heat-shocked for 30 min at 42 °C, pelleted (30 s, 4,200 x g) and the supernatant taken

off completely with a pipette. The pellets were resuspended in 50 µl sterile water and plated on CSM or YPD with antibiotic, respectively. The cells were incubated at 30 °C for 2 - 3 days.

2.2.2.5.2.2 Transformation of logarithmic *S. cerevisiae*

Overnight cultures were diluted in 50 ml YPD to an OD_{595} of ca. 0.2 and grown at 30 °C while shaking until an OD of 0.6 - 0.8 was reached. After harvesting the cells (5 min at 3,000 x g), they were washed with 25 ml water. Then, the cells were resuspended in 1 ml 0.1 M lithium acetate. 50 µl of the cell suspension were used for the transformation and again pelleted. The cells were resuspended in 240 µl PEG (50 % w/v), 36 µl 1 M lithium acetate, 6 µl ssDNA and 0.1 - 10 µg DNA. The suspension was filled to 360 µl with water, vortexed, incubated for 30 min at 30 °C and subsequently for 30 min at 42 °C. To remove the transformation mixture, the cells were spun down for 15 s at 5,200 g and 1 ml of warm YPD/CSM was added to allow the cells recover for 1 - 2 h. 200 µl were plated on selection media and incubated at 30 °C for 2 - 4 d. To select for correct positive clones, the colonies were transferred onto replica plates with the same selection marker after 3 d. Genomic insertion was checked with colony PCR and western blots.

2.2.2.6 Preparation of plasmid DNA from *E. coli*

Plasmid DNA from *E. coli* was isolated using WizardR Plus SV Minipreps DNA Purification System (Promega) according to the manufacturer´s instructions. The DNA was eluted with 50 µl nuclease-free water and stored at -20 °C.

2.2.2.7 Sanger Sequencing of DNA

Purified plasmids (50-100 ng/µl) or linear PCR products (10-50 ng/µl) were sent to MWG Eurofins or Genewiz for Sanger Sequencing to check if the sequence was correct. If the needed primers were not deposited in the company´s stock, they were added (10 pmol/µl) manually.

2.2.3 Transcriptomics

2.2.3.1 RNA Isolation

In this work, two different RNA isolation methods were applied. In the first protocol, spin columns (SV Total RNA Isolation System, Promega) were used to purify the RNA, in the second protocol, the RNA was isolated with hot phenol followed by phenol chloroform extraction. All work with RNA was done with nuclease-free tips and tubes.

2.2.3.1.1 RNA-Isolation with columns

1 ml of a logarithmic yeast cell suspension (OD_{595} 0.6 - 0.8) was transferred into a fresh Eppendorf tube and pelleted for 30 s at 14,000 x g. The pellets were resuspended in 100 µl freshly prepared 1 M sorbitol, 0.1 M EDTA, pH 7.4 with 0.1 % β-ME and 50 units lyticase

(Sigma). Degradation of the cell wall took place for 20 min at 30 °C. Subsequently, 75 µl RNA lysis buffer (Promega) were added and it was mixed gently. Then, 350 µl RNA dilution buffer (Promega) were added, it was mixed by inversion and pelleted at maximum speed for 10 min. The lysate was transferred into a fresh Eppendorf tube and 200 µl of 95 % ethanol were added. The solution was mixed, pipetted into a spin column assembly and centrifuged at 12,000 x g for 1 min. Then, 50 µl freshly prepared DNase incubation mix (Promega) were pipetted onto the column and it was incubated for 15 min at RT. To stop the DNase digest, 200 µl DNase Stop Solution (Promega) were added and it was centrifuged for 1 min at 12,000x g. After addition of 250 µl RNA wash solution (Promega), it was centrifuged for 2 min at full speed. Finally, the RNA was eluted with 100 µl nuclease-free water into a fresh Eppendorf tube and stored at -80 °C.

2.2.3.1.2 RNA isolation with hot phenol

Cells were grown from OD_{595} 0.2 to 0.8 in 50 ml YPD-A. Heat stress was performed as described above. RNA isolation was performed based on a published protocol (Collart and Oliviero, 1993). First, 1 ml of the cells was harvested (9,000 x g for 1 min at 4 °C) and the pellets were shock frozen in liquid nitrogen. To isolate the RNA, the cell pellets were resuspended in 400 µl TES buffer (10 mM Tris/HCl, pH 7.5, 10 mM EDTA, 0.5 % SDS). Then, 400 µl phenol were added and the suspension incubated for 30 min at 65 °C with short vortexing steps in between. After 5 min on ice, the suspension was centrifuged for 5 min at 16,000 x g and 4 °C. The aqueous phase was transferred into a fresh 1.5 ml tube, further 400 µl phenol were added and the emulsion vortexed. Cooling on ice and centrifugation (5 min at 16,000 x g and 4 °C) were repeated. After the aqueous phase was again transferred into a fresh tube, 400 µl of chloroform were added, it was vortexed and centrifuged for 5 min at 16,000 x g and 4 °C. The aqueous phase was once more transferred into a fresh tube and the RNA precipitated by the addition of 40 µl 3 M sodium acetate (NaOAc; pH 5.3) and 1 ml ice-cold ethanol. The RNA was pelleted for 5 min at 16,000 x g and 4 °C and the supernatant discarded. To get rid of residual salt, the pellet was washed two times with 1 ml 70 % ice-cold ethanol, centrifuged once more as described above and the supernatant discarded. Finally, residual ethanol was carefully removed and the pellets were dried for 3 - 5 min. Subsequently, the pellets were dissolved in 50 µl RNAse-free water and incubated for 20 min at 37 °C while shaking (900 rpm). For short-time storage, the RNA solution was kept at -80 °C, for long-term storage, the RNA was again precipitated with NaOAc and ethanol and then stored at -80 °C.

2.2.3.2 RNA quality control

2.2.3.2.1 Concentration determination

The RNA concentration was determined with a Nanodrop spectrometer (ThermoFisher Scientific) at 260 nm (A_{260} = 1 equates 40 ng/µl RNA). Furthermore, the 260/280 and 260/230

values were determined. Pure RNA should show a 260/280 of approximately 2.0 (DNA 1.8) and a 260/230 bigger than 2.0 (Wilfinger et al., 1997).

2.2.3.2.2 Bioanalyzer

2.2.3.2.2.1 RNA integrity

More detailed quality control was performed with the help of an Agilent Bioanalyzer 2100 expert (Agilent) and the Agilent RNA 6,000 Nano Kit, which has a quantitative range from 25 - 500 ng/µl RNA. The chips were primed mostly according to the manufacturer´s instructions. First, the RNA dye concentrate was equilibrated at room temperature and mixed by vortexing. 1 µl of the RNA dye concentrate was added to 65 µl filtered gel matrix. The solution was vortexed again and spun down for 10 min at 13,000 x g and RT. 9 µl of the gel-dye mix were pipetted into the *gel* well (marked with white G) of a *DNA 1,000* chip, which was placed in the priming station. The plunger of the priming station was set to 1 ml, the syringe clip positioned at the top position and the priming station closed. Subsequently, the plunger was pressed down until it was held by the clip to fill the microfluidic channels with gel matrix. After exactly 30 s, the clip was released and after further 5 s and the plunger was carefully pulled back to the 1 ml position. The chip was taken out of the priming station and 9 µl of gel-dye mix were pipetted into the wells marked with a black G. 5 µl of the provided RNA maker (Agilent) were pipetted into the 12 sample wells and the ladder well. Subsequently, 1 µl of each sample was pipetted into the sample well and 1 µl of the provided RNA ladder into the ladder well. The chip was vortexed for 1 min at 2400 rpm in the provided vortexer (Agilent) and run on the Agilent 2100 Bioanalyzer as rapid as possible. The instrument was operated with the 2100 Expert Software (Agilent).

2.2.3.2.2.2 DNA analysis

DNA analysis was performed with the DNA 1,000 Assay kit, which works in the range between 25 and 1000 bp and concentrations from 0.1 - 50 ng/µl DNA. Priming was also performed according to the manufacturer´s instructions with the clip at lowest position.

2.2.3.2.2.3 Recovery of Bioanalyzer *DNA 1,000* chips

Used Bioanalyzer chips were emptied by centrifugation for 1 min at 1,800 x g (Hettich). The wells were filled with 12 µl 1xTAE buffer each, sealed tightly with parafilm and stored at 4 °C. For reuse of the chip, the wells were again emptied by centrifugation, then 9 µl gel-dye mix were pipetted into the gel well and the chip was primed as described before. After priming, residual gel was taken off again and all wells were filled with 12 µl 1xTAE buffer, vortexed and spun out again. Then, all G wells were filled with 6 µl gel-dye mix and the chip was loaded as described by the manufacturer.

2.2.3.3 Quantitative real time PCR

For qRT-PCRs, the Brilliant III Ultra-Fast SYBR Green QRT-PCR Master Mix (Agilent) was used. 10 µl 2x SYBR Green QRT-PCR Master Mix, 1 µl of each primer, 0.2 µl 100 mM DTT, 1 µl RT/RNase Block were mixed and 100 ng total RNA were added. The reactions were filled to a total volume of 20 µl with nuclease-free water. QRT-PCRs were performed with the following cycling parameters on a Mx3000P System (Agilent) or a CFX Connect Real-Time PCR detection system (BioRad) (Table 16).

Table 16: Cycling scheme for qRT-PCRs.

time [min]	temperature [°C]	cycles
10	50	1
3	95	1
0.5	95	41
0.5	56 (dependent on the primer)	
1	72	
1	95	1
0.5	55	
0.5	95	

2.2.3.4 RNA-seq library preparation

Libraries were generated with the help of the Lexogen SENSE mRNA-seq Library Prep Kit V2 (Lexogen).

2.2.3.4.1 Poly-A Selection

To wash the magnetic oligo-dT beads (15 µl per reaction), the tube was placed on a magnetic rack, incubated for 5 min until the solution was clear and the supernatant discarded with the tube remaining in the rack. Then, the tube was removed from the rack and the beads were washed with 200 µl of the provided bead wash buffer (BW) per reaction. The tube was placed back into the magnetic rack, incubated for 5 min and the supernatant was again discarded. This washing step was repeated once and finally the beads were resuspended bubble-free in 10 µl (per reaction) of the provided hybridization buffer (HYB). Before applying the RNA to the beads, 2 µg of the total RNA (in 10 µl water) were denatured for 1 min at 60 °C in a thermocycler and afterwards held at 25 °C. After adding 10 µl of the beads to the RNA, it was incubated for 20 min at 25 °C and 1,250 rpm rotation in a thermomixer (Eppendorf) to allow hybridization of the polyadenylated RNAs to the beads. Then, the tubes were again placed into the magnetic rack for 5 min. After removing the supernatant, 100 µl BW were applied to the

beads, it was mixed well and incubated at 25 °C for 5 min while rotating at 1,250 rpm in a thermomixer (Eppendorf). Subsequently, the tubes were placed back into the magnetic rack. After further 5 min the supernatant was taken off again and the washing step was repeated once.

2.2.3.4.2 Library Generation

After removing the supernatant, 15 µl of the provided reverse transcription and ligation mix as well as 2 µl Starter/Stopper mix were added and mixed by vortexing. The starter/stopper oligomers anneal to the RNA and work as primers for the reverse transcriptase. The reverse transcription reaction was incubated for 5 min at 25 °C and 1,250 rpm, then 3 µl of enzyme mix 1 were added to ligate the reverse transcribed cDNA fragments. It was vortexed again and incubated for additional 2 min at 25 °C and 1,250 rpm. Subsequently, the temperature of the thermomixer (Eppendorf) was increased to 37 °C and the samples were incubated for 1 h at 1,250 rpm. To stop the reaction, 100 µl BW were added, it was mixed thoroughly and the tubes were again placed into the magnetic rack until the solutions were clear and the supernatant could be discarded. The beads were washed with 100 µl BW once more and then they were resuspended in 17 µl second strand synthesis mix. At this point, 1 µl of the provided enzyme mix 2 was added. The second strand was synthesized with the following program in a PCR cycler: 1 cycle: 90 s at 98 °C, 60 s at 65 °C, 5 min at 72 °C, hold at 25 °C. The double stranded samples can be stored at -20 °C. To purify the samples, 14 µl of the provided purification beads and 20 µl purification solution (PS) were added (dependent on the library), it was mixed by pipetting and vortexing and incubated for 5 min at RT. Subsequently, the tubes were placed into the magnetic rack again until the solution was clear. The supernatant was carefully removed, the beads were resuspended in 50 µl elution buffer and incubated for 2 min at RT. After addition of 70 µl purification solution and thorough mixing, the samples were incubated for 5 min at RT and then they were put back into the magnetic rack until the suspension became clear again. The supernatant was discarded, 120 µl of freshly prepared 80 % ethanol were added and incubated for 30 s with the tubes still in the rack. After taking off the supernatant, the washing step was repeated once. Then, the beads were dried for 5-10 min until all ethanol was evaporated. The DNA was eluted from the beads by the addition of 20 µl elution buffer (2 min at RT). The beads were separated in the magnetic rack and 17 µl of the supernatant transferred into a fresh PCR tube. At this point, the samples can be stored at -20 °C.

2.2.3.4.3 Library amplification

For the PCR, a master-mix containing 7 µl of the provided PCR mix and 1 µl enzyme mix 2 per reaction was prepared. 8 µl of the master-mix were added to 17 µl of the eluted library. 5 µl indexed i7 primers were added and 11 - 16 cycles of PCR with the following program were run:

98 °C for 10 s, 65 °C for 20 s, 72 °C for 30 s and a final extension at 72 °C for 1 min (hold at 10 °C). The PCR products were purified with beads as described in 2.2.6.13. In this case, 30 µl of purification beads were used. The beads were washed with 30 µl of the provided EB + 30 µl PB. The quality of the libraries was checked with an Agilent Bioanalyzer (DNA 1,000 Kit).

2.2.4 Sample preparation for gene chip analyses

Yeast cells were grown from OD 0.2 to 0.8 in YPD at 25 °C while shaking. The logarithmic cells were heat-stressed in a water bath at 37 or 42 °C for 10, 30 or 40 min, respectively. After the stress, the cells were transferred into precooled 50 ml conical tubes on ice, they were pelleted for 1 min at 4,165 x g and washed with 20 ml sterile water (1 min, 4,165 x g). Pellets were shock-frozen and sent to the "KompetenzZentrum für Fluoreszente Bioanalytik" (KFB) in Regensburg. There, the RNA was isolated and the samples were prepared for analysis on Yeast Genome 2.0 arrays (Affymetrix), which enable the analysis of 5,717 *S. cerevisiae* transcripts.

2.2.5 Assay for transposase accessible chromatin sequencing (ATAC-seq)

Around 5 million logarithmic cells (OD_{595} 0.8) were aliquoted (312.5 µl) in 2 ml tubes and heat-stressed at 37 °C and 42 °C for 0, 5, 10 and 30 min, respectively in a thermomixer (Eppendorf). The cells were harvested for 1 min at 10,000 x g and washed once with 100 µl 1 M sorbitol, 0.1 M EDTA, 10 mM DTT. Subsequently, 90 µl sorbitol buffer (1.4 M sorbitol, 40 mM HEPES/KOH, pH 7.5, 0.5 mM $MgCl_2$) and 10 µl 8,000 U/ml lyticase were added and the cell wall was degraded for 5 min at 30 °C and 300 rpm in a thermomixer (Eppendorf). It was washed once with 100 µl sorbitol buffer (1 min, 12,000 x g) and then 5 µl Nextera Transposase, 25 µl 2x buffer (Nextera DNA Library Prep Kit 2017; Illumina) and 20 µl water were added on ice (Buenrostro et al., 2015). For the tagmentation reaction, the cells were vortexed and incubated in a thermomixer (Eppendorf) at 37 °C for 20 min at 300 rpm. Then, the DNA was purified via Qiagen MinElute PCR Purification kit according to the manufacturer´s protocol and the DNA was eluted with 10 µl elution buffer. At this point, the DNA can be stored at -20 °C. To PCR amplify the libraries, 10 µl transposed DNA were mixed with 5 µl of each adapter (i5 and i7 indices), 5 µl Primer Mix (Nextera DNA Library Prep Kit 2017; Illumina) and 25 µl Phusion HiFi Master Mix. The libraries were amplified according to the following PCR scheme: 1 cycle: 72 °C, 5 min; 98 °C 30 s and 10 cycles: 98 °C, 10 s; 63 °C, 30 s; 72 °C, 1 min. The PCR product was purified via Qiagen MinElute PCR purification columns and the DNA was eluted with 20 µl water. The quality of the libraries was assessed with an Agilent Bioanalyzer 2100 (DNA 1,000 Kit).

2.2.6 Ribosome Profiling - Translatomics

2.2.6.1 Cell extract preparation and footprinting

The ribosome profiling experiment was mostly executed according to a published protocol (Ingolia et al., 2009) and the instructions of the Illumina kit (Illumina TruSeq Ribo Profile Yeast Kit). Overnight cultures were inoculated to an initial $OD_{595} \approx 0.1$ in 500 ml YPD and grown at 25 °C and 150 rpm until an OD_{595} of about 0.8 was reached. After stressing the cells at 37 °C and 42 °C for 0, 10 and 30 min, respectively, 1 ml 50 mg/ml cycloheximide dissolved in ethanol was added and the cells were incubated for another two minutes at RT to stop ribosomal elongation and thus protein biosynthesis. From this step on, nuclease-free conditions were applied. The cells were harvested at 8,700 x g for two minutes at 4 °C (Beckman Coulter) and washed once with 30 ml buffer (150 mM KCl, 40 mM HEPES, pH 7.4, 2 mM EDTA; 2 min 4,000 x g; Hettich). Then, the pellets were resuspended in 3 ml of the provided yeast lysis buffer (Illumina) and transferred into a 50 ml Falcon tube filled with liquid nitrogen and holes in the caps. The tubes were incubated at -80 °C to slowly evaporate the nitrogen. Finally, the perforated caps were replaced with intact caps and the pellets kept at -80 °C until further usage. Cell lysis took place in a cryogenic mixer mill (Retsch MM400). To this end, the frozen pellets were placed into chambers (Retsch; 50 ml) that were prechilled in liquid nitrogen. The chambers were loosened (one quarter turn) and mounted on the mixer mill (3 min at 15 Hz). After each cycle, the chamber was retightened and placed again in liquid nitrogen until boiling ceased. This procedure was repeated for six cycles. Subsequently, the powder was transferred into a prechilled 50 ml Falcon tube with liquid nitrogen in it with a precooled metal spatula. The tubes were closed with punched lids and placed upright into a -80 °C freezer to let the nitrogen evaporate. After thawing the lysate in a 30 °C water bath, it was centrifuged for 5 min at 3000 x g and 4 °C. The supernatant was transferred into chilled 1.5 ml tubes and centrifuged for another 10 min at 16,900 x g and 4 °C. Subsequently, the supernatant was recovered and the lipid layer on the top as well as the pellet were discarded. Then 1 U/µl DNaseI was added to a final concentration of 10 U/ml and the solutions were incubated for additional 10 min on ice. After measuring the concentration (A_{260}), the solutions were diluted to A_{260}=200 with lysis buffer and aliquoted (100 and 200 µl), frozen in liquid nitrogen and stored at -80 °C until further usage. 10 µl of 10 % SDS were added to the total RNA sample (100 µl aliquot) and the RNA stored on ice until purification.

2.2.6.2 Ribosome footprinting

For ribosome footprinting, 15 U/A_{260} of 100 U/µl RNaseI (Ambion) were added to 200 µl of the cell lysate. Free nucleic acid polymers were degraded whereas ribosomal bound RNA fragments (28 - 30 nt) were protected. The reactions were incubated at RT and 350 rpm. After 1 h, the reactions were stopped by the addition of 10 µl 20 U/µl SUPERaseIn RNase Inhibitor

(Illumina) and the samples were chilled on ice until purification with MicroSpin S-400 columns (RPF samples).

2.2.6.3 Purification of RPFs

The supplied Microspin S-400 HR columns were inverted several times to resuspend the resin avoiding the formation of air bubbles. Then, the buffer was let drip out under gravity flow. Subsequently, the columns were equilibrated with 3 ml 1x yeast polysome buffer (Illumina) and finally centrifuged for 4 min at 400 x g. The flow through was discarded and the columns placed into new nuclease-free 1.5 ml tubes (Eppendorf). 100 µl of the RPF samples (the remaining 100 µl were stored at -80 °C) were loaded onto the column and eluted via centrifugation for 2 min at 600 x g. The flow-through was collected and 10 µl of 10 % SDS were added.

2.2.6.4 RNA Cleaning and Concentration (RNA Clean & Concentrator-25 Kit)

The RNA samples were purified and concentrated using the RNA Clean & Concentrator-25 Kit (Zymo Research). The total RNA samples (110 µl) were diluted in 220 µl RNA Binding Buffer + 220 µl 100 % ethanol and the RPF samples (110 µl) were diluted in 220 µl RNA Binding Buffer + 495 µl ethanol, respectively. The solutions were loaded onto the provided Zymo-Spin™ IIC columns and centrifuged for 30 s at 16,000 x g. Subsequently, the columns were washed with 400 µl RNA Prep Buffer (30 s, 16,000 x g), 700 µl RNA Wash Buffer (30 s, 16,000 x g) and 400 µl RNA Wash Buffer (2 min, 16,000 x g). Finally, the columns were transferred into fresh RNase-free 1.5 ml tubes and the RNA was eluted with 26 µl of nuclease-free water. The concentration was determined via Nanodrop (ThermoFisher Scientific) at 260 nm and the solutions were stored at -80 °C.

2.2.6.5 rRNA Depletion

To wash the magnetic beads that carry oligonucleotides complementary to the rRNA depletion nucleotides (Illumina Ribo-Zero rRNA depletion kit), they were equilibrated at RT and then vortexed to homogeneity. 2.7 ml of the beads (for 12 samples) were transferred into a Falcon tube and placed into a magnetic rack until the solution appeared clear. The supernatant was discarded with the tube still in the rack so that the beads were kept. Subsequently, the beads were washed two times with nuclease-free water (i.e. vigorously vortexed, placed in the magnetic rack for about 1 min and the supernatant discarded). Finally, the beads were resuspended in 720 µl Magnetic Bead Resuspension Solution (Illumina; 60 µl per sample) and 12 µl of RiboGuard RNase Inhibitor (Illumina; 1 µl per sample) were added and mixed well by vortexing. Aliquots of 66 µl were pipetted into new nuclease-free 1.5 ml tubes and stored at RT until further usage. For rRNA depletion, 5 µg of the RNA samples were mixed with 4 µl of Ribo-Zero Reaction Buffer (Illumina) and 10 µl Ribo-Zero Removal Solution (Illumina), which contains oligonucleotides that are complementary to the rRNA at one end and to the immobilized oligonucleotides of the magnetic beads at the other end. The samples were filled

to a total reaction volume of 40 µl with nuclease-free water. To anneal the rRNA with its complementary RNA in the removal solution, the reactions were incubated at 68 °C for 10 min in a thermomixer, centrifuged briefly and incubated at RT for additional 5 min. The probe-hybridized samples were then added to the washed beads and mixed well by pipetting up and down and by vortexing. After another incubation at RT for 5 min, the Eppendorf tubes were placed into the magnetic rack for at least 1 min and the supernatant was gently transferred into a fresh nuclease-free tube.

2.2.6.6 RNA Cleaning and Concentration (RNA Clean & Concentrator-5 Kit)

The rRNA-depleted samples were purified with the help of Zymo´s RNA Clean & Concentrator-5 Kit (Zymo Research). The total RNA samples (all of it) were mixed with 100 µl 100 % ethanol and 100 µl RNA Binding Buffer (Zymo Research) whereas the RPF RNA samples were mixed with 450 µl 100 % ethanol and 220 µl RNA Binding Buffer. The solutions were loaded onto Zymo-Spin™ IC columns and centrifuged for 30 s and 16,000 x g. Subsequently, the columns were washed with 400 µl RNA Prep Buffer (30 s, 16,000 x g), 700 µl RNA Wash Buffer (30 s, 16,000 x g) and 400 µl RNA Wash Buffer (2 min, 16,000 x g). Finally, the columns were transferred into fresh RNase free 1.5 ml tubes and the RNA eluted with 21 µl (total RNA) and 12 µl (RPF RNA) of nuclease-free water, respectively. The concentration was determined at 260 nm and the samples stored at -80 °C.

2.2.6.7 PAGE Purification of RPFs, cDNA or PCR product

The procedure is exemplarily described for RPF samples. It was equally performed for cDNA and PCR purification. First, 10 µl of the samples were mixed with 10 µl of denaturing gel loading dye (ThermoFisher Scientific) and separated via polyacrylamide gel electrophoresis. As a standard, 4 µl of a 20 bp DNA ladder (ThermoFisher Scientific) were diluted in 1 µl nuclease-free water and 5 µl denaturing gel loading dye and loaded, as well. As a control, 5 µl TruSeq Ribo Profile RNA (Illumina) were mixed with 5 µl denaturing gel loading dye. The solutions (except from the ladder) were incubated at 95 °C for 5 min and afterwards kept on ice. 20 µl RPF aliquots as well as 10 µl RNA control sample and ladder were pipetted into the wells of the 15 % urea polyacrylamide gels (running buffer: 1x TBE (0.1 M Tris, 90 mM boric acid, 1 mM EDTA); ThermoFisher Scientific) and separated at 210 V for 1 h until the bromophenol blue band reached the bottom. The gels were stained in 50 ml 1x SYBR Gold (ThermoFisher Scientific; diluted in 1xTBE buffer) for 15 min at 4 °C. Gel slices corresponding to 28-30 nt were excised (even if no band was observed) and transferred into 500 µl tubes with holes punched in the bottom (with a 20-gauge needle). These tubes with holes were put into 1.5 ml tubes and centrifuged at 12,000 x g to shred the gel slices into the 1.5 ml tube where they were dissolved in 440 µl 0.45 M ammonium acetate, 0.045 % (m/v) SDS solution and rocked at RT for 3 - 4 h at 400 rpm in a thermomixer (Eppendorf). The slurry was transferred

into 1.5 ml filter tubes (Merck) and centrifuged for 3 min at 2,000 x g to separate the gel pieces from the eluted RNA solution. The eluate was pipetted into a fresh 1.5 ml tube and 2 µl glycogen solution (Illumina) as well as 700 µl 100 % isopropanol (Roth) were added. Subsequently, the mixtures were incubated at -20 °C overnight to precipitate the RNA. After pelleting the RNA (14,000 x g, 20 min, 4 °C), it was washed once with 500 µl ice-cold 80 % ethanol (14,000 x g, 10 min, 4 °C) and the pellets were air-dried. The RPF RNA pellets were dissolved in 20 µl nuclease-free water and stored at -20 °C until further usage.

2.2.6.8 Fragmentation and End Repair

7.5 µl TruSeq Ribo Profile PNK (polynucleotide kinase) buffer were added to 20 µl of the total RNA and RPF RNA samples on ice. The total RNA samples were incubated at 94 °C for 25 min to heat-fragment them and then placed on ice again. To the heat-fragmented total RNA and RPF RNA samples, 44.4 µl nuclease-free H_2O and 3.0 µl TruSeq Ribo Profile PNK (Illumina) were added and the reactions were incubated for 2 h at 37 °C in a thermal cycler. PNK is able to dephosphorylate either terminus and therefore generates free 3´-hydroxyl groups, which are needed for further adapter ligation.

2.2.6.9 3´Adapter Ligation

To be able to reverse transcribe the RNA fragments, 1 µl of TruSeq RiboProfile 3´ adapter (Illumina; 5´AGATCGGAAGAGCACACGTCT 3´) was added, the samples were heat denatured for 2 min at 65 °C in a thermal cycler with heated lid and afterwards held at 4 °C. To the denatured samples, 3.5 µl TruSeq RiboProfile Ligation Buffer (Illumina), 1 µl 100 mM DTT (Illumina) and 1.5 µl TruSeq RiboProfile Ligase (Illumina) were added. It was mixed well by pipetting, shortly spun down and incubated at RT for 2 h. Subsequently, 2 µl of TruSeq RiboProfile AR Enzyme (Illumina) were added to each reaction and it was incubated for another 30 min at 30 °C.

2.2.6.10 Reverse Transcription

To each sample, 4.5 µl TruSeq RiboProfile RT Reaction Mix (Illumina), 1.5 µl 100 mM DTT (Illumina), 6.0 µl nuclease-free water and 1.0 µl EpiScript Reverse Transcriptase (Illumina) were added, mixed well and incubated for 30 min at 50 °C in a thermal cycler with heated lid. Afterwards, 1 µl of TruSeq RiboProfile Exonuclease (Illumina) was added to each reaction and it was incubated for 30 min at 37 °C. Subsequently, the samples were incubated at 80 °C for 15 min and then held at 4 °C. The samples can be frozen at -20 °C or lower at this point. Finally, 1 µl of TruSeq RiboProfile RNase Mix (Illumina) was added and the RNA was degraded at 55 °C for 5 min.

2.2.6.11 Circularization of cDNA

For the PCR amplification, the samples were circularized by the addition of 4 µl CircLigase Reaction Mix (Illumina), 2 µl ATP (Illumina), 2 µl $MnCl_2$ (Illumina) and 2 µl 1,000 U/ml CircLigase (Illumina). The reaction took place at 60 °C for 4 h. cDNA can be stored at 4 °C.

2.2.6.12 PCR amplification of the ribosome profiling library

2 µl of circularized cDNA, 19 µl H_2O, 2 µl TruSeq RiboProfile forward primer, 2 µl TruSeq RiboProfile Index PCR Primer of choice (CAAGCAGAAGACGGCATACGAGAT NNNNNN GTGACTGGAGTTCAGACGTGTGCTCTTCCGATCT) and 25 µl 2x Phusion MasterMix (NEB) were added. The primers carried variable 6 nucleotides long barcodes indicated in blue, which allowed to sequence multiple samples together (*multiplexing*). During the evaluation, the samples were *demultiplexed* according to the barcodes. The PCR parameters are shown in table 17. Heating and cooling took place with 1.5 K/s.

Table 17: PCR cycling parameters for final PCR amplification of processed RPF and total RNA samples from ribosome profiling.

	temperature [°C]	time [s]
Melting	98	30
9-14 cycles		
Melting	94	15
Annealing	55	5
Elongation	65	10
Hold	4	-

2.2.6.13 Purification of PCR products

The PCR products were purified using Agencourt AMPure XP beads (Beckman Coulter). To this end, 90 µl beads were added to 50 µl PCR product, mixed well and incubated at RT for 5 min. Subsequently, the tubes were placed into a magnetic rack for 2 min to separate the beads and the supernatant was discarded. After the beads were washed two times with 200 µl freshly prepared 70 % ethanol (30 s incubation), the DNA was eluted by resuspending the beads in 16 µl nuclease-free water. The tubes were again placed into the magnetic rack to remove the beads and the DNA solution was transferred into a new tube.

2.2.7 Next generation sequencing

DNA libraries were sequenced by Dr. Helmut Blum´s group at the Gene Centre (LMU München) on a HiSeq1500 sequencer (Illumina) with 200 - 240 million reads per lane.

Depending on the sequencing depth of the samples, the number of multiplexed libraries as well as the sequence length (50 or 75 bp, single end or paired end) varied. RNA-seq experiments for example were usually sequenced with 10 million 50 bp single end reads, whereas ATAC-seq experiments were sequenced in more depth with 40 million reads and 75 bp paired end reads. The raw data were processed by Prof. Ralf Zimmer´s group (LMU, München). For the bioinformatic RP evaluation, a detailed description of the methods can be found in the associated publication (Mühlhofer et al., 2019).

2.2.8 Proteomics

2.2.8.1 Sample preparation for LC-MS/MS

2.2.8.1.1 Cell cultivation and disruption

S. cerevisiae overnight cultures were diluted to an OD_{595} of 0.2 and grown to an OD of 0.8 in YPD. The cells (50 ml) were heat-stressed for 30 min at 37 °C or 42 °C in a water bath. If recovery was measured, the cells were shifted back to 25 °C for 60 min before they were harvested for 1 min at 4,165 x g (Hettich). The pellets were washed once in 1 ml ice-cold buffer S_0 (20 mM HEPES/KOH, pH 7.4, 120 mM KCl, 2 mM EDTA; 30 s at 5,000 x g and 4 °C) and the cell pellets were frozen in 2 ml Eppendorf tubes in liquid nitrogen. To lyse the cells, the thawed pellets were resuspended in 150 µl buffer S (20 mM HEPES/KOH, pH 7.4, 120 mM KCl, 2 mM EDTA, 0.5 mM DTT, 1:100 protease inhibitor MixFY (Serva), 1 mM PMSF). For the total protein sample (T), 75 µl of the cell suspension were taken off and 500 µl buffer T (20 mM HEPES/NaOH, pH 7.4, 150 mM KCl, 5 mM EDTA, 3 % (m/v) SDS, 2 mM DTT, 1:1,000 protease inhibitor MixFY (Serva), 10 µM PMSF) were added. After sealing the tubes with adhesive tape, the cells were lysed for 20 min at 95 °C and 1,000 rpm in a thermomixer (Eppendorf). The cells were centrifuged for 1 min at 5,500 x g and the supernatant was flash frozen and stored at -20 °C until further usage. The second aliquot of the cell suspension in buffer S was also flash frozen in liquid nitrogen and lysed in a mixer mill (Retsch) with 9 mm stainless steel balls (4 x 90 s at 30 Hz; Cole-Parmer) that were prechilled in liquid nitrogen. The tubes were cooled in liquid nitrogen between the lysis cycles. Before the lysate was centrifuged for 30 s at 3,000 x g and 4 °C, 400 µl ice-cold buffer S were added. The cleared supernatant was then transferred into a 1.5 ml ultracentrifuge tube (Beckman Coulter) and the insoluble fraction was separated from the soluble fraction by ultracentrifugation for 25 min at 41,000 rpm (TLA-45; 114,480 x g) and 4 °C (Optima Max E Ultracentrifuge; Beckman Coulter). The soluble fraction was transferred into a fresh, precooled tube (S) and the pellet was washed once with 500 µl buffer S (41,000 rpm for 25 min at 4 °C). The remaining pellet was dissolved in 500 µl buffer P (8 M urea, 20 mM HEPES/NaOH, pH 7.4, 150 mM KCl, 2 mM EDTA, 2 % (m/v) SDS, 2 mM DTT, 1:1,000 protease inhibitor MixFY (Serva), 10 µM PMSF) by vigorous vortexing in a thermal shaker for 30 min at RT. Finally, the solution was spun down for 5 min

at 20,000 x g and RT and the aqueous phase was taken as the pellet (P) fraction. The concentration of the samples was determined via BCA assay, which is described below.

2.2.8.1.1.1 Cycloheximide chase

Yeast cells were grown to an OD of 0.8 in YPD. Subsequently, translation was stopped by adding 100 µg/ml cycloheximide (CHX). The cells were incubated for 30 min at 25 °C, 37 °C or 42 °C. Then, they were harvested (1 min at 4,165 x g and 4 °C; Hettich) and washed once with 1 ml ice-cold buffer S_{CHX} (20 mM HEPES, pH 7.4, 120 mM KCl, 2 mM EDTA, 100 µg/ml CHX; 1 min at 4,165 x g; Hettich). The cell pellets were flash frozen in liquid nitrogen and stored at -80 °C.

2.2.8.1.1.2 Proteasome inhibition with bortezomib

Logarithmic growing cells (OD_{595} = 0.8) were treated with 50 µM bortezomib for 1 h to inhibit the proteasome (Samant et al., 2018) before stressing them for 30 min at 37 °C and 42 °C. Cells kept at 25 °C were used as a control. After the stress, the cells were harvested for 1 min at 4,165 x g at 4 °C and washed once with 1 ml ice-cold buffer S (20 mM HEPES, pH 7.4, 120 mM KCl, 2 mM EDTA; 1 min 4,165 x g; Hettich). The cell pellets were flash frozen in liquid nitrogen and stored at -80 °C.

2.2.8.1.2 Wessel Flügge Precipitation

For MS analysis, 250 µg protein were precipitated to get rid of detergents and inhibitors (Wessel and Flugge, 1984). From here on, only MS grade material and chemicals were used. First, the volume of the protein sample was adjusted to 160 µl with H_2O in LoBind Eppendorf tubes. 600 µl methanol (Sigma) were added and the emulsion was vortexed and centrifuged for 10 s at 16,200 x g and RT. This procedure was repeated with 225 µl chloroform (Sigma). Then 450 µl H_2O were added, it was vortexed again, incubated for 7 min in an ultrasonic bath (VWR) and centrifuged for 10 s at 16,200 x g. The upper phase was taken off until the precipitated proteins in the interphase were reached. Then, 450 µl methanol were added, the suspension was vortexed and centrifuged at 16,200 x g for 20 min at RT. Finally, the supernatant was discarded and the pellets were air-dried and stored at -20 °C.

2.2.8.1.3 Tryptic digest and desalting – whole proteome

The protein pellets were dissolved in 198 µl 8 M urea, 0.1 M Tris, pH 8.0 and 2 µl 5 M DTT were added. The samples were prepared according to the FASP protocol (Wiśniewski et al., 2009). To this end, protein solutions were loaded onto 30 kDa Microcon – 30 centrifugal filters (Merck) and centrifuged for 30 min at 14,000 x g. The samples on the filters were washed with 200 µl 8 M urea, 0.1 M Tris, pH 8.0 (30 min at 14,000 x g) and then alkylated by the addition of 100 µl of 50 mM iodoacetamide (IAA; Merck), 8 M Urea, 0.1 M Tris, pH 8.0 for 21 min at RT in the dark. During the first minute of incubation the filters where shaken at 600 rpm in a

thermomixer (Eppendorf). IAA was removed by centrifugation (20 min at 14,000 x g) and the filter collected samples were washed three times with 100 µl 8 M urea, 0.1 M Tris, pH 8.0 (20 min at 14,000 x g) and further three times with 50 mM ammonium bicarbonate (ABC; Merck) solution. The filters were placed into fresh collection tubes and 35 µl ABC + 5 µl 500 ng/µl sequencing grade Trypsin (Promega) were added. It was mixed for 1 min at 600 rpm and incubated over night at 37 °C in a plastic box filled with water to avoid drying of the filter-collected samples. On the next day, the peptides were eluted by centrifugation (15 min, 14,000 x g) and the filters were washed with 50 µl 500 mM NaCl (15 min, 14,000 x g). The tryptic digest was stopped by the addition of 0.5 µl trifluoroacetic acid (TFA; Sigma). For the MS measurements, the samples were desalted with 50 mg SEP PAK (tC18) columns (Waters). First, the columns were equilibrated with 1 ml acetonitrile (ACN; Sigma), 500 µl elution buffer (80 % (v/v) ACN, 0.5 % (v/v) formic acid (FA; Sigma)) and three times with 1 ml 0.1 % (v/v) TFA before the samples were loaded. After loading the samples, the columns were washed three times with 1 ml 0.1 % (v/v) TFA and one time with 250 µl 0.5 % (v/v) FA without letting the columns run dry. The peptides were eluted into fresh 2.0 ml LoBind tubes (Eppendorf) with two times 250 µl elution buffer under gravity flow. Then, another 250 µl of elution buffer were loaded, vacuum was applied and the column was let run dry. The solvent was evaporated in a speed vacuum concentrator (Eppendorf), first in the "alcohol" mode to remove ACN and finally in the "water" mode. The dried peptides were stored at -80 °C.

2.2.8.1.4 Ubiquitin immunoprecipitation

Yeast cells were grown to an OD of 0.8 and stressed for 30 min at 37 °C and 42 °C, respectively. The cells were harvested (1 min at 4,000 x g; 4 °C), washed once in 1 ml resuspension buffer (100 mM Tris/HCl, pH 8.0, 150 mM NaCl, 5 mM EDTA) and transferred into chilled 1.5 ml Eppendorf tubes. After another centrifugation for 30 s at 5,000 x g and 4 °C, the supernatant was removed and the cell pellets were flash frozen in liquid nitrogen. Subsequently, the pellets were resuspended in 200 µl lysis buffer (50 mM Tris/HCl, pH 7.5, 150 mM NaCl, 5 mM EDTA, 1 mM DTT, 0.1 % (v/v) NP-40 substitute, 1:100 protease inhibitor MixFY (Serva), 100 µM PR619 (Merck)) and the cell suspension was transferred into 2 ml tubes and flash frozen. The cells were lysed with 9 mm stainless steel balls (4 x 90s at 30 Hz and 4 °C; Retsch). Then, 300 µl ice-cold lysis buffer were added and the thawed lysate was clarified by centrifugation at 14,000 x g for 20 min at 4 °C. The concentration of the lysates was determined via BCA Assay as described below. During the BCA incubation, the beads were prepared. For each immunoprecipitation, 100 µl of the anti-ubiquitin antibody-linked beads (K-48 TUBE HF, ThermoFisher Scientific) were transferred into fresh 1.5 ml tubes. The beads were collected in a magnetic rack, resuspended in 750 µl lysis buffer without inhibitors (50 mM Tris/HCl, pH 7.5, 150 mM NaCl, 5 mM EDTA, 0.1 % (v/v) NP-40 substitute) and collected again. This washing step was repeated for two more times. 1.5 mg protein of the cell

lysate were added to the beads and the total volume adjusted to 500 µl with lysis buffer. After incubation on a rotating wheel (20 rpm; Stuart) for 3 h at 4 °C, the beads were collected for 3 min in the magnetic rack. To remove unspecifically bound proteins, the beads were washed with 750 µl wash buffer 1 (50 mM Tris pH 7.5, 250 mM NaCl, 0.2 % (v/v) NP-40 substitute). The beads were collected again and the washing procedure was repeated for two times. Subsequently, they were washed once with 750 µl wash buffer 2 (50 mM Tris, pH 7.5, 150 mM NaCl, 0.05 % (v/v) NP-40 substitute). Finally, the beads were collected and frozen at -80 °C.

2.2.8.1.5 On bead digest and desalting

The on bead digest was performed based on a published protocol (Keilhauer et al., 2015). First, the beads were thawed and resuspended in 25 µl digestion buffer (50 mM Tris/HCl, pH 7.5, 2 M urea, 1 mM DTT, 5 ng/µl Trypsin). The beads were incubated for 2 h at RT. Afterwards, 100 µl alkylation buffer (50 mM Tris/HCl, pH 7.5, 2 M urea, 5 mM IAA) were added and the beads were incubated at RT over night at 500 rpm in a thermomixer protected from light. To quench the tryptic digest, 1.5 µl FA were added. The samples were desalted with double C18 layer stage tips (Rappsilber et al., 2007). First, the tips were equilibrated with 70 µl methanol and washed three times with 70 µl 0.5 % FA by applying mild centrifugation steps (960 x g). Before the samples were loaded, the beads were separated by centrifugation for 1 min at 16,900 x g. The loaded sample volume should not exceed 200 µl. The bound peptides were washed three times with 70 µl 0.5 % FA and eluted with two times 30 µl 80 % ACN, 0.5 % FA (960 x g). The samples were dried in a speed vacuum concentrator (Eppendorf) and stored at -80 °C.

2.2.8.1.6 Filtering peptide solutions for MS measurements

The peptides were dissolved in 23 µl 1 % (v/v) FA and incubated for 15 min in an ultrasonic bath at RT. In the meantime, the centrifugal filters (0.22 µM; Merck) were washed with 300 µl 1 % (v/v) FA (2 min at 10,000 x g). The peptide solutions were transferred onto the filters and filtered by centrifugation (2 min at 10,000 x g). For the MS measurement, the solutions were pipetted bubble-free into Chromacol vials (ThermoFisher Scientific).

2.2.8.2 MS/MS measurements

MS/MS measurements were performed on an Orbitrap Fusion or a Q Exactive Plus instrument coupled to an Ultimate3000 Nano-HPLC via an electrospray easy source (all ThermoFisher Scientific). After loading the peptides on a 2 cm PepMap RSLC C18 trap column (particles 3 µm, 100 A, inner diameter 75 µm, ThermoFisher Scientific) with 0.1 % TFA, they were separated on a 50 cm PepMap RSLC C18 column (particles 2 µm, 100 A, inner diameter 75 µm, ThermoFisher Scientific) constantly held at 40 °C. The peptides were eluted with a gradient from 5 to 32 % ACN, 0.1 % FA during 152 min at a flow rate of 0.3 µl/min (7 min 5 % ACN, 105 min to 22 % ACN, 10 min to 32 % ACN, 10 min to 90 % ACN, 10 min wash at 90 %

ACN, 10 min equilibration at 5 % ACN).

Fusion: Survey scans (m/z 300 - 1,500) with a resolution of 120,000 were acquired. The resolution is defined by the measured m/z divided by the smallest m/z difference of two ions that can be separated (Δ m/z). The automatic gain control (AGC) target value was set to 2.0*e5 with a maximum injection time of 50 ms. This means that not more than 2.0*e5 ions will be present in the mass analyzer to minimize space-charge effects, which would decrease the mass accuracy (Kalli et al., 2013). For fragmentation with high-energy collisional dissociation, the most intense ions of charge states 2-7 were selected. The collision energy was set to 30 %. In the ion trap, the maximum injection time was also set to 50 ms but the AGC target value was reduced to 1.0*e4. Inject ions for all available parallelizable time was allowed. Dynamic exclusion of sequenced peptides was set to 60 s, which avoids repeated sequencing of the same peptide. Internally generated fluoroanthene ions were used for real-time mass calibration. Data were acquired using Xcalibur software version 3.0sp2 (ThermoFisher Scientific).

Q Exactive Plus: Survey scans (m/z 300 - 1,500) were acquired in the orbitrap with a resolution of 140,000. The AGC target value was set to 3.0*e6 with a maximum injection time of 80 ms. The 12 most intense ions of the survey scans were subjected to data-dependent high collision dissociation fragmentation at a resolution of 17,500 with a maximum injection time of 50 ms. The minimal AGC target value was set to 1.0*e3 and the isolation window was set to 1.6 m/z. Singly charged and unassigned ions were excluded from the measurement. Furthermore, the dynamic exclusion of peptides was enabled for 60 s. For real-time mass calibration on the Q Exactive Plus, the lock-mass ion option, polydimethylcyclosiloxane (m/z 445.12002) generated during ESI from ambient air, was applied. Data were acquired using the Xcalibur software version 3.1sp3 (ThermoFisher Scientific).

2.2.8.3 MS Data analysis

The MS data were analyzed quantitatively with MaxQuant (version 1.6.2.6) (Cox et al., 2014, Cox and Mann, 2008). The *S. cerevisiae* proteome database downloaded from UniprotDB was used for protein identification. For all files of one experimental setup, the same fraction was set, which means that the software is principally allowed to compare the elution profiles of all different measurements to enhance protein identification. Only tryptic peptides were searched and cleavage sites before proline were included. Peptides with up to two missed cleavage sites were included in the analysis and a peptide tolerance of 4.5 ppm was applied. N-terminal acetylation and methionine oxidation were selected as variable modifications. As fixed modification, carbamidomethylation (due to alkylation of the cysteine residues with IAA) was selected. Not more than five modifications per peptide were allowed. For the primary search in MaxQuant it was sufficient if a protein was identified by only one peptide (*min. ratio count*

was set to 1 and *Label min. ratio count* was also set to 1). Furthermore, proteins that could not be identified unambiguously as the corresponding peptide(s) could also come from another protein, were included in the primary protein identification procedure (*unique + razor peptides* were taken into account). Otherwise, the preset orbitrap instrument settings of MaxQuant were applied. The minimal peptide length was set to 7 amino acids, the maximal length was 25 amino acids. To improve protein identification, match between runs was applied (*match time window*: 0.7 min; *align window*: 20 min). This feature allows comparing the elution spectra of the single measurements if a peptide could not be identified with high confidence. If this peptide was found in another measurement after a comparable elution time, the hit was included for the protein identification, otherwise it was discarded. The identification parameters were left preset with a protein false discovery rate (FDR) of 1 %. To validate the results, the peptides were also searched against a decoy database (reverse database) generated by MaxQuant. Based on those parameters, MaxQuant generated protein and peptide tables with the respective LFQ intensity values from the MS .*raw* data.

The *protein groups* table that was generated by MaxQuant and contains the identified proteins was further evaluated in Perseus (version 1.6.2.1) (Tyanova et al., 2016). First, the table was filtered by *potential contaminant hits*, hits from the *reverse (decoy) database* and hits that were *only identified by side*, to remove contaminations, proteins that were only identified based on peptides that also were found by chance in the decoy database and proteins that were only identified by peptides with PTMs. After log_2 transformation of the LFQ intensities, the associated replicates were grouped into categories (each triplicate becomes one category group). Then, the rows were filtered on three valid values in each group. In this case, only proteins that were found in every single replicate were taken into account. To avoid loss of proteins that were only aggregating at a distinct temperature, the pellet fractions were filtered on three valid values in at least one group. In this case, e.g. proteins that were not found in the pellet at 25 °C but in all replicates at 42 °C were included in the evaluation. As the number of identified proteins in the CHX chase was not satisfactory with three valid values, this dataset was filtered on at least two valid values in each group to increase the number of identified proteins. Thus, in this case it was sufficient if a protein was identified in two of the total three replicates of each category group. In the last two cases, the missing values were calculated from the Gaussian distribution (*width*: 0.3; *downshift*: 1.8). This means that the software assumes that the protein was not identified due to low abundance and then assigns a LFQ intensity value based on the (Gaussian) distribution of all LFQ intensity values in the measurement. After this calculation, the LFQ intensity distribution should be plotted to check if the intensity values still end up in a Gaussian distribution. If too many values had to be calculated, the distribution will show two maxima. In this case, the calculation should be revised or it should be filtered more stringently, e.g. on three valid values in each group. To analyze

the fold changes, Volcano plots with a two-sided t-test (FDR: 0.05; $S_0 = 0.1$) were plotted (Benjamini and Hochberg, 1995) in Perseus. In this thesis, a protein was considered to be significantly up- or downregulated if $|log_2 fc| > 1$; FDR < 5 % and $S_0 = 0.1$. S_0 is principally a minimal fold change below which a protein cannot be statistically significant even if the p-value was infinite. Thus, by combining S_0 and the FDR, the fold change and the statistical significance are combined, which results in the hyperbola functions shown in the volcano plots. For comparisons with the transcriptome and the translatome data, only the fold changes were used. A gene/protein was considered to be *changed* if $|log_2 fc| > 1$ and *unchanged* if $|log_2 fc| <$ 0.3 if not stated differently (Mühlhofer et al., 2019). As a measure for the correlation between the transcriptomic and proteomic changes, Pearson correlations were calculated and 2D enrichment plots were visualized with Perseus. The 2D enriched presentation allows comparing the addressed pathways (GO categories) at the different levels. To correct for the internal normalization performed by MaxQuant, the CHX chase and the Bortezomib LFQ data were additionally histone-normalized using the mean protein level of the histones Hht1, Htb2 and Hhf1 or Htz1 and Hho1, respectively (Wiśniewski et al., 2014, Mühlhofer et al., 2019).

2.2.9 *In vivo* ^{35}S-methionine incorporation

De novo protein biosynthesis was measured based on a modified protocol described previously (Schopf et al., 2019, Esposito and Kinzy, 2014, Mühlhofer et al., 2019). Methionine prototroph R1158 (URA3::CMV-tTA MATa his3-1 leu2-0 MET15) yeast cells were grown in 5 ml CSM medium (-methionine; table 18) over night. The cells were transferred into 50 ml fresh CSM medium and grown for another 24 h at 30 °C. The overnight culture was diluted to an OD_{595} of 0.2 in CSM medium and grown to an OD_{595} of 0.8. Then, the cells were harvested (1 min at 4,000 x g) and resuspended in fresh CSM to a concentration of 1 OD_{595}/ml. 1 ml of the cell suspension was supplemented with 7 µl methionine mix (6 µl 10 mM "cold" methionine + 1 µl 10 mM ^{35}S-methionine; Hartmann Analytic). To be able to correct for cell growth, parallel cultures with 7 µl 10 mM non-radioactive methionine were prepared. The cells were grown/stressed (25 °C, 37 °C, 42 °C and 46 °C, respectively) for 90 min in a thermal shaker (Eppendorf). Samples were taken after 10, 30, 60 and 90 min. To check if protein biosynthesis is relaunched after the stress, 90 min recovery at 25 °C was additionally monitored. After taking the samples, translation was immediately stopped by the addition of 1 µl 100 mg/ml cycloheximide (in ethanol). Always 1 OD of cells was harvested (1 min 13,000 x g) and the cells were washed two times with 100 µg/ml CHX (in water). To facilitate the following cell lysis by boiling, the cells were resuspended in 400 µl 100 mM NaOH and incubated for 3 min at RT. Then, the cells were centrifuged once more at full speed and the supernatant was discarded. For lysis, the cells were resuspended in 25 µl 2.5x Laemmli buffer (5 % SDS (w/v), 25 % glycerol (v/v), 150 mM Tris/HCl, pH 6.8, 0.025 % (w/v) bromophenol blue, 2.5 % (v/v) 2-mercaptoethanol) and 15 µl of the sample were loaded on a 4 - 20 % gradient gel (Serva). The

proteins were separated at 25 mA constant current until the bromophenol blue front exited the gels. Subsequently, the gels were placed onto a ceramic plate, wrapped with plastic wrap and the screen exposed for 20 h. Autoradiography was recorded with a Typhoon Scanner (GE). The gels were evaluated densitometrically with the ImageQuantTL Software (GE) and the intensities normalized to 1 h at 25 °C.

Table 18: Composition of yeast CSM medium. *The medium used for the ^{35}S-methionine incorporation did not contain methionine.*

CSM medium	glucose	20 g/l
	yeast nitrogen base w/o aa	6.7 g/l
	amino acid/nucleobase mix	1 g/l
amino acid/nucleobase mix	adenine	10 mg/l
	arginine	50 mg/l
	aspartic acid	80 mg/l
	histidine	20 mg/l
	isoleucine	50 mg/l
	leucine	100 mg/l
	lysine	50 mg/l
	(methionine)	(20 mg/l)
	phenylalanine	50 mg/l
	threonine	100 mg/l
	tryptophan	50 mg/l
	tyrosine	50 mg/l
	uracil	20 mg/l
	valine	140 mg/l

2.2.10 Nuclear depletion of Hsf1 (Hsf1 anchor away)

Genetically engineered W303 yeast strains with FKBP12 fused to a ribosomal subunit (Rpl13A) and Hsf1 fused to the FKBP-rapamycin-binding domain (FRB) were grown in YPDA (YPD + 100 mg/l adenine) at 25 °C until an OD$_{595}$ of 0.7 - 0.8 was reached (Haruki et al., 2008, Solís et al., 2016). Rapamycin (in DMSO) was added to a final concentration of 1 µM and the cells were incubated for additional 45 min at 25 °C. Rapamycin induces the formation of a complex between FKBP12 and FRB. Hence, the tagged transcription factor is exported together with the ribosomal subunit out of the nucleus and cannot regulate transcription

anymore. The control cells were treated with an equal volume of DMSO. The cells were stressed and harvested as described above. RNA isolation was performed by Sarah Reschke.

2.2.11 Knock-down of Pab1

To remove essential proteins transiently, a tetracycline operator can be inserted upstream of the gene of interest and a tetracycline repressible transactivator is additionally expressed. By the addition of doxycycline, the transactivator cannot bind the operator anymore and transcription is repressed (Garí et al., 1997). To knock-down Pab1, genomic engineered R1158 PAB1::kanR-tet07-TATA cells were grown over night in 5 ml YPD supplemented with 4.5 µg/ml doxycycline. On the next day, the cells were inoculated to an OD_{595} of 0.4 in YPD supplemented with 10 µg/ml doxycycline and grown until an OD of 0.8 was reached. Effects of the knock-down of Pab1 on the expression of Hsp26, Hsp42 and Hsp104 were analyzed at 25 °C and after 30 min at 42 °C with western blots.

2.2.12 Protein analytic methods

2.2.12.1 Determination of the protein concentration

2.2.12.1.1 UV/Vis spectroscopy

The concentration of a purified protein was usually determined with UV/Vis spectroscopy. This technique is based on the biophysical properties of two chromophores in proteins. First, the peptide bonds, which comprise only a small system of delocalized electrons and therefore can only be excited by light of higher energy (230 nm) and second, the aromatic amino acids, phenylalanine, tyrosine and tryptophan, which mainly contribute to the absorption of light at 280 nm. Thus, the measured absorption of a protein strongly depends on its amino acid composition. This fact is reflected by the molar absorption coefficient ε (Pace et al., 1995), which is either known or can be predicted by Expasy´s ProtParam tool (Gill and von Hippel, 1989, Wilkins et al., 1999). The concentration was calculated according to Lambert-Beer´s Law (Swinehart, 1962):

$$A = \varepsilon \cdot c \cdot d$$

A is the measured absorption [a.u.] at 280 nm, ε the molar absorption coefficient [$M^{-1}cm^{-1}$], c the molar concentration [M] and d the path length of the cuvette [cm]. The absorption was measured either with a NanoDrop1000 or with an Ultrospec3000 spectrophotometer. The spectra were always corrected for the absorption of the respective buffer.

2.2.12.1.2 BCA Assay

To determine the concentration of complex protein solutions, such as whole proteomes for MS, which might additionally contain SDS and urea, BCA assays (Pierce™ BCA Protein Assay Kit; ThermoFisher Scientific) were performed. The concentration determination is based on the

formation of a purple colored complex between bicinchoninic acid (BCA) and Cu^+. Cu^+ is formed by the reduction of Cu^{2+} by peptide bonds (Smith et al., 1985). Complex formation was measured at 562 nm. As a standard, different BSA concentrations were measured and the concentrations of the unknown samples were calculated from the standard curve. Dependent on the number of samples, the assay was conducted in 1 ml cuvettes (1 ml reagent + 50 µl protein solution) or in 96 well plates (200 µl reagent + 25 µl protein solution). The reagent/protein mixture was incubated for 30 min at 37 °C, cooled down to RT and measured in a photometer or a Pherastar plate reader (BMG Labtech), respectively.

2.2.12.2 Sodium dodecyl sulfate polyacrylamide gel electrophoresis (SDS-PAGE)

SDS-PAGE allows the analytic separation of proteins according to their difference in size. Complex formation with SDS outcompetes the intrinsic charge of the protein so that all proteins are negatively charged and run to the anode in a size dependent manner (Laemmli, 1970). Thus, separation is based on the movement with different velocities through the gel after voltage application. The constitution of 15 % gels is shown in table 19.

Table 19: Constitution of 15 % SDS-PAGE gels.

Separation gel 15 %	Volume	Stacking gel 5 %	Volume
4x buffer (1.5 M Tris/HCl, pH 8.8, 0.8 % (w/v SDS))	2.5 ml	2x buffer (250 mM Tris/HCl, pH 6.8, 0.4 % (w/v SDS))	2.5 ml
40 % Acrylamide	3.75 ml	40 % Acrylamide	0.625 ml
H_2O	3.75 ml	H_2O	1.875 ml
10 % APS	100 µl	10 % APS	100 µl
TEMED	10 µl	TEMED	10 µl

At first, the separation gel was prepared. To obtain a smooth surface, the polymerizing gel was overlaid with isopropanol. After removal of the isopropanol, the stacking gel was poured on top of the polymerized separation gel. The proteins were diluted in Laemmli buffer and incubation for 5 min at 95 °C to induce unfolding and SDS binding (Laemmli, 1970). Protein separation took place at 35 mA per gel with 25 mM Tris, pH 8.3, 0.2 M glycine, 0.1 % (w/v) SDS as running buffer until the bromophenol blue front reached the bottom. As a standard, 6 µl low molecular weight marker were loaded (Serva test mixture 6). The gels were stained with Fairbanks A (25 % (v/v) isopropanol, 10 % (v/v) acetic acid, 0.05 % (m/v) Coomassie Brilliant Blue R-250) and destained with Fairbanks D (10 % (v/v) acetic acid) (Fairbanks et al., 1971).

2.2.12.3 Western Blot

To identify specific proteins within the cellular protein extract, semidry western blots (Biometra) were conducted. The proteins were transferred from SDS gels onto nitrocellulose (NC) membranes at a current of 75 mA per gel for 2 h. Before blotting, Whatman papers were soaked in transfer buffer (48 mM Tris/HCl, pH 9.2, 39 mM glycine, 20 % (v/v) methanol). The NC membrane was also shortly incubated in the transfer buffer. The setup of the blot was (from anode to cathode): Three layers Whatman paper, membrane, gel, three layers Whatman paper. After the protein transfer, the membrane was incubated for 60 min in 5 % (m/v) milk in PBS-T (2.66 mM KCl, 137.93 mM NaCl, 1.47 mM KH_2PO_4, 8.06 mM $Na_2HPO_4*2H_2O$, pH 7.4 and 0.05 % (v/v) Tween-20) to avoid unspecific antibody binding to the membrane. After blocking, the membrane was gently shaken in the respective antibody solution (1:1,000 - 1:5,000 in 2.5 % (m/v) milk in PBS-T) over night at 4 °C. After washing the membrane three times with PBS-T for 10 min each on the next day, the blots were treated with the secondary antibody solution (1:15,000 in 2.5 % (m/v) milk in PBS-T), which binds the primary antibody and is coupled to horseradish peroxidase. After the membrane was incubated under constant shaking for 2 h at RT, it was washed five times for 10 min each with PBS-T. The chemiluminescent reaction catalysed by the horseradish peroxidase was induced by the addition of WesternBright™ ECL-Spray (Advansta) and detected using the ImageQuant LAS 4000 system (GE). The blots were densitometrically evaluated with the ImageQuant TL software (GE).

2.2.12.4 Stripping of Western Blots

If the blot should be treated with another antibody (e.g. loading control), which comes from the same animal as the first antibody and whose target is of a similar size as the first protein, the blots were stripped. To this end, the blots were incubated two times for 20 min in the stripping buffer (199.8 mM glycine/HCl, pH 2.2, 0.1 % (w/v) SDS, 1 % (v/v) Tween-20). Subsequently, the membranes were washed five times for 10 min with PBS-T. Finally, the membranes were blocked with 5 % (m/v) milk in PBS-T and treated with the next antibody.

2.2.13 Protein expression and purification

2.2.13.1 Cell disruption of *E. coli*

2.2.13.1.1 French press

E. coli cell pellets were resuspended in the buffer of the first column and mixed with protease inhibitor Mix G or HP (Serva), respectively. The cells were disrupted at 1.8 kbar (ConstantSystems) and the lysate was cleared by centrifugation for 45 min at 48,384 x g and 8 °C (Beckman Coulter Avanti J-26 XP; JA-25.50 rotor).

2.2.13.1.2 Ultra-sonication

The cell suspension was supplemented with protease inhibitor and sonicated four times for 45 s with 5 x 10 % duty cycle and 55 % output in watered ice (Bandelin). In between the sonication cycles, the suspension was cooled on ice for 45 s.

2.2.13.2 Concentrating protein solutions

Protein solutions with volumes exceeding 15 ml were concentrated in Amicon stirred ultrafiltration cells with suitable ultracel ultrafiltration discs (Merck). A pressure of 4.8 bar was applied with nitrogen to move the buffer through the filter membrane whereas the protein was retained. To prevent clogging of the membrane it was stirred gently. Proteins were concentrated at 4 °C.

Alternatively, smaller volumes were concentrated using Amicon Ultra Centrifugal Filter Units (Merck) with a suitable cut-off in a table top centrifuge at 4,000 x g and 4 °C.

2.2.13.3 Dialysis of proteins

To exchange the buffer in which the protein was dissolved, it was dialysed against 100-fold excess of target buffer over night at 4 °C and gentle stirring. The protein solution was filled into a Spectra/Por dialysis tube (Spectrum Laboratories) with an appropriate molecular weight cut-off. The dialysis tube was sealed with plastic clips.

2.2.13.4 Expression and purification of Hsp26 WT and phosphomimetic mutants

E. coli HB101 were freshly transformed with pQE60::*HSP26* plasmids. A 50 ml culture was inoculated with a single colony and the cells grown over night in LB_{Amp} (100 µg/ml ampicillin) at 37 °C while shaking in an incubator (Mytron). On the next day, a 2 l LB_{Amp} flask was inoculated with the overnight culture and the cells were grown at 37 °C under constant agitation until an OD_{600} of 0.6 - 0.8 was reached. Then, protein expression was induced by the addition of 2 ml 1 M IPTG (final concentration: 1 mM IPTG). Protein expression took place over night at 37 °C. On the next day, the cells were harvested in a Beckman Coulter Avanti J-26 XP centrifuge (JA-10 rotor) for 20 min and 8,671 x g at 4 °C. The pelleted cells were resuspended in 30 ml ice-cold buffer A (20 mM HEPES/KOH, pH 7.5, 50 mM KCl, 5 mM EDTA), transferred into 50 ml conical tubes and centrifuged again (4,165 x g and 4 °C for 20 min). The proteins were purified at 4 °C. After cell disruption, the clarified lysate was loaded onto an anion exchange column (Q-Sepharose) equilibrated in buffer A. The column was then washed with two column volumes (CV) buffer A and the protein was eluted with increasing salt concentration by anion displacement (320 ml linear gradient until 58 % buffer B (20 mM HEPES/KOH, pH 7.5, 1 M KCl, 5 mM EDTA)) at a flow rate of 2.8 ml/min. Finally, residual protein was eluted with 1.5 CV 100 % buffer B and 2 CV 2 M NaCl solution. The purity of the collected fractions was checked via SDS-PAGE. Selected fractions were pooled and concentrated to 10 ml with

a 10 kDa cut-off filter. Before loading the solution on the size exclusion column, it was filtered (0.22 µm) to remove aggregated proteins. 10 ml of the filtered solution were loaded onto a Superdex200 26/60 (GE) and separated at 2 ml/min with buffer A. The eluted fractions were again checked with SDS-PAGE and the pooled fractions loaded on a ResourceQ (6 ml, GE) equilibrated in buffer A. The bound protein was washed with 50 ml buffer A and then eluted by an increasing concentration of buffer B (200 ml linear gradient until 100 % B). Finally, the column was washed with 100 % buffer B for 10 CV. Fractions of sufficient purity were combined, dialysed against 4.5 l PBS (2.66 mM KCl, 137.93 mM NaCl, 1.47 mM KH_2PO_4, 8.06 mM Na_2HPO_4*$2H_2O$, pH 7.4), concentrated, flash frozen in liquid nitrogen and stored at -20 °C. The proteins all carry an artificial glycine residue as second amino acid due to former cloning with *Nco*I.

2.2.13.5 Expression and purification of Hsp26 *all-phospho* mutant

50 ml of an *E. coli* BL21 (DE3) overnight culture transformed with pESUMO::"*HSP26all-phospho*" were transferred into a 2 l LB medium flask containing 35 µg/ml Kanamycin and incubated at 37 °C and 150 rpm in an incubator (Mytron) until an OD_{600} of 0.8 was reached. Protein expression was induced by the addition of 2 ml 1 M IPTG. Expression took place over night at 37 °C and agitation. On the next day, the cells were pelleted at 4 °C and 8,671 x g for 20 min and washed in 35 ml buffer C (40 mM HEPES, 50 mM NaCl, 40 mM imidazole; pH 7.4; 20 min at 4,165 x g and 4 °C). The lysate was loaded onto an equilibrated His-Trap column (GE; 15 ml). Complex formation of the column bound Ni^{2+} cations with the histidine residues of the tagged proteins led to a retention of the target protein on the column. It was washed with 50 ml buffer C to remove unspecifically bound proteins and then the protein was eluted with an increasing concentration of buffer D (40 mM HEPES, 50 mM NaCl, 300 mM imidazole; pH 7.4; 0 - 80 %; 80 ml linear gradient). The high imidazole concentration in buffer D led to the replacement of the bound target protein. Elution took place in 3 ml fractions. Finally, the column was washed with 70 ml 100 % buffer D. Pooled fractions were dialysed over night against buffer C in the presence of SUMO-protease to remove both, the SUMO-module and the His-tag. Then, the protein solution was again loaded on the His-Trap column, which now retained the His-tagged protease and the SUMO-tag, but not the target protein. It was washed with 100 ml buffer C and the flow-through was fractionated. The second His-Trap purification step was followed by a ResourceQ as described for the WT. Instead of KCl, NaCl was used to elute the protein. After dialysis against PBS, the protein was concentrated, flash frozen in liquid nitrogen and stored at -20 °C.

2.2.13.6 Expression and purification of truncated Hsp26 variants

E. coli BL21 (DE3) were transformed with pET28b::*hsp26(82-195)* and cysteine mutants thereof. 50 ml cultures were inoculated with single colonies and grown over night in LB_{Kan} at

37 °C and shaking (Mytron). On the next day, 2 l LB_{Kan} flasks were inoculated with the overnight culture and the cells grown at 37 °C until an OD_{600} of 0.6 - 0.8 was reached. Then, protein expression was induced by the addition of 2 ml 1 M IPTG and protein expression took place over night at 30 °C.

For isotope-labelled constructs, expression was performed as described in the following. Single colonies were inoculated in 5 ml LB_{Kan} and grown at 37 °C over night. The cells were pelleted and resuspended in 50 ml $M9_{Kan}$ medium with $^{15}NH_4Cl$ (Table 20). After 6 h at 37 °C, the cells were pelleted for 5 min at 4,165 x g, resuspended in 100 ml $M9_{Kan}$ and grown over night at 37 °C under agitation. The overnight culture was transferred into 2 l $M9_{Kan}$ and the cells were grown at 37 °C while shaking until an OD_{600} of 0.8 was reached. Protein expression was induced with 1 mM IPTG and took place over night at 30 °C and 180 rpm. On the next day, the cells were harvested as described above (2.2.13.4). The pelleted cells were resuspended in 30 ml ice-cold buffer E (20 mM HEPES, pH 6.0, 50 mM NaCl, 5 mM EDTA, 1 mM DTT), transferred into 50 ml conical tubes and centrifuged at 4,165 x g and 4 °C for 20 min. Cell lysis was executed as described above (2.2.13.1). Purification started with a SP Sepharose (GE), a cation exchange column, which binds the positively charged Hsp26αM1 (aa 82 - 195) variant. The column with the bound protein was washed with 180 ml buffer E and the protein eluted with an increasing salt concentration (300 ml linear gradient until 50 % buffer F (20 mM HEPES, pH 6.0, 500 mM NaCl, 5 mM EDTA, 1 mM DTT)) at a flow rate of 2.8 ml/min. After checking the fractions on a SDS gel, selected fractions were pooled and concentrated to a volume of 10 ml for the following size exclusion chromatography (Superdex75 16/60; GE). Size exclusion chromatography was performed at a flow rate of 1 ml/min with buffer E. After checking the purity via SDS-PAGE, pure protein fractions were pooled, dialysed against NMR buffer (20 mM NaP, 50 mM NaCl), concentrated, frozen in liquid nitrogen and stored at -20 °C.

Table 20: Composition of M9 mineral medium.

M9 mineral medium	H_2O	867 ml
	M9 salt solution	100 ml
	20 % (w/v) glucose	20 ml
	1 M $MgSO_4$	1 ml
	1 M $CaCl_2$	0.3 ml
	1 mg/ml biotin	1ml
	1 mg/ml thiamine	1ml
	Trace element solution	10 ml

M9 salt solution	Na_2HPO_4-$2H_2O$	75.2 g/l
pH 7.2 (NaOH); autoclave	KH_2PO_4	30 g/l
	NaCl	5 g/l
	$^{15}NH_4Cl$	5 g/l
Trace element solution	EDTA	5 g/l
pH 7.5 (NaOH); sterile filtered	$FeCl_3$-$6H_2O$	0.83 g/l
	$ZnCl_2$	84 mg/l
	$CuCl_2$-$2H_2O$	13 mg/l
	$CoCl_2$-$2H_2O$	10 mg/l
	H_3BO_3	10 mg/l
	$MnCl_2$-$4H_2O$	1.6 mg/l

2.2.14 CD spectroscopy

2.2.14.1 Far UV CD spectroscopy

To analyse the secondary structure of proteins, circular dichroism spectroscopy was applied. This method it based on the physical principle that chiral molecules such as proteins differ in their absorption of right- and left-handed circularly polarized light. This difference in absorption is converted into the ellipticity (which is the measurement value) by multiplying ΔA with 32.98 (Johnson, 1988, Purdie, 1996). As the measured ellipticity θ is dependent on the concentration of the protein and the number of amino acids, the mean residual ellipticity per residue (θ $_{MRW}$) was calculated according to the following equation for plotting.

$$\theta_{MRW}\left[deg \cdot \frac{cm^2}{dmol}\right] = \frac{\theta_\lambda[mdeg] \cdot M\left[\frac{g}{mol}\right]}{c\left[\frac{mg}{ml}\right] \cdot d[cm] \cdot N_{AA} \cdot 10} = \frac{\theta_\lambda[mdeg]}{c\left[\frac{mol}{l}\right] \cdot d[cm] \cdot N_{AA} \cdot 10}$$

Where θ_λ is the measured ellipticity, c the concentration, d the path length through the cuvette, M the molar mass and N_{AA} the number of amino acids. Units are indicated in the equation. Far UV spectra were recorded from 280 – 200 nm with 15 repeats. Depending on the secondary structure, characteristic spectra are obtained. α-helical structures lead to a curve with two minima at around 208 and 222 nm whereas proteins with predominantly β-sheet structures lead to spectra with one minimum at 218 nm. Random coil structures show a minimum at around 200 nm (Johnson, 1988). CD spectra were measured in 0.5 mm cuvettes (Hellma) in a Chirascan™ - Circular Dichroism Spectrometer (Applied PhotoPhysics) at a concentration of 0.3 mg/ml in PBS. The spectra were corrected for the spectrum obtained for PBS.

2.2.14.2 Thermal transitions

To assess the thermal stability of a protein, thermal transitions from 20 °C to 90 °C with a heating rate of 1 K/min were measured with the Chirascan™ - Circular Dichroism Spectrometer (Applied PhotoPhysics) coupled to a waterbath (Vevor) and a Peltier element (Quantum Northwest). At each step one spectrum from 280 – 200 nm was taken. Thermal transitions were measured at a protein concentration of 0.3 mg/ml in PBS. The transition at 218 nm is shown in the plots.

2.2.15 Activity assays

The activity of sHsps *in vitro* was analyzed by determining their ability to suppress aggregation of different model substrates. Aggregation was measured via light scattering at 360 nm in a photometer (Cary 50; Agilent) with 10 mm quartz cuvettes (Hellma). Aggregation of the substrate was either induced chemically or by increased temperature. To keep the temperature in the cuvette constant, the cuvette holder was coupled to a water bath (Julabo). The reaction volume always was 200 µl and the reaction buffers were filtered and degassed on every measurement day. After thawing the proteins, they were centrifuged at 16,000 x g for 20 min at 4 °C to remove aggregates and the concentration was determined in the photometer.

2.2.15.1 Insulin assay

PBS, sHsps (0, 2, 4, 8 µM) and insulin (40 µM; Sigma) were added in a cuvette and mixed gently with a 200 µl pipette. The mixture was incubated for 5 min at 25 °C in the photometer. To reduce insulin and to initiate aggregation, 4 µl 1 M DTT (20 mM final concentration) were added. After adding DTT, the solutions were mixed once again and light scattering was measured at 360 nm for 70 min (Mymrikov et al., 2017). The activity of the Hsp26 phosphomimetic mutants was compared at 8 µM chaperone concentration.

2.2.15.2 Lysozyme assay

Lysozyme aggregation assays were conducted in PBS with 15 µM lysozyme (Sigma). Varying concentrations of sHsps were added to the buffer (0, 7.5, 15, 30 µM), mixed and incubated for 10 min at 37 °C in the cuvette holder of the photometer. To start the reaction, TCEP was added to a final concentration of 1 mM, the solution was mixed and the aggregation followed for 70 min (Peschek et al., 2009). The activity of the mutants was compared at a chaperone concentration of 15 µM.

2.2.15.3 Malate dehydrogenase assay

sHsps were diluted in PBS (0.6, 1.3, 2.0 µM) in a cuvette and incubated for 10 min at 44 °C in the cuvette holder. The reaction was started by the addition of 2 µM malate dehydrogenase (MDH (pig heart); Roche) and followed for 70 min (Mymrikov et al., 2017). Activity comparisons were performed with 1.3 µM chaperone.

2.2.15.4 Lysate assay

Yeast cells (BY4741 *HSP26Δ*) were grown in 400 ml YPD from OD_{595} 0.2 to OD_{595} 0.9 at 25 °C. Subsequently, the cells were harvested at 7,000 x g for 10 min and 4 °C (Beckman Coulter) and the pellets washed one time with 40 ml PBS (4,163 x g for 10 min and 4 °C; Hettich). Then, the cells were resuspended in 5 ml PBS supplemented with 1 mM DTT, 1:100 protease inhibitor MixFY (Serva) and 1:100 Phosphatase Mix 2 and 3 (Sigma). For cell lysis with glass beads in a mixer mill (Retsch; 4 x 90 s at 30 Hz), the suspension was aliquoted into 2 ml tubes. The cell debris was pelleted for 10 min at 16,000 x g and 4 °C and the supernatants were combined. Cellular ATP was degraded by the addition of hexokinase (Roche) to a final concentration of 30 U/ml together with 2 mM $MgCl_2$. The reaction was incubated for 20 min at 20 °C. Subsequently, the protein concentration was determined via BCA assay, 300 µl aliquots (5.3 mg/ml) were frozen in liquid nitrogen and stored at -80 °C. After thawing, the protein solution was centrifuged for 10 min at 16,000 x g and 4 °C to remove aggregates. The assay volume was 50 µl with a lysate protein concentration set to 0.8 mg/ml and 1 mM DTT. The sHsps were activated for 60 min at 42 °C, titrated to the lysate (0, 0.5, 1, 2, 4, 6, 8, 12, 16 µM) and the mixtures were incubated for 90 min at 42 °C. Then, the samples were centrifuged for 10 min at 8,600 x g and 4 °C, the supernatant was taken off, supplemented with 5x Laemmli buffer, boiled for 5 min at 95 °C and loaded on a 15 % SDS gel. The pellets were washed two times with 100 µl ice-cold PBS. Finally, they were dissolved in 40 µl 1x Laemmli buffer and boiled for 5 min at 95 °C. 22 µl were loaded on 4 - 20 % gradient gels (Serva) and run at 20 mA per gel until the bromophenol blue band reached the bottom. The gels were stained with Coomassie Quick Stain (Serva) for at least 2 h and destained with water while shaking. Densitometric analysis was performed with the ImageQuant TL software (GE).

2.2.16 High-performance liquid chromatography

2.2.16.1 Analytical size exclusion chromatography (SEC)

Size exclusion high-performance liquid chromatography (SEC-HPLC) allows the size analysis of protein complexes. Here, analytical size exclusion columns (Superdex200 increase 10/300GL or Superdex75 increase 10/300GL; GE), which separate proteins according to their size were attached to the HPLC system (Shimadzu). The proteins were detected by UV absorption and fluorescence with a SPD-20A detector (Shimadzu) and a fluorescence detection system RF-10A XL (Shimadzu). Furthermore, the HPLC system was equipped with a SIL-20AC auto sampler (Shimadzu) and a DGU-20A$_3$ degasser unit (Shimadzu). The retention times of the investigated proteins were compared with the retention times of standard proteins from the BioRad gel filtration standard (BioRad) which contains Thyroglobulin (670 kDa), γ-Globulin (158 kDa), Ovalbumin (44 kDa), Myoglobin (17 kDa) and Vitamin B12

(1.35 kDa). The HPLC runs were performed in PBS at a flow rate of 0.5 ml/min and at room temperature. 20 µl of 20 µM protein solution were loaded.

2.2.16.2 Analytical size exclusion chromatography-multi-angle light scattering (SEC-MALS)

A more precise determination of the size of protein complexes can be obtained by combining SEC with multi angle light scattering (MALS). To this end, the HPLC system (Shimadzu) was equipped with a refractive index (RI) (Shimadzu) and MALS detector (Wyatt). 2 nmol of the protein were loaded onto a Superdex200 increase 10/300GL (GE). The proteins were separated at a flow-rate of 0.45 ml/min in PBS for 60 min and the data evaluated using the ASTRA software (Wyatt). BSA (ThermoFisher Scientific) was used for calibration.

2.2.17 Analytical ultracentrifugation (AUC)

AUC measurements were carried out using a ProteomLab XL-I (Beckman Coulter) equipped with absorbance optics. The protein concentrations for the measurements were 23 µM, 7 µM and 2.3 µM (in PBS), respectively. The samples (350 µl) were loaded into assembled cells with quartz windows and 12-mm-path-length charcoal-filled epon double-sector centerpieces. The measurements took place at 35,000 rpm in an eight-hole Beckman Coulter AN50-ti rotor at 20 °C. Sedimentation was continuously scanned with a radial resolution of 30 µm and monitored at 280 nm. Data analysis was carried out with SEDFIT using the continuous c(S) distribution mode (Brown and Schuck, 2006, Schuck, 2000). Pamina Kazman performed the measurements and the SEDFIT analysis.

2.2.18 Hydrogen/deuterium exchange mass spectrometry

By hydrogen/deuterium exchange coupled to mass spectrometry (H/DX-MS), information about conformational dynamics and function linked to the structure of the investigated protein can be obtained (Masson et al., 2019). The method is based on the principle that hydrogen atoms of the amide backbone rapidly exchange with hydrogen atoms of the surrounding solvent (Hvidt and Nielsen, 1966). The exchange rates depend on the accessibility of the backbone, which is closely linked to the structure, physicochemical properties of the surrounding amino acids and protein dynamics (Konermann et al., 2011). H/DX-MS was performed with a Leap PAL RTC, a Waters ACQUITY M-Class UPLC, a HDX manager, and the Synapt G2-S ESI-TOF mass spectrometer (Waters), fully automated as described before (Boczek et al., 2015). Protein samples (30 µM) were diluted to 1.5 µM in deuterium oxide containing PBS, pH 7.4 and incubated at 20 °C for 0.167 min, 1 min, 10 min, 30 min and 120 min. By diluting the protein solution in an equal volume of H/DX quenching buffer (50 mM Na_2HPO_4/NaH_2PO_4, pH 2.6, 35 mM TCEP, 4 M guanidine hydrochloride) at 1 °C, the exchange reaction was stopped. The proteins were digested on an Enzymate BEH Pepsin Column (2.1 x 30 mm; Waters) at 20 °C and subsequently separated on an ACQUITY UPLC

BEH C18 column (1.7 µm, 1.0 x 100 mm; Waters) applying an acetonitrile/ 0.1 % (v/v) formic acid and 0.1 % (v/v) formic acid in water gradient. To minimize back exchange, chromatography was performed at 0 °C. Eluting peptides from the HPLC were directly subjected to the attached ESI-TOF (electron spray ionization-time of flight) mass spectrometer. After an additional separation by drift time within the mobility cell, the peptides were fragmented via MSE, a modified collision induced fragmentation protocol (Helm and Baginsky, 2018). The raw data were processed with the Protein Lynx Global Server PLGS and DynamX (Waters). H/DX MS was performed by Florian Rührnößl.

2.2.19 Microscopy

2.2.19.1 Fluorescence microscopy

Yeast cells were analyzed by light microscopy (Leica Axiovert 200 with attached Hamamatsu C4742-95 camera) at a magnification of 1,000 – 1,600x. Images were processed with ImageJ (Schindelin et al., 2012).

2.2.19.2 Scanning electron microscopy (SEM)

SEM was performed according to a protocol published by Spector and coworkers (Spector et al., 1998). 1 ml of logarithmic yeast cells were harvested for 5 min at 4,000 x g and washed one time with 500 µl PBS. The cells were fixed in 2.5 % (v/v) glutaraldehyde (in PBS) for 1 h at room temperature under gentle shaking. Then, the cells were centrifuged again and washed once more with PBS (5 min at 4,000 x g). After resuspending the cells in 300 µl PBS, 30 µL were incubated for 1 - 2 min at room temperature on a Thermanox® Plastic Coverslip (ThermoFisher Scientific). Then, the slides were washed in a petri dish with increasing ethanol concentrations, starting with 7.5 ml 50 % ethanol, followed by 7.5 ml 70 % ethanol, 7.5 ml 80 % ethanol, 7.5 ml 95 % ethanol and three more washing steps with 7.5 ml 100 % ethanol. The slides were dried over night under vacuum. Before microscopy, the cells were sputtered with gold. Pictures of the cells were taken at a constant voltage of 20 kV and a spot size of 20 nm at a magnification of 5,000 or 10,000x with a JEOL 5900 LV microscope (JEOL, Eching, Germany). The samples were prepared by Bettina Richter.

2.2.19.3 Negative stain transmission electron microscopy

The protein solution was pipetted onto a 200-mesh activated copper grid (Merck) and incubated for 1 min at room temperature. The grids were washed two times with 10 µl H_2O. For negative staining, the samples were treated with 8 µl 1.5 % (w/v) uranyl acetate solution for 1 min. Excess liquid was removed with a filter paper. TEM micrographs were recorded on a JEOL JEM-1400 Plus transmission electron microscope (JEOL Germany GmbH) at 120 kV and a magnification of 50,000 x. Negative stain TEM was performed by Pamina Kazman and Dr. Carsten Peters, respectively.

2.2.19.4 Cryo-EM

The protein samples were incubated for 1 h at room temperature at a concentration of 2-3.3 mg/ml. The grids (Quantifoil R1.2/1.3 or R2/1; Jena Biosciences) were glow discharged for 20 min. 5 µl of the sample were plunged in an ethane/propane mixture for cryo preparation using a Vitribot MK4 (ThermoFisher Scientific). Cryo-EM pictures were taken with a 300 kV Titan Krios transmission electron microscope (ThermoFisher Scientific) equipped with a K2 Summit camera (Gatan) and an energy filter operated with SerialEM (Mastronarde, 2005). A nominal magnification of 105,000x with a varying defocus (0.7-2.2 µm) was applied. The resulting pixel size was 1.35 Å/pixel. Pictures were recorded for 8 and 10 s, respectively with 5 frames per second. The dose was adjusted to 25-40 e/Å^2. Frames were aligned using motioncor (Zheng et al., 2017) with dose weightage. The contrast transfer function (CTF) correction was performed with gCTF (v1.06) (Zhang, 2016) to remove pictures of too low quality. The information content of the pictures had reach at least 4.5 Å, the defocus had to be in between 0.4 and 2.8 µm. The astigmatism did not have to be above 900 and a figure of merit within 0.04 and 9999 was applied. If those criteria were not fulfilled, the pictures were discarded. The particles were picked with Gautomatch and extracted with Relion (v3.0.6) (Scheres, 2012a, Scheres, 2012b). Only particles that fitted to the class averages and exhibited a resolution below 7 Å were used for the following analysis. The model was generated without bias using the *ab initio* function of cryoSPARC (v2) (Punjani et al., 2017). The generated structure was further refined with cryoSPARC and Relion. The final structure was generated from 85,425 particles. The final resolution was determined with the CTF validation server (EMBL-EBI). Cryo-EM was performed by Dr. Carsten Peters.

2.2.20 GO Analysis

For GO term enrichment analysis, the DAVID tool (Huang da et al., 2009, Ashburner et al., 2000), GOrilla (Eden et al., 2009) or the UniProt annotation table (2015) downloaded from the Perseus GitHub (for the 2D enrichment plots) (PerseusDigitalLibrary) were used.

2.2.21 Nuclear magnetic resonance (NMR) spectroscopy

All the Hsp26aM1 NMR samples were prepared in 20 mM sodium phosphate (pH 6.5), 50 mM NaCl, and 5 - 10 % ^{2}H$_2$O to determine the lock signal at a concentration of 50 - 100 µM. NMR spectra were recorded at 298 K using a 500 MHz Bruker spectrometer with a cryogenic triple resonance gradient probe. The backbone assignments were first performed for the wild type Hsp26αM1 using the standard triple resonance experiments (HNCACB, CBCACONH) (Frueh, 2014) at a protein concentration of 200 µM and then transferred to the S155C and T163C mutants, with the help of ^{15}N-edited NOESY experiments, for the subsequent PRE analyses. For the intermolecular PRE measurements, IPSL (3-(2-Iodoacetamido)-PROXYL) was covalently attached to the cysteine in the non-isotopically-labeled S155C or T163C mutants

(Mackereth et al., 2011), followed by mixing with an equimolar ^{15}N-labeled wild type Hsp26αM1, resulting in 50 μM of the final sample. The residual PRE effects were obtained based on the ratio of the peak intensities in the ^{1}H, ^{15}N-HSQCs before (paramagnetic) and after adding ascorbic acid (diamagnetic). NMR experiments were performed by Dr. Hyun-Seo Kang.

3 Results

3.1 Characterization of Hsp26 and the effects of its phosphorylation

3.1.1 Biochemical analysis of Hsp26 and phosphomimetic mutants

3.1.1.1 Hsp26 purification via a three-step protocol

To analyze the effects of Hsp26 phosphorylation *in vitro*, reported phosphorylation sites were substituted with glutamate to mimic the negative charge (Table 21) (Dissmeyer and Schnittger, 2011).

Table 21: Phosphorylation of Hsp26 was observed in several phospho-proteomic studies (Albuquerque et al., 2008, Bodenmiller et al., 2010, Ficarro et al., 2002, Holt et al., 2009, Smolka et al., 2007, Helbig et al., 2010, Chen et al., 2010b, Huber et al., 2009, Schreiber et al., 2012, Kanshin et al., 2015). Asterisks indicate positions at which diphosphorylated peptides were observed. All sites except from S144 and T48 are also listed in the BioGrid database. K: kinase; P: phosphatase.

phosporylation site	location in Hsp26	resource
T42	NTR (MD)	Albuquerque et al., 2008 (DNA damage); Bodenmiller et al., 2010 (Ptk1 (K); Ssn3 (K); Akl1 (K); Ptc4 (P); Sit4 (P)); Ficarro et al., 2002 (non-stress); Holt et al., 2009 (Cdk1); Smolka et al., 2007 (DNA damage); Kanshin et al., 2015 (heat)
S47*	NTR (MD)	Bodenmiller et al., 2010
T48*	NTR (MD)	Schreiber et al., 2012 (Ppt1 (P))
S90	NTR (MD)	Albuquerque et al., 2008
S144	ACD	Schreiber et al., 2012
T163	ACD	Albuquerque et al., 2008; Helbig et al., 2010 (Nat3 inhibition)
S207	CTR	Helbig et al., 2010; Holt et al., 2009
S208*	CTR	Albuquerque et al., 2008; Chen et al., 2010b (DNA damage); Ficarro et al., 2002; Holt et al., 2009; Huber et al., 2009 (TORK inhibition)
S211*	CTR	Albuquerque et al., 2008; Chen et al., 2010b; Ficarro et al., 2002; Holt et al., 2009; Huber et al., 2009

Point-mutants were cloned as described above (2.2.1.6). The proteins were overexpressed in *E. coli* HB101. Expression was induced with 1 mM IPTG and the proteins were expressed at 37 °C over night (2.2.13). Hsp26 was purified tagless according to the following strategy (Figure 10).
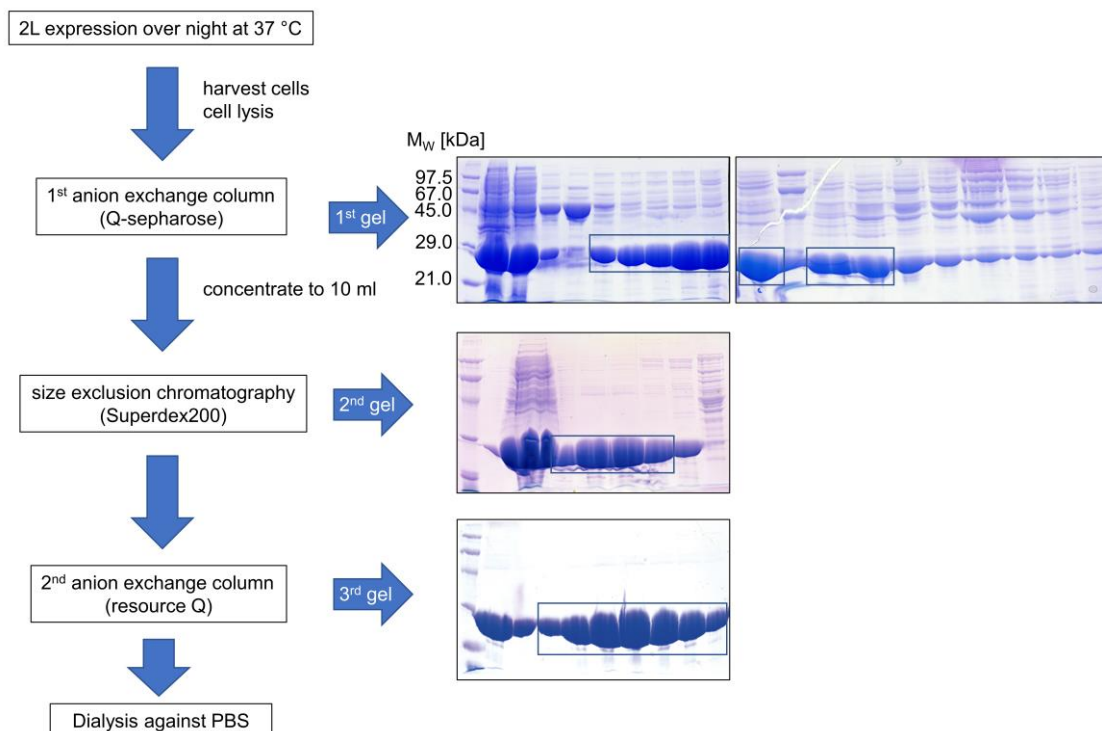
Figure 10: Three-step purification strategy for Hsp26*. The protein was purified tagless via an anion exchange column, a size exclusion column and another anion exchange column. A detailed protocol can be found in 2.2.13.4.*

The protein solution was concentrated to approximately 11 mg/ml. From a 2 l overexpression, around 100 mg Hsp26 were yielded. For the single/double mutants, similar yields were obtained. The gene for the mutant, in which all described phosphorylation sites were substituted (T42E/S47E/T48E/S90E/S144E/T163E/S207E/S208E/S211E) was synthesized by GeneArt (ThermoFisher Scientific). It should be noted that there is no evidence that such a phosphorylated Hsp26 variant occurs *in vivo*. T69 is not substituted in this mutant, as there are no reports that this threonine residue is phosphorylated. This single mutant was used as a control to check if a random substitution has a similar effect as substitutions at reported phosphorylation sites. As the *all-phospho* Hsp26 could not be expressed in *E. coli* without tag, the gene was cloned into a pESUMO vector (LifeSensors) as described in 2.2.1. The SUMO tagged protein was expressed in good yields and purified as described in 2.2.13.5, via two Ni-NTA columns and a SEC column. The His-SUMO tag was cleaved off between the first and

the second column. In this case, around 60 mg protein were obtained, which could also be concentrated to 10 mg/ml.

3.1.1.2 The secondary structure and thermal stability of phosphomimetic Hsp26 mutants is comparable to the WT

After the purification of the proteins, their secondary structure was analyzed with far UV CD spectroscopy (see 2.2.14) (Figure 11A). As it was described before, Hsp26 mainly consists of β-sheets (Stromer et al., 2004). From the spectra, a β-sheet content of around 33 % was predicted for the wild type (WT), which fits to the structure prediction from the primary sequence (Figure 11B, C) (Micsonai et al., 2018, Kelley et al., 2015). The far UV spectra of all single or double phosphomimetic mutants were very comparable to the WT spectrum. They all show a global minimum at around 218 nm, which is indicative for a high β-sheet content (Greenfield, 2006). Interestingly, the mutant with all possible phosphorylation sites substituted (*all-phospho*) showed a divergent behavior. The CD spectrum differs strongly from the WT spectrum (Figure 11D). In this case, the minimum is significantly blue-shifted to 205 nm. According to the secondary structure prediction, the β-sheet content is reduced in this mutant, which indicates that more parts of the protein are unstructured (Figure 11E). As the α-helix content is also decreased in comparison to the WT and these helical sequences are mostly modeled in the NTR, the mutations might possibly also affect the NTR of the protein, which is known to be the thermosensor domain. Noteworthy, the far UV CD spectrum of the *all-phospho* mutant at 20 °C resembled the spectrum of the WT at 45 °C, thus after the oligomer had dissociated. This implies that the *all-phospho* mutant might be a dimer or even a monomer.
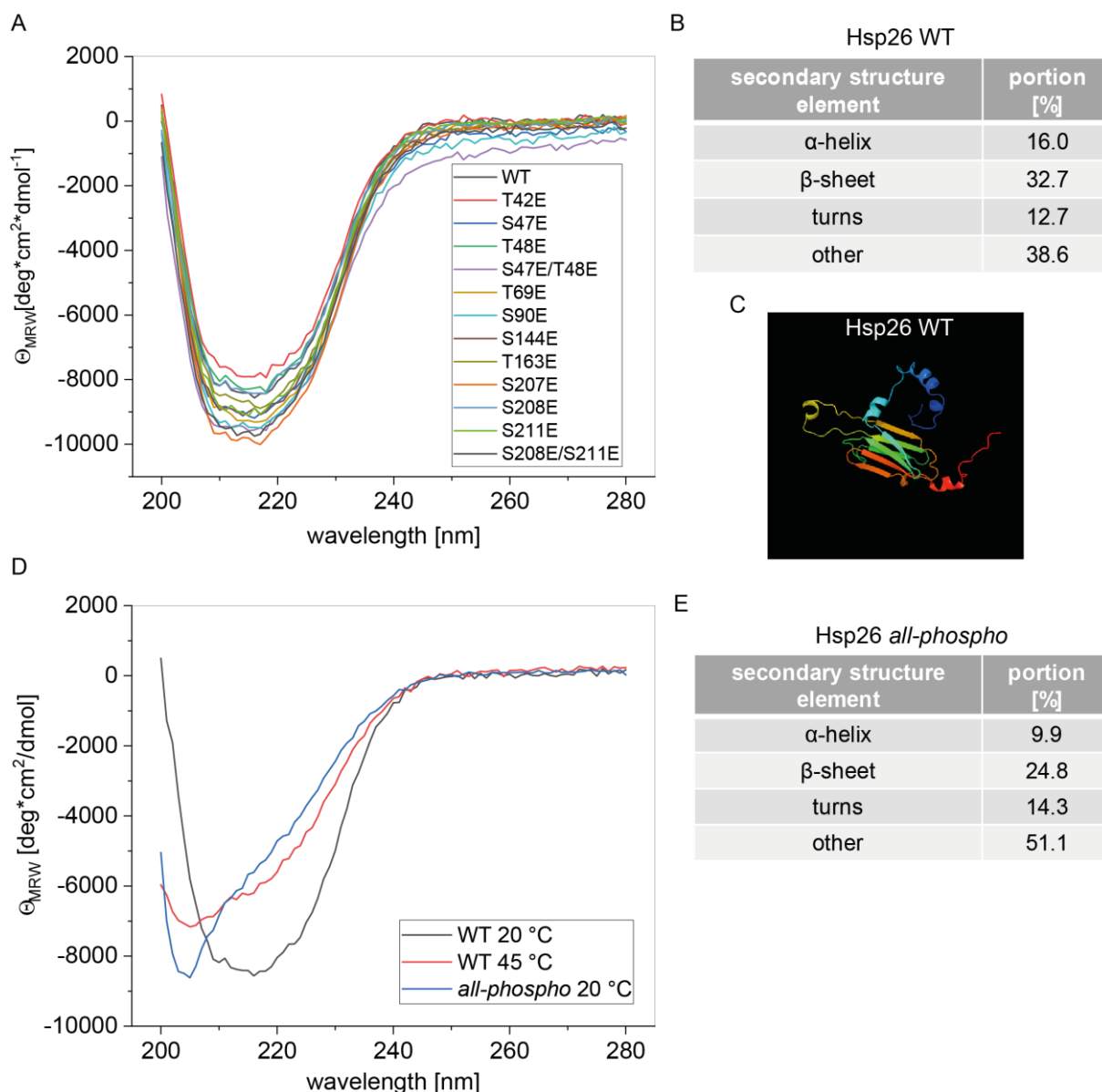
Figure 11: Secondary structure analysis of Hsp26 and the phosphomimetic mutants reveals a high β-sheet content. *A) Far UV CD spectra were recorded in a Chirascan spectrometer from 280 - 200 nm in 1 nm steps at 20 °C in PBS. The proteins were measured in a 0.5 mm cuvette at a concentration of 0.3 mg/ml. B) Secondary structure prediction with BeStSel for the WT protein according to the CD spectrum (Micsonai et al., 2018). C) Structure prediction of Hsp26 WT based on the primary sequence performed with PHYRE[2] (Kelley et al., 2015). The algorithm modeled amino acids 55 - 207 and selected PDB: d1gmea as template structure. D) Far UV CD spectra of the all-phospho mutant were also recorded on a Chirascan spectrometer from 280 nm to 200 nm in 1 nm steps at 20 °C in PBS (blue line). The mutant spectrum was compared to the WT spectrum at 20 °C (black line) and at 45 °C (red line), respectively. The proteins were measured in a 0.5 mm cuvette at a concentration of 0.3 mg/ml. E) Secondary structure prediction with BeStSel for the all-phospho mutant protein according to the CD spectrum at 20 °C.*

Furthermore, the thermal stability of the WT and the mutants was assessed with thermal transitions in the CD spectrometer as described in 2.2.14.2. As it was shown for the WT before, two transitions were expected, whereupon the first transition presumably reflects the oligomer dissociation and the second transition the unfolding of the protein (Haslbeck et al., 2004b).

Indeed, this observation could be reproduced (Figure 12A). Furthermore, all single or double phosphomimetic mutants showed the same two-phase transition. All proteins, except for T163E, unfolded (second transition) between 68 °C and 72 °C, thus overall the stability of the proteins was almost identical (Figure 12B). The T163E mutant unfolded already at 65 °C, hence was a bit less stable, but still comparable to the others. Hsp26 WT unfolded at 69.5 °C. For the first transition, the WT showed a T_M1 of 42 °C, which represents severe heat stress for *S. cerevisiae*. All phosphomimetic mutants had lower T_M1 values. The mutations in the ACD had the most pronounced effects and decreased the T_M1 by 7 K to 35 °C. The T_M1 values of all other mutants were between 37 °C, which represents mild heat stress, and 41 °C. The *all-phospho* mutant however, showed a different behavior. The protein unfolded at 68.7 °C and therefore was as stable as the other proteins. Interestingly, this protein did not exhibit the first transition, which is another indication that it does not form oligomers (Figure 12A).
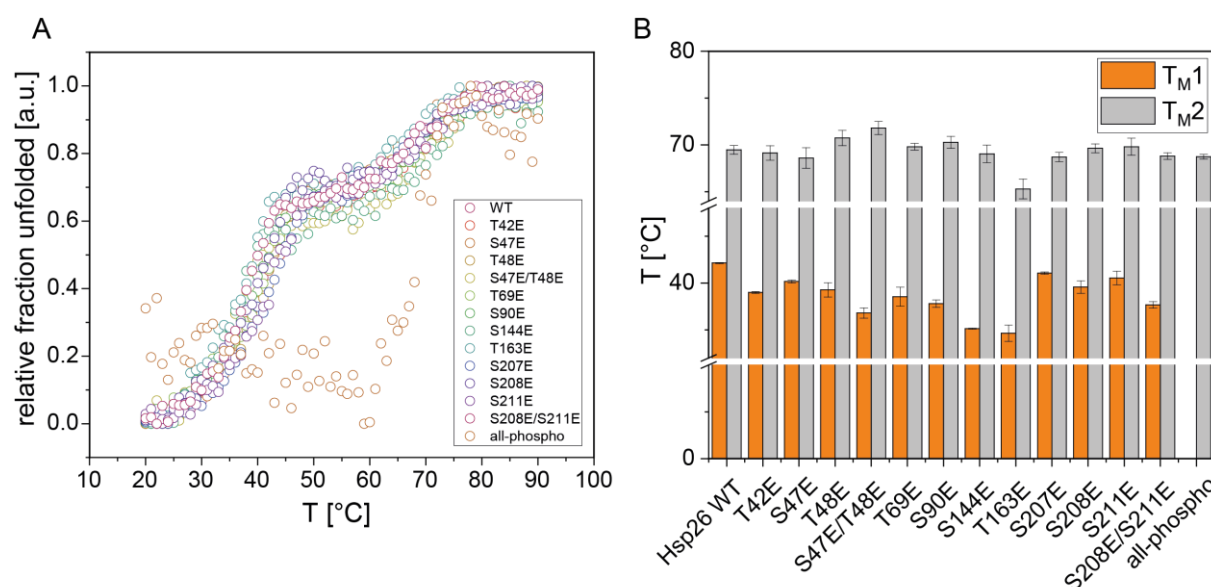
Figure 12: Phosphomimetic mutants affect the oligomer dissociation but not the overall stability. *A) Thermal transitions were recorded from 20 °C - 90 °C in a Chirascan CD spectrometer at 218 nm with a heating rate of 1 K/min. One transition curve of each protein is shown. B) The transition curves of the WT and single/double mutants were fitted with two sigmoidal Boltzmann fits to obtain both T_M values. The transition of the all-phospho mutant was fitted with a sigmoidal Boltzmann fit. Mean values and standard deviation were calculated from three replicates.*

3.1.1.3 Phosphomimetic mutants tend to form less stable Hsp26 oligomers

To analyze the oligomer size of the Hsp26 complexes in more detail, SEC-HPLC, SEC-MALS and AUC were performed as described in 2.2.16 and 2.2.17. In the SEC-HPLC analyses, two main species were observed. The WT and several mutants formed 24-meric complexes according to the size standard (Figure 13A). Except for T48E, all substitutions in the MD and ACD led to the dissociation of the oligomers into dimers on the SEC column. Interestingly, the CTR single mutants mostly were not dissociated.
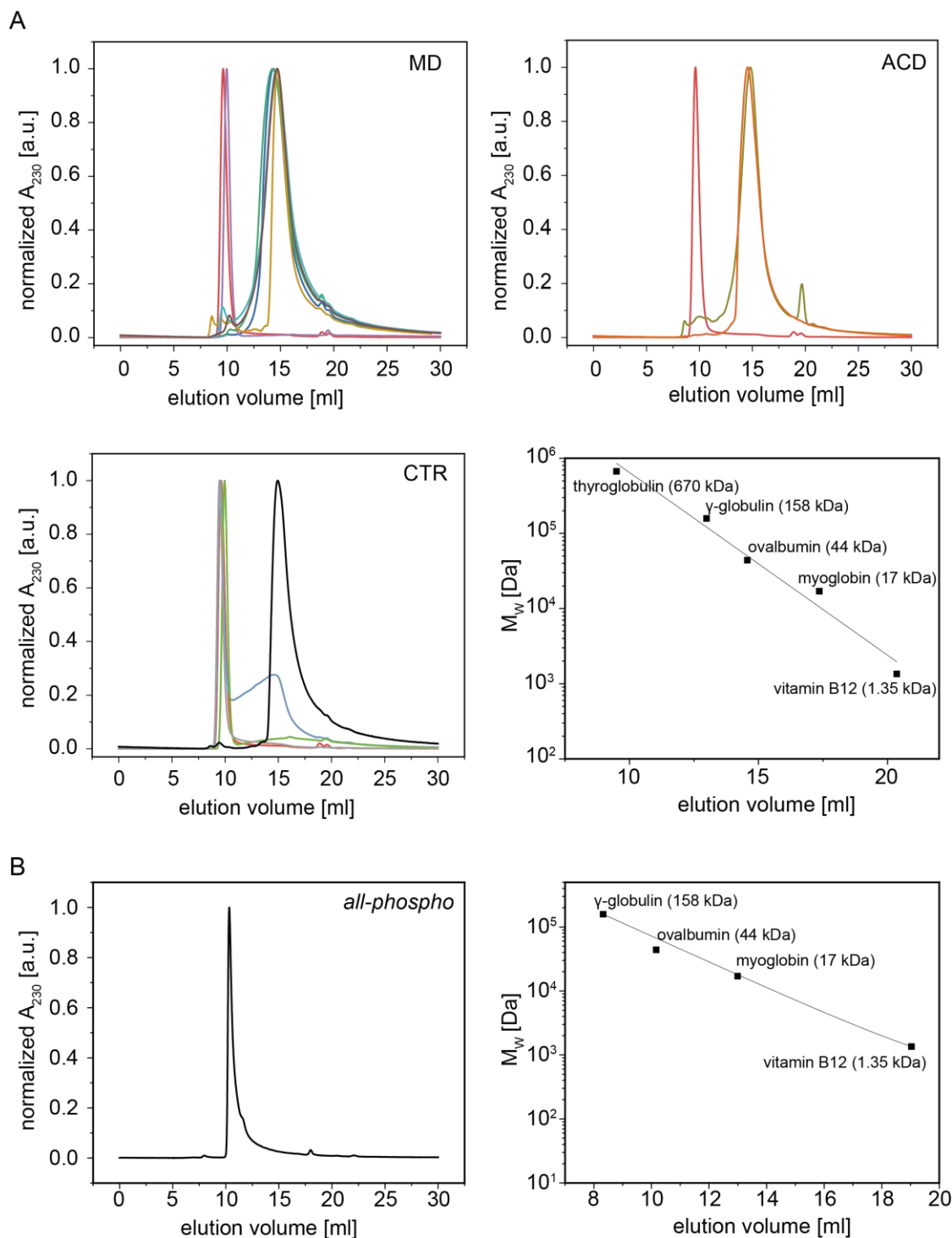
Figure 13: Phosphomimetic mutations lead to less stable Hsp26 complexes. *The oligomer size was measured with SEC-HPLC. The protein samples (0.4 nmol) were separated with a Superdex200 increase 10/300GL (GE) column (A) or a Superdex75 (B) at a flow rate of 0.5 ml/min in PBS. Elution of the protein was followed at 230 nm. Normalized absorption values are plotted. A) Elution profiles of the single/double mutants of the MD, ACD and CTR in comparison to the WT. The oligomer size was determined according to the SEC-HPLC marker (BioRad). The elution profile of the marker was fitted with an exponential decay function. Upper left panel: Mutants of the MD: WT: red, T42E: blue, S47E: green, T48E: purple, S47E/T48E: beige, T69E: cyan, S90E: brown. Upper right panel: Mutants of the ACD: WT: red, S144E: green, T163E: orange. Center left panel: mutants of the CTR: S207E: blue, S208E: green, S211E: gray, S208E/S211E: black. B) Elution profile of the all-phospho mutant. The size was calculated based on the exponential decay fit of the marker peaks (BioRad).*

In the elution profile of the S207E mutant, where the mutation sits directly next to the IEV motif, also a smaller dimeric species was observed. Substitution of both, S208 and S211, led to complete oligomer dissociation. As it was already expected from the CD analysis, the *all-phospho* mutant did not form oligomers anymore. The protein eluted comparable to ovalbumin (44 kDa), which clearly indicates that it only forms dimers (Figure 13B).

SEC-MALS allows determining the size of protein oligomers more precisely (2.2.16.2). For Hsp26, this was difficult as the complexes are dynamic and did not seem to be monodisperse (Figure 14). Therefore, the size prediction by light scattering was not so accurate. For SEC-MALS, higher protein concentrations were used, to prevent oligomer dissociation on the column. All proteins eluted after approximately 9.2 ml, the elution profile of the S47E/T48E mutant exhibited a second smaller peak, which eluted a bit earlier. Nevertheless, the oligomer sizes that were derived from the light scattering signal differed strongly and ranged from a tetramer (S90E) to bigger than 40-mers (S144E, T163E) (Table 22). For the WT, a 24-mer was obtained, which fits to the HPLC measurement. As already mentioned above, an accurate size determination via light scattering was not possible as the proteins were not monodisperse. Based on the elution profile the oligomers should be of a similar size. Presumably, there are different species present, which are very dynamic and convert into each other. Overall, based on the elution volume also this measurement confirmed the formation of big complexes.

Table 22: Size and stability of Hsp26 complexes.

	WT	T42E	S47E	T48E	S47E/T48E	S90E
T_M1 [°C]	42.1	39.0	40.1	39.2	36.8	37.8
AUC	24-mer	24-mer	24-mer	24-mer	12-mer	12-mer/18-mer
SEC-HPLC	24-mer	Dimer	Dimer	24-mer	Dimer	Dimer
SEC-MALS	24-mer	18-mer	18-mer	18-mer	6-mer/40-mer	4-mer

	S144E	T163E	S207E	S208E	S211E	S208/S211E
T_M1 [°C]	35.1	34.6	41.0	39.4	40.5	37.25
AUC	24-mer	24-mer	24-mer	24-mer	24-mer	24-mer
SEC-HPLC	Dimer	Dimer	24-mer	24-mer	24-mer	Dimer
SEC-MALS	4-mer/>40-mer	>40-mer	24-mer	12-mer	30-mer	12-mer
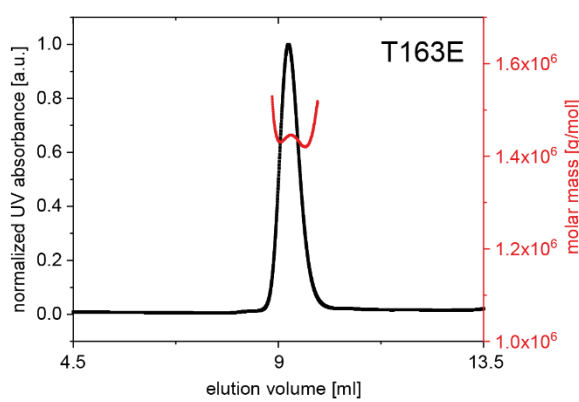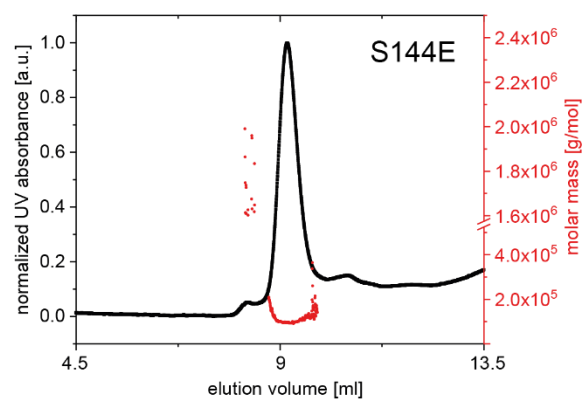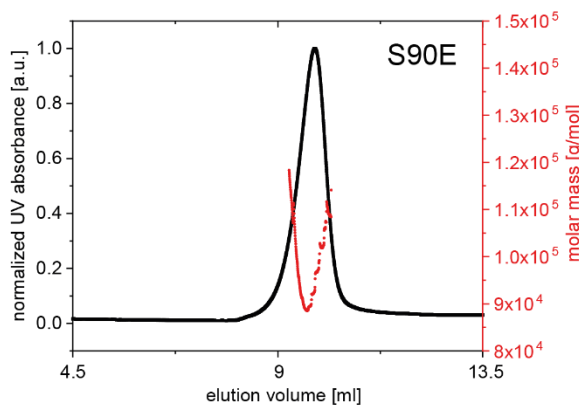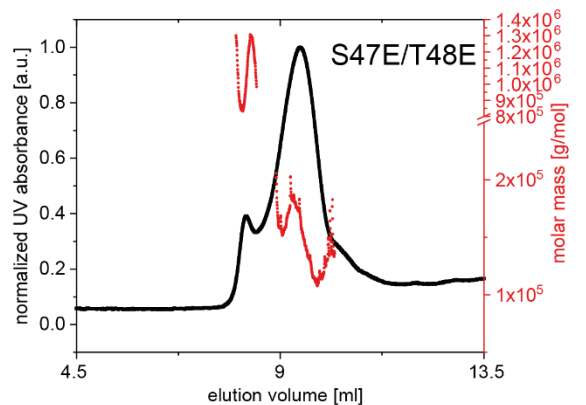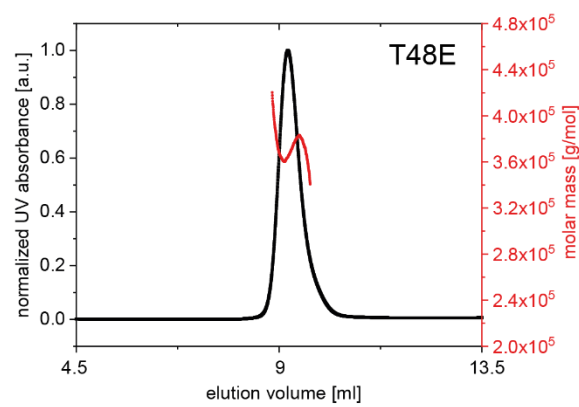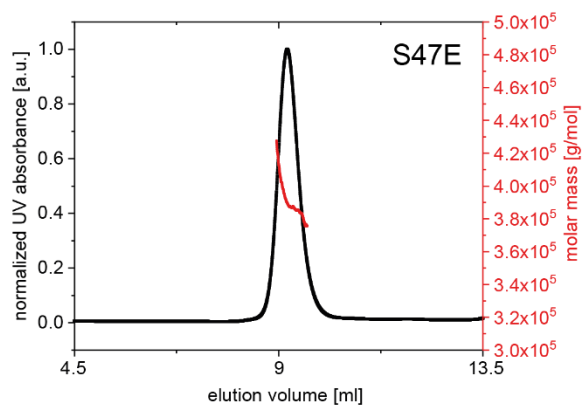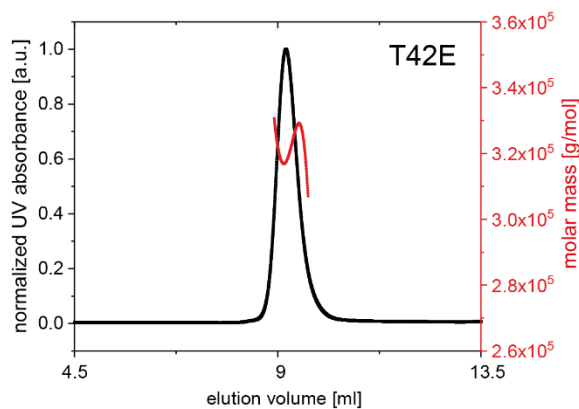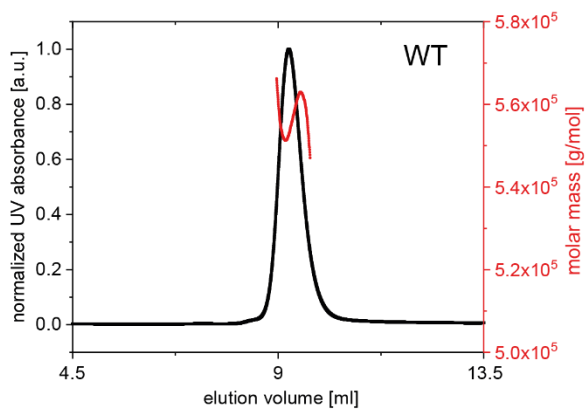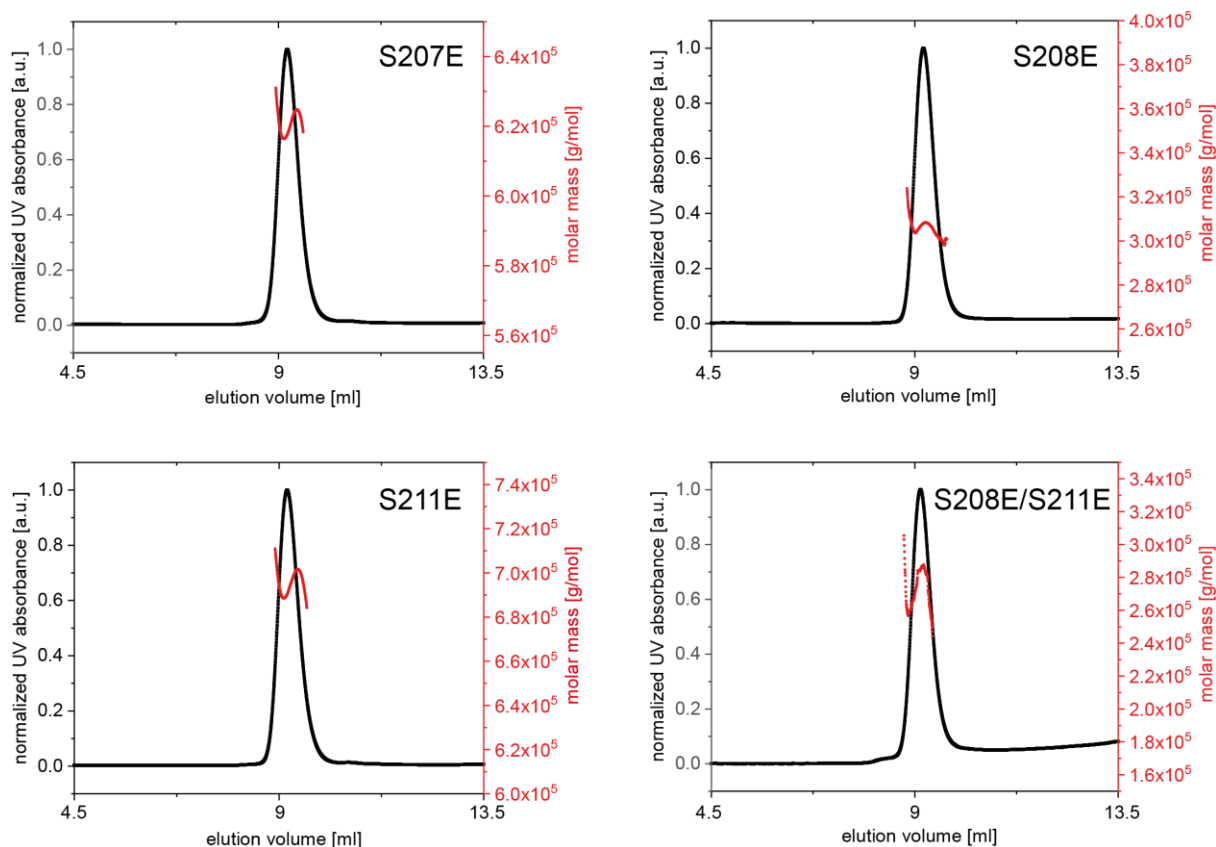
Figure 14: Hsp26 oligomers are polydisperse. *The oligomer size of the proteins was determined with SEC-MALS. 2 nmol of the protein samples were separated with a Superdex200 increase 10/300GL column at a flow rate of 0.45 ml/min.*

As a third method to determine the size of oligomer complexes, AUC was used (see 2.2.17). In this case, the samples were not diluted during the measurement and no interaction with the column matrix was taking place, which could also have an influence on the oligomer size. All protein complexes except for the S47E/T48E and the S90E mutant exhibited a sedimentation coefficient of 24 - 25 S, which corresponds to a 24-mer according to the size prediction (Figure 15A). For the S90E two species were observed in the AUC. One with a sedimentation coefficient of ca. 16 S and the second with a sedimentation coefficient of ca. 20.5 S. The calculated masses would fit to a 12- and an 18-mer. The S47E/T48E complexes also sedimented at ca. 16 S, which corresponds to a 12-mer. In summary, at 25 °C most of the mutants form big, WT-like complexes. As expected from the HPLC and CD measurements, the *all-phospho* mutant did not form oligomers and the main peak sedimented at 2 S. Even though the mass prediction indicated rather a monomer, presumably dimers are formed based on the results from the SEC-HPLC measurements, as the mass predication from the S-value is usually not very accurate. Furthermore, it could be shown with AUC that the complexes dissociate upon dilution, exemplary shown for the WT and the S144E mutant (Figure 15B). This might explain the dimer formation on the SEC column.

A
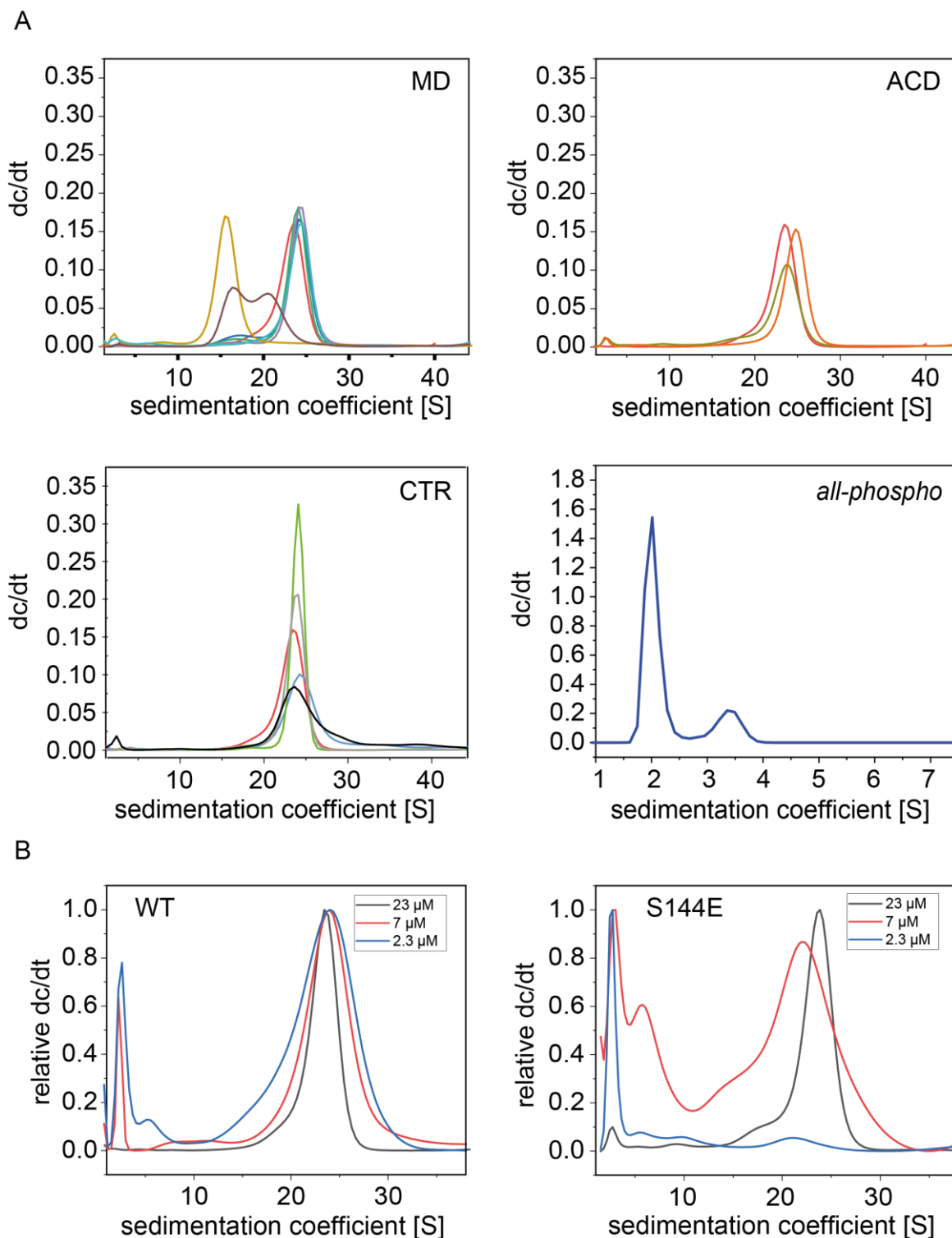
Figure 15: Hsp26 forms big oligomers dependent on the concentration. *A) AUC was measured at a concentration of 23 µM at 35,000 rpm and 20 °C in PBS. Sedimentation was followed by UV absorption at 280 nm. Upper left panel: Mutants of the MD: WT: red, T42E: blue, S47E: green, T48E: purple, S47E/T48E: beige, T69E: cyan, S90E: brown. Upper right panel: Mutants of the ACD: S144E: green, T163E: orange. Center left panel: mutants of the CTR: S207E: blue, S208E: green, S211E: gray, S208E/S211E: black. Center right panel: all-phospho mutant. B) To analyze concentration dependent oligomerization, the proteins were measured at different concentrations (black: 23 µM, red: 7 µM and blue: 2.3 µM). On the left, the WT protein is shown, on the right an exemplary mutant (S144E). AUC runs were performed by Pamina Kazman.*

3.1.2 Phosphomimetic mutations modulate the activity of Hsp26 *in vitro*

The activity of Hsp26 and the mutants was measured *in vitro* at different temperatures and with different substrate proteins. At 25 °C, aggregation of chemically denatured insulin was measured, at 37 °C and reducing conditions the aggregation of lysozyme, at 42 °C yeast lysate assays were performed and at 44 °C MDH was used as a substrate.

3.1.2.1 Phosphorylation in the ACD and CTR activates Hsp26 at 25 °C

To check whether phosphomimetic mutations lead to activated Hsp26 already at 25 °C under reducing conditions, insulin assays were performed (2.2.15.1). As expected, the WT protein was not able to efficiently suppress the aggregation of chemically denatured insulin under the tested conditions (Figure 16A). Nevertheless, almost 50 % suppression of the signal for aggregation were reached with 8 µM Hsp26 WT. This concentration was selected for the comparison with the mutants, as it seemed well suited to determine differences. Most substitutions in the MD suppressed insulin aggregation efficiently for approximately 30 min (Figure 16B). Then, an increase of the light scattering signal was observed. The effect was small for the T69E mutant and the double mutant S47E/T48E. The curve of the S90E mutant showed the sharpest increase and finally even more light scattering than in the *insulin alone* sample was observed, which indicates co-aggregation. Both ACD mutants were fully active and suppressed insulin aggregation completely (Figure 16C, F). The CTR mutants also were more active than the WT (Figure 16D, F). The S211E and S208E/S211E mutant completely suppressed insulin aggregation over 70 min. The other two mutants did not work as efficiently but still led to a 70 % suppression of the aggregation signal. The *all-phospho* mutant was also fully active, even at 4 µM, which fits to the results of the previous paragraph, in which a small, possibly activated species was suggested (Figure 16E). As the assay kinetics with the MD mutants implied the formation of fibrillary aggregates (Mainz et al., 2015), the morphology of the aggregates was analyzed in more detail with TEM (2.2.19.3). Indeed, in the presence of Hsp26, long stretched aggregates, which resembled fibrils, were formed. Insulin alone formed rather amorphous aggregates (Figure 16G). Hsp26 alone did not form any aggregates over 60 min.
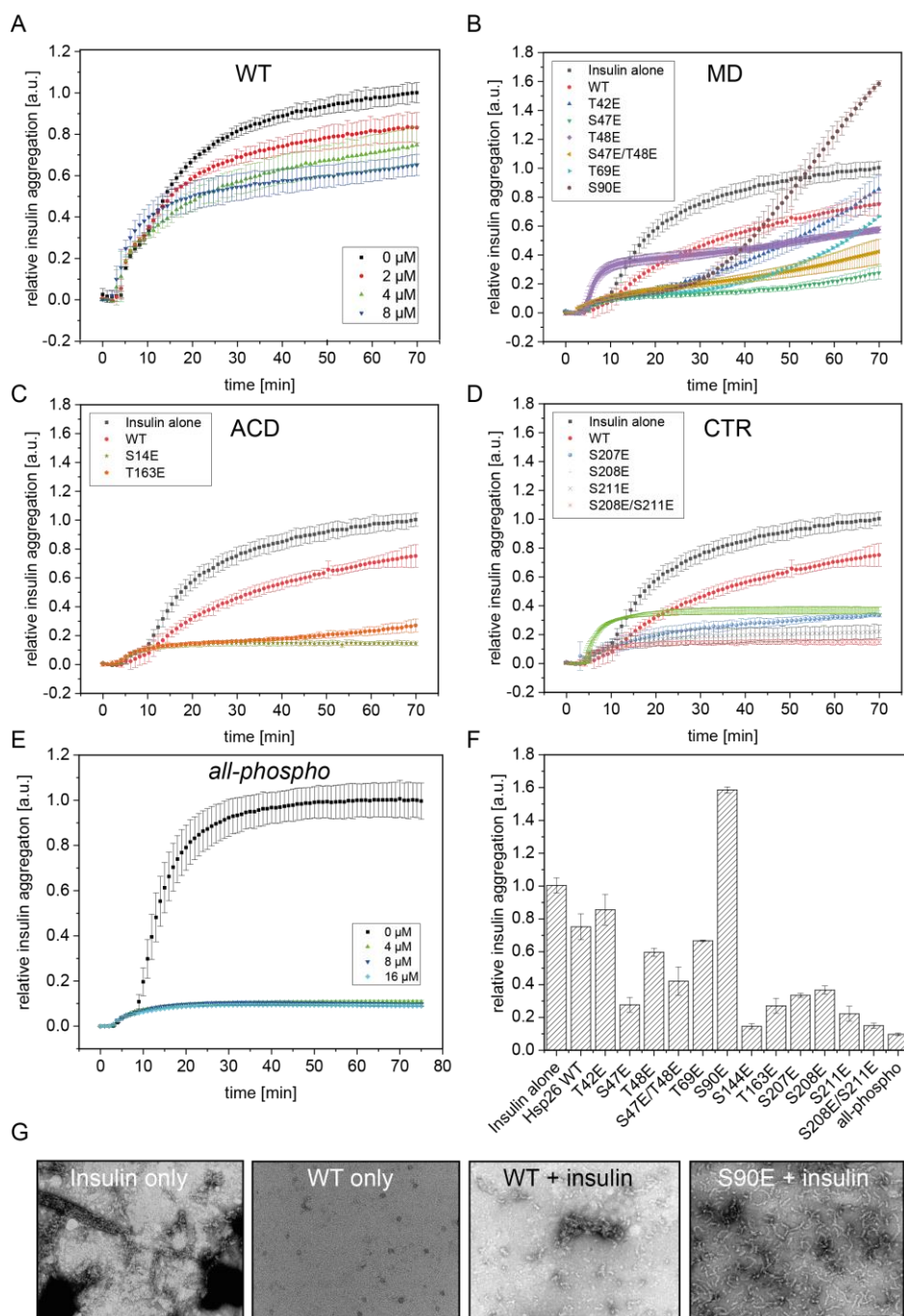
Figure 16: Phosphomimetic mutations in the ACD and CTR activate Hsp26 at 25 °C. *A) Hsp26 was titrated to 40 μM insulin at different concentrations (0 μM (black square), 2 μM (red circle), 4 μM (green triangle) and 8 μM (blue inverted triangle)). The reaction was started by the addition of 20 mM DTT to reduce the substrate. Light scattering was measured for 70 min at 360 nm. B) In comparison to the WT (red circle), the insulin assay was performed with 8 μM of the MD phosphomimetic mutants. T42E: blue triangle, S47E: green inverted triangle, T48E: purple diamond, S47E/T48E: beige triangle (pointing left), T69E: cyan triangle (pointing right), S90E: brown hexagon. C) Insulin assay with the ACD mutants. S144E: green star, T163E: orange pentagon. D) Insulin assay with the CTR mutants: S207E: blue circle, S208E: green line, S211E: black cross, S208E/S211E: red cross. E) Insulin assay with the all-phospho mutant (titration: 0 μM (black square), 4 μM (green triangle), 8 μM (blue inverted triangle) and 16 μM (cyan diamond)). Mean values and standard deviation were calculated from three replicates. F) Comparison of the endpoints of the aggregation assays shown in figure parts B-E. G) After 60 min, samples were taken off for TEM analysis. The pictures were taken at a magnification of 50,000x. Scale bar: 200 nm. TEM pictures were taken by Pamina Kazman.*

3.1.2.2 Heat activation does not activate the phosphomimetic mutants additionally

Next, the *in vitro* activity of the chaperones was measured with lysozyme as a model substrate at 37 °C under reducing conditions (see 2.2.15.2), which represents mild heat shock for *S. cerevisiae*. The WT already became activated at 37 °C and suppressed the aggregation of lysozyme in equimolar ratio or molar excess (Figure 17A). In substoichiometric ratio (1:2), the aggregation was only primarily suppressed. After 25 min, Hsp26 seemed to co-aggregate. Thus, equimolar substrate-chaperone concentrations were chosen for the comparisons. Most of the MD mutants were not active anymore in the lysozyme assay (Figure 17B). Only the S47E and the T69E mutant behaved WT-like. All other mutants co-aggregated whereas the course of the curve again implied that the aggregates might be fibrillary. The ACD mutants that were fully active in the insulin assay lost their activity at 37 °C (Figure 17C, F). Except from the S208E mutant, the CTR mutants were all fully active and thus retained their activated conformation (Figure 17D, F). The *all-phospho* mutant still suppressed the aggregation of lysozyme but not as efficiently as the WT (Figure 17E). In 1:1 ratio, around 80 % suppression was achieved. At 2-fold chaperone excess, lysozyme aggregation was approximately 70 % suppressed. Interestingly, also with this mutant co-aggregation was observed after 25 min in a substoichiometric ratio (1:2).

At 44 °C, MDH was used as a model substrate (see 2.2.15.3). As expected, the WT inhibits MDH aggregation efficiently even in substoichiometric concentrations (Figure 18A). In the MDH assay, most of the single/double mutants suppressed the aggregation comparably to the WT (Figure 18B-D, F). The T48E and the S208E mutant alone, which were both reported to occur as double phosphorylations (in combination with S47 or S211), were less active than the WT. The *all-phospho* mutant did not suppress MDH aggregation efficiently (Figure 18E). Even in 2-fold excess, only a delayed and approximately 10 % reduced aggregation were observed. Notably, the *all-phospho* mutant was not completely inactive at 44 °C. In an insulin assay performed at 44 °C, it still suppressed the aggregation of this model substrate (Figure 18E).
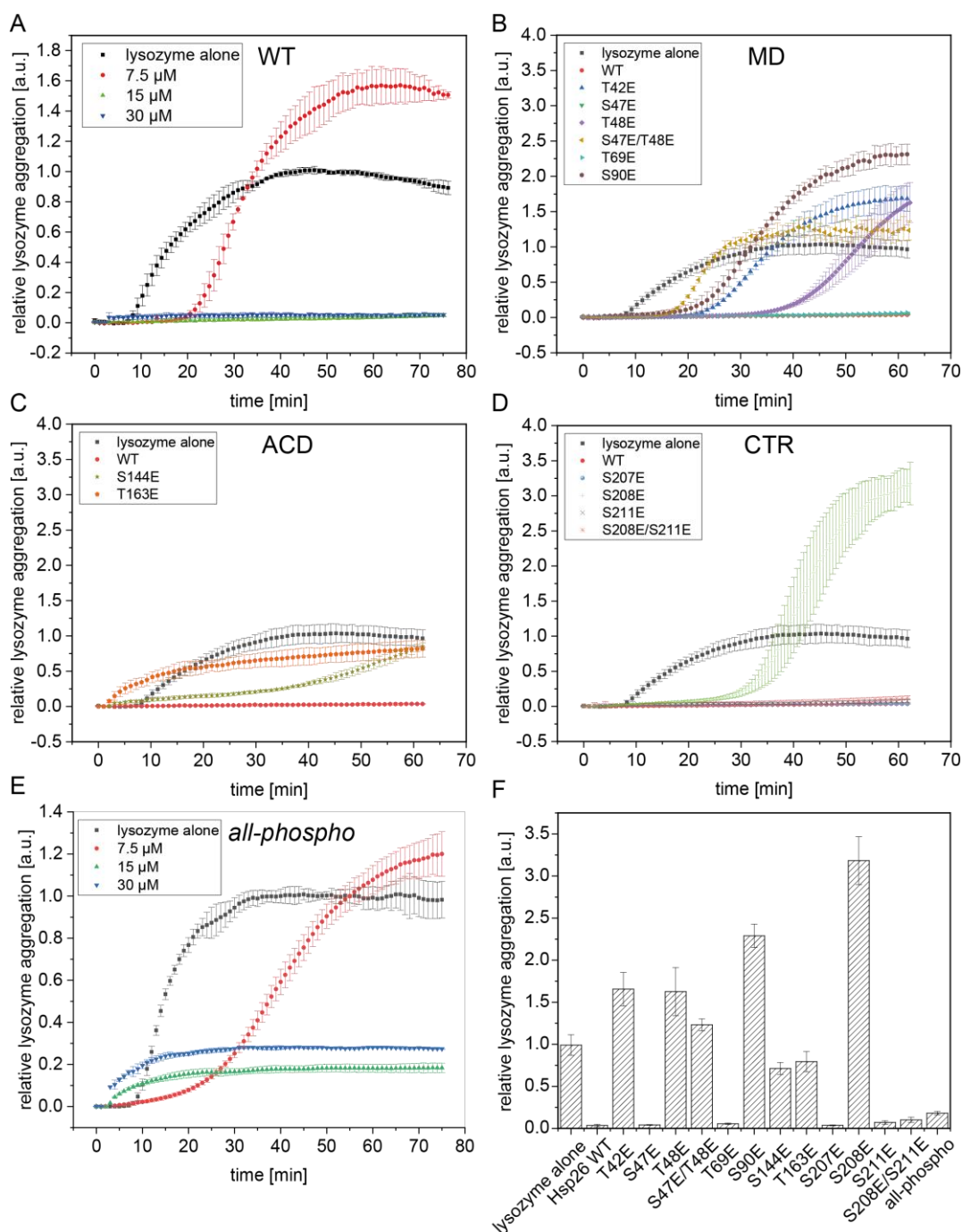
Figure 17: Phosphomimetic mutations in the CTR are activating under mild heat stress.
A) Hsp26 was titrated to the lysozyme assay at different concentrations (0 μM (black square),
7.5 μM (red circle), 15 μM (green triangle) and 30 μM (blue inverted triangle)). After 10 min
pre-incubation at 37 °C, the reaction was started by the addition of 1 mM TCEP. Aggregation
was followed in a photometer at 360 nm. B) In comparison to the WT (red circle), the lysozyme
assay was performed with 15 μM of the MD phosphomimetic mutants. T42E: blue triangle,
S47E: green inverted triangle, T48E: purple diamond, S47E/T48E: beige triangle (pointing left),
T69E: cyan triangle (pointing right), S90E: brown hexagon. C) Lysozyme assay with the ACD
mutants. S144E: green star, T163E: orange pentagon. D) Lysozyme assay with the CTR
mutants: S207E: blue circle, S208E: green line, S211E: black cross, S208E/S211E: red cross.
E) Lysozyme assay with the all-phospho mutant (titration: 0 μM (black square), 7.5 μM (red
circle), 15 μM (green triangle) and 30 μM (blue inverted triangle)). Mean values and standard
deviation were calculated from three replicates. F) The endpoints of all measurements shown
in figure parts B-E are plotted in a bar chart.
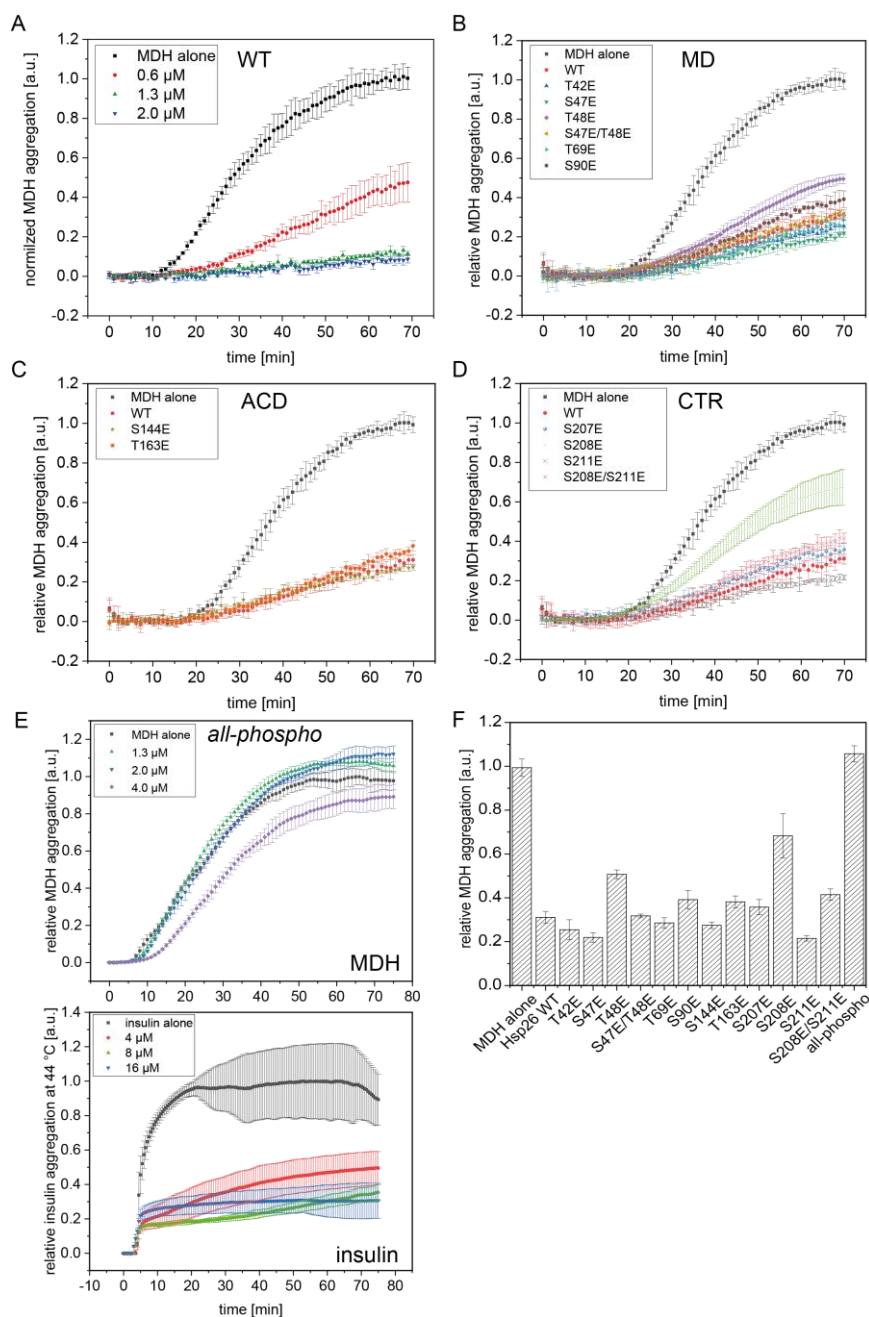
Figure 18: Heat activated Hsp26 is not activated further by phosphomimetic mutations.
A) Hsp26 was titrated to the MDH assay at different concentrations (0 µM (black square), 0.6 µM (red circle), 1.3 µM (green triangle) and 2 µM (blue inverted triangle)). After 10 min pre-incubation at 44 °C, the reaction was started by the addition of 2 µM MDH. MDH aggregation was followed in a photometer for 75 min at 360 nm. B) In comparison to the WT (red circle), the MDH assay was performed with 1.3 µM of the MD phosphomimetic mutants. T42E: blue triangle, S47E: green inverted triangle, T48E: purple diamond, S47E/T48E: beige triangle (pointing left), T69E: cyan triangle (pointing right), S90E: brown hexagon. C) MDH assay with the ACD mutants. S144E: green star, T163E: orange pentagon. D) MDH assay with the CTR mutants: S207E: blue circle, S208E: green line, S211E: black cross, S208E/S211E: red cross. E) Upper panel: MDH assay with the all-phospho mutant (titration: 0 µM (black square), 1.3 µM (green triangle), 2.0 µM (blue inverted triangle) and 4 µM (purple diamond)). Lower panel: Insulin assay at 44 °C with the all-phospho mutant (titration: 0 µM (black square), 4 µM (red circle), 8 µM (green triangle) and 16 µM (blue inverted triangle)). Mean values and standard deviations were calculated from three replicates. F) The endpoints of all measurements shown in figure parts B-E are plotted in a bar chart.

Finally, the lysate of the *HSP26Δ* BY4741 yeast strain was used to provide authentic substrates and to imitate the physiological conditions better. This assay was performed at 42 °C as described in 2.2.15.4. Hsp26 variants were spiked in at different concentrations and the reactions were incubated for 1.5 h at 42 °C. After centrifugation, the pellet fraction was analyzed by SDS-PAGE (Figure 19A). The presence of Hsp26 WT (16 µM) led to a 50 % reduction of aggregation. The mutants seemed to be comparably active as the WT. The substitutions T42E and T48E in the MD increased the activity in comparison to the WT (Figure 19B). S47E and T69E were as active as the WT and S47E/T48E as well as S90E performed slightly less well than the WT but still led to 40 % less aggregation than without chaperone.
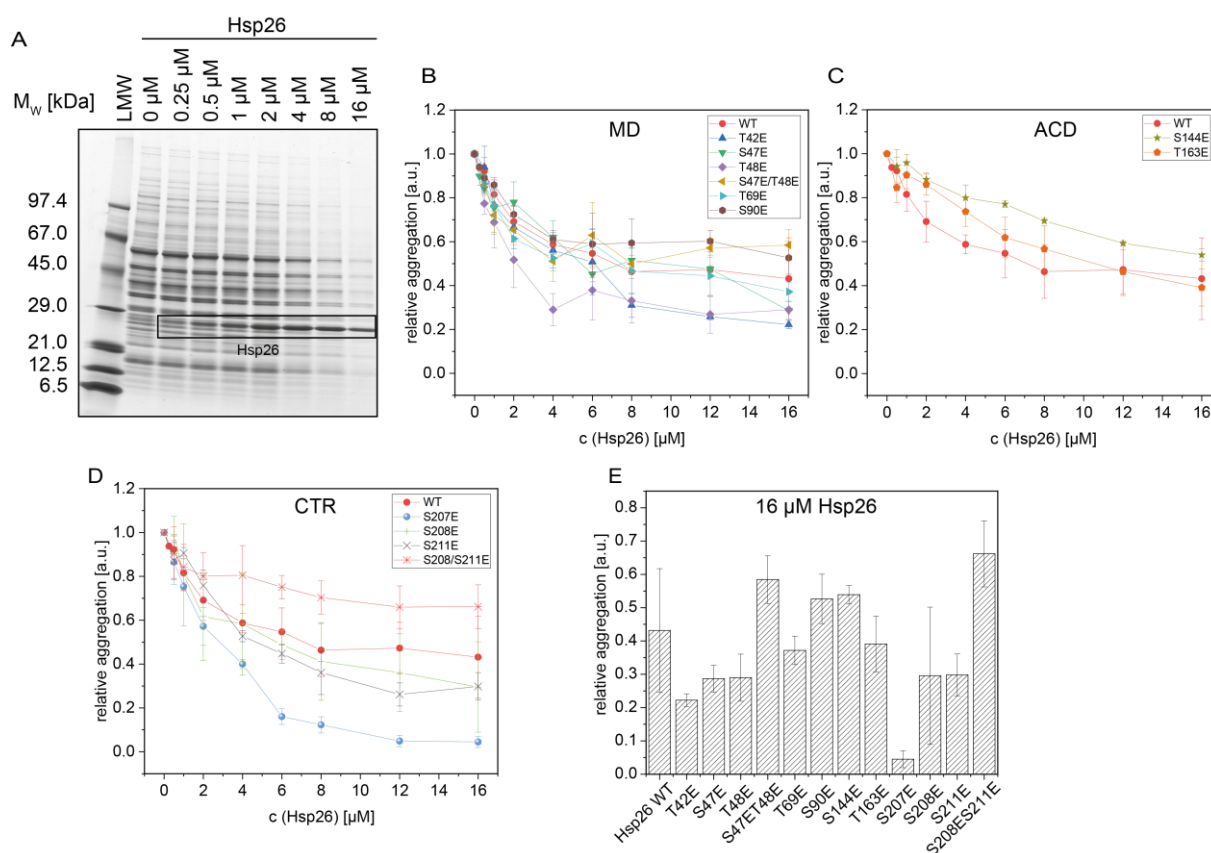
Figure 19: Hsp26 efficiently suppresses aggregation of proteins in the yeast lysate. A) Exemplary gel of one replicate of a lysate assay with Hsp26 WT. The chaperone was titrated at different concentrations to 0.8 mg/ml lysate protein solution and incubated for 90 min at 42 °C. Afterwards, the soluble fraction was loaded onto a SDS gel and the lane intensities were quantified. The Hsp26 band was excluded from the quantification. For each protein, triplicate measurements were performed. LMW: low molecular weight marker. B) Lysate assay with MD phosphomimetic substitutions. WT: red circle, T42E: blue triangle, S47E: green inverted triangle, T48E: purple diamond, S47E/T48E: beige triangle (pointing left), T69E: cyan triangle (pointing right), S90E: brown hexagon. C) Lysate assay with ACD mutants. S144E: green star, T163E: orange pentagon. D) Lysate assay with the CTR mutants: S207E: blue circle, S208E: green line, S211E: black cross, S208E/S211E: red cross. Mean values and the standard deviation are shown. E) The aggregation suppression (mean ± SD) at 16 µM Hsp26 concentration was plotted to compare all mutants.

For the S90E mutant this was not astonishing, as this mutation turned out as compromised in all experiments. Substitution of S144 also led to a decline of the activity in comparison to the WT, T163E was equally active as the WT (Figure 19C). The CTR mutations tended to be more effective than the WT in the lysate assay. Although the single mutants S208E and S211E were slightly more efficient than the WT, the combination of both led to an activity decline in comparison to the WT. The best performing mutant in this assay was the S207E mutant, which suppressed the aggregation of the lysate proteins by 90 % (Figure 19E).

3.1.3 Phosphomimetic Hsp26 mutants do not lead to a changed phenotype *in vivo*

To analyze the effect of the different mutations *in vivo*, the gene sequences were cloned into p416GPD vectors and transformed into BY4741 *HSP26Δ* (2.2.1.1-2.2.1.5; 2.2.2.5.2). From this vector, the proteins were constitutively expressed. Thus, the expression levels were approximately 10-times higher than the levels of non-stressed logarithmic growing BY4741 cells (Figure 20A). The expression levels of the proteins expressed from the vector seemed to be comparable. Spot assays did not indicate a difference in growth, neither at 25 °C nor under mild heat stress at 37 °C, ethanol (8 %) stress or proteotoxic stress induced by 10 mM azetidine-2-carboxilic acid (AZC) (Figure 20B). On AZC, the cells did not grow well. With the *all-phospho* mutant and the WT, also heat shock cycles (30 min 42 °C, 30 min 25 °C; three times) were tested. Again, no difference in comparison to the *HSP26* KO cells was observed.
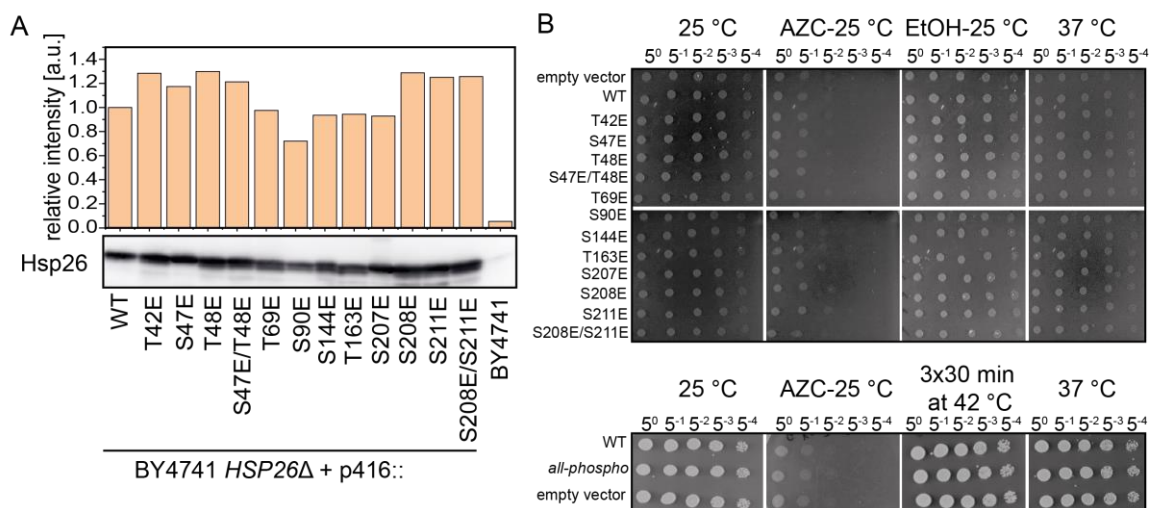
Figure 20: Expression of phosphomimetic mutants only has small phenotypic effects.
A) The Hsp26 content in the total protein fraction of BY4741 HSP26Δ cells transformed with p416::HSP26 WT or mutants that were expressed constitutively under a GPD promoter was analyzed with western blot. The band intensities were quantified densitometrically and normalized to the intensity of the overexpressed WT protein. To be able to estimate the overexpression from the vector, the lysate of unstressed BY4741 WT cells was loaded as a reference. B) Yeast cells were spotted in 1/5 dilution steps onto CSM plates and grown for 48 h. Besides temperature, 8 % ethanol (EtOH) or 10 mM AZC were used as stressors.

As a more sensitive approach to analyze the activity of the chaperones *in vivo*, the cells were additionally transformed with destabilized firefly luciferase-GFP, which also was constitutively expressed under the GPD promoter (Gupta et al., 2011). This firefly luciferase is prone to aggregation and works well as a reporter for proteotoxic stress. Because of the fusion to GFP, aggregate formation can be well followed via fluorescence microscopy *in vivo* (Figure 21A). For the evaluation, the cells were classified into cells without aggregates (orange bars), cells with small and multiple aggregates (n ≥ 3; green bars) and cells with one or two big aggregates (purple bars). Aggregate formation was induced by heat stress (42 °C for 30 min). Interestingly, Hsp26 WT was the best chaperone concerning the suppression of luciferase-GFP aggregation. Around 70 % of the cells expressing Hsp26 WT showed no aggregates and if there were aggregates, they were packed in big foci and not in small/numerous aggregates. Cells expressing the S47E mutant also showed decreased aggregation (64 %). Nevertheless, if the cells had aggregates, those were small and numerous. In contrast, all other mutants exhibited comparable phenotypes as the empty vector control (19 % no aggregates, 35 % big aggregates, 46 % small aggregates). Hence, proteostasis under heat stress is clearly not improved by the expression of the mutants. Notably, in the *all-phospho* mutant, an extraordinary high amount of cells with foci was observed and all of them were small and granular (80 % small aggregates, 20 % no aggregates). To shed more light on Hsp26 aggregate sequestration, yeast cells transformed with the respective Hsp26 variants, were stressed for 30 min at 46 °C to induce the formation of stress granules and other cellular deposits (Cherkasov et al., 2015). After the stress, the cells were recovered to check if Hsp26 becomes soluble again and if the phosphomimetic mutations affect the resolubilisation during recovery. Therefore, the cells were lysed after the stress and the insoluble fraction was separated by centrifugation. The Hsp26 content in the supernatant and pellet fraction was determined by western blots (2.2.12.3). As expected, Hsp26 WT was found to be completely soluble at 25 °C (Figure 21B). After 30 min at 46 °C, it was also present in the pellet and accordingly decreased in the soluble fraction. After 30 min of recovery, Hsp26 WT was completely soluble again. Thus, Hsp26-containing pelleted deposits became soluble again. Principally, the same behavior was observed for all tested Hsp26 mutants. However, some mutants such as T48E, T69E or S144E were already present in the insoluble fraction at 25 °C. Under heat stress, the levels in the pellets increased strongly and after 30 min of recovery, there was still some Hsp26 present in the insoluble fraction. Mutations in the CTR mostly led to a strong enrichment in the pellet fraction under stress but also a very efficient dissolution of the aggregates during recovery. Additionally, the amount of insoluble Hsp26 S211E and S208E/S211E after recovery seemed to be smaller than before the HS. BY4741 WT cells were also included in the analysis, but could not be evaluated equally as the endogenous Hsp26 levels were too low. The S47E mutant that looked active in the microscopic analysis of firefly

luciferase behaved WT-like concerning aggregate formation and recovery in this experiment, as well.
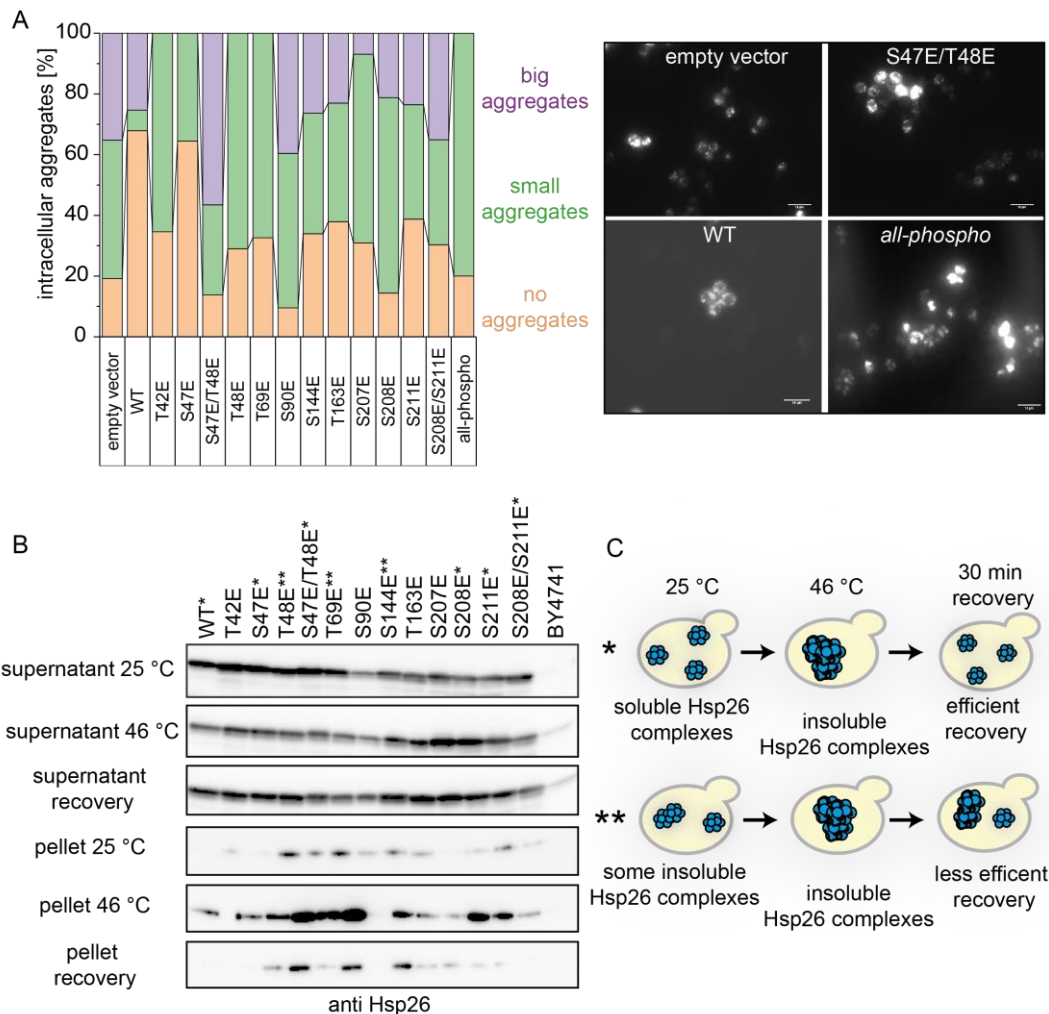
Figure 21: The heat-activated Hsp26 WT is the best performing chaperone in vivo. *A) BY4741 HSP26Δ were transformed with the indicated Hsp26 variants and destabilized firefly luciferase-GFP fusion constructs that were also expressed constitutively from p425GPD. The cells were stressed for 30 min at 42 °C to induce aggregation of the luciferase. For the classification of the aggregation phenotype, 100 cells were counted. Pictures of the cells were taken at a magnification of 1,600x. The scale bar represents 10 µm. B) To analyze the Hsp26 content in the supernatant and pellet fraction under non-stress, stress (30 min at 46 °C) and after recovery (30 min at 25 °C), respectively, the cell lysate was separated by centrifugation and analyzed with western blots. Mutants that behaved WT-like are marked with an asterisk (*). Mutants that were enriched in the pellet and less efficient in their recovery are marked with two asterisks (**). C) Model for the effects observed in figure part D. *: Hsp26 is soluble under non-stress condition and enriched in the pellet after incubation of the cells at 46 °C. After 30 min at 25 °C (recovery), Hsp26 is (almost) completely soluble again. **: Hsp26 is already present in the pellet at 25 °C. Upon heat stress, it is further pellet-enriched and during recovery, Hsp26 cannot be dissolved again completely.*

In conclusion, two groups were observed (Figure 21C). One that behaved WT-like, soluble at 25 °C, enriched in the pellet at 46 °C and again soluble after recovery (*). Several mutants however, tended to be more pellet-enriched already under non-stress conditions and the

insoluble Hsp26 complexes could not be cleared completely during recovery (second group: **) (Figure 21C). Although some differences were observed in the *in vivo* experiments, the effects were rather small. It became clear that under the tested conditions, that mostly included heat stress, the WT chaperone is the most efficient and none of the phosphomimetic mutants led to more stress-resistant yeast cells. This is in accordance with the *in vitro* activity measurements, in which no mutant could clearly outcompete the heat-activated Hsp26 WT.

3.1.4 Hsp26 forms big substrate complexes

As it was described before, Hsp26 is able to suppress the temperature-induced aggregation of lysozyme and MDH *in vitro*. To gain more insight into the complex formation with the substrates, the morphology as well as dynamics of the Hsp26 – substrate complex formation were followed with TEM (2.2.19.3). Lysozyme was chosen as a first model substrate because this aggregation assay is performed at 37 °C. According to the thermal transition measurements, the oligomer should not dissociate at 37 °C and thus be visible in TEM throughout the whole time course of the experiment. Indeed, the Hsp26 oligomers were stable (Figure 22A). As expected, lysozyme alone initially formed small aggregates, which grew to big filamentous aggregates within 30 min at 37 °C (Figure 22B). The addition of 15 µM Hsp26 (1:1 ratio) suppressed lysozyme aggregation completely as it was also observed in the *in vitro* aggregation experiments (Figure 22C). With TEM, the structural changes that occur during substrate complex formation could be followed. After 10 min, the originally spherical Hsp26 complexes formed big drawn-out structures that were quite heterogeneous. After 20 min, the complexes remained oval but overall the shapes were more similar to each other than 10 min earlier. The biggest complexes were around 1.5 times as big as the Hsp26 WT alone. After 30 min the Hsp26 – substrate complexes became mostly spherical again but still seemed to be slightly bigger than the Hsp26 complexes alone. Importantly, at no time point oligomer dissociation was observed in the Hsp26 alone sample. This implies that the Hsp26 oligomer can interact with the unfolded substrate and does not necessarily have to decompose into smaller species to be activated and to be able to interact with the substrate.
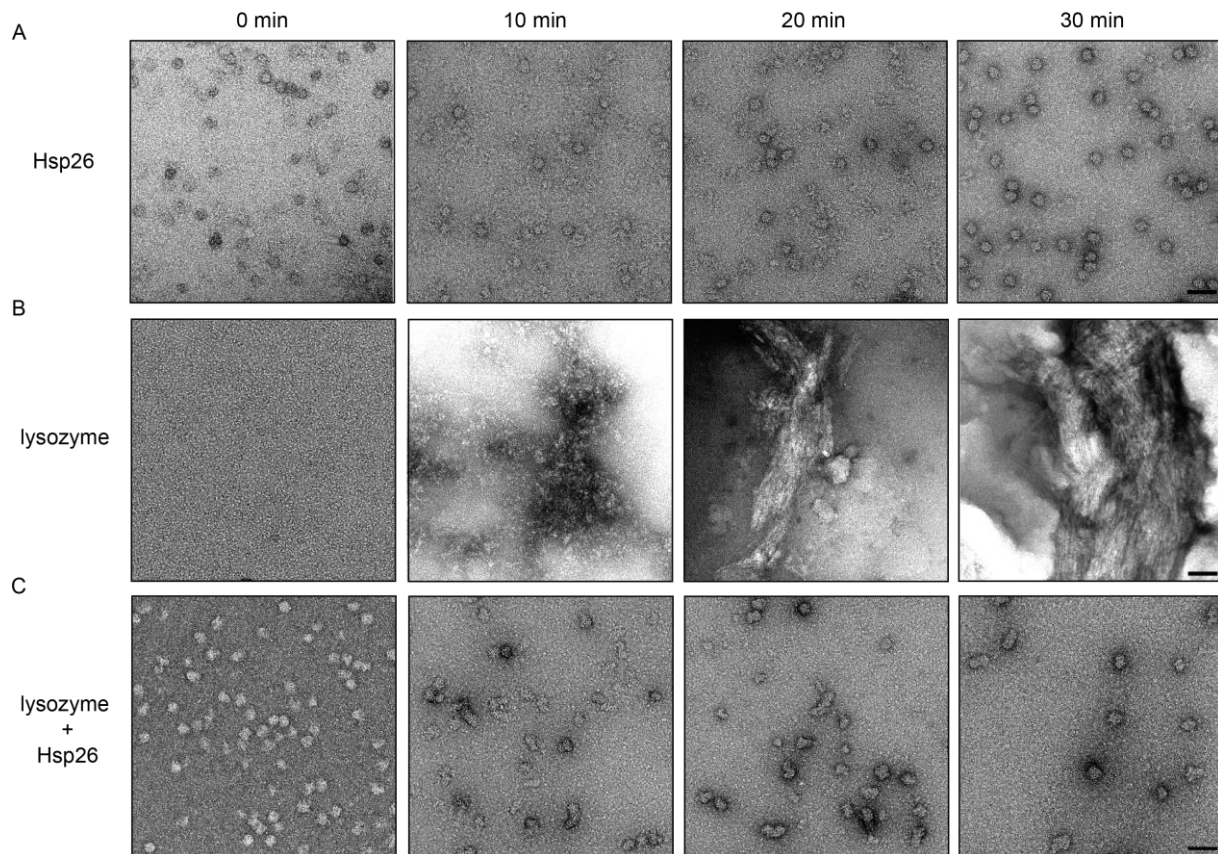
Figure 22: Hsp26 and lysozyme form big sHsp - substrate complexes. *The lysozyme aggregation assay was performed as described in the caption of figure 17 with 15 µM Hsp26 and 15 µM lysozyme. The first sample for TEM was taken immediately after the reaction was started, the other samples were taken after 10 min, 20 min and 30 min, respectively. A) Hsp26 alone. B) Lysozyme alone. C) Hsp26 and lysozyme. Scale bar: 50 nm. TEM pictures were taken by Dr. Carsten Peters (Prof. Sevil Weinkauf).*

Next, MDH was chosen as a model substrate for complex formation at 44 °C. At this temperature, the oligomer should dissociate according to the thermal transition measurements. MDH alone forms big amorphous aggregates at 44 °C as expected (Figure 23A). The previous observation that the Hsp26 oligomer dissociates at this temperature could be confirmed with TEM. The amount of big oligomers rapidly decreased and within 5 min almost all large oligomers were gone (Figure 23B). Nevertheless, some heterogeneous smaller oligomers were still observable up to 20 min. When MDH (2 µM) and Hsp26 (1.3 µM) were incubated together, the oligomers dissociated much faster and were already gone after the first minute (Figure 23C). Interestingly, already after 2 min, a few bigger complexes were visible. Those complexes grew in size and number until 20 min with the biggest substrate complexes exhibiting about double the size of the Hsp26 oligomer. Big Hsp26 - substrate complexes were also observed with other substrates such as citrate synthase or rhodanese (Stromer et al., 2003). Similarly to the lysozyme assay, the big sHsp – substrate complexes seemed to decrease in size again and most of the protein persisted in complexes that were much smaller than the Hsp26 complexes alone (40 min and 60 min).

A MDH

0 min | 2 min | 5 min | 20 min

B Hsp26

0 min | 1 min | 2 min | 5 min

10 min | 20 min | 40 min | 60 min

C MDH + Hsp26

0 min | 1 min | 2 min | 5 min

10 min | 20 min | 40 min | 60 min
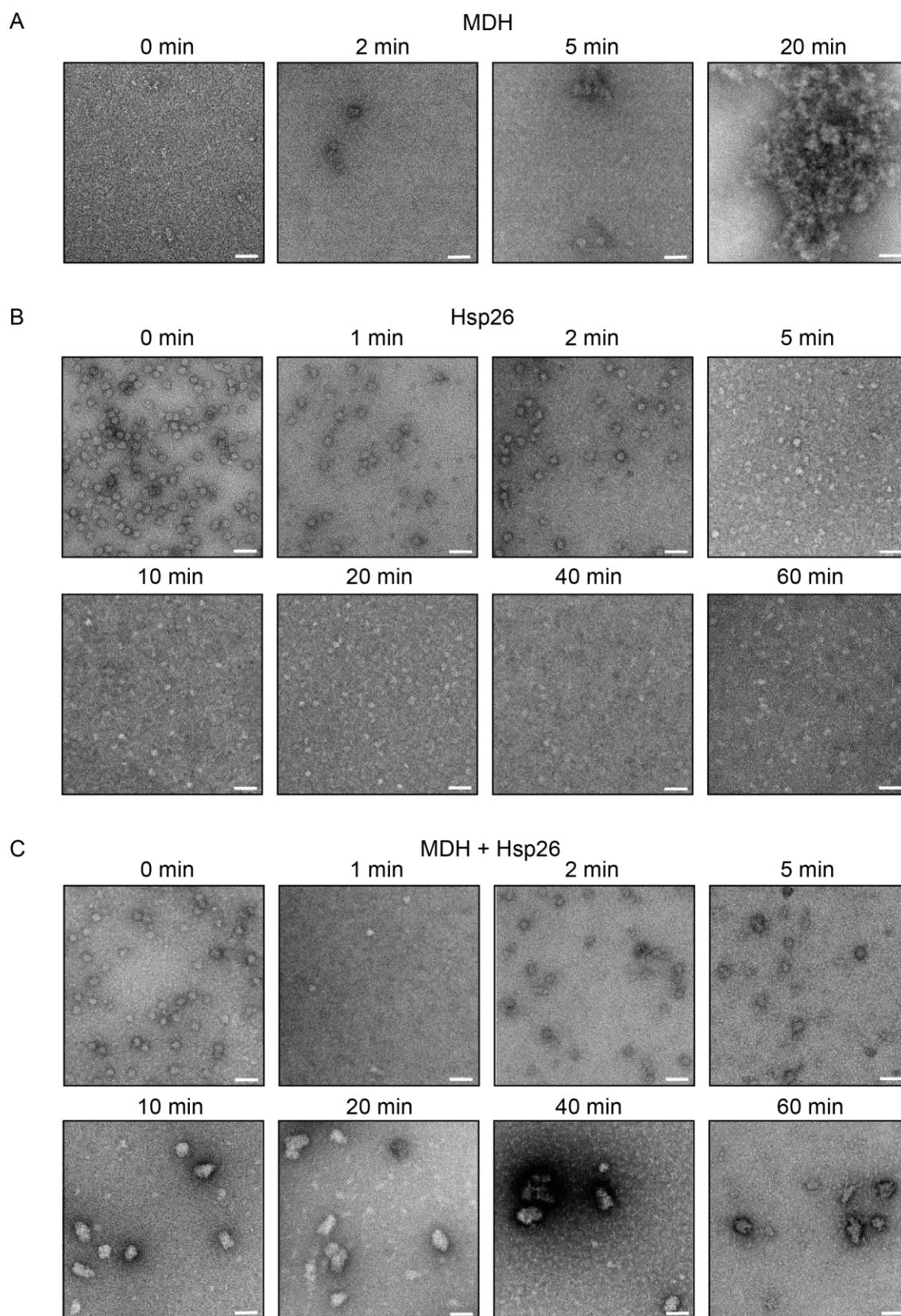
Figure 23: Hsp26 dissociates before big substrate complexes with MDH are formed. *The aggregation assay was performed as described in the caption of figure 18 with 1.3 µM Hsp26 and 2 µM MDH. The first sample for TEM was taken immediately after the reaction was started. The other samples were taken after 1, 2, 5, 10, 20, 40 and 60 min, respectively. A) MDH alone. B) Hsp26 alone. C) Hsp26 and MDH. Scale bar: 50 nm. TEM pictures were taken by Dr. Carsten Peters (Prof. Sevil Weinkauf).*

Hence, in this case the oligomer was activated, dissociated and the substrate complexes seemed to assemble from smaller Hsp26 species, which is in contrast to the observation made with lysozyme. Both experiments together imply that the formation of Hsp26 – substrate complexes is possible with an activated oligomer as well as with an activated smaller species.

3.1.5 Structure and dynamics of the Hsp26 oligomer

3.1.5.1 H/DX indicates an interaction of the Hsp26 MD and an ACD-loop

To understand the mechanism of the function and substrate interaction of Hsp26 in more detail, the protein structure was studied extensively. First, the dynamics of the exchange of hydrogen atoms of Hsp26 in the context of the oligomer were analyzed. As shown above, the oligomer seems to be able to interact with unfolding substrates. If this is the case, substrate interaction sites have to be accessible also in the oligomer and should not be buried completely. Hydrogen/deuterium exchange (H/DX) coupled to mass spectrometry is well suited to analyze the accessibility of amino acids with peptide resolution (see 2.2.18). To cover the dynamics of the hydrogen exchange, mass spectra were measured after 10 s, 1 min, 10 min, 30 min and 120 min, respectively. In comparison to the WT, two phosphomimetic mutants that were conspicuous in the *in vitro* assays were measured to see if and how phosphorylation changes the exposure of peptide stretches. The WT sequence was covered from amino acid (aa) 3 to 211 (Figure 24A; Figure S1A). Thus, four amino acids of the CTR were missing. Furthermore, the MS spectrum of the WT lacked the peptide 148 - 152. In the NTS (aa 1 - 30) of the WT, moderate exchange rates were observed. The first N-terminal amino acids exhibited 32 % exchange that already occurred within the initial 10 s and hardly changed further. In the MD, a 28 aa long sequence (aa 34 - 62) exhibited 52 % exchange rates, which indicates that this part is flexible and accessible also in the oligomer. The rest of the MD seemed to be more buried again (21 % - 44 %) except from residues 69 - 71 (~ 60 % exchange). The ACD consists of β-sheets and is mostly well structured. Therefore, in this domain of the protein low exchange rates were observed (mostly between 10 and 30 %). Only in one loop (aa 139 - 143), high H/DX rates of 56 % were observed. The CTR also seemed to be buried in the oligomer and was not solvent accessible as it exhibited comparable or only slightly higher exchange rates of around 20 %. In order to identify the parts of the protein, in which structural changes have to occur that facilitate oligomer decomposition, S47E/T48E and S144E were analyzed in comparison to the WT protein. Those mutants tended to form smaller species or at least formed less stable oligomers, which should be reflected by partially higher exchange rates in the H/DX profile. Unfortunately, in both mutants, the CTR was almost missing completely (Figure S1B, C). Furthermore, the first nine N-terminal amino acids were lacking in the mutant spectra. The rest of the NTS of both mutants looked almost exactly the same as the WT NTS.
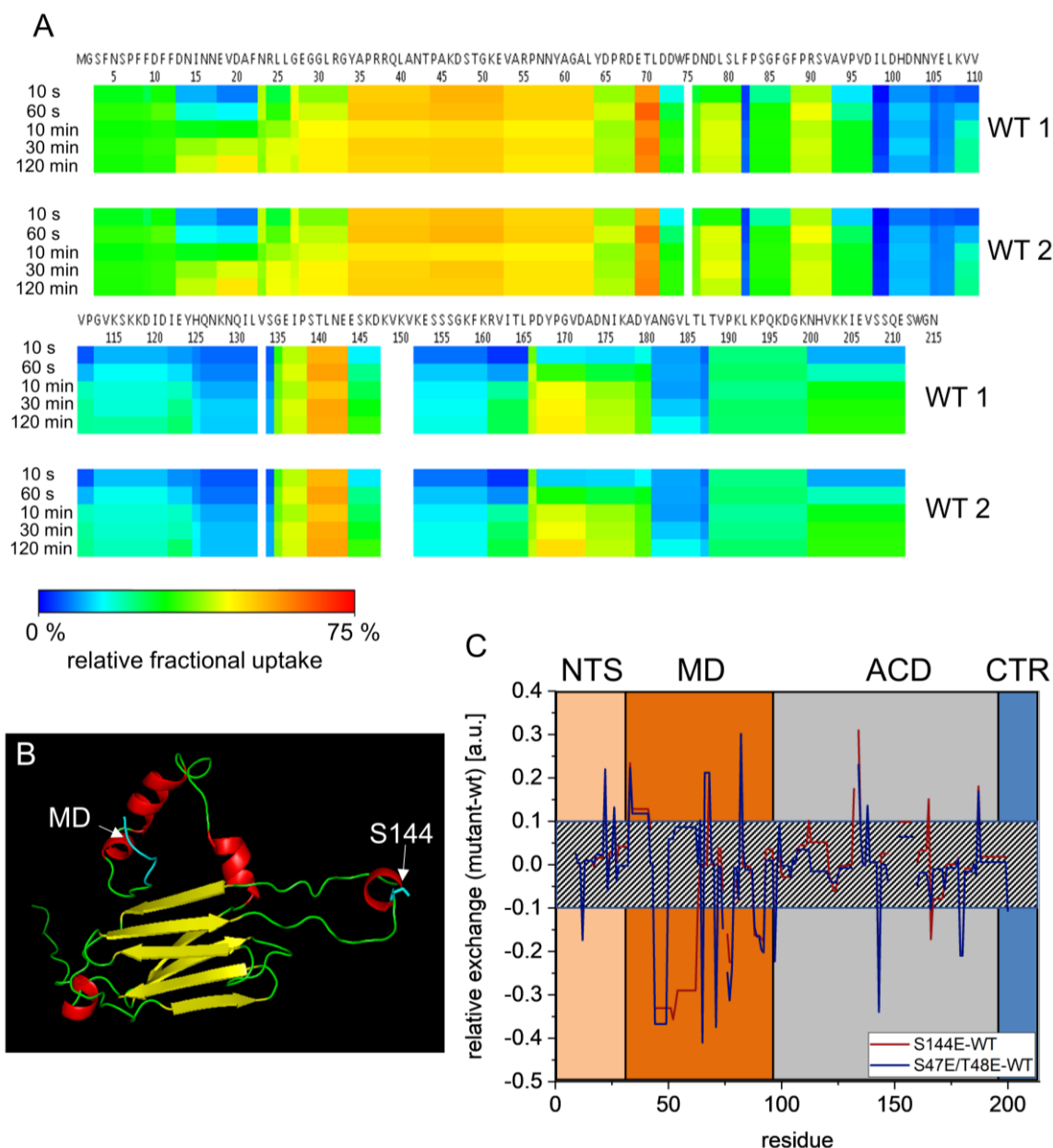
Figure 24: Phosphomimetic mutations affect the hydrogen deuterium exchange rate in the MD of Hsp26. *A) H/DX MS was measured with Hsp26 WT after 10 s, 1 min, 10 min, 30 min and 60 min. The exchange rates for each residue are indicated in the heat map according to the color code below the map. B) Model of Hsp26 from aa 55 to 207 (Kelley et al., 2015). Secondary structure elements are colored differentially (α-helix: red; β-sheet: yellow; unstructured: green). S144 (cyan) is located in a big loop within the ACD. S47 and T48 are not included in the model. It can be expected that also the rest of the NTR is unstructured, thus in the model, the rest of the MD that is included is stained cyan, as well. The cyan parts might interact in the oligomer according to the H/DX measurements. C) The exchange rates of the mutants were subtracted by the WT exchange rates after 1 min and plotted (B-value$_{mutant}$ - B-value$_{WT}$). Differences within the dashed box were not considered to be a robust effect due to the mutation. The single domains of Hsp26 are highlighted by colored boxes. The peptide coverage is shown in the appendix (Figure S1).*

In the first seven amino acids (34 - 41) of the MD, more exchange was observed in the mutant proteins compared to the WT (Figure 24B). This peptide sequence with higher exchange rates

was followed by a stretch with less exchange in comparison to the WT. The less accessible region is shorter in the S47E/T48E (5 aa) than in the S144E mutant (19 aa). In the ACD, the effects of the mutations were less pronounced than in the MD. Summarizing, in the S47E/S48E mutant, the exchange in the ACD was slightly reduced, which indicates that the ACD is well folded and buried within the oligomer. Interestingly, the loop in which S144 is located was affected by the mutation in the MD and showed higher exchange rates (Figure 24C). In the S144E mutant, the exchange rates were slightly increased N-terminally of the mutation site.

3.1.5.2 Cryo-EM structure of the Hsp26 40-mer

Since 2006, the cryo-EM structure of the Hsp26 24-mer is known. The oligomer complexes were resolved to approximately 11 Å and two states, a compacted and an expanded were postulated (White et al., 2006). Hsp16.9 from wheat was used as a model to fit the ACD dimer into the electron density map. Nevertheless, there were some uncertainties concerning the dimerization mode. First, it was tried to perform NMR with a (spin-) labelled truncated Hsp26 variant Hsp26αM1 (aa 82-194), which should form dimers (see 2.2.21) (Chen et al., 2010a). For spin-abelling, positions 155 or 163 were mutated to cysteine, respectively. Spin-labelled (3-(2-Iodoacetamido)-proxyl; IPSL) Hsp26αM1 mutants were mixed with the ^{15}N-labelled Hsp26αM1 (Figure 25A). The results of the NMR experiment were inconclusive, as it seemed that the truncated versions did not form stable dimers under the conditions used for NMR and no intermolecular paramagnetic relaxation enhancement (PRE) effect was observed (Figure 25B).
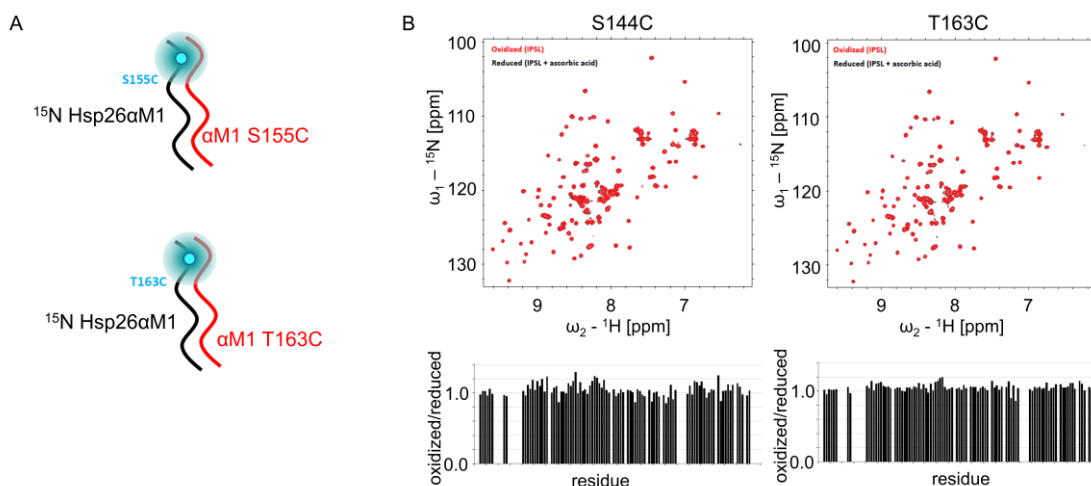
Figure 25: No dimerization of Hsp26αM1 was observed with NMR. *A) Setup of the PRE-NMR experiment. ^{15}N Hsp26αM1 was mixed with spin-labelled Hsp26αM1. B) No differences between oxidized (red) and reduced (black) IPSL were observed. NMR experiments were performed by Dr. Hyun Seo Kang (Prof. Sattler, TUM).*

In parallel to NMR, additional cryo-EM measurements were performed as described in 2.2.19.4. The Hsp26 WT structure was reconstructed from 85,425 particles. Ten class averages could be identified, thus more than for the published structure (Figure 26A) (White et al., 2006). In contrast to the published structure, the class averages did not fit to a 3-fold symmetry. Even though, the results of the *in vitro* characterization fitted well to the 24-mer, the obtained cryo-EM structure turned out to be much bigger, namely a 40-mer with a diameter of 17.5 nm consisting of 20 dimers (Figure 26B). This might be due to the higher concentrations used for EM (ca. 2.5 mg/ml). The oligomer forms a hollow sphere, is built up by four rings of dimers (4+4+8+4) and the best *ab initio* prediction was obtained with a 4-fold symmetric structure that structurally resembles a strawberry with a flat bottom and a pointed top (Figure 26C, D). The 40-mer could be resolved on average to 8 Å. Importantly the structure is very dynamic, which resulted in an uneven resolution across the oligomer from 6 - 9 Å (Figure 26D). Within the hollow sphere, a mass of approximately 136 kDa was detected. This mass most likely comes from the N-terminal regions of the upper two rings and one monomer of the third ring (3x8) (Figure 26C). As the NTRs are highly dynamic and hardly structured, they were not resolved well. For a homology model of the ACD we used wheat Hsp16.9 as for the previous Hsp26 structure. As the new structure is much better resolved, it became clear that only a domain-swapped dimer fits into the measured densities (Figure 27A). Thus, the assumption that had been made in 2006 could be confirmed by the new structure. Furthermore, we were able to identify the IEV binding pocket, which is indicated in a section of two dimers from the upper rings. This part of the oligomer was resolved to 6.3 Å (Figure 27B).
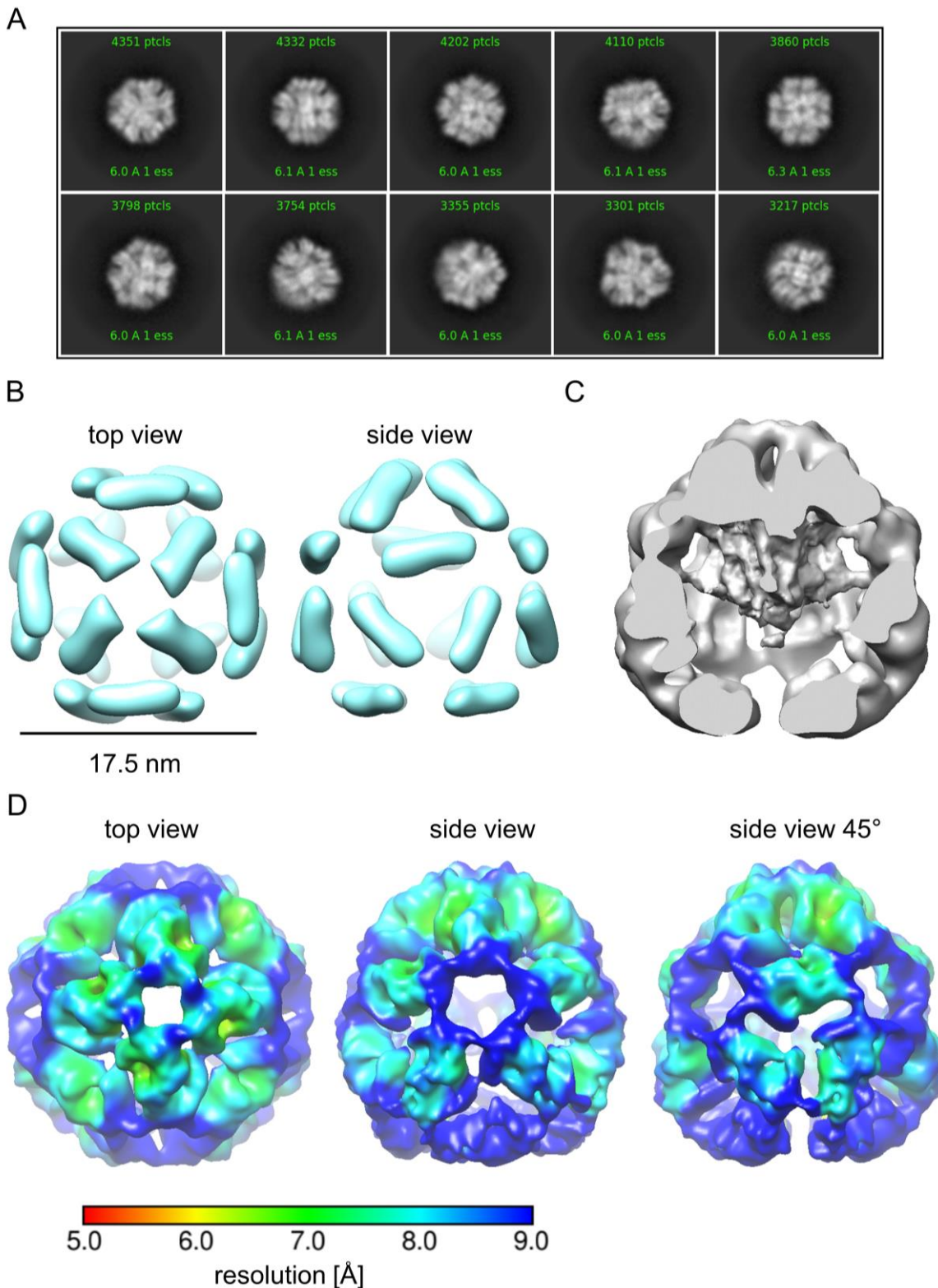
Figure 26: High-resolution cryo-EM structure of the Hsp26 40-mer. *A) Hsp26 cryo-EM was performed with a Titan Krios TEM. Ten class averages were determined from the obtained particles. B) The 40-mer is constituted of 20 dimers and has a diameter of 17.5 nm. C) The N-termini of 24 subunits seem to meet in the inner cavity of the oligomer. D) Electron density maps were reconstructed with a resolution of 9 Å and below. Not all parts of the oligomer are equally flexible, which leads to differences in the resolution. The color code indicates the resolution at specific positions in the 40-mer. Cryo-EM was performed by Dr. Carsten Peters (Prof. Sevil Weinkauf, TUM).*
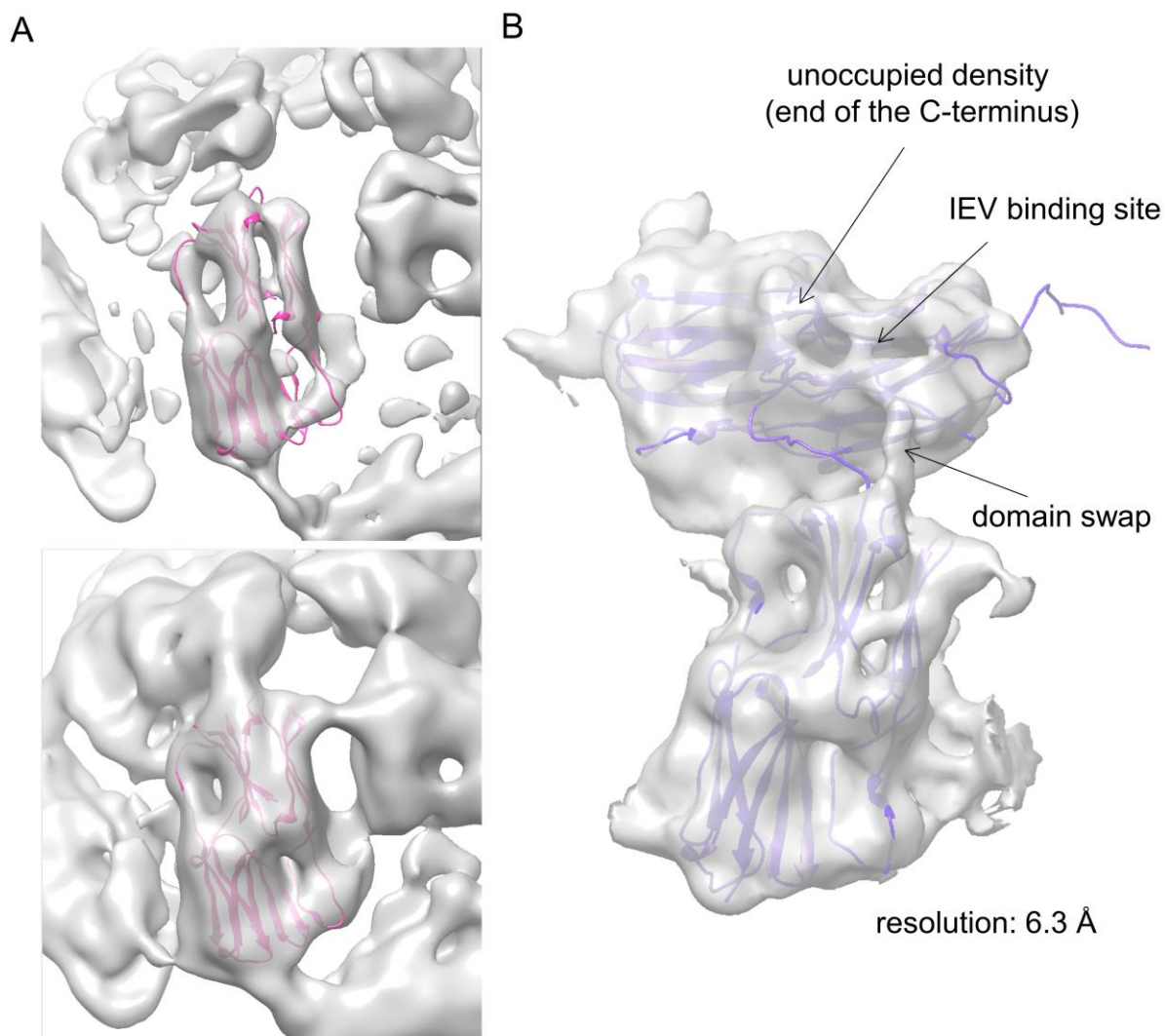
Figure 27: Hsp26 forms a domain swapped dimer. *A) Wheat Hsp16.9 was used as a homology model for the ACD (aa 84 - 133) and the dimer was fitted into the density map. B) Structure of two dimers from the upper rings resolved to 6.3 Å. The domain swap is indicated, as well as the IEV binding pocket. Cryo-EM was performed by Dr. Carsten Peters (Prof. Sevil Weinkauf, TUM).*

3.2 Global analysis of the heat shock response in *S. cerevisiae*

The findings of this project have mostly been published in *Cell Reports* (Mühlhofer et al., 2019).

3.2.1 Mild and severe heat shock do not affect the phenotype of *S. cerevisiae*

Before the heat shock response (HSR) will be analyzed in depth, general phenotypic effects that were observed will be presented shortly. First, cell growth was checked under the applied heat shock conditions at 37 °C, 42 °C and 46 °C. In all HS experiments, yeast cells were grown from an OD_{595} of ~0.2 to an OD_{595} of 0.8 and then they were shifted to the respective temperature. Thus, the stressed cells were in the logarithmic growth phase (Figure 28A). Interestingly, within 30 min of heat stress, cell growth was mostly unaffected. There was even a boost of cell growth observable, at least in the first 15 min. After shifting the cells back to 25 °C, differences in cell growth became visible. Cells stressed at 37 °C continued growth comparable to the control cells kept at 25 °C. Cells stressed at 42 °C exhibited a lag phase of approximately 1 h before logarithmic growth was resumed. Cells that were stressed for 30 min at 46 °C did not recover within 2 h, but were also not dead and continued growth over night. The observation that growth was continued within the first 15 min of stress was probably due to the heating of the media, as it took a few minutes until the stress temperature was reached. Cooling back to 25 °C even took longer, which also should be considered and certainly affects restart of growth during the recovery phase.

A spot assay performed on a temperature gradient plate (2.2.2.4.4) indicated that from 43 °C onwards *S. cerevisiae* BY4741 does not grow anymore (Figure 28B). Up to 39 °C, cell growth was unaffected. Temperature sensitivity of W303 yeast cells was also tested as those cells were used for the transcription factor analyses. *S. cerevisiae* W303 was more heat-sensitive and stopped growth at around 41 °C. The deletion of the two transcription factors Msn2/4 did not lead to an increased heat sensitivity in this assay.

The shape and surface of heat-stressed BY4741 cells was analyzed with SEM as described in 2.2.19.2. Up to 42 °C, no effects on the phenotype were observed (Figure 28C). Only the morphology of cells stressed at 46 °C was changed in comparison to the other cells, which fits to the observations made in the growth assays. The cell surface of many cells was uneven and showed dents after incubation for 30 min at 46 °C, which indicates severe damage induced by the sublethal stress.
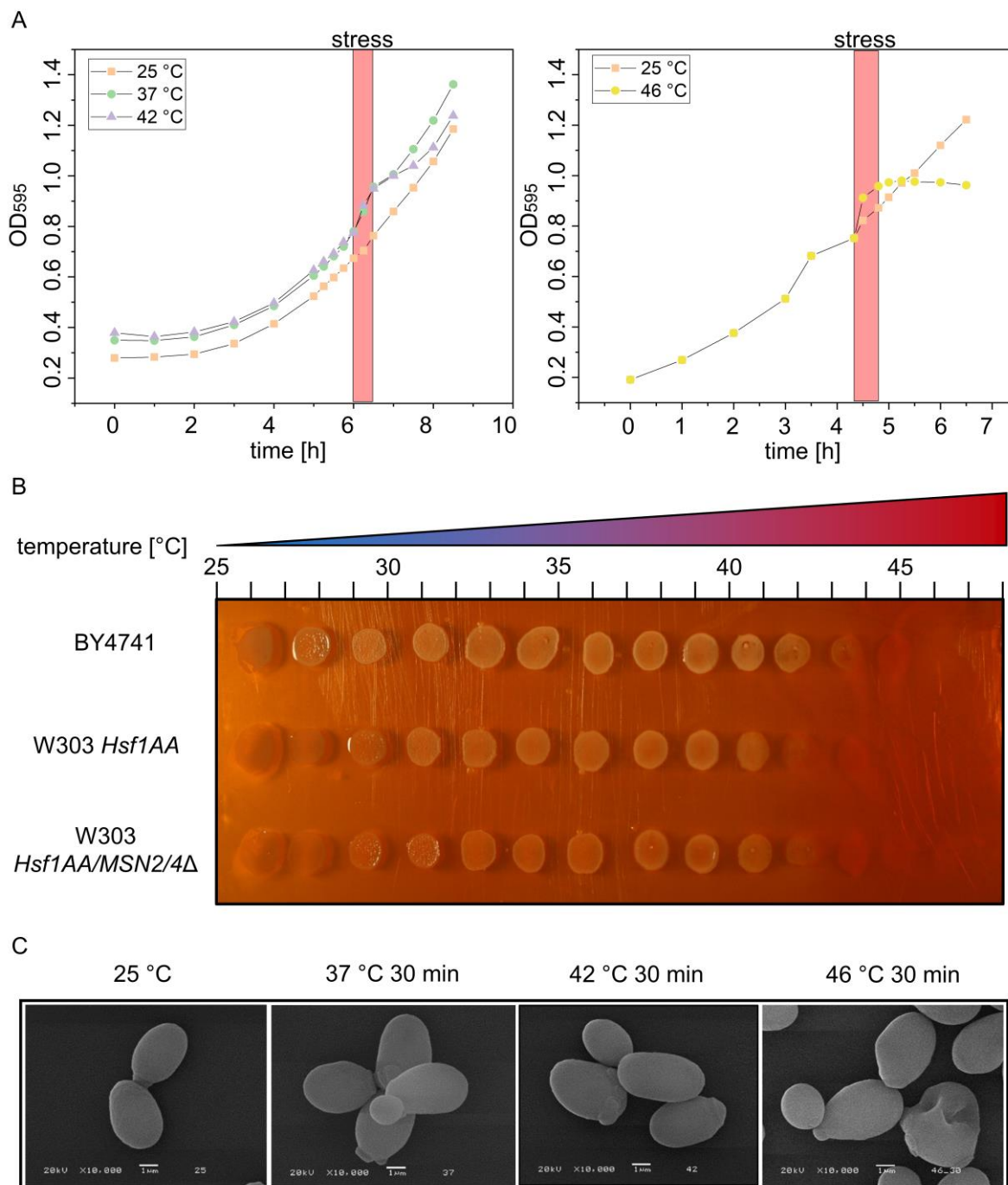
Figure 28: Up to 42 °C, only small phenotypic effects were observed – at 46 °C, cell growth was stopped. *A) BY4741 cells were grown in YPD at 25 °C to an OD$_{595}$ of 0.8. Then the cells were stressed for 30 min at 37 °C (green circle), 42 °C (purple triangle) and 46 °C (yellow circle), respectively. Recovery was measured for further 2 h at 25 °C. B) Spot assay to test for thermosensitivity of different yeast strains. Overnight cultures were diluted to an OD$_{595}$ of 1 and 5 µl were spotted onto an YPD agar plate. The cells were incubated for 24 h on a gradient heater plate (25 °C – 48 °C). C) Logarithmic cells were stressed at the indicated temperature for 30 min and prepared for SEM. SEM pictures were taken at a magnification of 10,000x and a voltage of 20 kV. The scale bars represent 1 µm. Parts of the figure are shown equally in the associated publication (Mühlhofer et al., 2019).*

3.2.2 The transcriptomic response to heat stress is fast and affects more than 1,000 genes

Time-resolved transcriptomic analyses of cells stressed at 37 °C and 42 °C have already been performed by my predecessor who started this project (Stratil, 2015) and will only be shortly summarized as the outcomes are important for further analyses and comparisons that had been performed in the context of this work. Transcriptomic analyses of cells stressed at 46 °C were performed by me.

Kinetic analysis of the transcriptome revealed that the stress response at this level is extremely fast and comprises 1,800 genes after 15 min at 37 °C and up to 3,100 genes at 42 °C, which are up- or downregulated by at least two-fold (Figure 29A). Actually, only a small fraction (~5 %) of the changed genes were clearly functionally linked to the HSR. Furthermore, it was shown that the response to mild heat stress (37 °C) peaked at 15 min and then decreased again, which indicates that the transient reprogramming of the cells led to a successful adaption to the stress. At severe heat stress (42 °C) however, the stress response was continued throughout the measured 80 min. The transcriptomic stress response of cells exposed to sublethal heat stress (46 °C) was only measured after 10 min and 30 min. At this temperature, less than 1,000 genes were changed by the factor of two or more. GO analysis (see 2.2.20) revealed that the transcriptomic response induced at 46 °C was mostly limited to the core HSR. Thus, it mainly comprised *chaperones* and *trehalose biosynthesis enzymes*, *glycolysis enzymes* and *ubiquitin-conjugating enzymes* (Figure 29B). Another important finding of the mRNA analysis was that each temperature distinguished itself by a specific fingerprint at the transcriptomic level. At 37 °C, genes annotated to mitochondria and membranes were uniquely upregulated, which indicates that the cell maintains growth and metabolism. Between 37 °C and 42 °C there was a big overlap of regulated genes involved in the clearance of damaged proteins, including *autophagy* and *ubiquitin-conjugating processes*. In addition, at 42 °C, genes associated with *sporulation* were upregulated. Thus, there was a clear shift towards life rescuing pathways with increasing temperature. Based on those observations, a modular setup of the HSR was proposed (Mühlhofer et al., 2019). The HSR is characterized by a stepwise activation, which was supported by the observation that there was almost no overlap of genes that were only upregulated at 37 °C and at 46 °C, but not at 42 °C. The third important finding was that the kinetics of the regulation are strikingly different for single genes (Figure 29C). Whereas *HSP26* was upregulated 158-fold within 5 min at 42 °C, the levels of a gene involved in sporulation, *OSW1*, stayed unchanged within the first 5 min and subsequently were upregulated 68-fold within 80 min. This implies that for yeast also transcriptional waves exist similarly as described for mammalian cells (Mahat et al., 2016, Mühlhofer et al., 2019, Stratil, 2015).
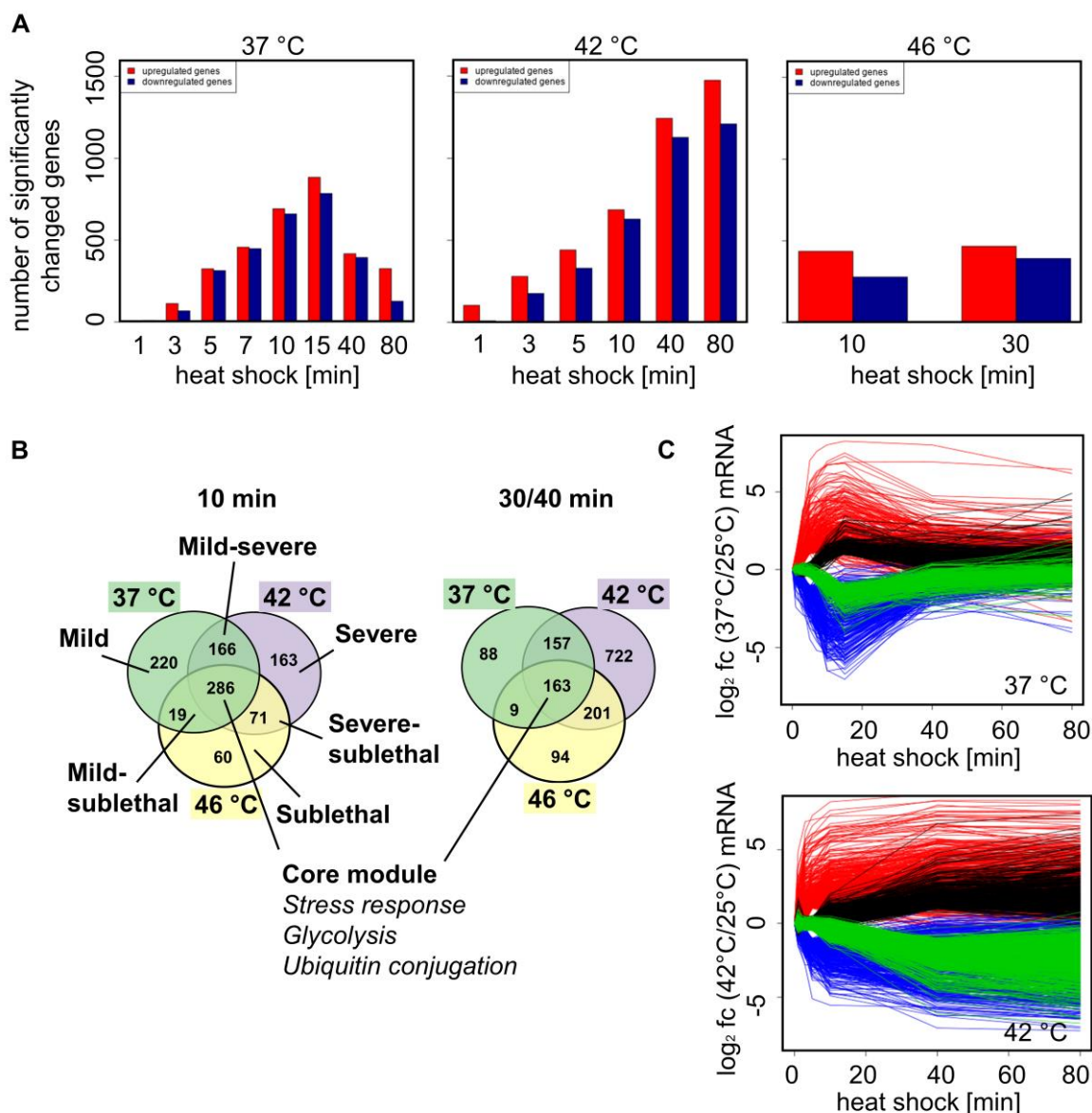
Figure 29: The transcriptomic response involves hundreds of genes, is modular and is activated in waves. *A) Yeast cells (BY4741) were grown to an OD$_{595}$ of 0.8 and stressed at 37 °C, 42 °C and 46 °C, respectively. Cells were harvested for transcriptomic microarray analysis after the indicated time points. The measurements were conducted in biological duplicates and the mean value was calculated. Genes that were changed at least two-fold were assumed to be up- or downregulated. B) Comparison of the responses at the different temperatures revealed distinct modules that are activated dependent on the severity of the stress. C) Detailed kinetic analysis of the HSR at 37 °C and 42 °C. The figure was adapted from the associated publication (Mühlhofer et al., 2019). The kinetics shown in figure part C can also be found in the PhD thesis of Dr. Chris Stratil (Stratil, 2015).*

As throughout the literature not always the same "WT" yeast strains are used, it was checked how well the transcriptomic responses to mild heat stress (37 °C) correlate between the different "WT" strains. Therefore, BY4741, the strain mainly used in this thesis was compared to the W303 strain, which will be the strain of choice in the last chapter of the thesis. As a third strain, DBY7286 was chosen as this strain was used for the original transcriptome analyses

(Eisen et al., 1998). After 10 min at 37 °C, the responses were very comparable and high Pearson correlation values were obtained, whereas BY4741 correlated better with DBY7286 than with W303 (BY4741/DBY7286: R = 0.90; BY4741/W303: R = 0.80; Figure 30). Thus, the HSR seems to be initiated in a very comparable manner. After 40 min at 37 °C, yeast cells adapt to the heat stress as shown above. Notably, the strains obviously exhibited different kinetics concerning the stress adaption process, which led to a worse correlation after 40 min at 37 °C (Figure 30).
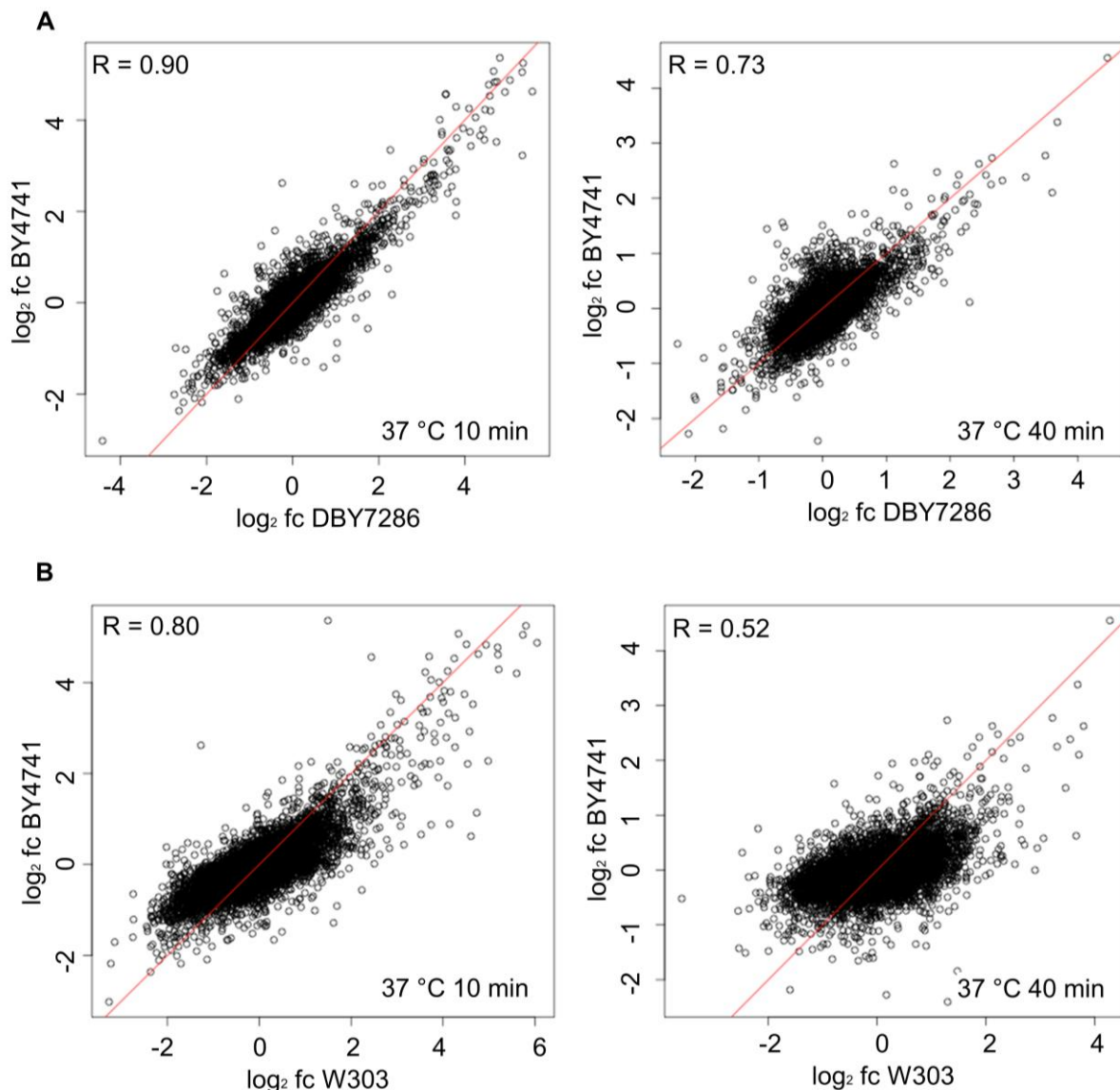
Figure 30: The primary heat stress response is comparable between different WT yeast strains. A) Comparison of the HSR of BY4741 and DBY7286 induced by mild HS. Yeast cells were grown to an OD_{595} of 0.8 and heat stressed for 40 min at 37 °C. After 10 min, the first samples were taken for the transcriptome analyses. Gene chip analyses were performed in duplicates and mean values are shown. B) Comparison of the HSR of BY4741 and W303 induced by mild HS. Gene chip analysis was performed as described above. R: Pearson correlation.

Whereas BY4741 and DBY7286 still correlated well (R = 0.73), the correlation between BY4741 and W303 dropped to 0.52. It appeared that W303 adapts slower to the stress than the other two strains. The differences observed with the W303 strain might also be due to the adenine synthesis defect of this strain, which possibly affected the stress response and the adaption process. Therefore, this strain was grown on YPD supplemented with adenine whenever it was used in the next chapter.

3.2.3 Changes in transcription are well reflected at the level of translation

3.2.3.1 Pab1 and Ded1 stay mostly soluble up to 42 °C

The poly(A) binding protein Pab1 as well as the RNA helicase Ded1 were both reported to be involved in translation and to be prone to phase separation under heat stress (Riback et al., 2017, Wallace et al., 2015, Iserman et al., 2020). Therefore, a regulatory role on translation under stress is assumed. To check at which temperature the proteins phase-separate *in vivo*, yeast cells expressing GFP-tagged Pab1 or Ded1 were heat-stressed for 30 min at 37 °C, 42 °C or 46 °C. Foci formation was analyzed by fluorescence microscopy as described in 2.2.19.1. Notably, Pab1 was completely soluble up to 42 °C. Furthermore, cells expressing Ded1-GFP exhibited hardly any foci up to 42 °C within 30 min (Figure 31). At 46 °C however, both proteins completely phase-separated and localized to stress-induced deposit sites (Cherkasov et al., 2015). As no phase separation was observed under mild and severe heat stress up to 42 °C, those results imply that translation continues up to 42 °C or at least that those two factors do not play a major regulatory role under mild and severe heat stress.
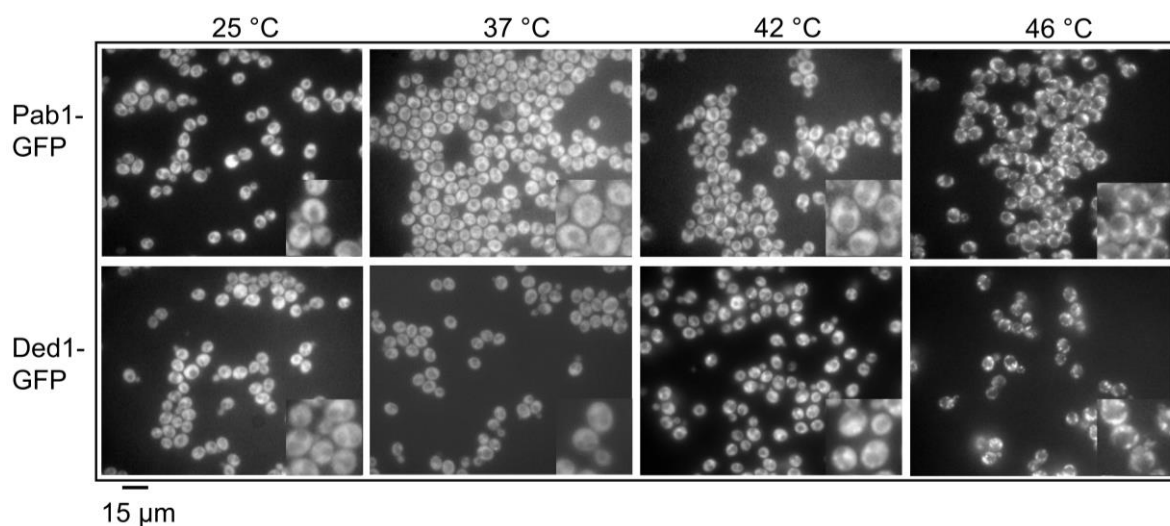
Figure 31: Pab1 and Ded1 foci formation is observed at 46 °C. *Logarithmic growing yeast cells (OD$_{595}$ 0.8) with GFP tagged Pab1 or Ded1 were heat-stressed for 30 min at 37 °C, 42 °C or 46 °C. As a control, non-stressed cells were analyzed under the microscope. Pictures of the cells were taken at a magnification of 1,600x. Insets represent 3,200x magnification. The scale bar represents 15 µm. The pictures were taken from the associated publication (Mühlhofer et al., 2019).*

As it was shown that Pab1 suppresses the translation of genes that carry poly(A) sequences in their 5´ UTR and Hsps tend to be enriched in such 5´ poly(A) stretches, one could imagine that Pab1 is important to suppress translation of Hsps under non-stress conditions (Xia et al., 2011). By its phase separation, Pab1 might possibly liberate the *HSP* coding mRNA and induce an immediate upregulation of those stress-protective proteins. As *PAB1* is an essential gene and cannot be deleted, a knock-down was performed as described in 2.2.11. After the addition of doxycycline, the transcription of *PAB1* was blocked and the protein could be almost completely depleted (Figure 32). After depletion of Pab1, the levels of Hsp26, Hsp42 and Hsp104 were measured with western blots and compared to the WT cells. Importantly, only the levels of Hsp42 were increased by the knock-down of Pab1, the levels of Hsp26 and Hsp104 were not increased. This finding does not support the hypothesis that phase separation of Pab1 leads to an initial boost in the chaperone levels. In heat-stressed cells, the chaperone levels were all increased more than two-fold, as expected. Thus, the effect of Pab1 in regulating the heat stress response up to 42 °C seems to be rather negligible.

gene	40 bp 5´ UTR
HSP104	AAAGAAATCAACTACACGTACCATAAAATATACAGAATAT
HSP42	CCATATCCCACACAAATTAAGATCATACCAAGCCGAAGCA
HSP26	GGTATCCAAAAAAGCAAACAAACAAACTAAACAAATTAAC

	log$_2$fc WT (42/25) °C	log$_2$fc (knock-down/WT)
Hsp104	1.1	-0.1
Hsp42	5.4	2.0
Hsp26	1.4	-1.4
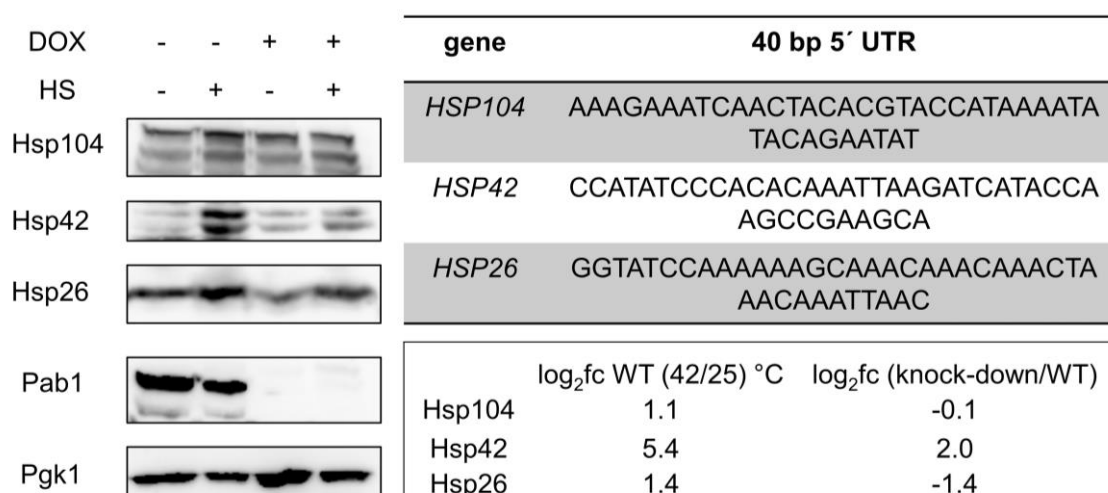
Figure 32: Knock-down of Pab1 did not lead to a robust increase of Hsp26 and Hsp104 levels. *Pab1 was expressed under the control of a tetracycline operator and expression repressed by the addition of doxycycline (DOX). In addition to the knock-down, cells were stressed for 30 min at 42 °C (HS) and the Hsp26, Hsp42 and Hsp104 levels determined with western blots. Pgk1 was used as a loading control and the efficiency of the knock down was tested with an anti Pab1 antibody. Changes in the chaperone levels induced by heat stress in the WT were compared to the effect of Pab1 knock-down at 25 °C versus the WT chaperone levels. The fold changes calculated from the band intensities that were normalized to the Pgk1 levels and are shown in the box next to the western blots. In the upper table the 40 bp 5´UTRs of the three chaperones are shown.*

3.2.3.2 *De novo* protein biosynthesis is maintained up to 42 °C

As all previous results indicated that translation is not stopped at 42 °C, *de novo* protein biosynthesis was directly studied by the incorporation of radioactively labelled methionine that was added just before the cells were subjected to the heat stress as described in 2.2.9. The

cells were again stressed at 37 °C, 42 °C or 46 °C. In parallel, protein biosynthesis was measured at 25 °C. Additionally, recovery was monitored to see how fast protein biosynthesis was restarted after a heat-induced pause. The band intensities were normalized using the amount of synthesized proteins after 1 h at 25 °C. In accordance to the data shown above, proteins were actively translated at 37 °C throughout the 90 min heat stress (Figure 33). Interestingly, the total amount of newly synthesized proteins under mild heat stress even exceeded the synthesis observed at 25 °C. The increase of the protein amount seemed to be linear at 37 °C and at 25 °C (Figure 33B). When the cells were shifted back from 37 °C to 25 °C, synthesis was continued with no obvious change in the synthesis rate.
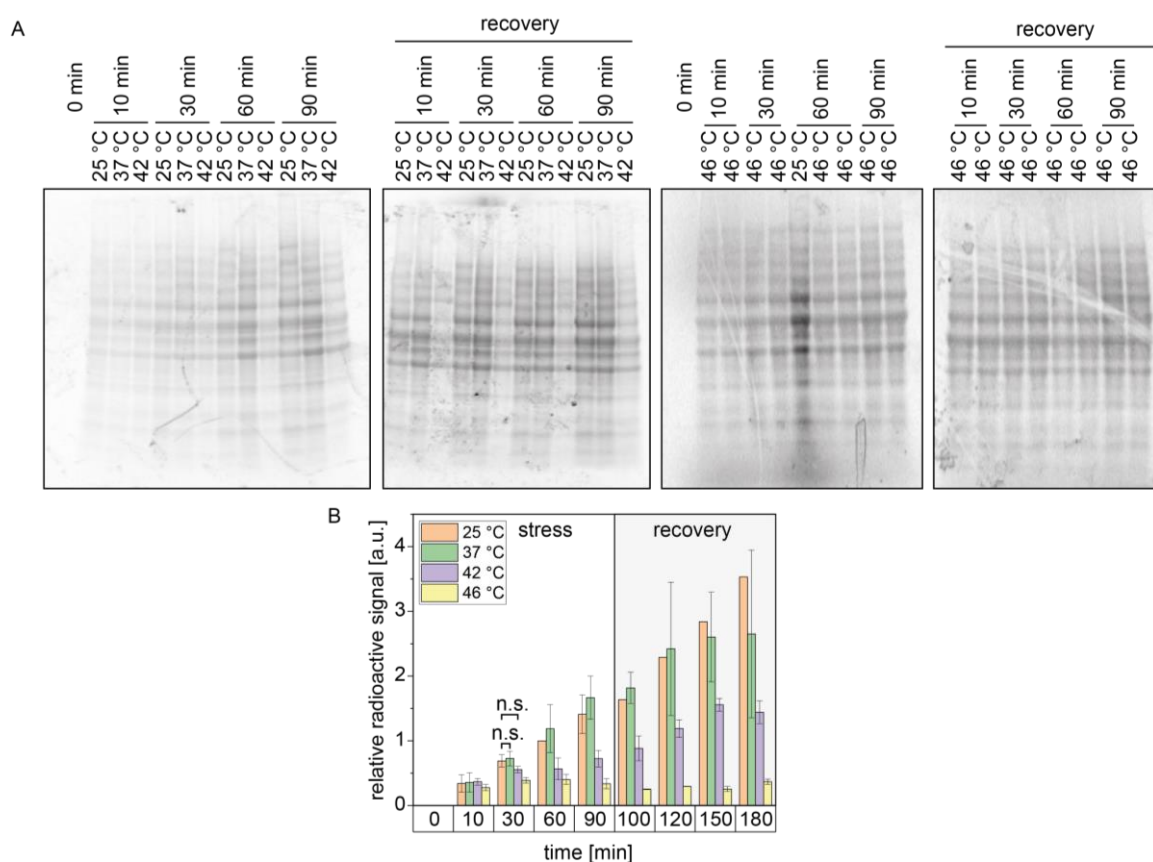
Figure 33: Protein biosynthesis is stopped after prolonged severe and under sublethal heat stress. A) Yeast cells were grown to an OD_{595} of 0.8 at 25 °C in medium without methionine. The cells were harvested and resuspended (OD_{595} = 1) in CSM (-Met). Directly before the heat stress, ^{35}S-methione was added and one OD harvested at the indicated time points. Lysates were separated via SDS-PAGE and the storage phosphor screen exposed for 20 h. B) The lane intensities of the gels were determined densitometrically with Image Quant. Mean values and standard deviation were calculated from at least two biological replicates. For 30 min and 60 min at 25 °C, 37 °C and 42 °C biological triplicates were measured. The band intensities were normalized on the amount of synthesized proteins after 60 min at 25 °C. After 30 min the changes in protein biosynthesis between 25 °C and 37 °C or 42 °C were not significant according to a two sided t-test (p > 5 %). The plot and the gels can also be found in the associated publication (Mühlhofer et al., 2019).

Protein synthesis was also initially continued after a shift to 42 °C. However, after 30 min the protein amount was around 15 % lower than the amount of synthesized proteins in the control cells kept at 25 °C. This decrease was not statistically significant. From 30 min onwards, *de novo* protein synthesis was almost completely paused at 42 °C. Notably, soon after the shift back to 25 °C, protein biosynthesis was resumed. At 46 °C from 10 min onwards, no further protein biosynthesis was observed, which indicates a very fast stop of translation. Furthermore, the cells did not resume translation within 90 min of recovery.

3.2.3.3 Changed mRNAs are quantitatively translated

To analyze which proteins are translated under mild or severe heat stress, ribosome profiling experiments were performed as described in 2.2.6. In parallel to the ribosome footprint analysis, total RNA-seq samples were prepared to be able to directly compare the translatome with the transcriptome. After 10 min at 37 °C, the translational profiles of 4,411 genes were obtained (Figure 34A). Of those, the translation of 725 genes was increased at least two-fold in comparison to the non-stress control. As expected, *protein folding* and *trehalose biosynthesis* were the most significantly enriched processes according to the GO analysis (Figure 34B). Concomitantly, 489 genes were translationally repressed by at least two-fold. Those were mostly involved in *RNA processing*, *ribosome assembly* and *nuclear transport*. Thus, *translation* is downregulated on different levels. After 30 min at 37 °C, translational data of 3,680 genes were obtained. The translation of 846 genes was increased whereas translation of 556 genes was repressed. In this case, the profile was shifted more towards *metabolic processes*, which indicates that the cells can well handle the mild stress and continue growth. The downregulated categories could still be summarized by *translation*. 10 min incubation at 42 °C led to the upregulated translation of 779 genes out of 3,607 detected genes under this condition. The amount of genes with decreased translation was 515. Hence, the amount of downregulated genes was again lower than the amount of upregulated genes. The addressed pathways were very comparable to the pathways observed for cells stressed at 37 °C for 10 min. *Chaperones* and *sugar/trehalose metabolism* were upregulated and *translation* as well as *RNA processing* were downregulated. After 30 min at 42 °C, 892 of 2,901 measured genes were upregulated at the level of translation. As expected, the targeted pathways were again dominated by the *stress response*. In addition, *proteasomal degradation* seemed to gain importance after prolonged stress. 583 genes were found to be repressed in the ribosome profiling experiment after 30 min at 42 °C. The repression of translation after 30 min at 42 °C, which was observed in the radioactive incorporation experiment, is supported by the gene ontology analysis, which again almost exclusively pinpointed *translation*.
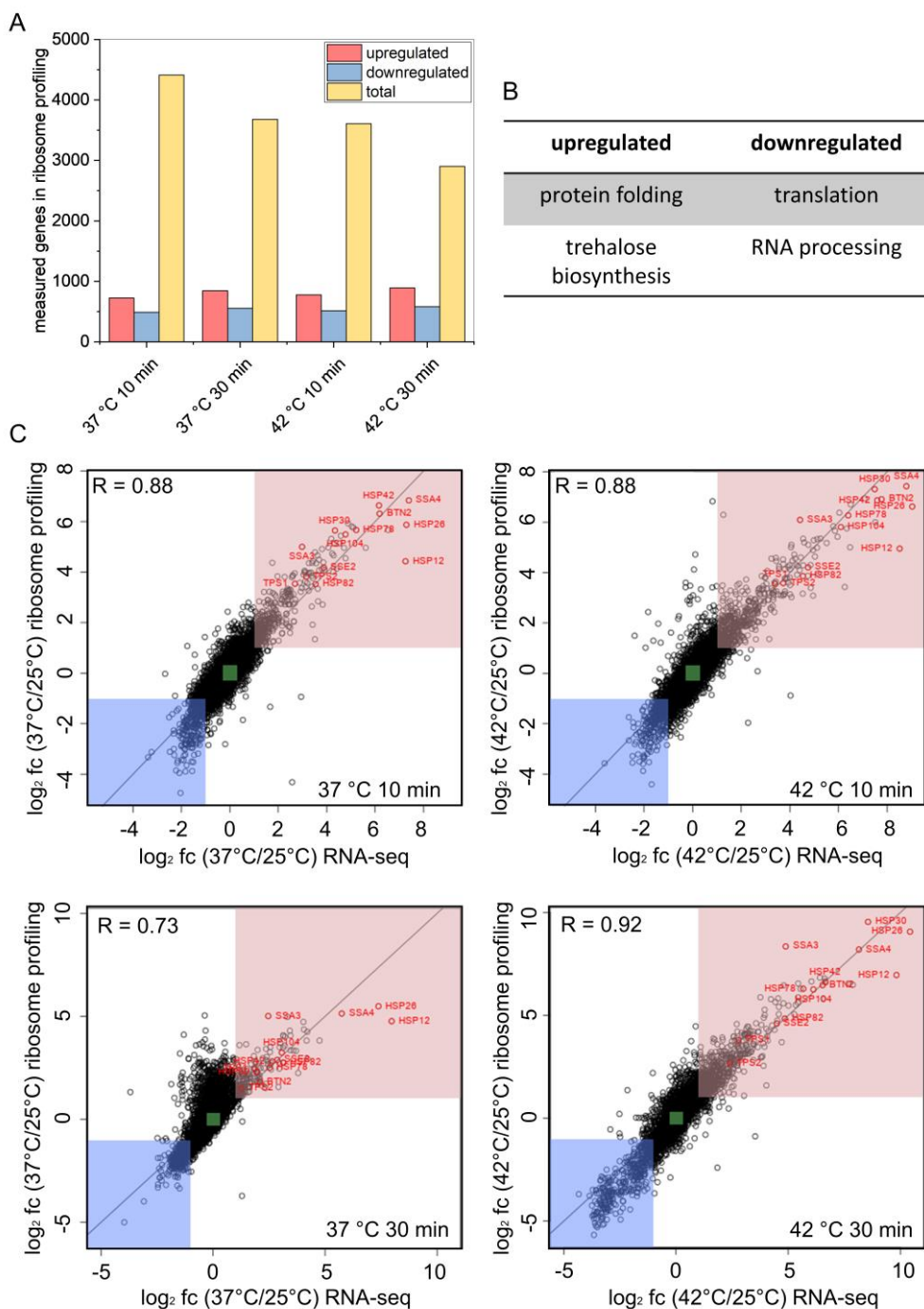
Figure 34: The translational and the transcriptional HSRs correlate very well. *A) Amount of genes that were found to be regulated at the translational level. Cells were grown to an OD_{595} of 0.8 and then stressed for 10 and 30 min at 37 °C and 42 °C, respectively. Ribosome profiling experiments were mostly performed in biological duplicates, partially in triplicates. Upregulated genes (log_2 fold change (fc) > 1) are indicated by red bars, downregulated genes (log_2 fc < -1) are indicated by blue bars. The yellow bars indicate the amount of genes that could be identified under each condition. B) Main cellular processes that were affected at the translational level under heat stress. GO analysis was performed with GOrilla (Eden et al., 2009). C) Correlation between the transcriptomic and the translatomic changes. Genes that were downregulated at both levels (log_2 fc < -1) are indicated by the blue box, genes that were upregulated at both levels (log_2 fc > 1) are indicated by the red box. The green box comprises unchanged genes ($|log_2 fc| < 0.3$). HSR related genes are indicated red. R: Pearson correlation. The correlations can be found equally in the associated publication (Mühlhofer et al., 2019).*

The correlation between the ribosome profiling data and the transcriptome was very high under almost all conditions (Figure 34C). After 10 min at 37 °C and 42 °C, respectively, a Pearson correlation of 0.88 was obtained. After 30 min at 42 °C, the transcriptome and the translatome correlated even better (R = 0.92). Only after 30 min at 37 °C, the correlation was not as good as under the other conditions. In this case, the adaption process at the transcriptional level that was described before did not seem to be equally reflected in the ribosomal footprints, which indicates that translation lags a bit behind transcription (R = 0.73). Summarizing, it was evident that the transcriptional and the translational response are very similar and hence seem to be closely linked to each other.

Besides looking at pure fold changes (fc), ribosome profiling also allows the analysis of the translation efficiency (TE), which is calculated by dividing the ribosome footprint counts by the RNA-seq counts (Ingolia et al., 2011). Closely linked, ribosome profiling also allows the analysis of the ribosomal distribution across the mRNAs. Overall, the TE was not strongly reduced by heat stress up to 42 °C within 30 min, which was expected from the results shown above (Figure 35A). The observed TE of the cells stressed for 10 min at 37 °C seemed to be even slightly increased, whereas after 30 min the relative TE was shifted towards lower values. In this context, the rRNA levels (RDN5-1 and RDN18-1) of stressed yeast cells at 37 °C and 42 °C were analyzed with qRT-PCR as described in 2.2.3.3, to check whether the amount of ribosomes was changed under stress. Notably, no differences in the rRNA levels were observed. This indicates that the amount of ribosomes was not significantly different under stress and non-stress conditions (Figure 35B). The analysis of the ribosomal distribution on the mRNAs revealed a slight accumulation in early regions of the transcripts (Figure 35C). The strongest stalling effect was observed in cells stressed for 30 min at 42 °C, whereas the ribosomes were almost equally distributed across the transcripts at 25 °C. The effect after 10 min at 37 °C and 42 °C was similar. After 30 min at 37 °C, much less stalling was observed. This supports the hypothesis that the cells adapt to the mild stress. The stress-dependent stalling effect was especially pronounced after stretches of hydrophobic amino acids within the first 30 aa (Figure 35D). Similar effects had been observed for mammalian cells (Shalgi et al., 2013). Inversely, non-stalled transcripts showed less hydrophobic sequences in those early regions than the average.
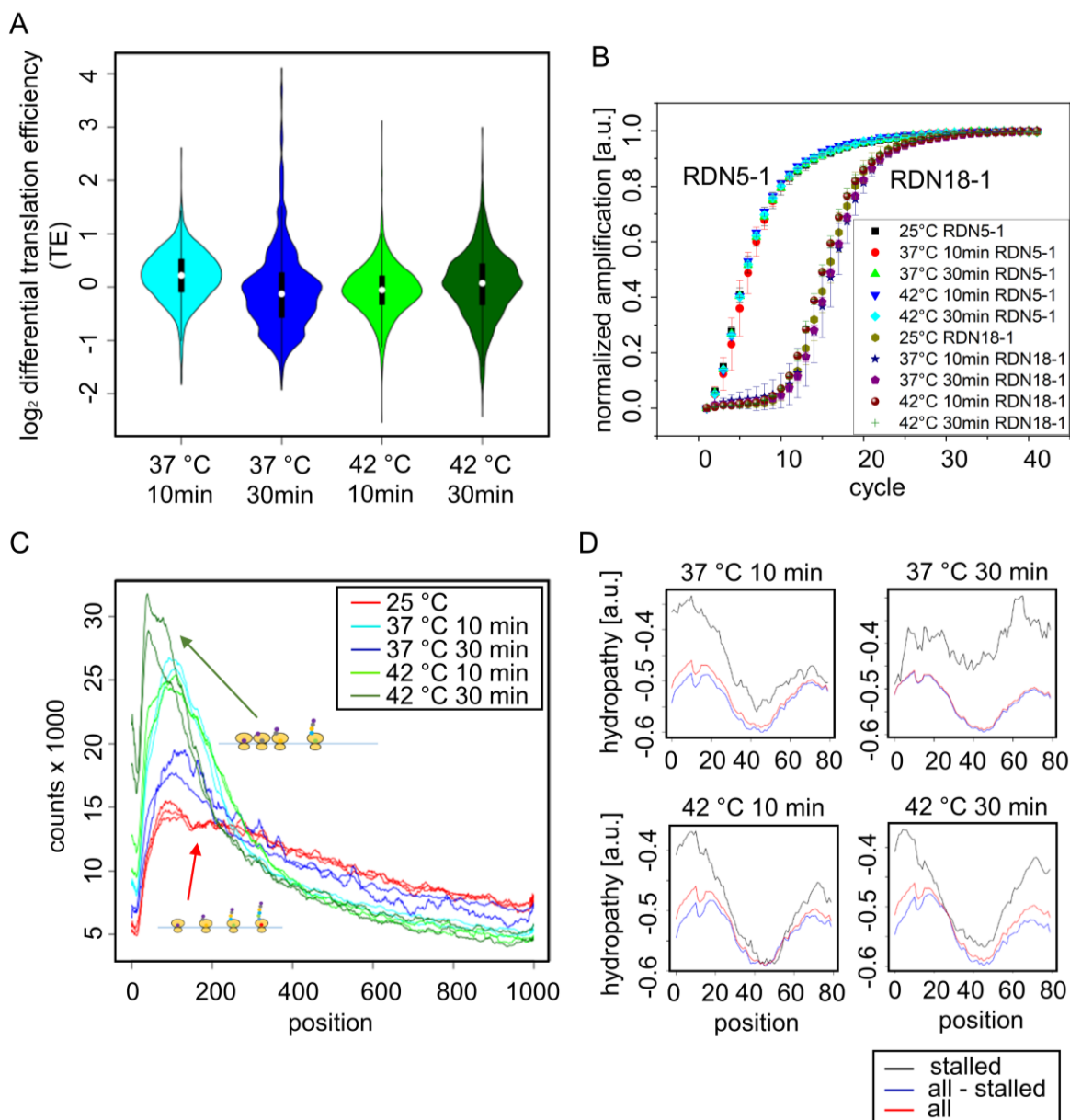
Figure 35: Only slight stalling effects were induced by heat stress up to 42 °C within 30 min. *Ribosome profiling was performed as described in the caption of figure 34. A) The distribution of the differential TE values, measured with ribosome profiling under stress in comparison to non-stress, was plotted. B) Quantification of the rRNA levels of heat-stressed yeast cells. Logarithmic growing cells were stressed at 37 °C and 42 °C, respectively. The RNA was isolated after 10 min and 30 min and the rRNA quantified with qRT-PCR. Mean values and the standard deviation were calculated from duplicate measurements. The color code can be found in the figure. C) Ribosomal distribution on the transcripts under heat stress and non-stress conditions derived from the ribosome footprint reads. Stress led to the accumulation of ribosomes in early regions. All single ribosome profiling replicates are plotted. The color code can be found in the figure. D) Stalled transcripts were enriched in hydrophobic sequences within the first 30 amino acids (black lines). Inversely, non-stalled transcripts (blue lines) exhibited less of those hydrophobic sequences than the average of the transcripts (red lines). The figure was assembled based on two figures from the associated publication (Mühlhofer et al., 2019).*

As noted above, translation of several genes is dependent on the RNA helicase Ded1, which was shown to phase separate under heat stress and hence to negatively regulate translation under stress (Wallace et al., 2015). Next, it was checked whether the TE of Ded1-dependent genes (Sen et al., 2015) is changing at 37 °C and 42 °C, where almost no foci formation was observed under the microscope. To this end, the TE values derived from ribosome profiling of the two time points at one temperature were combined and the mean TE was calculated for 37 °C and 42 °C, respectively (Figure 36). At 37 °C, the differences between the time points were bigger as already seen in figure 35A, which resulted worse p-values after the combination of both datasets. Nevertheless, it suffices to get an idea of the general effects on Ded1-dependent genes. Indeed, genes whose translation depends on Ded1 (indicated in red) tended to be slightly less efficiently translated under stress, but since Ded1 phase separation was negligible up to 42 °C, presumably only the onset of the effect was observed. It should be stated once more that the overall TE was hardly affected by those stalling events, which leads to the conclusion that translation continues at a similar level within the first 30 min of mild and severe heat stress.
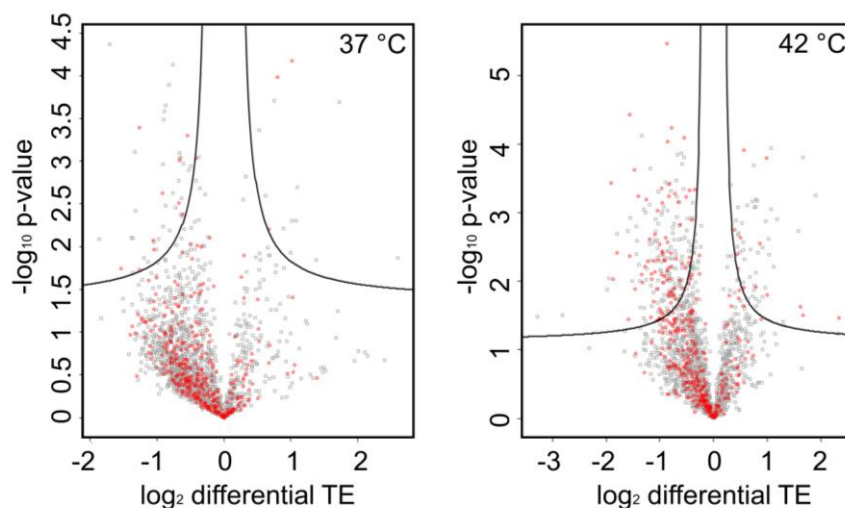
Figure 36: Translation of Ded1-dependent genes is only slightly affected up to 30 min at 37 °C or 42 °C. *All time points of the single stress conditions were combined and the TE difference in comparison to non-stressed cells was calculated. In the Volcano plots, Ded1-dependent genes are indicated by red dots.*

3.2.4 Protein turnover is replenished by protein synthesis under tolerable stress

3.2.4.1 Changes in the soluble proteome induced by mild and severe heat stress are small

At the transcriptomic as well as at the translatomic level, extensive reprogramming was observed, which included more than 1,000 genes. To check how this response is reflected at the level of the proteome, label-free quantification mass spectrometry (LFQ-MS) was applied as described in 2.2.8. Importantly, the amount of changed proteins ($|\log_2 fc| > 1$) was much smaller than the number of gene transcripts with changed levels. At 37 °C and 42 °C, 2,044 and 1,955 proteins, respectively, were identified. The overlap of those measurements contained 1,857 soluble proteins, which were used for further comparisons. Of those, 63 proteins were significantly upregulated whereas 10 proteins were significantly downregulated ($|\log_2 fc| > 1$; false discovery rate (FDR) < 0.05; $S_0 = 0.1$) at 37 °C (Figure 37A). At 42 °C, 54 proteins were significantly upregulated whereas 92 were downregulated. The increase of downregulated proteins in the supernatant was even stronger at 46 °C. Of the almost 1,800 proteins identified in the supernatant, 47 proteins were found to be significantly upregulated and 220 proteins were downregulated.

As expected, chaperones such as Hsp26, Hsp42, Hsp82 and Hsp104, as well as the stress inducible Hsp70 homologues Ssa3/4 were upregulated at 37 °C and 42 °C. Besides *trehalose biosynthesis enzymes* (Hxk1, Tps1, Tps2, Tsl1, and Nth1), proteins involved in *glycerol metabolism* (e.g., Gcy1 and Ald3) were found to be upregulated. In addition to trehalose, glycerol is also known to increase stress resistance in yeast (Conlin and Nelson, 2007, Klein et al., 2017). To validate the MS results, western blots were performed as described in 2.2.12.3. Hsp26, Hsp42 and Hsp104 were selected as positive controls that should be upregulated. As proteins that should not change, Cmk2, Tdh1, Cnb1, Hch1 and Pgk1 were chosen. Those five were neither up- nor downregulated in the MS measurements. Accordingly, they also were completely unchanged in the western blots, whereas the three tested chaperones were all upregulated as expected (Figure 37B).
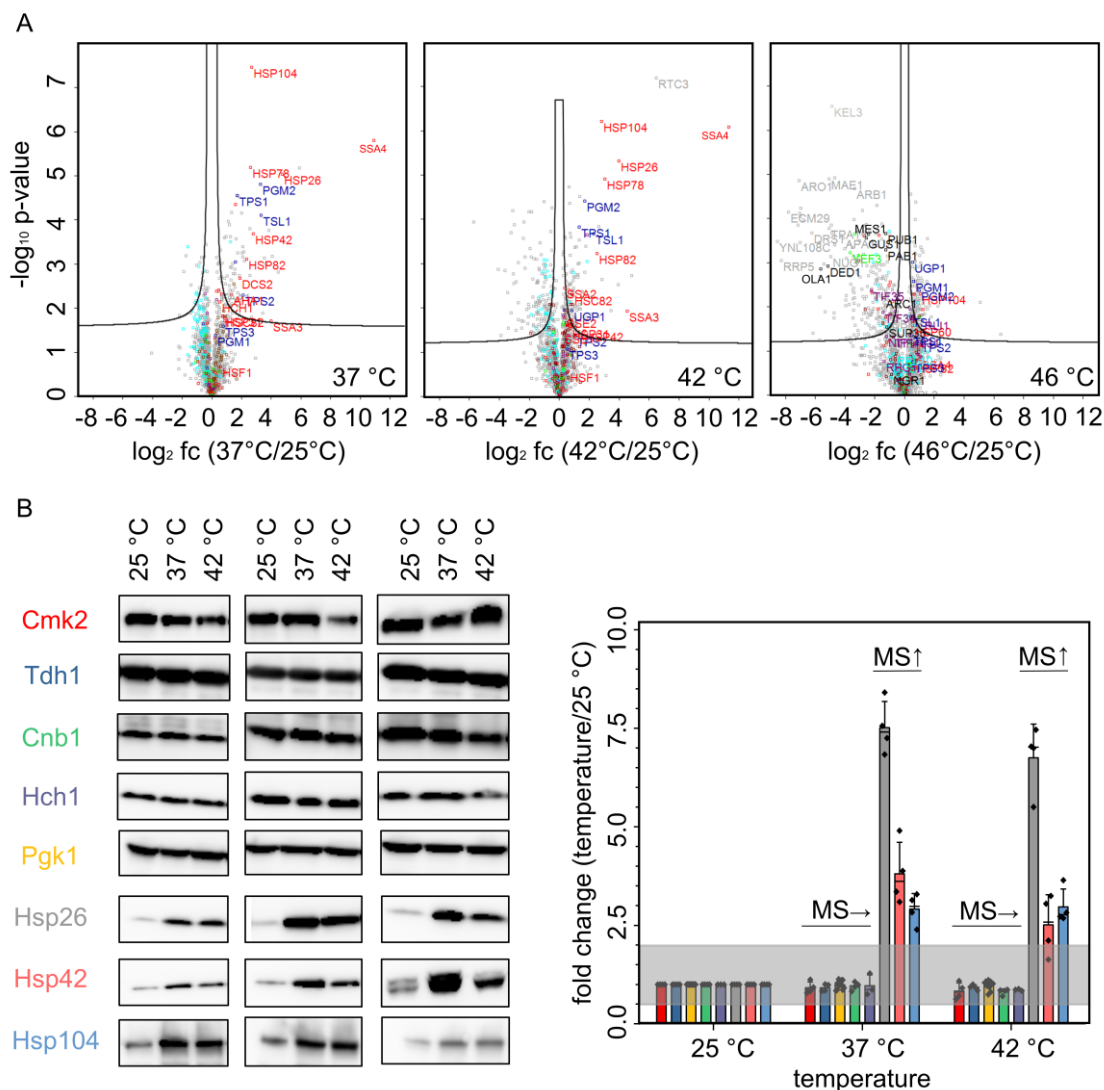
Figure 37: Proteomic changes induced by heat stress comprise less than 150 proteins up to 42 °C. *A) Logarithmic growing yeast cells were heat stressed for 30 min at 37 °C (left panel), 42 °C (middle panel) and 46 °C (right panel), respectively. Relative changes in the soluble proteome were measured with LFQ-MS in biological triplicates. Fold changes were calculated with the supernatant of non-stressed cells as a base. Two-sample t-tests with a FDR < 0.05 were applied for the Volcano plots. Proteins were clustered according to the Uniprot GO BP annotation downloaded in 2015. Proteins that are associated with response to heat are stained red, trehalose biosynthesis enzymes are colored blue, proteins involved in translation generally cyan, in translation initiation purple, in translation elongation green and in ubiquitin-dependent catabolic processes brown. At 46 °C, known phase separators are colored black. B) The soluble protein fraction of heat stressed cells was analyzed with western blots to validate the MS results. The fold changes were calculated by the division of the band intensity under stress by the corresponding band intensity at 25 °C. On the left, three western blot replicates for each protein are shown. In the bar plot on the right, the single measurements (black dots), the mean value (bar height), the median (black line) and the standard deviation are shown. Hch1 was measured in triplicates, all other proteins in quadruplicates. The proteins that were not upregulated in the MS measurement are indicated by: MS→; the upregulated proteins are indicated by: MS↑. The gray box indicates the space, in which a protein was assumed not to be changed (0.5 < fc < 2). The five unchanged proteins were: Red: Cmk2, blue: Tdh1, yellow: Pgk1, green: Cnb1, purple: Hch1. The three upregulated proteins: Gray: Hsp26, light red: Hsp42, light blue: Hsp104. Cmk2 was tagged with hemagglutinin (HA) and hence detected with an anti-HA antibody. The figure was assembled from two figures from the associated publication (Mühlhofer et al., 2019).*

The further analysis was continued with less stringent criteria for protein up- or downregulation to increase the amount of changed proteins, with a view to better cover the targeted processes. Now, only a two-fold change was set as a threshold to consider a protein to be changed. In addition to the chaperones, this expanded analysis revealed that specific metabolic processes are affected by the HSR. Besides Hxk1, which was already mentioned above in the context of trehalose biosynthesis, pyruvate kinase, another key enzyme of glycolysis was upregulated. In addition, other enzymes involved in glycolysis (e.g. Gcy1, Glk1, Dak1, Ald3, Tdh1, Gpd1, Gpm2, Pyc1) tended to be upregulated at least 1.4-fold (Figure 38B). Upstream of glycolysis, enzymes involved in glycogen catabolism were found to be upregulated (Figure 38A) and downstream of glycolysis, pyruvate turnover to citrate seemed to be an upregulated process under mild heat stress (Cit2). Additionally, enzymes, which are involved in the clearance of the toxic glycolysis side-product methylglyoxal (Gre3, Gor1), were upregulated under mild heat stress (Figure 38C). At 42 °C besides Hsps, more proteins involved in the control of the cell cycle and division showed changed levels. Under mild and severe heat stress, proteins involved in translation, and more specifically, ribosomal proteins tended to be downregulated (Figure 37A). The effect was stronger at 42 °C, where 50 downregulated proteins sorted into this category, whereas at 37 °C, only 28 proteins of this group were identified. This fits well to the observation shown above, that after prolonged, severe heat stress, protein biosynthesis is paused. Importantly, the soluble levels of translation initiation factors were not found to be affected up to 42 °C and hence were mostly unchanged. This is in accordance with the ribosome profiling measurements and supports the findings concerning translation up to 42 °C. Interestingly, three enzymes (Dph1, Jjj3 and Rrt2), which are involved in the diphthamide biosynthesis pathway were downregulated under mild and severe heat stress (Figure 38D). In the elongation factor eEF2, a histidine residue is modified to diphthamide, which enhances translation fidelity (Schaffrath and Stark, 2014). Thus, this is another indication for a translational pause upon prolonged stress conditions.
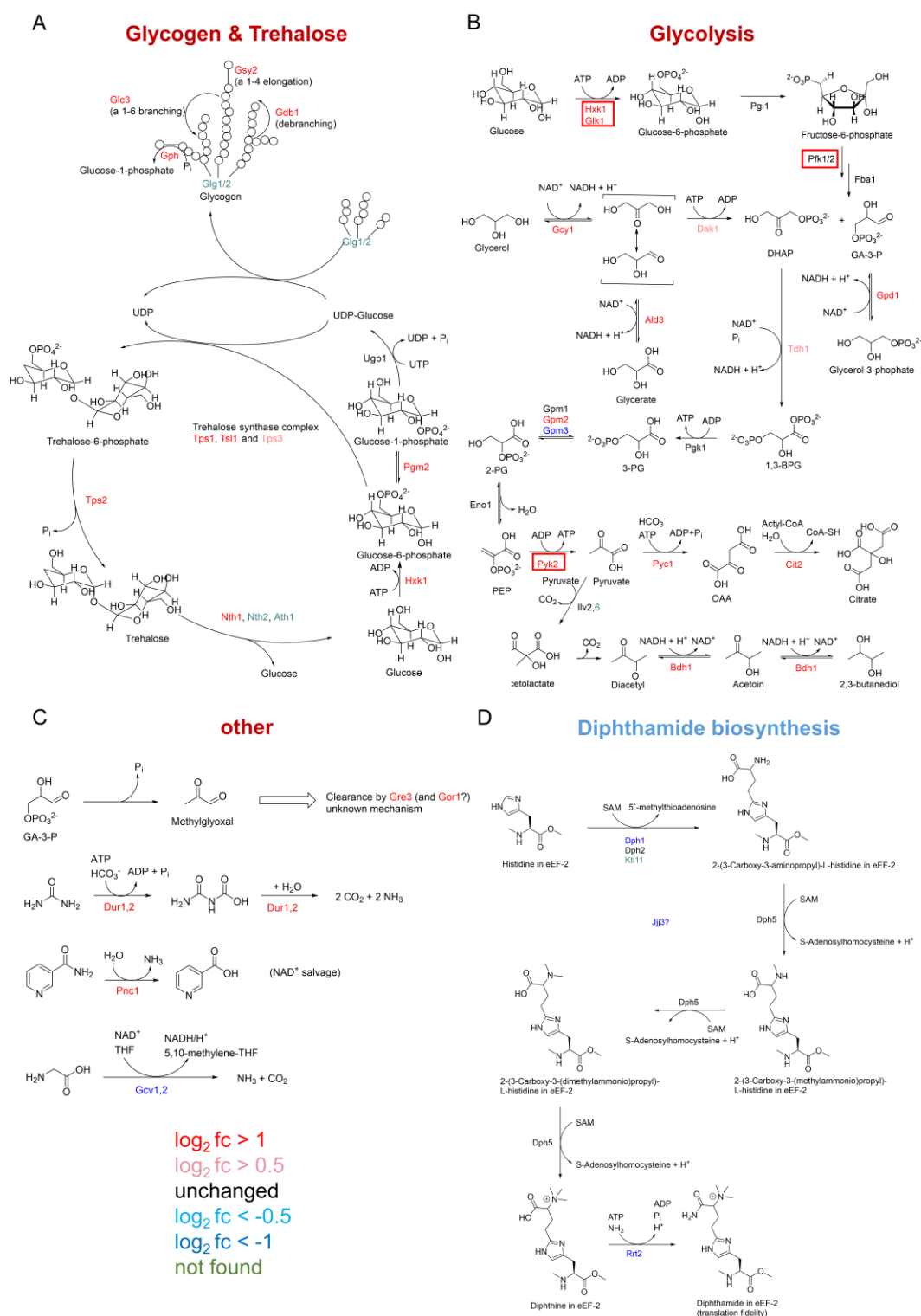
Figure 38: Metabolic processes targeted by mild heat stress in yeast according to the LFQ-MS analyses. *A) Glycogen and trehalose metabolism enzymes are mostly upregulated. B) Several glycolysis enzymes are upregulated under mild heat stress. C) Other metabolic reactions that were upregulated under mild heat stress and could not be directly integrated into a larger metabolic pathway. D) Diphthamide biosynthesis enzymes (3 of 6) were downregulated under mild and severe heat stress. The color code can be found in the figure. The figure is shown equally in the supplemental information of the associated publication (Mühlhofer et al., 2019).*

Even though the proteomic changes made sense, the correlations between the changes in the transcriptome and the proteome were not good. After 30 min at 37 °C, the correlation was moderate (R = 0.57; Figure 39A). More severe stress led to an even worse correlation (R = 0.33; Figure 39B) and after sublethal stress at 46 °C, the transcriptome and the proteome changes appeared to be completely decoupled (Figure 39C). This resulted in a Pearson correlation of 0.12. Under mild and severe heat stress, many more transcripts were changed in their expression levels whereas the corresponding proteins stayed unchanged. As the transcriptional response after 30 min at 37 °C was already reduced due to adaption, the correlation between the transcriptome and the proteome was better at this temperature. Based on these observations, the proteins were grouped into different categories. Some proteins, mainly heat shock proteins, constitute the first group: Proteins whose gene expression as well as the protein levels were upregulated (red box). The second group, downregulated at both levels, consisted of even less proteins (blue box). Many proteins were unchanged at both levels (green box). Of note, *unchanged* was defined rather strict ($|\log_2 fc| < 0.3$) in this case.

In the fourth group, proteins can be found that were upregulated at the level of transcription but stayed unchanged in the proteome (beige box). Especially under severe stress, this group was populated. In the last group, proteins whose transcripts were downregulated, but whose protein levels were still unchanged (gray box) were sorted. Those proteins possibly are relatively stable.
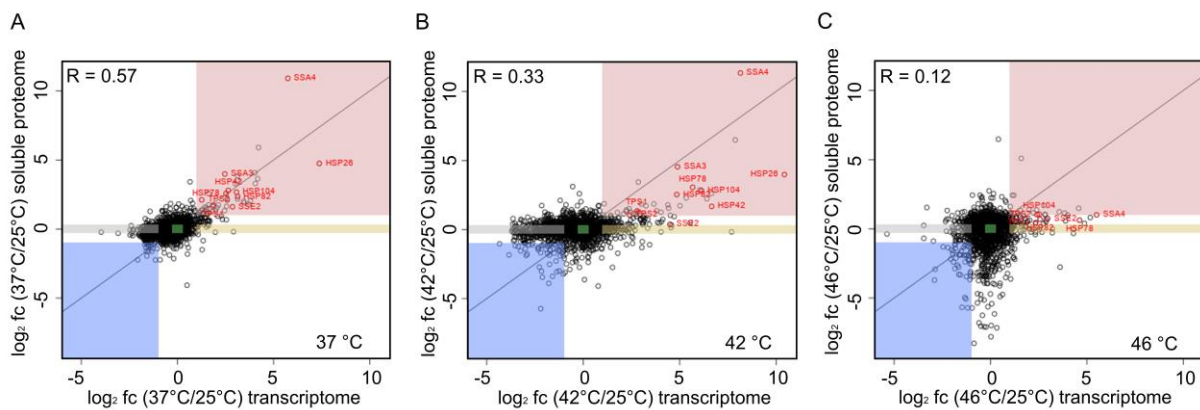
Figure 39: Transcriptome and proteome changes induced by heat shock do not correlate well. *Cells were stressed at 37 °C (A), 42 °C (B) and 46 °C (C), respectively for 30 min. The transcriptomic changes were measured in biological duplicates, the proteomic changes in triplicates. The red box comprises proteins that were upregulated at both levels ($\log_2 fc > 1$). The blue box comprises proteins that were downregulated at both levels ($\log_2 fc < -1$) and the green box proteins that were unchanged at both levels ($|\log_2 fc| < 0.3$). The beige box comprises proteins that were upregulated in transcription ($\log_2 fc > 1$) and unchanged in the proteome ($|\log_2 fc| < 0.3$) and the gray box proteins that were downregulated in transcription ($\log_2 fc < -1$) and unchanged in the proteome ($|\log_2 fc| < 0.3$). R: Pearson correlation. The figure is equally shown in the associated publication (Mühlhofer et al., 2019).*

As the comparison at the level of single proteins resulted in such low correlation values, the comparison was performed on a bigger scale by summarizing the proteins/genes into GO terms. Subsequently, the targeted pathways at both levels were compared. *Chaperones*, *trehalose*, *vacuolar catabolic processes*, *autophagy*, *monosaccharide metabolism* and *respiratory chain* were upregulated at 37 °C and 42 °C at the level of translation. Interestingly, all groups except for *respiratory chain* and *autophagy* were also enriched in the MS measurements at 37 °C or 42 °C (Figure 40A). As already mentioned above, *monosaccharide metabolism* was only enriched in cells stressed at 37 °C. At 37 °C, *vacuolar catabolic processes* were more enriched at the proteomic level in comparison to 42 °C, whereas at 42 °C, *autophagic processes* were targeted slightly stronger by the proteomic response than at 37 °C, even though the increase in this category was not statistically significant. Thus, those pathways constitute the main response to mild and severe heat stress. Proteins that belong to those classes are also upregulated at the level of the proteome. This analysis can be further expanded using 2D enrichment plots (Figure 40B). According to this evaluation, *(proteasomal) degradation* should also be added to the main pathways that are targeted by the response to mild and severe heat stress. In addition, also the downregulated categories were clear and coherent. As already mentioned above, the terms *ribosome*, *translation* and *RNA processing* are unambiguously linked to stress-dependent downregulation. At the level of GO terms, the correlation between the translatome and the proteome was astonishingly high at both temperatures. At 37 °C a Pearson correlation of 0.72 was observed and at 42 °C the correlation was even a bit better (R = 0.78). At 46 °C, the HSR seemed to be mostly overwhelmed by the stress and specific processes that are targeted at this temperature could not be identified. Some chaperones and trehalose enzymes were still slightly upregulated, but not comparable to the levels observed for the other temperatures (Figure 37A). Notably, components of the proteasomal degradation machinery were not upregulated anymore. As a shutdown of translation was observed at 46 °C, those observations were not surprising. At 46 °C, protein loss in the soluble fraction was the dominating process. Consistent with the literature, phase separators such as Gus1, Mes1, Ola1, Ded1, Pub1 and Pab1 were depleted from the supernatant at 46 °C (Wallace et al., 2015). Overall, translation initiation factors were found to be downregulated in the soluble proteome under sublethal stress, which resulted in the observed stop of translation. Interestingly, elongation and termination factors were mostly unchanged, which supports the general assumption that translation initiation is the main regulatory point of translation (Crawford and Pavitt, 2019). Thus, the enormous discrepancy between the transcriptome and the proteome can be explained by stopped translation and extensive aggregation processes at 46 °C. To understand the differences between the transcriptome and the proteome under mild and severe heat stress, the insoluble protein fraction was analyzed next.
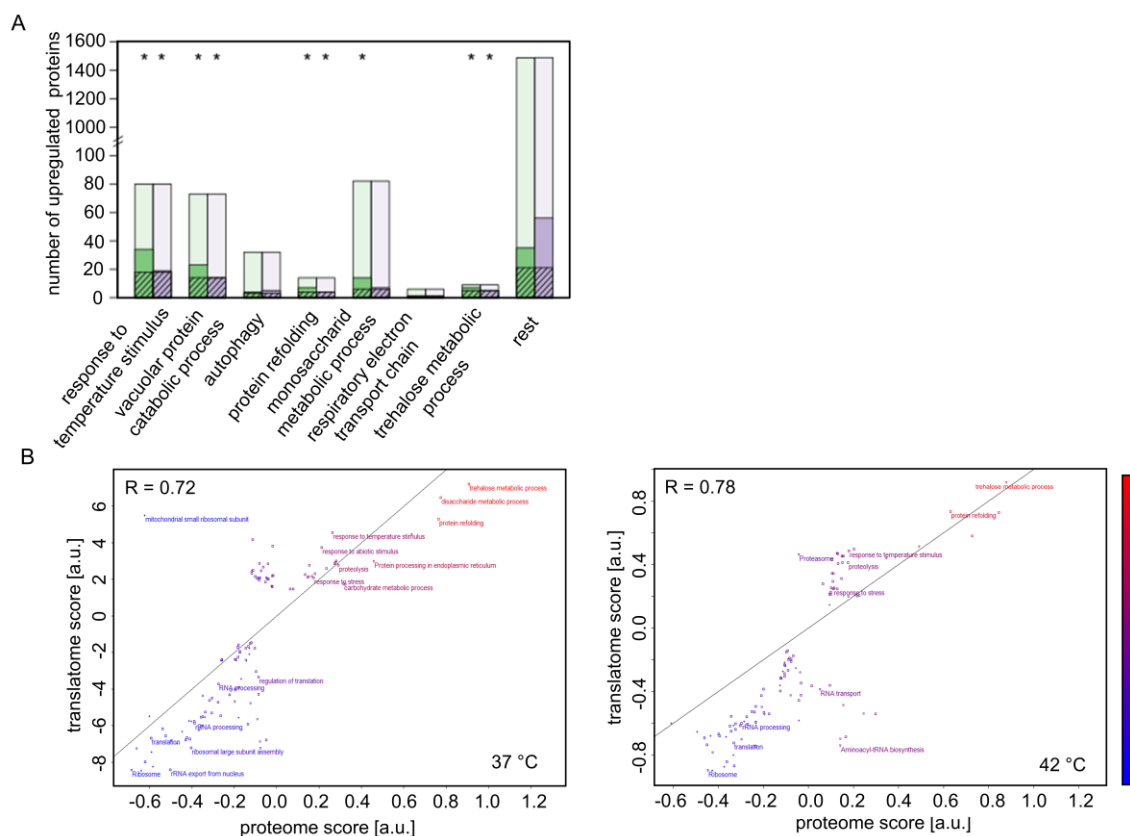
Figure 40: The main pathways targeted by transcriptomic and proteomic changes are consistent. *A) Upregulated proteins (log_2 fc > 1) were sorted into the main enriched upregulated categories of the ribosome profiling experiments (Huang da et al., 2009). Green bars: 37 °C; purple bars: 42 °C. The number of proteins that were upregulated at 37 °C and 42 °C is indicated by the black-striped parts of the bars. Faded parts indicate the number of measured genes of each group at each temperature. Asterisks indicate if the respective category was also enriched in the MS measurement. B) 2D enriched comparison of the MS and ribosome profiling data revealed a better correlation than the comparison of single genes and proteins (Cox and Mann, 2012). Proteins and genes were clustered according to the Uniprot GO annotation downloaded in 2015. Biological process (□), cellular component (+), molecular function (o) and KEGG (Δ). The groups are colored from red (upregulated) to blue (downregulated). R: Pearson correlation. The figure was adapted from the associated publication (Mühlhofer et al., 2019).*

3.2.4.2 Protein loss due to aggregation is a key determinant of sublethal heat stress

One possibility that might explain how numerous genes can be upregulated whereas the soluble protein levels remain unchanged is that protein aggregation is balanced by protein synthesis. Thus, the insoluble fraction of cells stressed at 37 °C and 42 °C was analyzed by LFQ-MS as described in 2.2.8. To achieve an optimal protein identification, the protein groups table exported from MaxQuant was filtered on 3 valid values in at least one condition (2.2.8.3). Thus, LFQ intensities for proteins that were absent in the pellet at lower temperatures were calculated by Perseus to prevent loss of proteins that were only aggregating at 42 °C. After this calculation, 2,144 proteins could be identified in the pellet fraction. At 37 °C, no protein was significantly enriched in the pellet ($|log_2$ fc$| > 1$; FDR < 0.05; $S_0 = 0.1$), even though the

pellet fraction analyzed by SDS-PAGE was increased in comparison to the 25 °C control cells (Figure 41A, B). If the stringency was reduced and a two-fold enrichment with a p-value < 5 % was set as a threshold for pellet enrichment, 48 proteins were found to be pellet-enriched at 37 °C. At 42 °C, more proteins were found in the pellet fraction. 22 proteins were significantly aggregated applying the standard statistics ($|\log_2 fc| > 1$; FDR < 0.05; $S_0 = 0.1$). If only a two-fold increase and p-value < 5 % was applied, 80 proteins were found to be pellet-enriched. Among those pellet-enriched proteins, Hsp42, Btn2 and Hsp104 were identified. Those components of the cellular folding machinery are known to be involved in the formation and removal of cellular aggregates (Alberti, 2012, Grousl et al., 2018, Miller et al., 2015b). Consistent with the *in vivo* microscopy results, Pab1 and Ded1 were not found to be enriched in the pellet up to 42 °C. As already speculated before, at 46 °C, aggregation processes are strongly increased (Figure 41A). The MS experiments of the pellet fraction of cells stressed at 46 °C are not shown as the single replicates did not correlate well. This was possibly due to technical reasons during sample preparation. Nevertheless, the soluble and total protein fractions allow the indirect identification of aggregated and degraded proteins, as well. Therefore, the soluble protein fraction was compared with the total protein measurement (Figure 41C). A decrease of the protein level in the total and the soluble fraction means that the protein was degraded under stress (brown box). If proteins were decreased in the supernatant but unchanged or even elevated in the total proteome, the proteins aggregated under stress (blue box). The same is true for proteins that appeared to be unchanged in the supernatant but were enriched in the total proteome. As expected, much more proteins were found in the blue box, thus aggregating, whereas only a few proteins seemed to be degraded under sublethal stress, which fits to the observation that proteasomal components are not upregulated at 46 °C anymore. The massive aggregation processes also resulted in a non-existent correlation between the soluble and the total proteome (R=0.02). In summary, the strength of aggregation varied strongly across the investigated temperature range, from few aggregates at 37 °C to extensive aggregation under sublethal stress. As the aggregation processes up to 42 °C were too small to provoke the observed discrepancy between the translatome and the proteome alone, it was next checked whether the effects at the proteomic level are delayed.
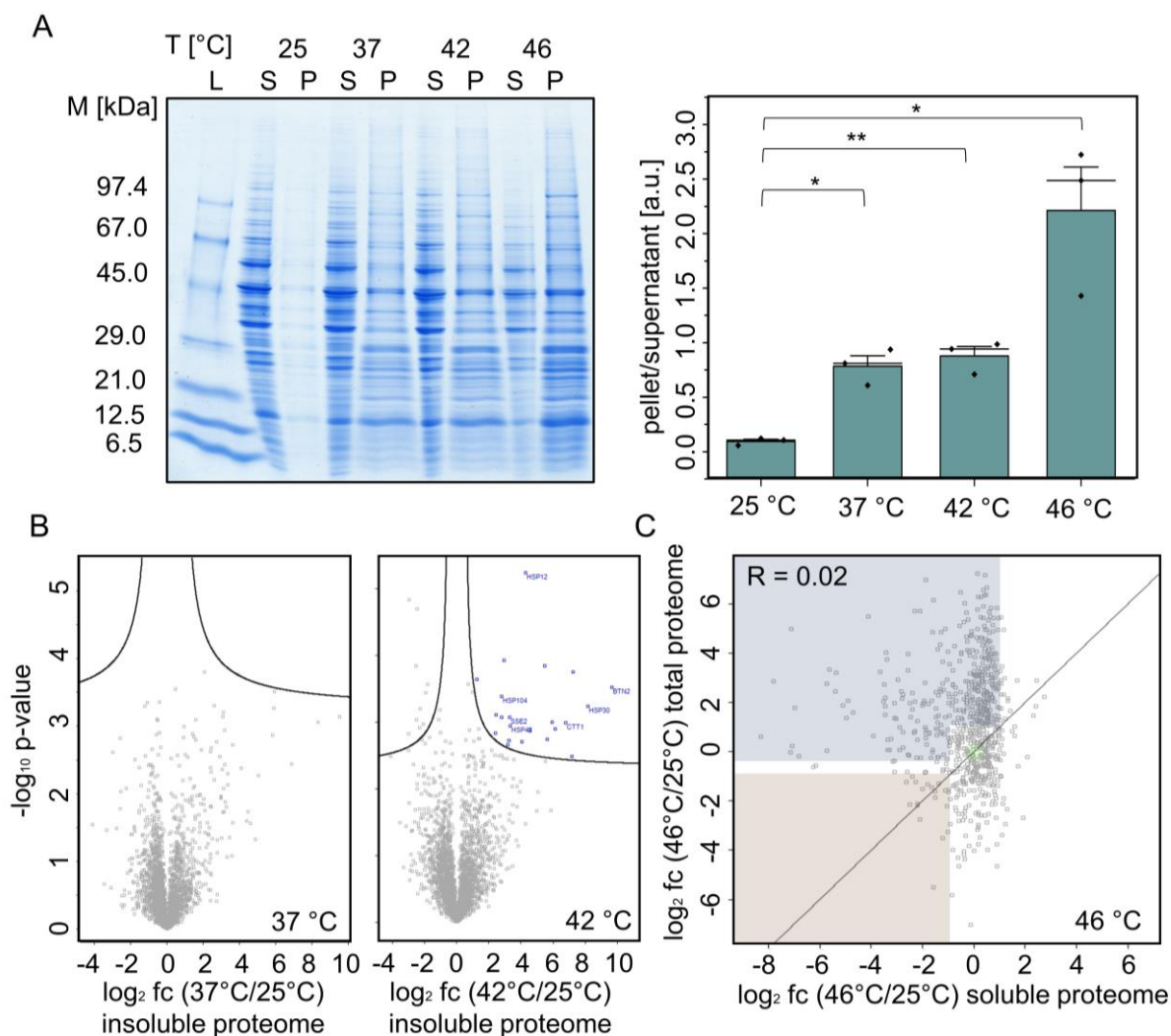
Figure 41: Aggregation processes gain importance with increasing temperature. *A) The amount of insoluble proteins increased with elevated temperature. Lysates of heat-stressed yeast cells (30 min at 37 °C, 42 °C and 46 °C, respectively) were separated by centrifugation. Subsequently, the supernatant (S) and the pellet (P) fraction were analyzed via SDS-PAGE. A representative gel is shown. The lane intensities were quantified densitometrically and the pellet intensity divided by the supernatant intensity. In the bar plots, mean values (bar height), the results of the single replicates (black dots), the median (black line) and the standard deviation from three biological replicates are shown. To estimate the significance of the changes, two sample t-tests were performed (N.s.: $p > 5$ %; *: $p < 5$ %; **: $p < 1$ %). B) Only a few proteins were identified to be pellet enriched up to 42 °C by LFQ-MS. MS spectra of the pellet fractions of cells stressed for 30 min at 37 °C and 42 °C, respectively were measured in biological triplicates. For the Volcano plots a FDR < 5 % ($S_0 = 0.1$) was applied and significantly pellet enriched proteins were colored blue. C) Sublethal heat stress led to massive aggregation processes. The soluble and the total proteome of cells stressed for 30 min at 46 °C were measured in biological triplicates with LFQ-MS. The fold changes compared to cells kept at 25 °C are shown. Brown box: degraded proteins; blue box: aggregated proteins. R: Pearson correlation. This figure can be found similarly in the associated publication (Mühlhofer et al., 2019).*

3.2.4.3 The proteome of recovered cells after severe stress correlates better with the translatome

One could imagine that the HSR is maintained during recovery or that maybe even more changes in the proteome are observed after recovery as the cells had more time to translate the changed mRNAs. To check this, another LFQ-MS measurement was performed with cells that were recovered for 1 h at 25 °C after a 30 min heat shock at 37 °C and 42 °C, respectively. 1,857 overlapping proteins were identified. At 37 °C, 97 proteins were significantly upregulated, whereas 73 proteins were downregulated (Figure 42A). At 42 °C, 54 proteins were significantly upregulated and 92 proteins were downregulated. The indicated GO categories in the Volcano plots already implied similarities to the proteome of stressed cells. Indeed, the proteome of cells that were recovered after HS at 37 °C correlated well with the corresponding proteome of cells stressed at 37 °C (R = 0.72) (Figure 42B). The correlation between the proteome of recovered cells after stress at 42 °C and the corresponding proteome of stressed cells was not as good (R = 0.57). Nevertheless, it was obvious that the stress-induced proteome was largely maintained during recovery and that it takes more than 1 h until the non-stressed state is reached again at the proteomic level. Comparisons of the proteomes of recovered cells with the ribosome profiling data even revealed that the proteome of cells that were recovered after stress at 42 °C correlated better with the translatome of stressed cells (R = 0.53), than the proteome of cells stressed at 42 °C with the respective translatome (Figure 43). The proteome of cells that were recovered after stress at 37 °C correlated not as good with the translatome at 37 °C (R = 0.46). Hence, the proteomic response under severe heat stress seemed to be slightly delayed. In summary, this delay was too small to explain the discrepancy between the proteome and the transcriptome/translatome.
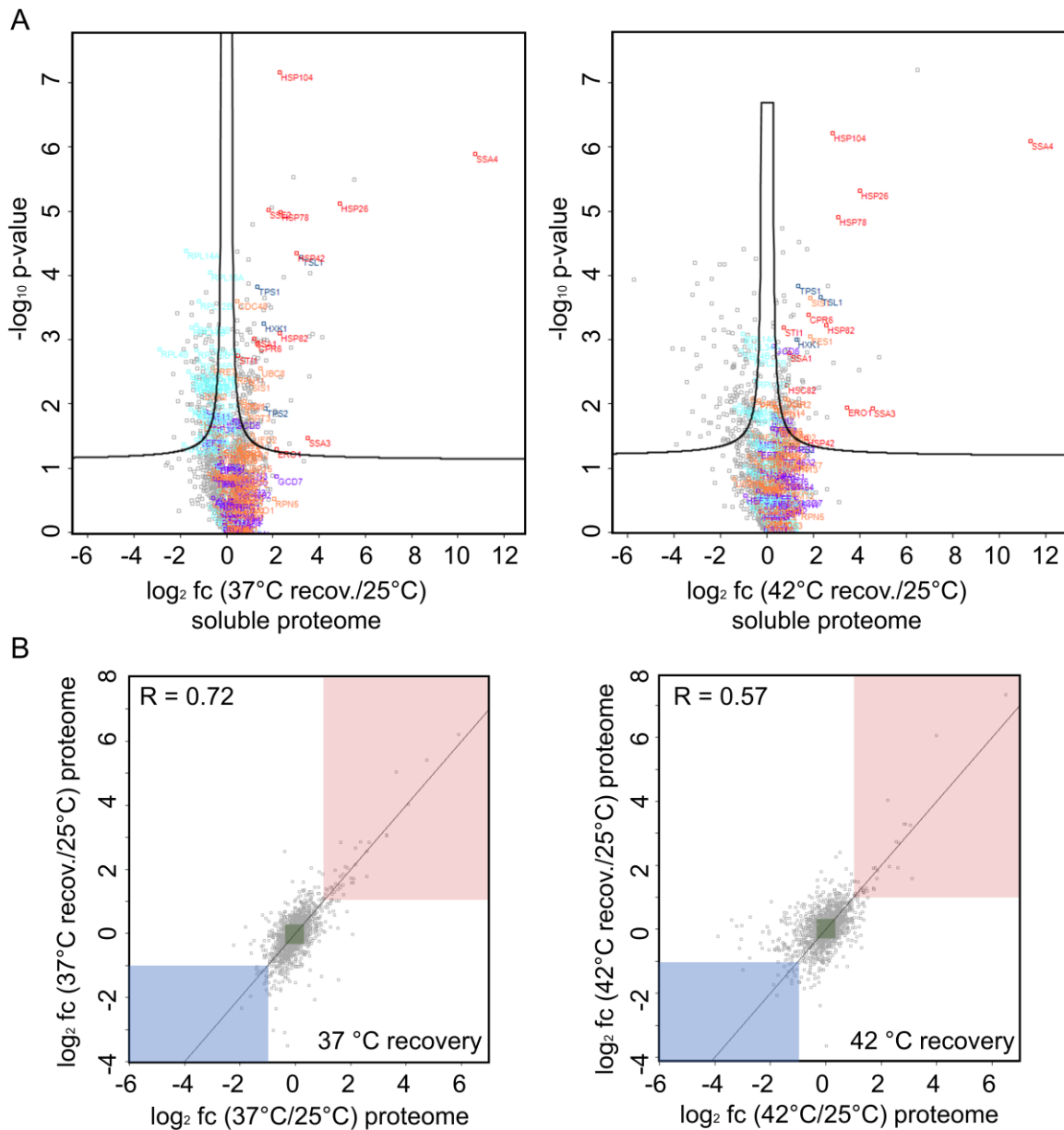
Figure 42: The proteome of recovered cells resembles the proteome of heat-stressed cells. *A) Logarithmic cells were stressed for 30 min at 37 °C or 42 °C. After the stress, the cells were shifted back to 25 °C for 60 min. The soluble proteome was measured with LFQ-MS in biological triplicates. Fold changes were calculated with the supernatant of non-stressed cells as a base. Two-sample t-tests with a FDR < 0.05 were performed for the Volcano plots. Proteins were clustered according to the Uniprot GO BP annotation table downloaded in 2015. Proteins that are associated with response to heat are stained red, trehalose biosynthesis enzymes are colored blue, ribosomal proteins cyan, translation initiation purple and ubiquitin-dependent catabolic processes orange. B) Comparison of the proteome of recovered cells with the proteome of stressed cells reveals that the proteome of stressed cells is largely maintained within 1 h of recovery. The red box comprises proteins that were at least two-fold upregulated under stress and after recovery in comparison to non-stress. The blue box comprises proteins that were at least two-fold downregulated under stress and after recovery in comparison to non-stress. In the green box, unchanged proteins are located. Parts of the figure can be equally found in the associated publication (Mühlhofer et al., 2019).*
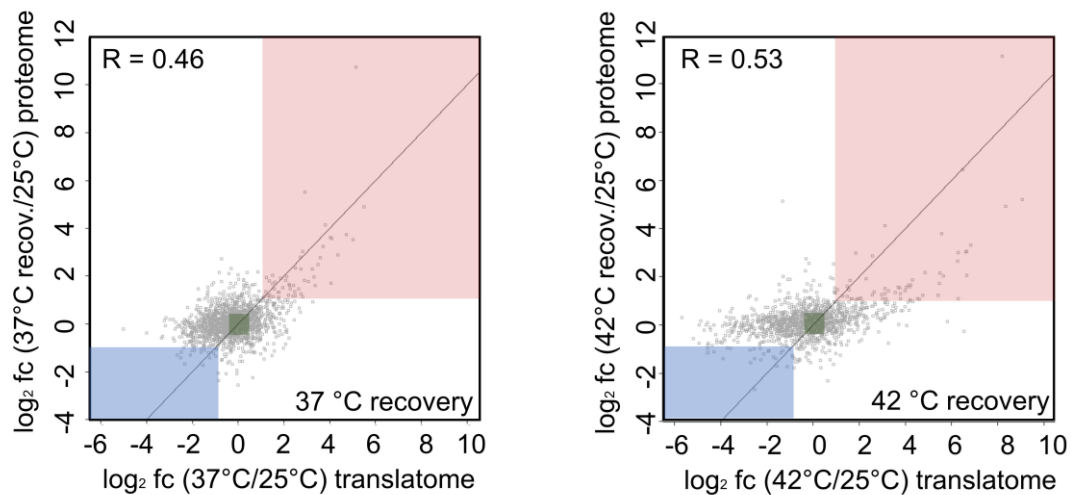
Figure 43: The proteomic response to severe heat stress is slightly delayed. *Comparison of the proteome of recovered cells with the translatome of stressed cells revealed that after severe HS the correlation was improved. The red box comprises proteins that were at least two-fold upregulated under stress in the translatome and after recovery in the proteome in comparison to non-stress. The blue box comprises proteins that were at least two-fold downregulated under stress in the translatome and after recovery in the proteome in comparison to non-stress. In the green box, unchanged proteins at both levels are located. R: Pearson correlation.*

To check if and how fast the cells recover at the transcriptomic level, qRT-PCRs were performed as described in 2.2.3.3. Two *HSP* transcripts, *HSP12* and *HSP42* were chosen, which both were strongly upregulated upon heat stress. As expected, the levels of both transcripts were increased already after 10 min at 37 °C or 42 °C (Figure 44). The *HSP42* transcripts nicely reflected the adaption process to mild stress as those transcript levels were decreased again after 30 min at 37 °C whereas at 42 °C they remained strongly increased. During recovery, the mRNAs responded fast. The *HSP42* levels in cells stressed at 37 °C reached the 25 °C level already after 5 min of recovery (Table 23). The *HSP12* levels, for which no adaption at 37 °C was observed also decreased fast, but still were elevated in comparison to the non-stressed cells after 1 h of recovery. The same was true for the *HSP12* and *HSP42* levels in cells stressed at 42 °C. Thus, the recovery process can be very well followed at the transcriptional level. Its kinetics support the proteomic observation that the "stressed proteome" is maintained for at least 1 h.
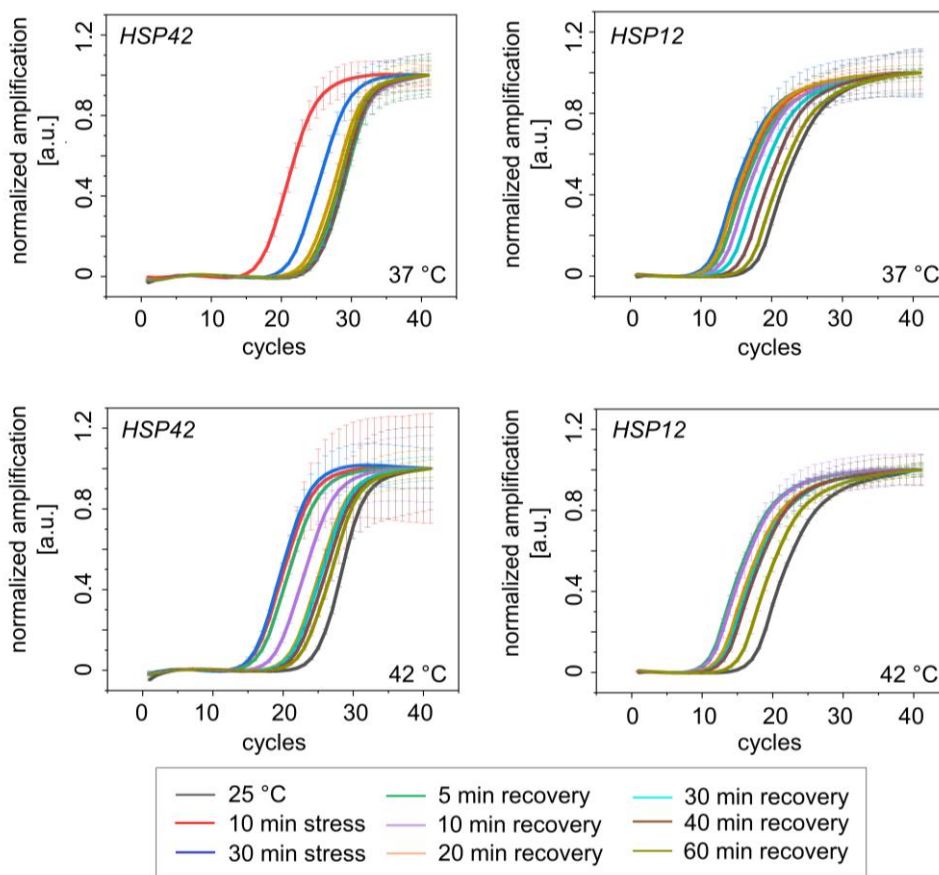
Figure 44: Recovery at the transcriptional level was followed via qRT-PCR. *Cells were stressed at 37 °C and 42 °C, respectively and the RNA isolated after 10 min and 30 min, respectively. During recovery, sampels were taken after 5, 10, 20, 30, 40 and 60 min. Mean values and the standard deviation from duplicate measurements are shown. The color code can be found in the figure. The inflection points of the amplification curves are shown in table 23. The figure was taken from the associated publication (Mühlhofer et al., 2019).*

Table 23: Inflection points derived from the qRT-PCR amplification plots shown in figure 44. *This table can be equally found in the associated publication (Mühlhofer et al., 2019).*

timepoint	Inflection point (cycle number)			
	HSP12		HSP42	
	37 °C	42 °C	37 °C	42 °C
0 min	20	20	29	28
10 min	15	15	21	19
30 min	14	14	26	19
5 min recovery	15	13	30	20
10 min recovery	17	14	29	23
20 min recovery	14	15	28	25
30 min recovery	17	15	29	26
40 min recovery	18	16	29	27
60 min recovery	19	18	29	27

3.2.4.4 Protein degradation and protein aggregation are counterbalanced by translation

As aggregation processes or a delayed proteomic response insufficiently described the discrepancy between the transcriptomic and the proteomic changes at 37 °C and 42 °C, degradation under heat stress was analyzed next. According to the translatome and proteome data, proteasomal degradation should be upregulated under mild and severe heat stress. To analyze this in more detail, the ubiquitination state in stressed cells was compared to non-stressed cells with western blots (Figure 45A, B). At 25 °C, not many ubiquitinated proteins were observed. After a temperature increase to 37 °C or 42 °C, the amount of ubiquitinated proteins was significantly increased. A further temperature increase to 46 °C however, did not lead to increased ubiquitination compared to the cells kept at 25 °C. Those results are in line with the other analyses that only implied increased proteasomal degradation under mild and severe heat stress but not under sublethal stress. Interestingly, the ubiquitinated proteins were efficiently cleared during recovery. After shifting the cells back to 25 °C for 60 min, the ubiquitination dropped back to the levels of non-stressed cells. To investigate protein ubiquitination in more detail, ubiquitin immunoprecipitation in combination with mass spectrometry was performed as described in 2.2.8.1.4 and 2.2.8.1.5. After 30 min at 37 °C, 77 proteins were found to be significantly enriched (log_2 fc > 1; p < 5 %). Tma10, a protein of unknown function which is associated to the ribosome (Fleischer et al., 2006), was enriched strongest (512-fold) (Figure 45C). Even though Tma10 is associated with translation, the overall GO categories that were identified amongst the enriched proteins correlated well with the upregulated processes under stress, thus *chaperones* and *trehalose*. Furthermore, *ubiquitin dependent ERAD pathway* was identified whereas translation was not enriched. At 42 °C, a few more (86) proteins were significantly enriched under stress. Again, Tma10 was the strongest hit. The GO categories stayed mostly the same, *protein transport* and *ubiquitin dependent degradation* were additionally found to be enriched under severe stress.
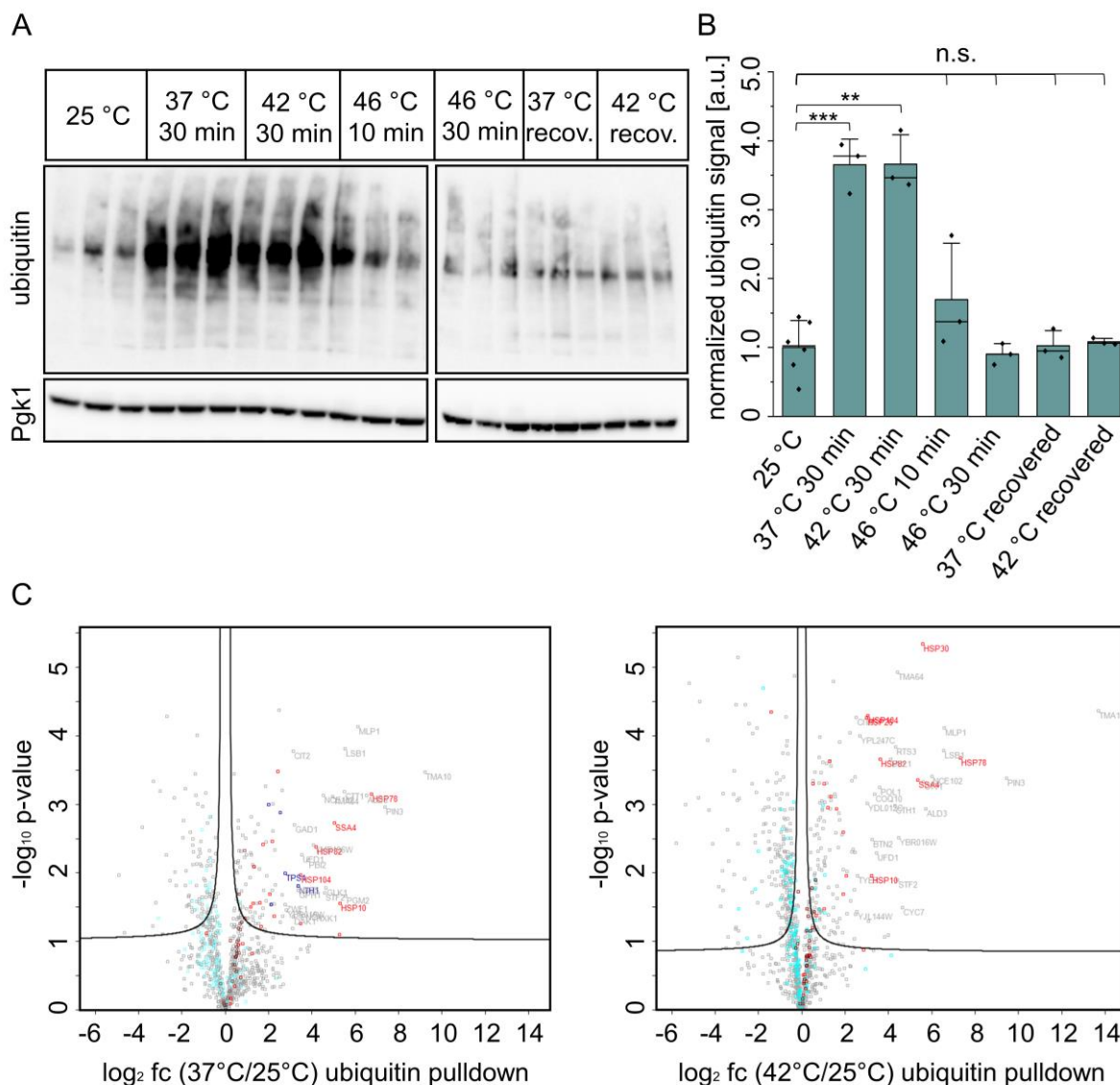
Figure 45: Ubiquitinated proteins accumulate under mild and severe heat stress. *Cells were stressed for 30 min at 37 °C, 42 °C and 46 °C. At 46 °C, also a sample after 10 min stress was analyzed. After mild and severe heat stress, the cells were recovered for 60 min at 25 °C to check the ubiquitination state in recovered cells. Biological triplicates were analyzed with western blots. Pgk1 was used as a loading control. The band intensities were quantified densitometrically and normalized to the Pgk1 intensity. In the bar plots, mean values (bar height), the standard deviation, the median (black line) and the single replicates (black dots) are shown. To estimate the significance of the changes, two sample t-tests were performed (N.s.: p > 5 %; *: p < 5 %; **: p < 1 %; ***: p < 0.1 %). C) Ubiquitin immunoprecipitation (IP) coupled to MS. Cells were stressed for 30 min at 37 °C and 42 °C, respectively. Ubiquitinated proteins were enriched via IP out of the cell lysates. Fold changes were calculated with the IP of non-stressed cells as a base. Two-sample t-tests with a FDR < 0.05 were applied for the Volcano plots. Proteins were clustered according to the Uniprot GO BP annotation table downloaded in 2015. Chaperones are stained red, trehalose biosynthesis enzymes are colored blue, ribosomal proteins cyan, and proteasomal proteins brown. The 30 strongest enriched proteins are labelled by names. The figure parts A and B can be equally found in the associated publication (Mühlhofer et al., 2019).*

Increased ubiquitination does not necessarily mean that more proteasomal degradation is taking place. It could also indicate less efficient clearance and hence accumulation of

ubiquitinated proteins. To test whether proteasomal degradation is in fact increased under stress, the proteasome was inhibited by the addition of bortezomib as described in 2.2.8.1.1.2 (Groll et al., 2006, Samant et al., 2018). Astonishingly, the proteomes of cells treated with bortezomib did not look strikingly different to the control cells kept at 25 °C. Thus, no big effect was observable (Figure 46A). At 37 °C, 47 proteins and at 42 °C, 25 proteins were significantly upregulated. At 46 °C, no protein was significantly upregulated. These unexpected results were due to the internal normalization performed by the analysis software MaxQuant. It was shown before that histone proteins are suitable to normalize proteome data that exhibit extreme and possibly asymmetric changes (Wiśniewski et al., 2014). Exactly such changes would be expected according to our hypothesis that the levels of many proteins should now be increased as instable proteins cannot be cleared by the proteasome anymore. Normalization on the measured histone proteins had very strong effects on the proteome, especially at 42 °C (Figure 46B).
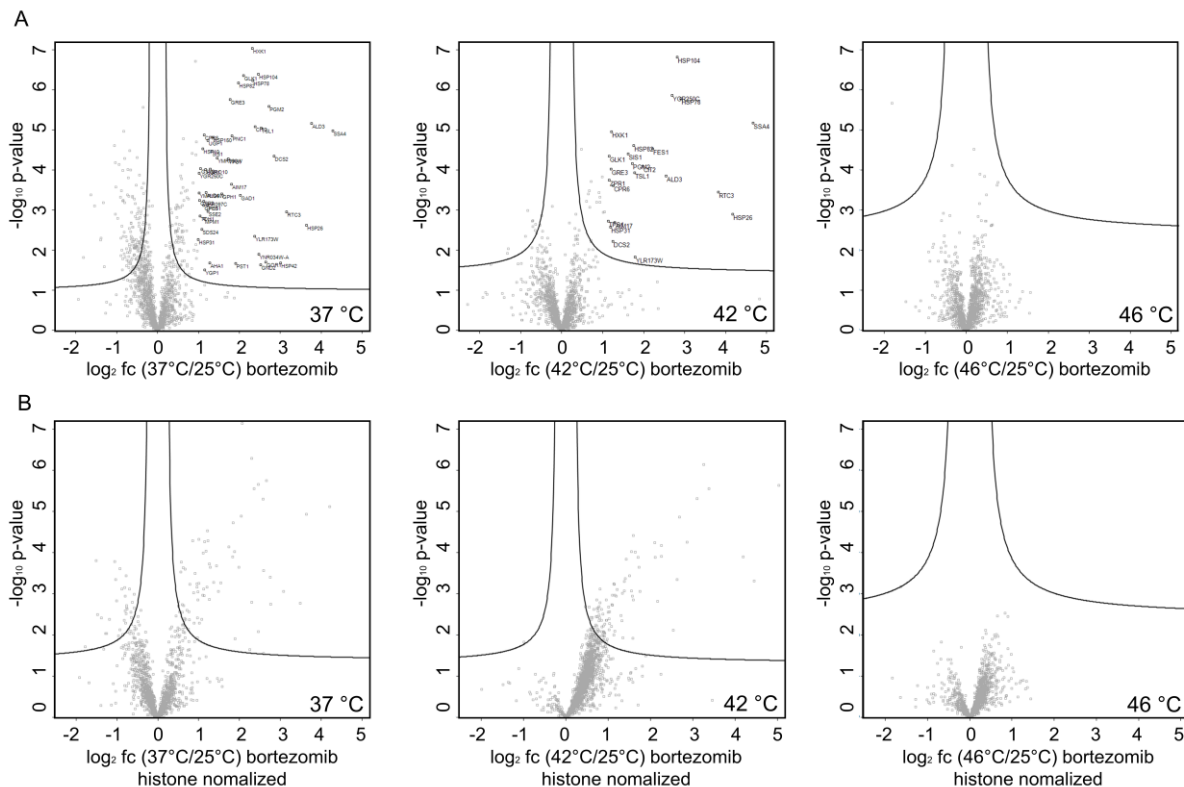
Figure 46: Inhibition of the proteasome had the strongest effects at 42 °C. *A) Logarithmic yeast cells were treated with 50 µM bortezomib for 1 h and then were heat stressed for 30 min at the indicated temperatures. The total proteomes were measured with LFQ-MS. Fold changes were calculated with the non-stressed cells as a control. Two-sample t-tests with a FDR < 0.05 were performed for the Volcano plots. Significantly enriched proteins are labelled with names. B) To overcome the internal normalization by MaxQuant, the measured LFQ intensities were normalized on the measured histone intensities. Some of the plots are taken from the associated publication (Mühlhofer et al., 2019).*

This observation strongly supports our hypothesis, that protein turnover is counterbalanced by translation. At 37 °C, the number of significantly changed genes was unchanged and the Volcano plots looked similar. At 46 °C, also no significant changes in the total proteome after normalization on the histones was observed, which fits to the other results that did not indicate proteasomal degradation under sublethal heat stress. The overall protein upregulation by the inhibition of the proteasome was not extraordinarily strong suggesting that besides proteasomal degradation also other degradation processes might play a role.

To include all possible degradation processes in the analysis, the experimental setup was changed and translation was inhibited by the addition of cycloheximide as described in 2.2.8.1.1.1. The total protein fractions were again measured with LFQ-MS. Now, a global decrease of the protein levels was expected as degraded proteins will not be refilled by translation. Also with this dataset, problems induced by the normalization in MaxQuant were observed. After performing the standard evaluation, several proteins seemed to be significantly upregulated at 37 °C and 42 °C, which does not make sense when translation is blocked. After the data were normalized on the histones again, the Volcano plots confirmed the expectation, that almost no proteins should be upregulated and most of the protein levels should be decreased or at least unchanged after the addition of CHX (Figure 47A). At both temperatures, strongly decreased protein levels were observed after the normalization. At 42 °C, 242 of 2,576 proteins showed significantly decreased levels ($\log_2$ fc < -1; FDR < 0.05; $S_0 = 0.1$) and at 37 °C, the levels of even 550 proteins were found to be significantly reduced. In the plots, a few chaperones were highlighted, which prove that translation really was blocked as those were now unchanged or even slightly reduced in their levels (Hsp82). Next, the degradation and aggregation data were integrated into the comparison of the proteome and the translatome. To cover as many proteins as possible, once more only the fold changes were taken into account whereas an at least two-fold change was premised for a protein to be degraded (brown dots; proteasomal degradation: brown crosses) or aggregating (blue dots; Figure 47B). At 37 °C, the group of less stable proteins, that were upregulated at the level of translation ($\log_2$ fc > 1) but were unchanged in the soluble proteome ($|\log_2$ fc| < 0.3), comprised 35 proteins. Two of those were found to be pellet-enriched, thus their aggregation was compensated by translation. As stated above, aggregation was a minor factor at 37 °C. Furthermore, 10 of those proteins were found to be downregulated in the CHX chase experiment and thus their stress-dependent degradation was compensated by translation. This indicates that protein turnover is a key determinant of the heat stress response at 37 °C. At 42 °C, the group of less stable proteins comprised 72 members of which 17 were found to be pellet-enriched and five were found to be degraded under stress. Thus, at 42 °C aggregation seems to become more important.
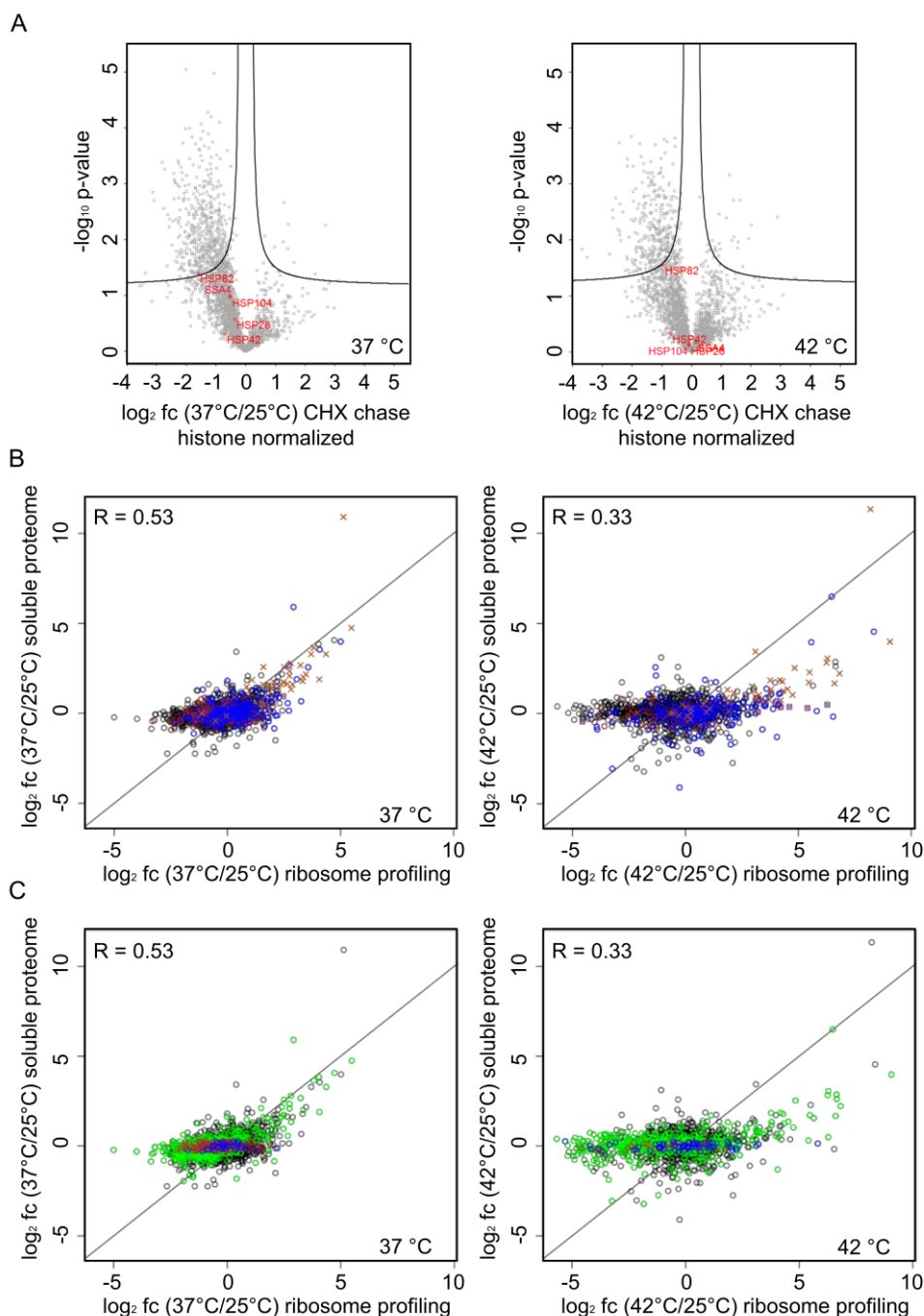
Figure 47: Protein degradation processes are strongly upregulated under mild and severe heat stress. *A) Protein translation was blocked to analyze stress dependent degradation. Logarithmic yeast cells were treated with 100 µg/ml CHX and stressed for 30 min at 37 C and 42 °C, respectively. The total proteome was analyzed with LFQ-MS. Cells kept at 25 °C were used as a control. For the Volcano plots two-sample t-tests with a FDR < 0.05 were performed. To correct for the internal normalization by MaxQuant, the intensities were normalized on the histone signals. Some chaperones are highlighted in red. B) Pellet enriched (blue dots) and degraded (blown dots; brown crosses in case of proteasomal degradation) proteins are highlighted in a pairwise comparison of the translatome and the soluble proteome. A protein was assumed to be pellet enriched if log$_2$ fc (pellet) > 1. A protein was assumed to be degraded if log$_2$ fc (CHX chase) < -1. A protein was assumed to be degraded by the proteasome if log$_2$ fc (bortezomib MS) > 1. C) In addition to degradation and aggregation, the 20 % most abundant proteins were highlighted in green (Kulak et al., 2014). R: Pearson correlation. The shown plots are taken from the associated publication (Mühlhofer et al., 2019).*

142

A big bottleneck of those comparisons was that in the different MS measurements not always the same proteins could be identified. If the analysis was narrowed down to proteins that were found in every experiment, the numbers became even smaller. In this case, for 8 of 14 proteins, it could be shown that translation compensates protein aggregation and degradation at 37 °C and at 42 °C, aggregation or degradation of 17 out of 52 proteins was balanced by upregulated translation. Hence, the reason for the partially bad correlation between the translatome and the proteome seems to be that increased protein turnover under stress has to be replenished by protein biosynthesis so that the pool of functional soluble proteins is maintained. Another main determinant for the reason why so many proteins apparently maintain their levels is most possibly the copy number per cell (cpc). Especially those proteins that were sorted into the group with a seemingly increased stability under heat stress exhibited relatively high cpcs (green dots) (Figure 47C). This allows transcriptional downregulation with no significant downregulation effects in the proteome within 30 min of heat stress.

3.2.4.5 Biophysical determinants of the different protein groups

Finally, biophysical properties that are characteristic for proteins that sort into one of the before defined five groups were analyzed (Table 24). Furthermore, pellet-enriched proteins ($\log_2$ fc > 1 and p-value < 0.05) were also included in the analysis. For this analysis, the fold change range of unchanged proteins was expanded to $|\log_2$ fc$| < 0.6$, in order to increase the amount of proteins and to potentially obtain more reliable results. The proteins were analyzed based on their molecular weight, the isoelectric point, the hydrophobicity, the aromaticity, the instability index, reported half-life, content of intrinsically disordered regions and the copy number per cell.

Table 24: Protein groups under heat stress that were defined in the global analysis.

group	translatome fold change	proteome fold change
both upregulated	$\log_2 > 1$	$\log_2 > 1$
both downregulated	$\log_2 < -1$	$\log_2 < -1$
less stable	$\log_2 > 1$	$|\log_2| < 0.6$
stable	$|\log_2| < 0.6$	$|\log_2| < 0.6$
more stable	$\log_2 < -1$	$|\log_2| < 0.6$
pellet enriched 37 °C	---	$\log_2$ (pellet 37 °C) > 1 p-value < 5 %
pellet enriched 42 °C	---	$\log_2$ (pellet 42 °C) > 1 p-value < 5 %

As pointwise correlations were confusing and also distribution plots were rather unclear, in the end, means and medians of the single groups were calculated and compared with the overall mean/median of the measured proteins. The mean values were often strongly influenced by extreme values, thus only the median values will be shown in the figure. As already mentioned above, members of the *more stable* group tended to have very high cpcs (Figure 48A). Additionally, the *less stable* members at 37 °C tended to be present in lesser copies. Whereas the cpcs of *both up* members appear to be slightly increased at 37 °C, the proteins upregulated at 42 °C exhibited a smaller median cpc, which was expected as proteins with smaller cpcs in the beginning are easier to be duplicated within 30 min. At 42 °C, also the mean cpc of the members of *both down* was strongly decreased. As the median was not conspicuous, this might rather be an artifact of single examples with extremely low cpcs and not a general characteristic of this group. The molecular weight was less meaningful (Figure 48B). At 37 °C, the *less stable* proteins seemed to be slightly bigger, at 42 °C, the *both up* and *down* group members exhibited a median M_W bigger than the average. At 37 °C, the *less stable* members had a smaller Gravy score, which means that they were less hydrophobic than the average, whereas the *more stable* fraction was more hydrophobic (Figure 48C). The median indicated that the members of the *both down* fraction were less hydrophobic, the mean however, indicated that there are also very hydrophobic members present, which even shifted the mean above the average. At 42 °C, members of the *both up* group, *stable* and *pellet enriched* were more hydrophilic, whereas the *more stable* group was again more hydrophobic than the average. The aromaticity was increased in the *both up* and *down* groups, as well as the *pellet enriched* proteins at 37 °C (Figure 48D). In the *less stable* fraction, it was strongly decreased at 37 °C. At 42 °C, the aromaticity was less conspicuous. Only in the *both down* group, it seemed to be increased as it was observed for mild heat stress. The instability indices correlated very well with the observations made at 37 °C (Figure 48E). Members of *both up* and *more stable* had much smaller instability values than the average, which means that they are relatively stable. The *pellet enriched* proteins at both temperatures seemed to be less stable. In addition, members of the *both down* group and the *less stable* group at 37 °C exhibited high instability values. At more severe stress, the indices, which were determined for non-stress conditions, did not fit well anymore. Now, the *both up* group comprised proteins with higher median instability values, whereas in the *less stable* fraction, proteins that should be relatively stable in the test tube were found. The *stable* fraction also comprised more proteins that are thought to be less stable than expected. At 42 °C, only the group *more stable* fulfilled the expectation, as those proteins exhibited low instability values. At 37 °C, a high pI correlated with less stability (Figure 48F). The *stable* fractions at both temperatures tended to exhibit smaller pIs. The half-lives fitted again quite well, especially with the observations made under mild heat stress (Figure 48G). At both temperatures, members of *both up* exhibited long

half-lives. This effect was especially strong at 37 °C. Members of *both down* had short half-lives, as expected. At 37 °C, also the members of *less stable* had half-lives below the average. At 42 °C, the median half-life of proteins in this group was inconspicuous and the mean was even increased. Members of *stable* exhibited reduced half-lives at 37 °C. At 42 °C, only the mean was reduced but not the median. At 37 °C, the half-life of the *more stable* members was comparable to the average. At 42 °C, the median was increased, whereas the mean was smaller than the average. The half-lives of *pellet enriched* proteins was above the average at both temperatures. At 37 °C, proteins with predicted intrinsically disordered regions (IDR) were enriched in the *less stable* fraction (Figure 48H). In the *pellet* and *stable* fraction, as well but not as strong as in the *less stable* fraction. In the *more stable* fraction, fewer proteins with IDRs were found. At 42 °C, also members of *pellet enriched* and *stable* carried more IDRs. In addition, also members of *both up* carried 20 % more IDRs than the average at 42 °C. Surprisingly, the lack of IDRs seemed to lead to a significant stability decrease at 42 °C. All correlations are summarized in table 25.

Table 25: The defined protein groups were analyzed according to several biophysical properties. +++/++/+: higher median value in comparison to the average; ---/--/-: lower median value in comparison to the average; *: mean looked different.

37 °C	cpc	M_W	Gravy score	instability index	pI	half-live	IDR	aromaticity
both up	+	0	0	--	0	+++	0	+
both down	0	0	0	+	++	--	0	+
less stable	--	+	--	++	+	--	++	--
stable	0	0	0	0	-	-	+	0
more stable	+++	0	+	--	0	0	-	0
pellet up	0	0	0	+	0	++	+	+

42 °C	cpc	M_W	Gravy score	instability index	pI	half-live	IDR	aromaticity
both up	-	+	-	+	0	+	+	0
both down	0*	+	0	0	0	--	---	+
less stable	0	0	0	-	0	0*	--	0
stable	0	0	-	+	-	0*	+	0
more stable	+++	0	+	--	0	+*	0	0
pellet up	0	-	-	+	0	+	+	0
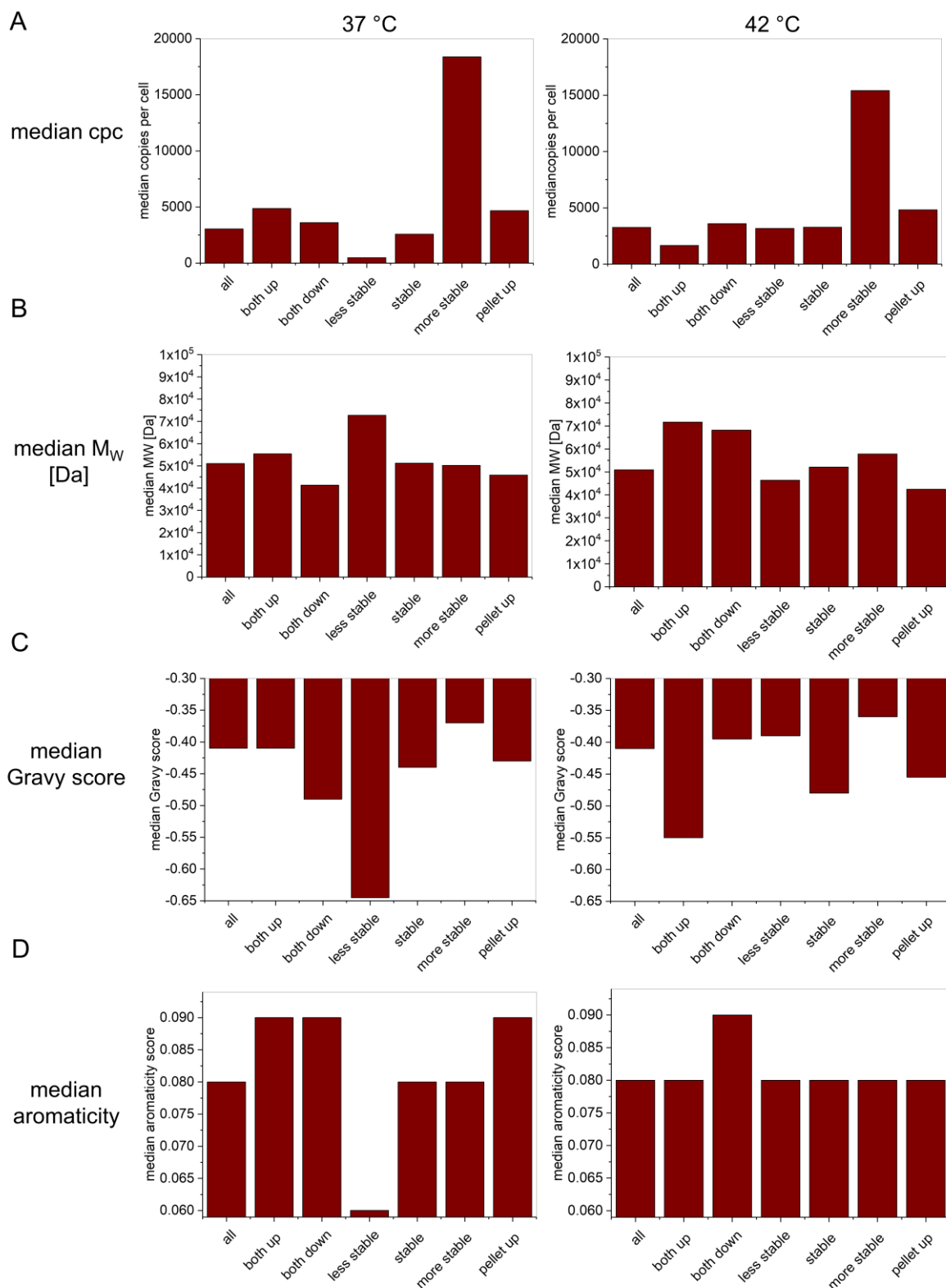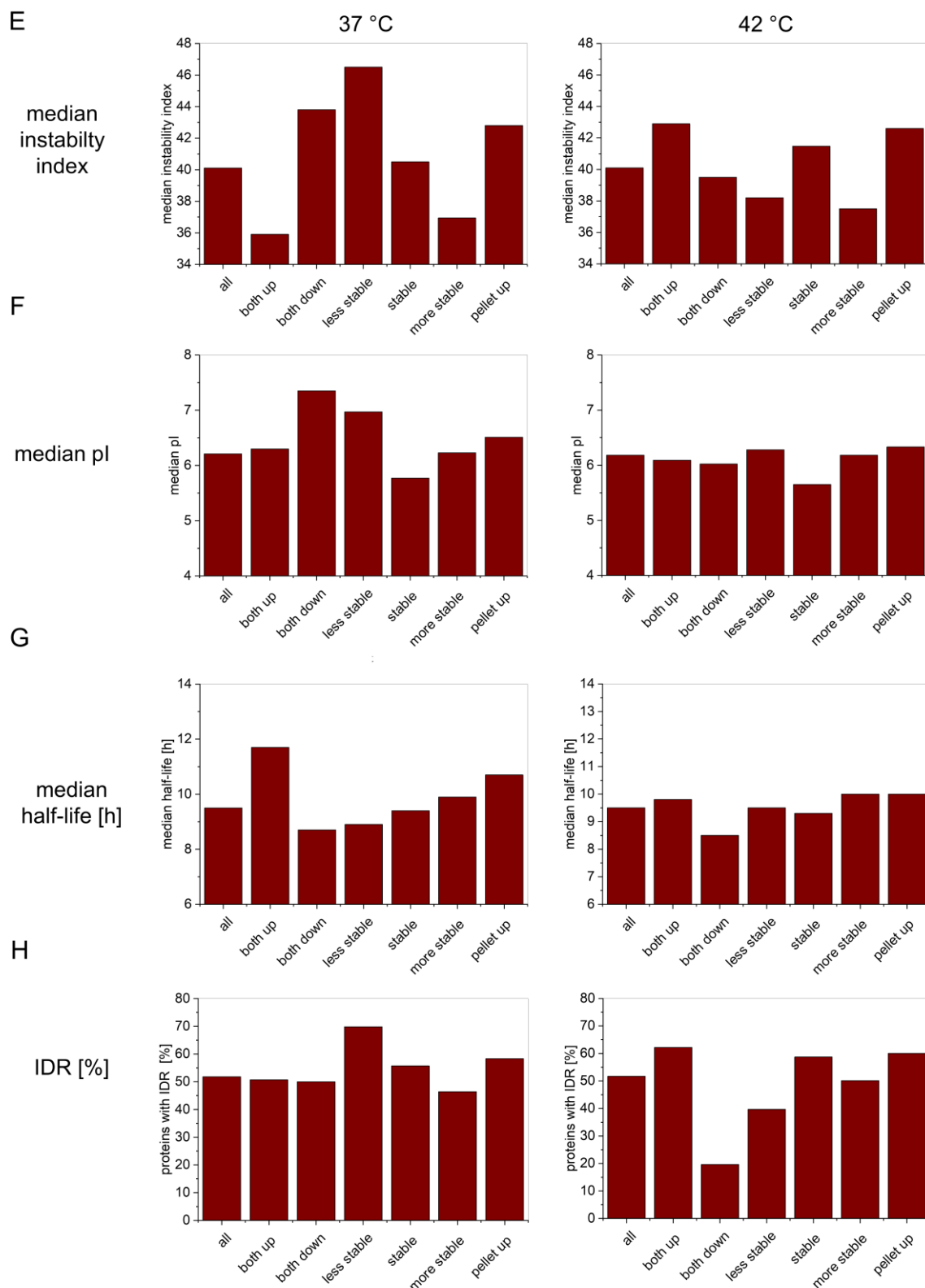
Figure 48: The proteins were grouped into both up, both down, less stable, stable, more stable and pellet up based on the ribosome profiling and mass spectrometry results. *For each group the median cpc (A), M$_W$ (B), Gravy score (C), aromaticity (D), instability index (E), pI (F), half-life (G) and IDR (H) are shown. The biophysical information was downloaded from BioGrid/Yeast mine (Balakrishnan et al., 2012). The IDR prediction was obtained from a recent publication (Macossay-Castillo et al., 2019). A classification scheme for the different groups can be found in table 24.*

147

3.3 Transcriptional regulation of the HSR in yeast

3.3.1 Depletion of Hsf1 in combination with deletion of Msn2/4 turns off the central HSR

Depletion of Hsf1, which is commonly assumed to be the main regulator of the HSR in eukaryotic cells, revealed that only 18 genes are Hsf1-dependent (HDGs) in yeast cells stressed at 39 °C (HDGs: *SSA1/2*, *HCH1*, *HSP82*, *HSC82*, *BTN2*, *HSP42*, *SIS1*, *HSP104*, *MBF1*, *STI1*, *HSP78*, *CUR1*, *AHA1*, *FES1*, *YDJ1*, *CPR6* and *MDJ1*) (Solís et al., 2016). Its essential function could be even further narrowed down to the regulation of *HSP90* and *HSP70* expression. To test what happens to yeast in the absence of the three main stress-responsive transcription factors, Hsf1 depletion was combined with the deletion of Msn2/4, which orchestrate the general environmental stress response in yeast. The hypothesis was that the central transcriptional HSR should be turned off in this mutant. The *MSN2/4* genes were deleted in the W303 Hsf1 anchor-away (AA) strain as described in 2.2.1.1 and 2.2.2.5.2.2. In addition to the strain that lacked all three TFs, depletion of Hsf1 or deletion of *MSN2/4* alone were studied in parallel. The respective cells were stressed at 37 °C or 42 °C for 10 min or 30 min, respectively. Before the stress, Hsf1 was depleted from the nucleus as described in 2.2.10 (Figure 49). The RNA was isolated after the heat shock experiment as described in 2.2.3.1.2 and libraries prepared as described in 2.2.3.4.
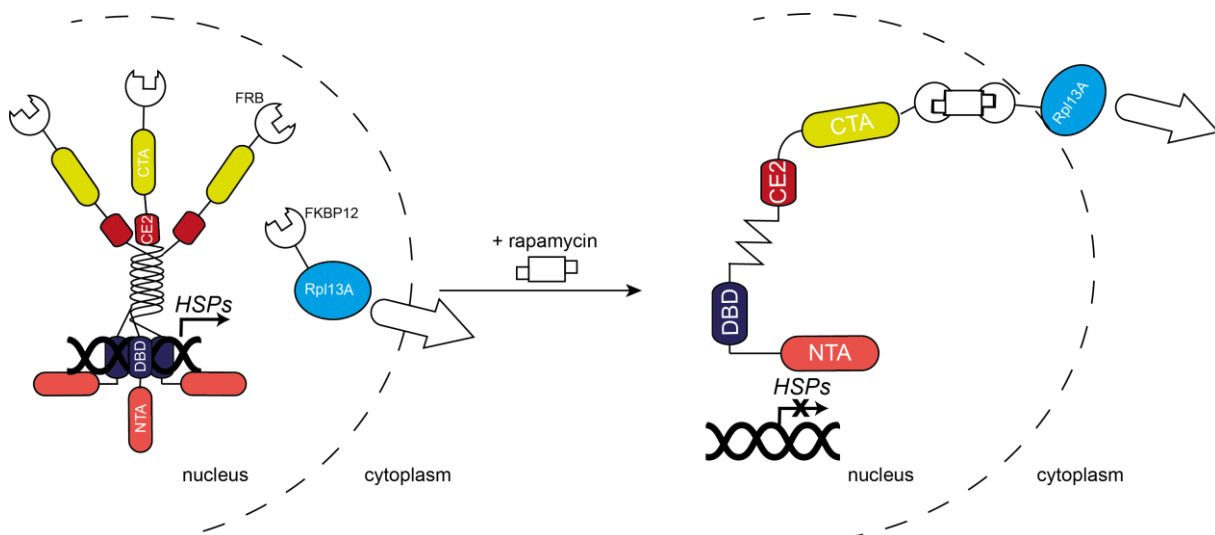
Figure 49: General scheme of the Hsf1 anchor-away system (Solís et al., 2016). *The FRB domain is fused to Hsf1 and the FKBP12 domain to a ribosomal subunit (Rpl13A). Upon addition of rapamycin, FRB and FKBP12 form a heterodimeric complex and Hsf1 is exported together with the ribosomal subunit from the nucleus into the cytosol.*

37 °C 10 min

Deletion of the *MSN2/4* genes had effects on the expression profile of numerous transcripts after 10 min at 37 °C (Figure 50A). Nevertheless the correlation with the WT cells was quite good (R = 0.8). To analyze the changes in a dynamic manner, a threshold corridor was defined with the functions $y = x-1$ (blue line) and $y = x+1$ (red line) (y: $\log_2$ fc mutant strain; x: $\log_2$ fc WT strain). It makes more sense to analyze changes in this way, as a decrease of e.g. 32-fold upregulated to 2.5-fold upregulated would be excluded if fix thresholds (e.g. $|\log_2$ fc| < 1) were applied. In this case, this change will be included. Using this dynamic threshold, the levels of 210 genes were reduced in the *MSN2/4Δ* cells in comparison to the WT after 10 min at 37 °C. Of those 210 genes, 149 genes were at least two-fold upregulated in the WT. GO analysis revealed that almost exclusively *carbohydrate metabolism,* mostly *trehalose biosynthesis* and *glycolysis enzymes* were negatively affected in the absence of Msn2/4. This represents the metabolic branch of the HSR at 37 °C. *Energy generation*, which is linked to glucose turnover, was also negatively affected in the knock-out strain, as well as the term *environmental stress response*. The deletion of these transcription factors also led to elevated levels of many genes (252). Of those, 204 were at least two-fold downregulated in the WT whereas *RNA processing* was enriched. Notably, half of the previously defined (and measured) HDGs exhibited reduced levels in the *MSN2/4Δ* strain after 10 min at 37 °C.

The overall effects of Hsf1 depletion were smaller than the deletion of *MSN2/4*. The transcriptome of Hsf1-depleted cells correlated very well with the WT transcriptome after 10 min at 37 °C (R = 0.92). The levels of almost all defined HDGs were reduced as expected. Only *MBF1* was not strongly affected at 37 °C. Furthermore, *SSA1*, *HSP104* and *HSP42* were at the borderline, but within the defined threshold corridor. Interestingly, many of the HDGs were not even elevated in the WT under heat stress, which underlines the importance of Hsf1 under physiological conditions. 33 genes were found to be decreased in the Hsf1-depleted strain. Of those, only 22 were upregulated in the WT, which were unambiguously linked to *protein folding*. Furthermore, the data revealed that Hsf1 plays an important role in the repression of gene expression. In the Hsf1-depleted strain, 256 genes showed increased expression in comparison to the WT whereas 249 of those were downregulated in the WT. Those genes were mostly involved in *RNA processing*, especially rRNA and tRNA, which indicates that Hsf1 is involved in the translational repression under heat stress.

In the absence of all three transcription factors, the correlation of the transcriptomes after 10 min at 37 °C was worse but still not bad (R = 0.70). The scatter plot already indicated that the response in both directions was strongly reduced. There were still changes observable but much weaker than in the WT. Of 241 genes that were repressed in those cells compared to the WT, 204 were upregulated in the WT. *Protein folding*, *response to (heat) stress* and

carbohydrate metabolism were found to be the negatively affected GO terms, consistent with the results obtained for the "single knock-outs".
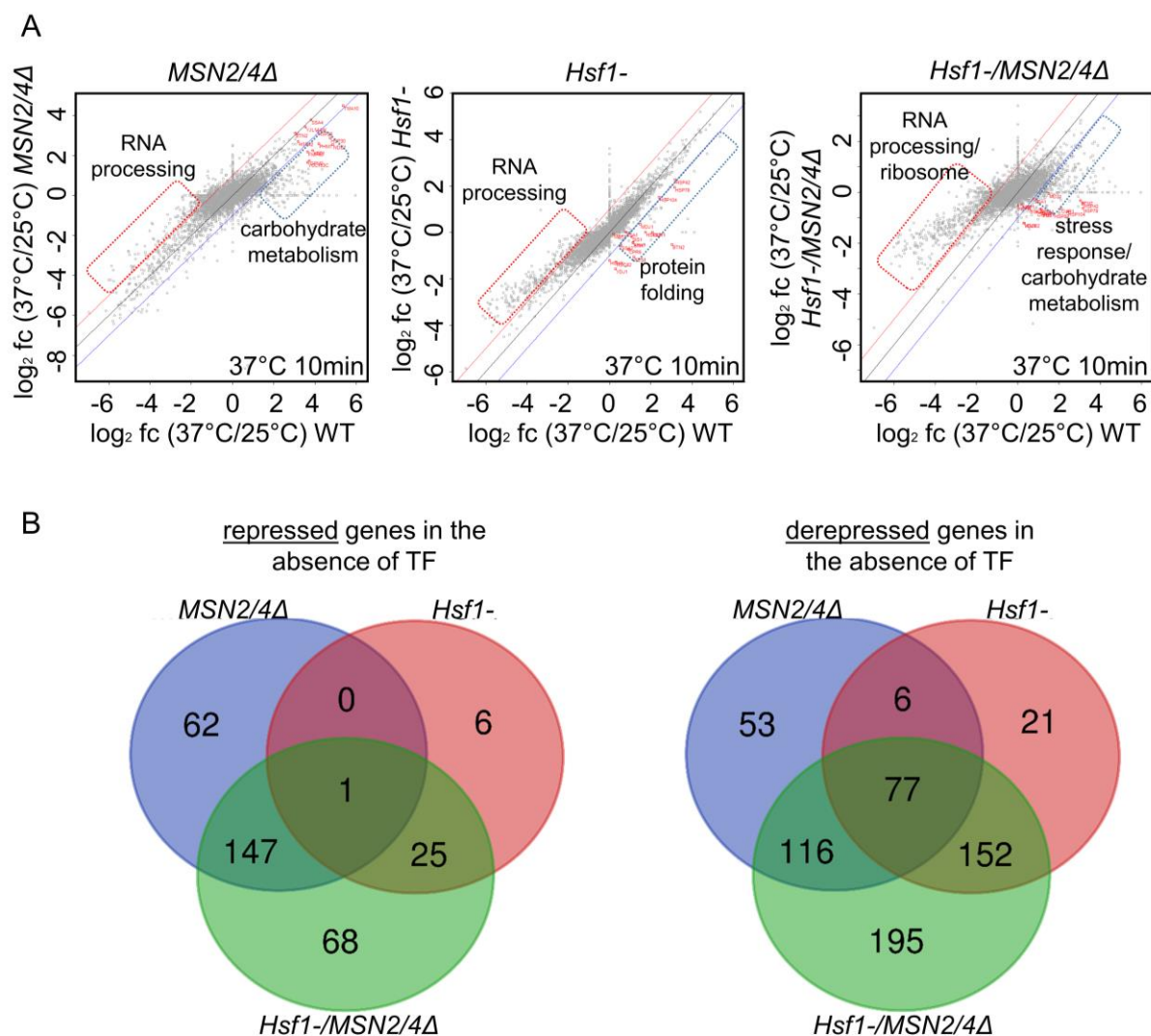
Figure 50: Deletion of MSN2/4 in combination with depletion of Hsf1 abolishes the central HSR at 37 °C. A) Pairwise comparisons of the transcriptomes of MSN2/4-deleted and/or Hsf1-depleted cells with the WT transcriptome. Logarithmic cells were stressed for 10 min at 37 °C. Cells that should be depleted of Hsf1 were treated with 1 µM rapamycin for 45 min before the stress was applied. The control cells were treated with DMSO. The RNA was isolated and sequenced. The experiments were performed in biological triplicates. Fold changes were calculated with unstressed WT cells as a base. The blue line indicates the lower threshold barrier, the red line the upper barrier. Genes that are located outside the corridor were assumed to be affected by the TFs. Hsf1-dependent genes (HDGs) (Solís et al., 2016) are highlighted in red. Blue framed genes are repressed in the cells lacking the respective TFs and red framed genes are derepressed in those strains. The main GO categories of the affected genes can be found next to the boxes (Eden et al., 2009). B) Repressed and derepressed genes in the different strains were compared with Venn plots (blue: MSN2/4 deletion; red: Hsf1 depletion (Hsf1-); green: MSN2/4 deletion and Hsf1 depletion). The transcriptomes were isolated and sequenced by Sarah Reschke.

Notably, the levels of 540 genes were increased in the strain without Msn2/4 and Hsf1 in comparison to the WT. 487 of those genes were downregulated in the WT and can be grouped in *RNA processing* (rRNA, tRNA and ncRNA), *ribosome biogenesis* and *nucleic acid biosynthesis*. This also goes in line with the results obtained for the *MSN2/4* deletion strain and the Hsf1-depleted strain alone. Although the expression profile was strongly changed in this strain, still 162 genes were upregulated at least two-fold. Those genes were involved in *sporulation*, thus no classical HSR was present anymore. The comparison of the overlap of repressed genes in the different TF-lacking strains revealed several unique targets of Msn2/4 and Hsf1 after 10 min at 37 °C (Figure 50B). Nevertheless, they also exhibit an overlapping target gene spectrum. In the strain with deleted *MSN2/4* and depleted Hsf1, 68 genes were repressed that were not conspicuous in the strains with either Msn2/4 or Hsf1 absent. According to the GO analysis, the TF target spectra of the repressed genes are more similar. Interestingly, for the derepression of 195 genes all three TFs had to be absent.

37 °C 30 min

It was shown above that yeast cells adapt to prolonged stress at 37 °C. Even though, the adaption seemed to result in a better correlation of the WT transcriptome with the transcriptome of *MSN2/4Δ* cells, the Pearson correlation was not better than after 10 min (R = 0.78; Figure 51A). None of the HDGs was affected anymore after 30 min at 37 °C in the *MSN2/4* knock-out (KO) strain. The impression of a better correlation was confirmed by the amount of repressed genes in the *MSN2/4* KO strain in comparison to the WT, which was decreased to 65. Of those, 49 genes were at least two-fold upregulated in the WT and associated with *energy generation* and *carbohydrate catabolic processes* as described before. The amount of derepressed genes dropped even more to 43 genes, of which 34 were at least two-fold downregulated in the WT and involved in *RNA processing* (rRNA and ncRNA).

The comparison of the WT with the Hsf1-depleted strain was surprising, as no adaption was observed in the strain lacking Hsf1. Thus, the HSR in this strain was more pronounced after 30 min and the stress response seemed to react slower even though the correlation was still better than expected (R = 0.84). 646 genes were downregulated in the strain with depleted Hsf1 in comparison to the WT. Only seven of those genes were upregulated in the WT, thus in this case almost no proteins were repressed. 245 of those genes were also downregulated in the WT and the rest was unchanged. *Ribosome biogenesis* and *RNA processing* were enriched in the repressed group, which supported the notion form the scatter plot that adaption does not work in the Hsf1 depleted strain or at least not as fast as in the WT. In the other direction the effect was not as strong but still 125 genes were upregulated in the strain without Hsf1 in comparison to the WT. Of those, only six were downregulated in the WT, 67 were upregulated in the WT and the rest was unchanged.
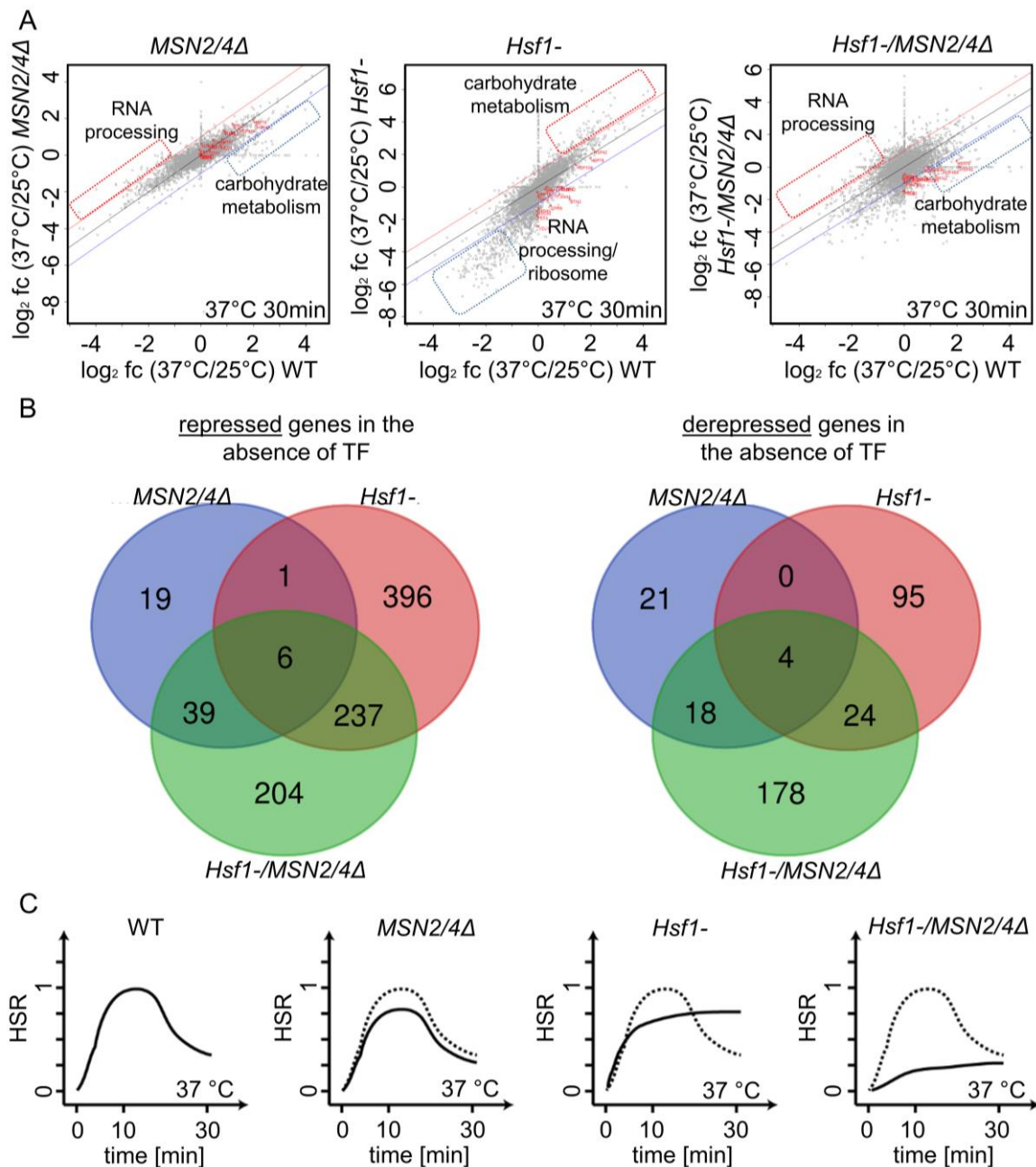
Figure 51: Depletion of Hsf1 slows down the adaption process at 37 °C. *A) Pairwise comparisons of the transcriptomes of MSN2/4-deleted and/or Hsf1-depleted cells with the WT transcriptome. Logarithmic cells were stressed for 30 min at 37 °C. For Hsf1 depletion, the cells were treated with 1 µM rapamycin for 45 min before the stress was applied. The control cells were treated with DMSO. The RNA was isolated and sequenced. The experiments were performed in biological triplicates. Fold changes were calculated with unstressed WT cells as a base. The blue line indicates the lower threshold barrier, the red line the upper barrier. Genes that are located outside the corridor are assumed to be affected by the TFs. Hsf1-dependent genes (HDGs) (Solís et al., 2016) are highlighted in red. Blue framed genes are repressed/downregulated in the cells lacking the respective TFs and red framed genes are derepressed/upregulated in those strains. The main GO categories of the affected genes can be found next to the boxes (Eden et al., 2009). B) Repressed and derepressed genes in the different strains were compared with Venn plots (blue: MSN2/4 deletion; red: Hsf1 depletion (Hsf1-); green: MSN2/4 deletion and Hsf1 depletion). C) Schematic time course of the transcriptional HSR at 37 °C of the different genotypes. The WT curve is shown in all mutant strains as a dotted line. The transcriptomes were isolated and sequenced by S. Reschke.*

Importantly, the upregulated genes were involved in *carbohydrate metabolism* and *energy generation* and not in the Hsf1-dependent chaperone branch. Thus, HDGs were not upregulated with time and were indeed dependent on Hsf1.

When all TFs were absent, only a weak response was observed. Even though numerous genes (421) were at least two-fold upregulated, exclusively *autophagy* and *sporulation* were found to be enriched. This branch is only a minor factor in the HSR induced by mild heat stress in WT cells. Changed genes in comparison to the WT were spread all over the plot. No trend was observable. Hence, the correlation between the WT and the mutant strain was bad (R = 0.55). HDGs were downregulated in comparison to the WT. Overall, 488 genes were downregulated in comparison to the WT, whereas 95 of those were upregulated in the WT and thus repressed in the mutant strain. As expected, the additional deletion of *MSN2/4* led to the suppression of *trehalose biosynthesis* and *glycolysis* (*carbohydrate metabolism*) under stress. 50 of 225 genes that were upregulated in the mutant strain compared to the WT, were downregulated in the WT. Consistently with the observations made before, those genes are involved in *RNA processing*. In summary, it can be stated that deletion of *MSN2/4* negatively affects the *metabolic branch* of the HSR whereas Hsf1 is essential for the efficient upregulation of the *chaperone branch* at 37 °C. All TFs seem to suppress *translation* and in the absence of them, the downregulation of *ribosome biogenesis* and *RNA processing* was reduced. In addition, depletion of Hsf1 slows down the adaption process and thus has contrary effects that led to a more pronounced HSR after 30 min at 37 °C in the Hsf1-depleted strain (Figure 51C). This is also visible in the comparison of the repressed and derepressed genes in the different genotypes, in which the Hsf1-depleted strain shows many unique genes (Figure 51B). After 30 min, it was again observed that more than 100 genes seem to be targeted by Hsf1 and Msn2/4. Thus, they were only changed if all three TFs were missing. Furthermore, the data clearly show that the target spectrum of Hsf1 is smaller and much more heat stress specific than the spectrum of Msn2/4.

42 °C 10 min

After 10 min at severe heat stress (42 °C), the correlation of the WT transcriptome with the *MSN2/4* deletion strain was still good (R = 0.76; Figure 52A). The transcriptome of the Hsf1-depleted strain correlated extremely well with the WT (R = 0.91). The transcriptome of the strain lacking all three TFs exhibited the worst correlation (R = 0.68). In the *MSN2/4* deletion strain, 198 genes were repressed in comparison to the WT, 160 of those were at least two-fold upregulated in the WT. The affected pathways were the same as at 37 °C: *carbohydrate metabolism* and *energy generation*. On the other hand, 156 genes were derepressed in the *MSN2/4* KO strain. Two-thirds (101) of those, were downregulated at least two-fold in the WT and again were involved in *RNA processing* and *ribosome biogenesis*.

In the Hsf1-depleted strain, the number of repressed genes was again smaller than in the *MSN2/4* deletion strain (65) but higher than at 37 °C. 38 proteins of those were upregulated in the WT and clearly linked to *protein folding*.
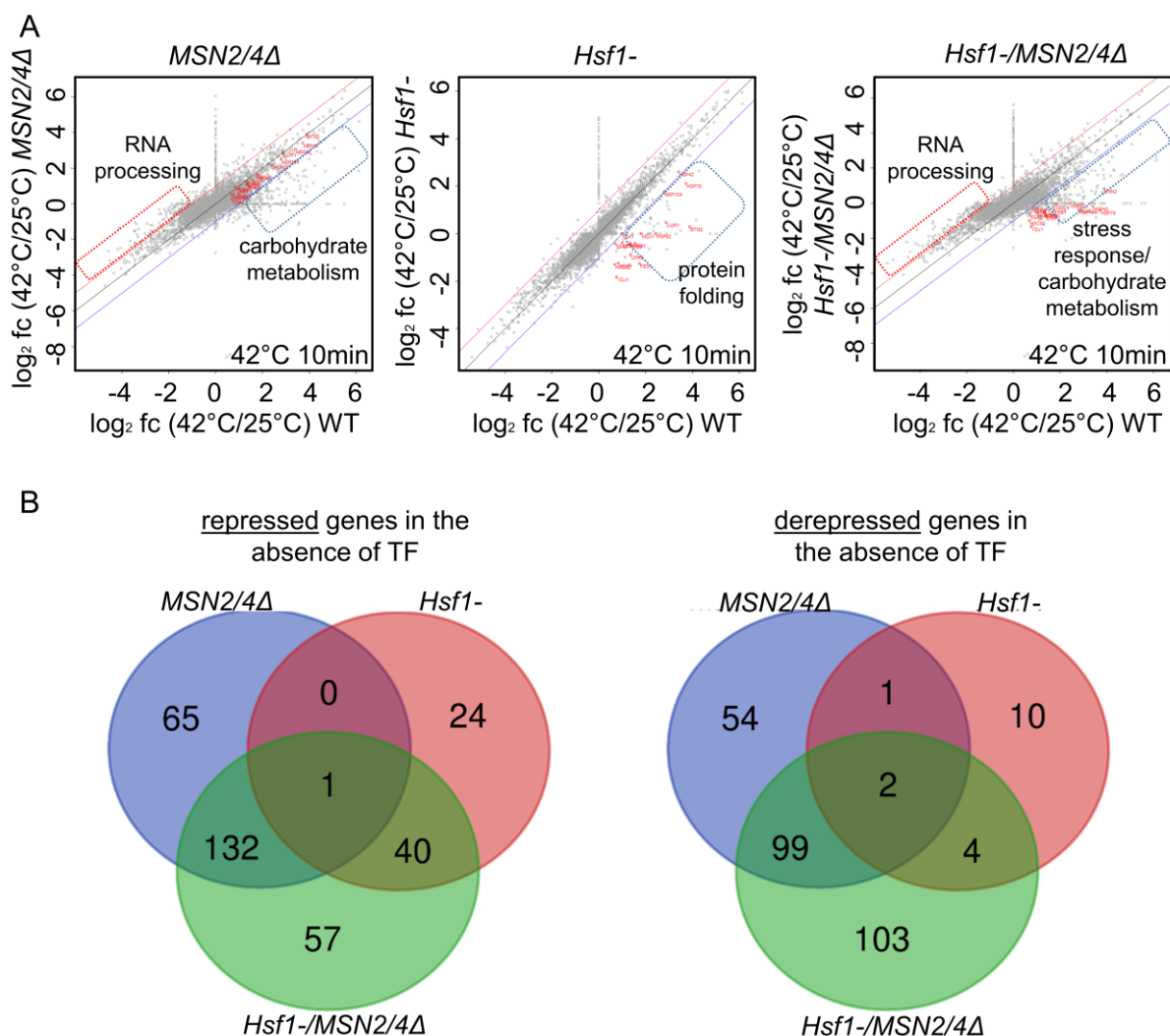
Figure 52: The central HSR is switched off in the mutant without all three TFs after 10 min at 42 °C. *A) Pairwise comparisons of the transcriptomes of MSN2/4-deleted and/or Hsf1-depleted cells with the WT transcriptome. Logarithmic cells were stressed for 10 min at 42 °C. Cells that should be depleted of Hsf1 were treated with 1 µM rapamycin for 45 min before the stress was applied. The control cells were treated with DMSO. The RNA was isolated and sequenced. The experiments were performed in biological triplicates. Fold changes were calculated with unstressed WT cells as a base. The blue line indicates the lower threshold barrier, the red line the upper barrier. Genes that are located outside the corridor are assumed to be affected by the TFs. Hsf1-dependent genes (HDGs) (Solís et al., 2016) are highlighted in red. Blue framed genes are repressed/downregulated in the cells lacking the respective TFs and red framed genes are derepressed/upregulated in those strains. The main GO categories of the affected genes can be found next to the boxes (Eden et al., 2009). B) Repressed and derepressed genes in the different strains were compared with Venn plots (blue: MSN2/4 deletion; red: Hsf1 depletion (Hsf1-); green: MSN2/4 deletion and Hsf1 depletion). The transcriptomes were isolated and sequenced by S. Reschke.*

The HDGs were more efficiently repressed at 42 °C. All HDGs lay outside the threshold corridor or at least on the border (*HSP42*, *SSA1* and *HSP104*). Interestingly, only 17 genes were derepressed in the Hsf1-depleted strain after 10 min at 42 °C and only seven of those were downregulated in the WT. As the regulation of the vast majority of other genes was similar to the WT cells, it became again evident that Hsf1 targets a very specific, relatively small set of genes.

The combination of Hsf1 depletion and *MSN2/4* deletion led to the repression of 230 genes in comparison to the WT after 10 min at 42 °C. Of those, 194 genes were upregulated in the WT. Similarly to the effects at 37 °C, also at 42 °C *carbohydrate metabolism* and *protein folding* were negatively affected. 208 genes were derepressed in this mutant whereas 157 of those were downregulated in the WT. As observed at 37 °C, those were involved in *RNA processing* and *ribosome biogenesis*. Hence, also under more severe stress the central stress responsive program seems to be abolished in the strain that lacks all three TFs. Nevertheless, 625 genes were still found to be at least two-fold upregulated after 10 min at 42 °C. GO analysis indicated again that the cells were once more preparing for sporulation. The results obtained with cells stressed for 10 min at 42 °C support the impression that there are Msn2/4 and Hsf1 specific genes as well as a shared gene set (Figure 52B). Especially the set of derepressed genes appeared to be highly overlapping (103 genes). This indicates that the suppression of transcription follows a more common principle and that only one TF suffices to inhibit the transcription of numerous genes. In contrast, the induction of gene expression seems to be a more specific process and only for 57 upregulated genes, all three TFs had to be absent to repress their transcription. Also at 42 °C, it was visible that Msn2/4 exhibit a much broader target spectrum concerning both, activation and repression of genes.

42 °C 30 min

After 30 min at 42 °C, the correlation between the *MSN2/4*-deleted and the WT strain was still quite good (R = 0.81; Figure 53A). The depletion of Hsf1 alone also had no big effect on the overall correlation of the transcriptomes (R = 0.92). The absence of all three transcription factors resulted in a worse correlation (R = 0.72). In the *MSN2/4* deletion strain, 331 genes were transcriptionally repressed in comparison to the WT, whereas 209 of those were at least two-fold upregulated in the WT. As in all other experiments, those genes were linked to *carbohydrate metabolism*. Even 414 genes were derepressed in the double KO strain. 332 of those were at least two-fold downregulated in the WT and associated with *RNA processing* (ncRNA, rRNA, tRNA) and *ribosome biogenesis*.

Whereas in the double KO the HDGs were completely unaffected, they were strongly and specifically repressed in the strain depleted of Hsf1. After 30 min at 42 °C, 75 genes were repressed in the absence of Hsf1. More than half of them (42) were upregulated in the WT and

again *protein folding* was the enriched GO term. When Hsf1 was absent, 44 genes were derepressed. Almost all of those genes (39) were at least two-fold downregulated in the WT and involved in *ribosome biogenesis* and *RNA processing*.

In the *MSN2/4Δ*/Hsf1 depletion strain, 363 genes were transcriptionally repressed. 259 of those were upregulated in the WT and linked to *carbohydrate metabolism* and *stress response* as expected. Of 732 genes that were derepressed in this mutant, 576 genes were downregulated in the WT. Those genes sorted again in *RNA processing* and *ribosome biogenesis*. Interestingly, 991 genes were still upregulated in this mutant strain after 30 min at 42 °C. The term *sporulation* was obtained with a p-value of 7.4×10^{-18}, which underlines that exclusively sporulation is initiated under severe heat stress, when the cell cannot respond adequately by the upregulation of stress protective factors. A comparison of the repressed and derepressed gene sets in the different genotypes showed once more that there are transcription factor-specific genes and genes whose regulation is redundantly orchestrated by Msn2/4 and Hsf1 (Figure 53B). As seen before, the set of repressed genes seems to be more overlapping (355 genes) than the set of activated genes (102 genes). Interestingly, for the strain lacking Msn2/4, several genes that were uniquely affected in the *MSN2/4* KO strain were identified (e.g. 118 uniquely repressed genes). As those genes were not affected in the strain that lacked all three TFs, it is implied that for some genes, Msn2/4 and Hsf1 fulfill opposite regulatory functions. GO analysis of those 118 genes pointed towards *positive regulation of growth*. This means that Hsf1 suppresses those genes in the absence of Msn2/4, possibly as a protective measure to prevent further growth. After the additional depletion of Hsf1, this protective function is lost and those genes were not repressed anymore.

In summary, those results clearly indicate that the central HSR was switched off if Msn2/4 and Hsf1 were absent (Figure 53C). Nevertheless, the cells were still able to initiate an emergency program that might rescue them into sporulation.
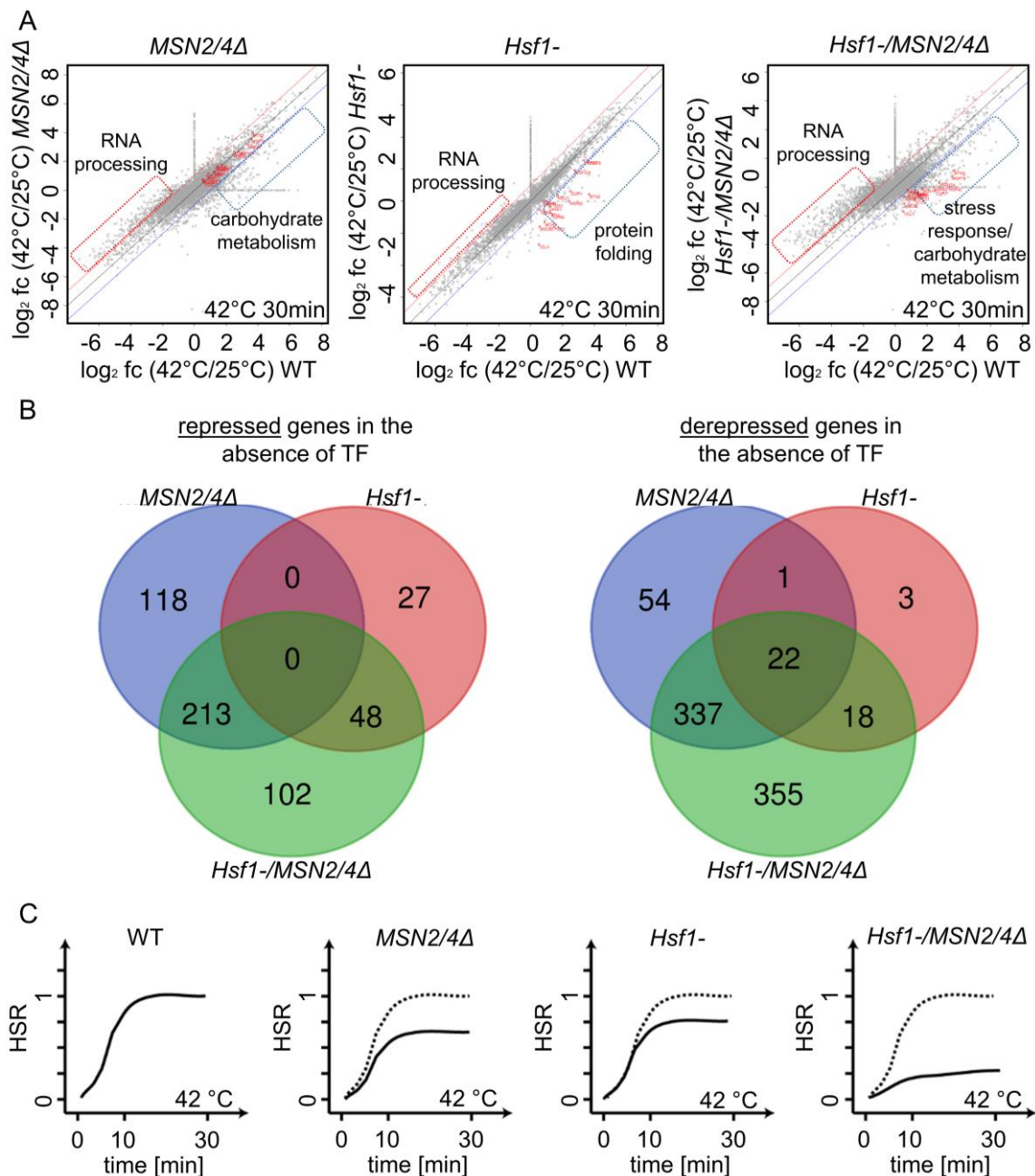
Figure 53: The central HSR is switched off in the mutant without all three TFs at 42 °C.
A) Pairwise comparisons of the transcriptomes of MSN2/4-deleted and/or Hsf1-depleted cells with the WT transcriptome. Logarithmic cells were stressed for 30 min at 42 °C. Cells that should be depleted of Hsf1 were treated with 1 µM rapamycin for 45 min before the stress was applied. The control cells were treated with DMSO. The RNA was isolated and sequenced. The experiments were performed in biological triplicates. Fold changes were calculated with unstressed WT cells as a base. The blue line indicates the lower threshold barrier, the red line the upper barrier. Genes that are located outside the corridor are assumed to be affected by the TFs. Hsf1-dependent genes (HDGs) (Solís et al., 2016) are highlighted in red. Blue framed genes are repressed in the cells lacking the respective TFs and red framed genes are derepressed in those strains. The main GO categories of the affected genes can be found next to the boxes (Eden et al., 2009). B) Repressed and derepressed genes in the different strains were compared with Venn plots (blue: MSN2/4 deletion; red: Hsf1 depletion (Hsf1-); green: MSN2/4 deletion and Hsf1 depletion). C) Schematic time course of the transcriptional HSR of the different genotypes at 42 °C. The WT curve is shown in all mutant strains as a dotted line. The transcriptomes were isolated and sequenced by S. Reschke.

157

3.3.2 Identification of additional HSR transcription factors – Establishment of ATAC-seq

As there was still some regulation in the absence of the main HS transcription factors Hsf1 and Msn2/4 observed, a relatively new method was established in the lab: *Assay for Transposase Accessible Chromatin (ATAC).* This method is based on the changes in the chromatin accessibility induced by TF binding or more general, transcriptional activity. To this end, a transposase was added to the genomic DNA, which inserts a specific transposon DNA sequence at positions where the DNA is loose (Figure 54A) (Schep et al., 2015, Buenrostro et al., 2013). It is important that the amount of added transposase, the reaction time and the number of cells are matched, to avoid too many or too few insertion events. The best results were obtained with the protocol that can be found in 2.2.5. Approximately 5,000,000 cells were treated with 5 µl of the transposase and the reaction was incubated for 20 min at 37 °C. Notably, the experiment did not work well, if the cells were flash-frozen after the heat stress. It turned out to be important to perform the transposase reaction directly after the stress (and after cell wall degradation). The transposed DNA can then be stored frozen. The ATAC library should contain fragments of a mean length of approximately 200 bp as the nucleosome length is 147 bp (Figure 54B) (Chereji et al., 2018, Schep et al., 2015). After sequencing, the samples size distribution was determined more precisely. It ranged from 50 bp to >250 bp. Notably, the amount of reads decreased with increasing read length (Figure 54C). This pattern is comparable to the published yeast dataset even though in the dataset presented here, the second smaller peak at ~180 bp was missing. Thus, the read distribution was shifted towards smaller fragments, which is not necessarily bad, as especially the accessible regions are important to identify new TFs. The ATAC profile exhibited periodicity, which arises from the nucleosome structure (Schep et al., 2015). As the DNA is tightly wrapped around the nucleosome, those parts were protected. This allows the analysis of the nucleosome pattern, as most reads are expected to be found around the center of the nucleosome (dyad). Thus, the most enriched fragment containing this position should be around 147 bp long. Equally as observed in the published yeast dataset, this fragment was 143 bp long (Figure 54D) (Schep et al., 2015). Furthermore, some shorter fragments were observed around the dyad, which reflects the dynamics of the wrapped DNA (down to 117 bp). The bioinformatic evaluation of the data is still ongoing. Changes in Hsf1 and Msn2 promoter regions are shown exemplary (Figure 54E). Unfortunately, the effects that were observed up to now for those positive controls were not extraordinarily big. This complicates the identification of additional factors, as those are not assumed to exhibit stronger effects under heat stress than Hsf1. Nevertheless, the p-values of Hsf1 and Msn2/4 were very low, which further indicated that the method principally works. Of note, the TFs involved in the cell wall integrity pathway (CWI) exhibited low p-values in this analysis, as well.
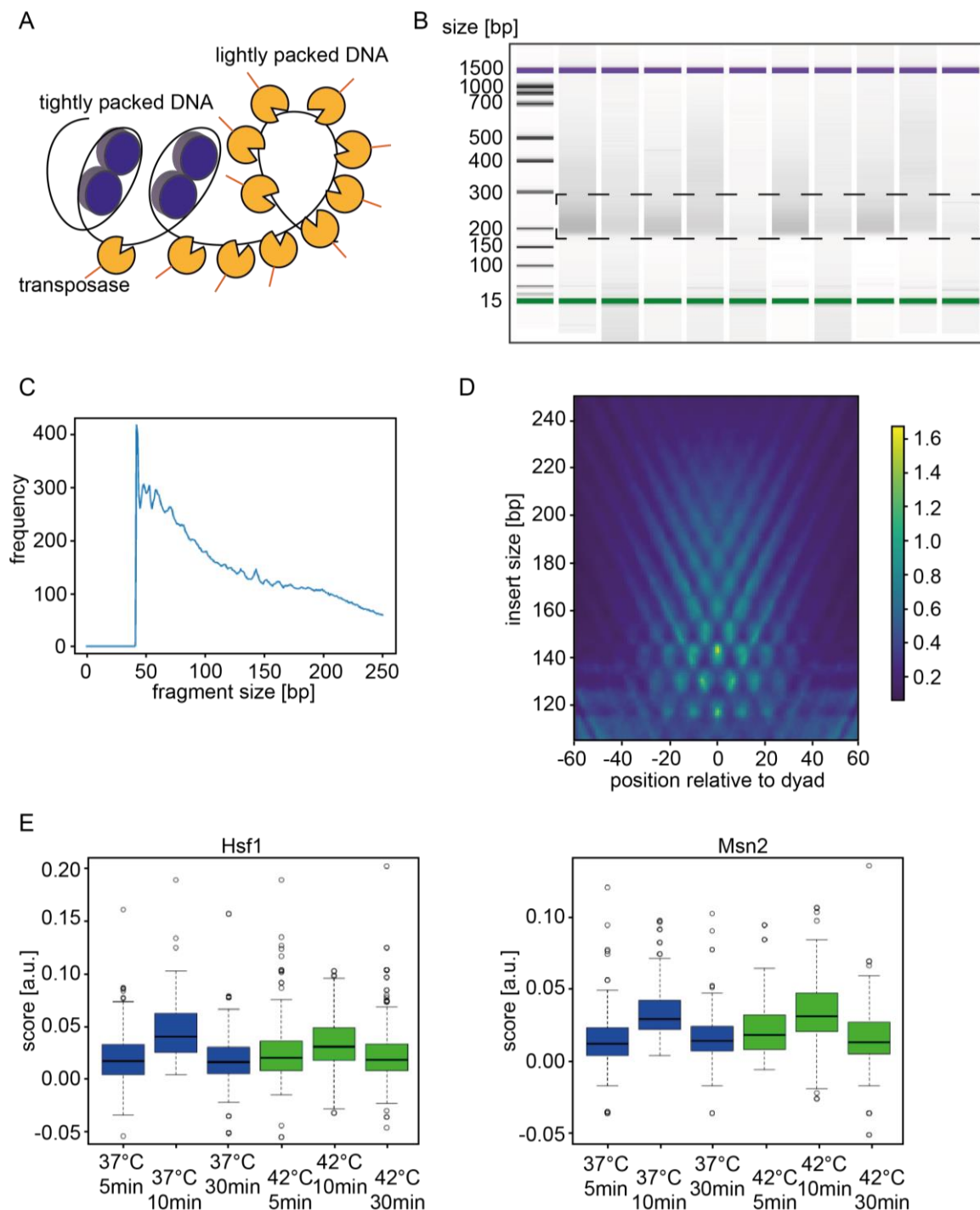
Figure 54: Establishment of ATAC-seq to search for unknown transcription factors that are involved in the regulation of the HSR in S. cerevisiae. *A) General scheme of ATAC. Accessible chromatin can be attacked by a transposase whereupon a known transposon that allows PCR amplification of the tagmented DNA is inserted. B) Bioanalyzer electropherogram of a good transposase reaction. Logarithmic yeast cells were stressed for 5 min, 10 min and 30 min, respectively at 37 °C or 42 °C. Subsequently, the cells were treated with a transposase and the tagmentation reaction was performed for 20 min at 37 °C in biological quadruplicates. Fragments for ATAC-seq should be approximately 200 bp long (black box). C) Size distribution of the sequenced fragments. D) V-plot (fragment size versus fragment center) of the ATAC-seq reads. One nucleosome-spanning region is shown. E) Scores for Hsf1 and Msn2 transcription factor binding sites determined by ATAC-seq. Bioinformatic analyses were performed by Dr. Gergely Csaba and Dr. Evi Berchtold (Prof. Ralf Zimmer, LMU).*

First results implied that some transcription factors became significant at later time points, which might be interesting and possibly will allow us to understand the origin of transcriptional waves in more detail. At 37 °C, e.g. Hot1 and Set1 were not significant after 5 min and 10 min but after 30 min. Hot1 is linked to the response to high osmolarity and Set1 is a histone methyltransferase and main constituent of the COMPASS complex. At 42 °C, Sub1 (hyperosmotic stress), Rtf1 (chromatin remodeling Paf1 complex), Mcm6 (DNA helicase domain), Gcn4 (aa biosynthesis; homologue to metazoan ATF4), Ino4 (phosphatidylcholine synthesis), Set1, Cbf2 (kinetochore assembly) and Rfa1 (DNA replication, repair and stability) were the most significant hits of those later enriched TFs. ATF4 (yeast Gcn4) is know to be a very important effector TF of the ISR (Costa-Mattioli and Walter, 2020). Thus, it makes sense that Gcn4 was found amongst the secondary TFs under heat stress, as it first had to be translated. If and how the other TFs are linked to the HSR will have to be determined.

4 Discussion

4.1 Hsp26

According to the far UV CD spectra, the phosphomimetic mutant proteins were very similar to the WT and exhibited a high β-sheet content. Only the *all-phospho* mutant differed from the other proteins. In this case, the spectrum was more similar to the WT at 45 °C. This indicates that the structure of the *all-phospho* mutant might come close to the heat-activated form of Hsp26 and that phosphorylation destabilizes the oligomer. The latter was supported by the observation that single mutations decreased the temperature, at which the oligomers dissociated. Especially the substitutions in the ACD were effective in this context. These observations are interesting because they imply that phosphorylation also decreases the temperature at which the protein is activated. Oligomer dissociation is expected to be closely linked to sHsp activation, thus phosphorylation of Hsp26 might allow the cells to react faster to elevated temperatures. As already indicated in the far UV CD spectrum, the *all-phospho* mutant does not form oligomers and exhibits only one transition at a temperature comparable to the second transition of the other Hsp26 mutants. HPLC and AUC confirmed the occurrence of the *all-phospho* mutant as a dimer. HPLC results further implied that especially the NTR and the ACD are important to stabilize the oligomer, which is in accordance to the literature (Haslbeck et al., 2004b). Upon dilution on the size exclusion column, the less stable oligomers dissociated whereas the stable ones did not. The decreased oligomer stability perfectly fits to the earlier oligomer dissociation observed in the thermal transition experiments. The IXI motif also seems to be involved in the oligomerization. Interestingly, this interaction was harder to disturb than the other interactions, as two substitutions were necessary to abrogate it. This again is in accordance to the thermal transition measurements, in which the single CTR mutant oligomers decomposed only at slightly lower temperatures than the WT, the double mutant however much earlier. Unfortunately, the size of the complexes could not be determined more precisely with SEC-MALS as the complexes are too dynamic and not monodisperse. Because of higher protein concentrations in this measurement, the complexes tended to be bigger and for some proteins, it seemed that even 40-mers were present. The analysis of the oligomers was completed with analytical ultracentrifugation experiments, a method that does not include a column and therefore no interaction with a column matrix and no dilution effect during the measurement takes place. All single/double mutants except for S47E/T48E and S90E form 24-mers according to the size prediction based on the AUC measurements. The concentration-dependent oligomerization could also be proven in the AUC as dilution led to oligomer dissociation.

Besides modulating the stability of the oligomer, phosphomimetic mutations in the ACD and CTR have an activating effect on Hsp26. Those mutants are able to suppress the aggregation

of insulin at 25 °C in contrast to the WT protein (Figure 55). Mutations in the MD also modulated the activity but only delayed the aggregation of insulin. In addition, those mutants induce the formation of rather fibrillary insulin aggregates and even seem to co-aggregate. The interaction of the MD with the substrate, which is essential for the activity of Hsp26 (Haslbeck et al., 2004b), seems to be less strong in those mutants and thus, is negatively affected by the phosphomimetic mutations. The *all-phospho* mutant however is fully active at 25 °C. An increase of the temperature did not lead to an additional activation of the mutants. Some mutants were even deactivated (e.g. ACD mutants at 37 °C). Interestingly, several of the MD mutants also induce the formation of fibrillary lysozyme aggregates. This effect was observed with WT at lower concentrations, as well and indicates that oversaturation of the chaperone might lead to fibril formation, at least of substrates that are prone to form fibrils such as lysozyme (Cao et al., 2004). When Hsp26 binds the partially unfolded substrate, processes such as α-β transition might be favored by keeping the substrate in this not completely unfolded state. Introducing a negative charge in the MD of Hsp26 by phosphomimetic mutations might weaken the interaction with the substrate and therefore decrease the maximum aggregation suppression capacity of the chaperone. Thus, co-aggregation is observed earlier with those mutants. The *all-phospho* mutant was not able to suppress heat-induced aggregation of MDH at 44 °C. Nevertheless, it is not inactive at 44 °C, as it was still able to suppress the aggregation of insulin at this temperature. Insulin is aggregating extremely fast under these conditions, which rules out the possibility that MDH is simply aggregating to fast. The different behavior might be due to the size of the substrate. Overall, mutations in the MD seem to lead to an intermediate state, between activated and not activated. Those proteins suppress aggregation to some extent also at lower temperatures but are exhausted by higher substrate concentrations and tend to co-aggregate as a result. The proteins can be heat-activated and behave quite comparable to the WT at temperatures above 40 °C. Substitution of S90 seems to be less favorable. The mutations in the ACD lead to activated species at 25 °C, which tend to loose activity relatively to the WT at mild stress temperature. Mutations in the CTR however might come close to the heat-activated state, as those proteins are already active at 25 °C and mostly retain their activity at elevated temperatures. Again, no additive effect between activation by heat and phosphomimetic mutations was observed. It should be noted that the differences in the activity could also be due to the different substrates. However, big differences in the substrate specificity induced by single phosphomimetic mutations in Hsp26 are not expected. A summary of the activity of all the point-mutants in the different assays is shown in figure (55).
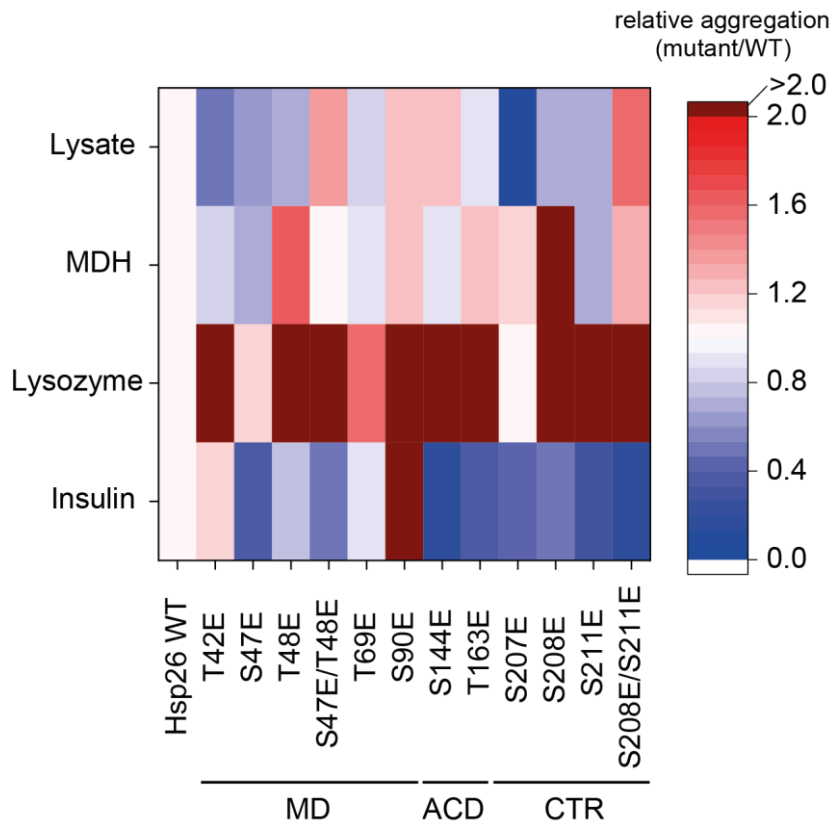
Figure 55: Phosphomimetic mutations lead to an activation of Hsp26 at lower temperatures. *The assays were performed as described in the captions of figures 16-19. The endpoints of the assays with the mutants were divided by the WT endpoints and the quotients were plotted in the shown heat map. Values below 1 (blue) indicate that the mutant was more active than the WT, values above 1 (red) indicate that the mutant was less active than the WT Hsp26. Values above 2 are indicated in dark red.*

The *in vivo* analysis was more challenging as the Hsp26 deletion strain does not exhibit a clear phenotype (Petko and Lindquist, 1986). Thus, the effects that can be expected by the mutants are small. Indeed *in vivo*, the effects were much smaller than the effects observed *in vitro*. Under the tested stress conditions, no growth phenotype was observed. Next, proteostasis under heat stress was analyzed using destabilized firefly luciferase (Gupta et al., 2011). In accordance to the *in vitro* data, the phosphomimetic mutants did not improve proteostasis under heat stress in comparison to the WT. Thus, it does not seem that phosphorylation increases the activity of Hsp26 at elevated temperature and is most probably induced under other stress conditions. This fits to the published phospho-proteome data in which Hsp26 phosphorylation was reported to occur upon DNA damage stress, inhibition of Ptk1, deletion of Ppt1 or perturbation of the N-acetyl transferase NatB complex (Albuquerque et al., 2008, Bodenmiller et al., 2010, Ficarro et al., 2002, Holt et al., 2009, Smolka et al., 2007, Helbig et al., 2010, Chen et al., 2010b, Huber et al., 2009, Schreiber et al., 2012). Only T42E was reported to be phosphorylated under heat stress (Kanshin et al., 2015). Interestingly, cells expressing the mutant proteins even tended to exhibit numerous smaller heat-induced aggregates, which are associated with more severe stress (Specht et al., 2011). Especially

cells expressing the *all-phospho* mutant showed an impaired proteostasis, which indicates that this mutant loses its activity at elevated temperatures. Analysis of the soluble and insoluble protein fractions at 25 °C and 46 °C confirmed the assumption that Hsp26 localizes to the insoluble pellet under stress but efficiently becomes soluble again during recovery. Some mutants (e.g. T48E) were already found in the pellet at 25 °C. Under stress, they were extremely enriched, which implies that they might be either less stable or more sensitive to the unfolded proteins. During recovery, the amount of those mutants in the pellet also decreased but they could not be resolubilized completely. A problem of the *in vivo* studies could be that natural occurring PTMs during stress might be affected by the mutations, which cannot be controlled in this experimental setup. To prevent phosphorylation of Hsp26 *in vivo*, a mutant in which all phosphorylation sites are mutated to alanine might be included in future studies.

The analysis of the substrate complexes by TEM revealed that the complexes are very dynamic and undergo morphological changes. Interestingly, Hsp26 substrate complexes can be formed with an activated sHsp oligomer as well as with the activated dimer. These processes seem to be temperature-dependent. At 37 °C, no oligomer dissociation was observed but still the formation of substrate complexes was visible by a changed morphology of the oligomer. At 44 °C, the Hsp26 oligomer first dissociated and then big complexes were formed anew. Thus, those results confirm the observations from former activity assays that for Hsp26 two activation modes exist and that dissociation of the oligomer is not a prerequisite for activation (Franzmann et al., 2005, Haslbeck et al., 1999). It seems that also rearrangements in the intact oligomer suffice to reach an active high affinity state that is able to bind substrate proteins and prevent their aggregation (Franzmann et al., 2005).

To find out more about the mechanism behind this observation, the structure of the Hsp26 oligomer was studied in detail. First, the dynamics of the Hsp26 complexes were analyzed with H/DX. As expected, not much exchange was observed in the mostly well-structured ACD. Furthermore, the CTR appeared to be quite stably packed in the oligomer complexes. This is presumably due to the interaction of the IEV motif with the ACD. The NTR, which is known to be less structured, consequently exhibited patches of very high exchanges rates. To understand how phosphomimetic mutations destabilize the oligomers, H/DX of two mutants (S47E/T48E and S144E) was measured. It could be shown that the mutation in the ACD has long-range effects on the MD as it affected the exchange rates comparable to the mutation in the MD. This implies that the ACD loop, in which S144E is located, interacts with the MD of another subunit, most likely with the N-terminal part of the MD. According to the H/D exchange profile, this interaction is weakened or relocated to a downstream patch (around aa 48) by the negative charge introduced by the phosphomimetic mutations. As the MD was described to be the thermosensor and essential for oligomerization (Haslbeck et al., 2004b), it is likely that

modulation of the oligomers by phosphorylation targets the same effector domain. Based on those observations, it might be even possible to narrow down the essential part of the thermosensor for oligomerization to a few amino acids (aa 32-61). The observation that the double mutation in the MD (S47E/T48E) changed the H/DX profile in the big ACD loop, where S144 is located further supports the hypothesis that the N-terminal part of the MD interacts with this ACD loop. It cannot be ruled out completely that this observation is an artifact, as only two residues of the ACD seem to be really affected. Nevertheless, it is another indication that the regions where the selected mutations are located might indeed interact with each other in the oligomer.

With cryo-EM a well-resolved structure of an Hsp26 40-mer was obtained. The 40-meric structure was partially resolved to 6.3 Å, which is significantly better than the resolution of the published 24-mer structure (up to 11 Å) (White et al., 2006). The high resolution of the Hsp26 structure allows fitting in solely a β6-swapped ACD dimer, which is characteristic for non-metazoan sHsps. Thus, the "metazoan type" dimer based on antiparallel fused β6/7 strands can now be excluded for Hsp26. Furthermore, cryo-EM revealed that the oligomer is very dynamic and that the dimers interact with the neighboring dimers in an alternating manner, which implies that the dimers are in flux and leads to a constant stretching and bending movement in the structure simulation. For the 24-mer structure, two states (expanded and compact) were described which was possibly also based on the dynamics in the oligomer that are now resolved better (White et al., 2006). The 40-mer forms a hollow sphere whereas the NTRs of several subunits apparently meet within the inner cavity. One could speculate that this structure might allow taking up unfolded proteins in the inside of the sphere where the MD can interact and hold the substrate. This would also explain why oligomer dissociation is not necessary for the activation of Hsp26 (Franzmann et al., 2005). In this case, Hsp26 would be needed in higher concentrations to be active. However, when the Hsp26 oligomer first dissociates, lower Hsp26 concentrations might be sufficient to achieve comparable activity. This is in accordance with the MDH assay in which aggregation inhibition was achieved in substoichiometric chaperone ratios whereas in the lysozyme assay, at least equimolar ratios were needed.

4.2 Global analysis of the HSR

By combining transcriptomics, translatomics and proteomics, the HSR in yeast was studied in detail. Up to date, the analyses of the HSR have predominantly been focused on chaperones and phase separation or aggregation processes (Iserman et al., 2020, Mackenzie et al., 2016, Solís et al., 2016, Wallace et al., 2015, Cherkasov et al., 2015). Of note, our transcriptomic studies revealed that only roughly 5 % of the regulated genes were chaperones. Thus, in this thesis also the "rest" was integrated in the HSR model of yeast. The analyses implied that the

HSR consists of three main branches. The well-studied chaperone branch, which is crucial to maintain proteostasis under stress by aggregation suppression, protein (re-)folding and protein sequestration. Based on the experimental results, a second branch was defined, which comprises many genes and whose main function seems to be balancing increased stress induced protein aggregation and degradation. This branch allows the maintenance of metabolism and growth as long as possible. The first two branches are the key pathways that are addressed under mild and severe heat stress up to 42 °C. A further temperature increase to 46 °C activates the third branch, which is characterized by extensive aggregation and phase transition processes and leads to a shutdown of translation and growth (Figure 56). Thus, the stress response is dependent on the severity of the stress. Whereas under mild heat stress, besides chaperones, many metabolic pathways, such as glycolysis or trehalose biosynthesis were upregulated, the focus shifts more to a regulated repression of translation in combination with upregulation of chaperones at 42 °C. At 46 °C, an immediate cell growth arrest is induced by protein aggregation. *In vivo* experiments implied that for BY4741 yeast cells, the borderline temperature at which cell growth is stopped is around 43 °C. Up to 42 °C, cell growth was only slowed down and no phenotypic effects were observed which supports the assumption of a productive stress response.

The analysis of the transcriptome had already revealed earlier that temperature specific pathways are addressed and that there is a specific temporal regulation that divides the stress responsive genes in an immediate and a delayed group (Mahat et al., 2016). At 46 °C however, the transcriptomic response differed significantly from the other two temperatures. It seemed that a fast response was taking place, possibly during the initial phase of temperature increase upon shift to 46 °C. Afterwards not much was happening anymore at 46 °C. Furthermore, significantly fewer genes are affected at 46 °C. Nevertheless, the core set of the HSR, consisting mainly of chaperones and trehalose biosynthesis was still found to be upregulated. This indicates that, the more challenging the stress becomes, the more narrowed down to the core program the stress response becomes. Analysis of different laboratory WT strains revealed that comparisons between different studies with different strains should be handled with caution and some variation has to be considered. An inter-strain comparison of the early HSR at 37 °C seems to work. During adaption, the profiles differ stronger. Overall, the DBY7286 and the BY4741 strain exhibited a more closely related response than the BY4741 and the W303 strain, which might also be due to the adenine deficiency of W303 (Kokina et al., 2014).
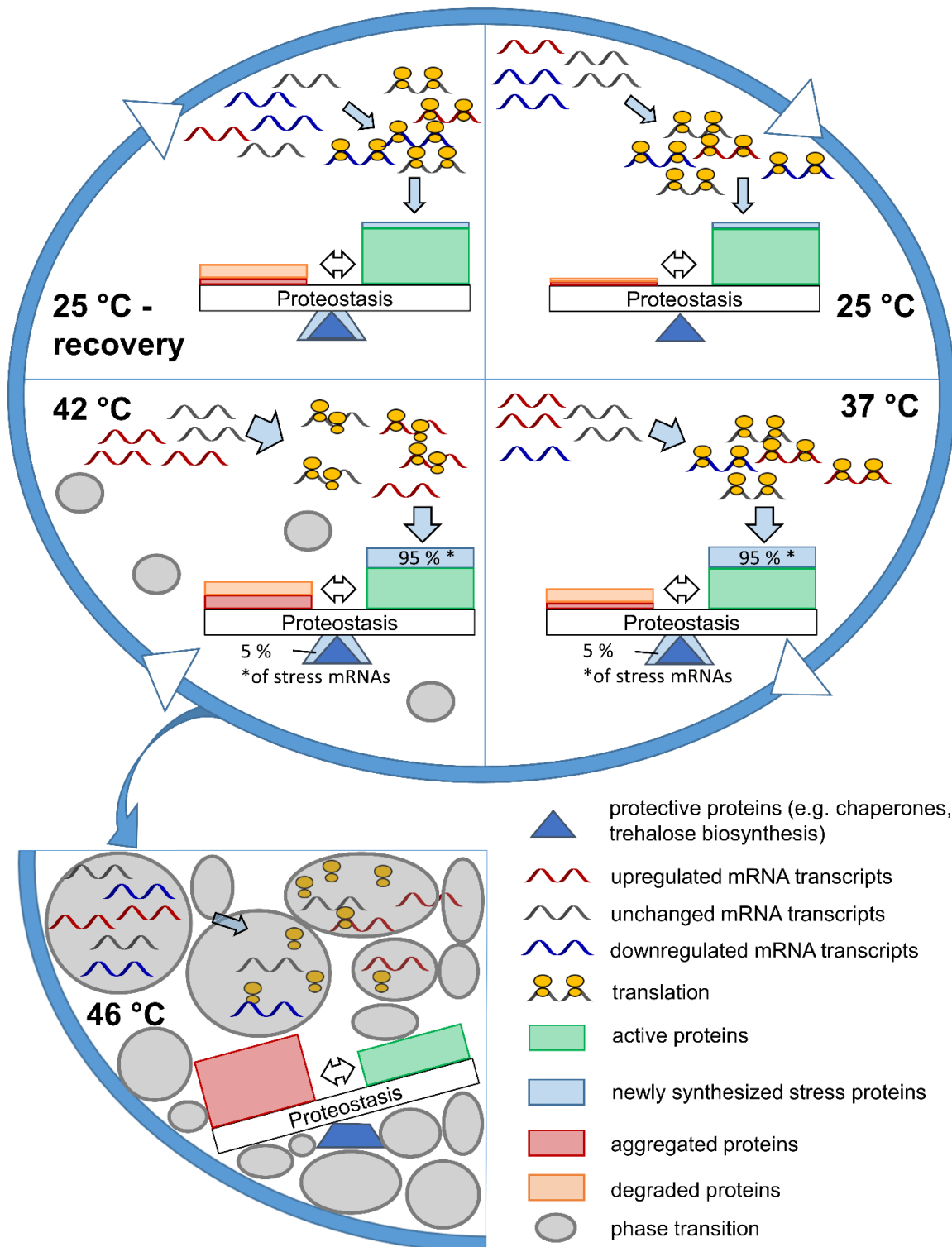
Figure 56: Model of the HSR. *Under mild and severe heat stress, ~90 % of the transcriptomic regulation takes place to replenish protein loss due to aggregation and degradation with no obvious changes in the proteome. At 42 °C, aggregation plays a more important role than at 37 °C. Degradation processes are similarly upregulated. Around 5 % of the stress induced mRNAs code for chaperones, which is thought to be the classical HSR. During recovery, proteins targeted for degradation are cleared and protein deposits dissolved again. At 46 °C, aggregation is the key determinant that shapes the HSR. Translation and growth are completely arrested. The model is equally shown in the associated publication (Mühlhofer et al., 2019).*

For the analysis of the regulation of translation, the *in vivo* behavior of two model proteins for phase separation (Ded1 and Pab1), which are involved in translation, was studied. It could be shown that the proteins mostly stay soluble until 42 °C, which implies that translation is perpetuated up to severe stress. Furthermore, those data suggest that phase separation of those proteins does only have a minor effect on the regulation of the HSR under mild and severe stress. In addition, the presented data show that the absence of Pab1 is not sufficient to induce the translation of Hsps. Thus, Pab1 does not seem to suppress translation of *HSP* coding genes under non-stress conditions. It should be noted that the tested chaperones do not have poly(A) stretches of 12 or longer without interruption even though especially *HSP26* and *HSP104* are strongly enriched in adenines in their 40 bp 5´ UTR (Figure 32). Thus, this observation fits to the published data which state that the poly(A) sequences need to be 12 bp or longer to achieve translational inhibition by Pab1 (Xia et al., 2011). Therefore, Pab1 might still affect translation of other genes under heat stress, but the effect on the selected chaperones was small under the tested conditions up to 42 °C. Nevertheless, it could be shown that stress at 42 °C seems to be the border to translational arrest for BY4741. While at 37 °C, *de novo* protein biosynthesis was unaffected, at 42 °C, it was continued but only for approximately 30 min. Then, a strong translational suppression of approximately 85 % compared to the initial synthesis rate was observed. The arrest is reversible, as translation was continued with a lag phase during recovery. At 46 °C, no translation was observed anymore due to extensive aggregation processes. Analysis of the translational profile by ribosome profiling revealed that hundreds of genes are changed in their ribosomal occupancy and that the ribosome profiling data correlate very well with the corresponding transcriptome data. Those data also imply that with prolonged stress, translation should be negatively affected. Importantly, the ribosomal distribution on the transcripts was affected by heat stress whereas the strongest stalling was observed after 30 min at 42 °C. This supports the observation from the protein biosynthesis experiments where almost no synthesis after 30 min at 42 °C was observed anymore. After 30 min at 37 °C however, the stalling effect was reduced and hence the stress adaption is reflected at the level of translation, as well. This is also in accordance with the protein biosynthesis experiment. As described for mammalian cells, the stalled transcripts are enriched in hydrophobic stretches within the first 30 amino acids (Shalgi et al., 2013). Most likely, the stalling is based on the recruitment of Hsp70 away from the ribosome under stress. As such hydrophobic sequences are dependent on Hsp70 to adopt their correct folding and to prevent unwanted interactions, translation of those transcripts might be stalled to avoid aggregation of newly synthesized proteins (Hartl et al., 2011). It should be noted that the stalling effects are minor and should not be over interpreted. As already mentioned in the introduction, stalling which is observed in the presence of CHX have to be handled with care, as it was shown that elongation inhibition with CHX is imperfect and still

allows some elongation (0.1 - 0.3 aa/s; normal speed 7 - 9 aa/s) (Hussmann et al., 2015, Lacroute, 1973). Thus under heat stress conditions, the rate-limiting step might be shifted from initiation towards elongation in the presence of CHX, which leads to stalling artifacts (Gerashchenko and Gladyshev, 2014, Hussmann et al., 2015, Lacroute, 1973) (Figure 57). Nevertheless, according to our bioinformatic analysis the slight effect, which is seen, is not an artifact. Furthermore, those effects do not challenge the assumption that translation initiation is the key process affected under heat stress (Crawford and Pavitt, 2019).
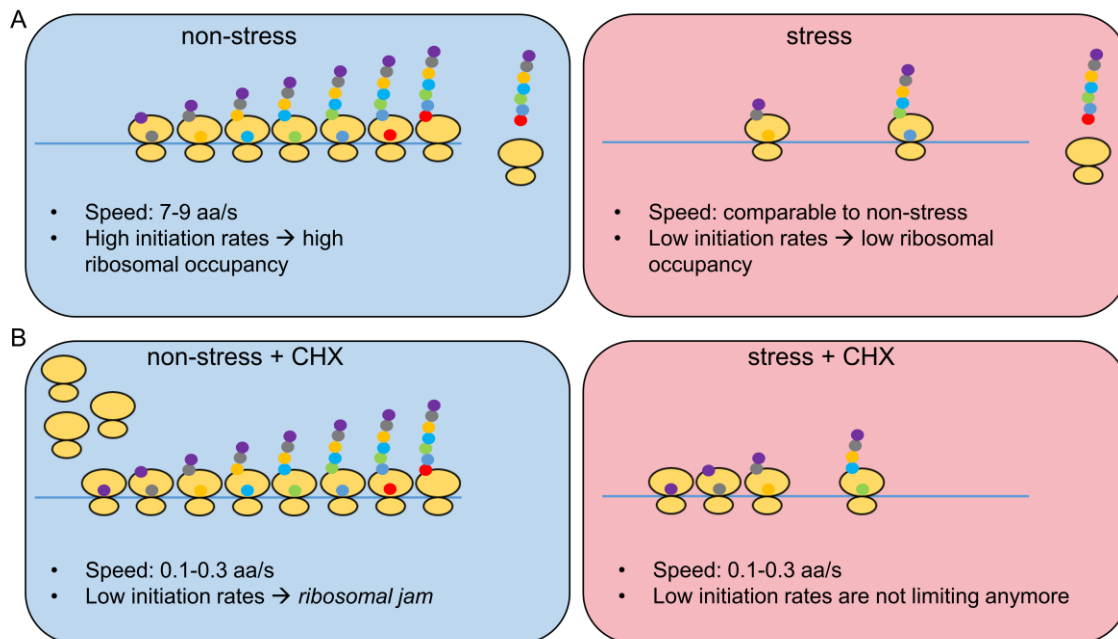
Figure 57: Schematic picture of the stalling effect that might be induced by CHX under heat stress. A) Under non-stress conditions (blue), translation initiation is fast and not limiting. Under stress (red), initiation becomes limiting whereas the elongation speed is unaffected. B) After the addition of CHX, translation elongation is only incompletely blocked and translation elongation becomes the rate-limiting step under both conditions. Hence, the occupancy profile under non-stress conditions looks principally the same. Under stress, the profile changes as the rate-limiting step has changed. Thus, early regions of the transcripts appear to be stronger occupied by ribosomes in comparison to the end of the transcripts.

In comparison to the transcriptomic and translatomic changes, the changes in the proteome are small. As expected, mostly heat-protective factors are upregulated. Under mild heat stress, *glycolysis* and *trehalose biosynthesis* were again upregulated. The correlation between the translatome and the proteome improved if only the targeted pathways were considered. Besides the before mentioned *trehalose biosynthesis*, as well as *glycolysis enzymes* and *chaperones*, also *proteasomal degradation* turned out to be upregulated under stress at both levels. Thus, the main message of the transcriptional regulation is transferred to the proteome. Interestingly, only a few proteins were downregulated and translation initiation factors were only found to be clearly downregulated at 46 °C, which again fits to the analysis of translation. Thus, downregulation of mRNAs tends to correlate even worse with the proteome. This

observation has already been made before and it was suggested that the main function of mRNA downregulation is to avoid a competition of those less needed mRNAs with mRNAs coding for stress-protective proteins at the ribosome (Lee et al., 2011). This hypothesis goes in line with the observations presented here. The MS analysis of recovered cells revealed that the heat stress proteome is mostly maintained within 1 h of recovery. Furthermore, the correlation of the translatome measured at 42 °C and the corresponding proteome of recovered cells is improved in comparison to the proteome measured directly after the stress. This indicates that the proteomic response is a bit slower than the response at the level of translation. Nevertheless, the improvement of the correlation was not strong enough to state that the proteomic measurements were performed too early and that the bad correlation was due to the measurement of a proteomic transition state and not a steady state proteome (Liu et al., 2016). In this context, it should be mentioned again that the changes induced by heat shock are dynamic at the mRNA level and undergo constant adjustments. Thus, it might be hard to measure a real steady state proteome under heat stress. Concerning the recovery time, it should be noted that cooling of the media was much slower than heating. Heating of 50 ml medium took approximately 8 min. For medium that was warmed to 42 °C, it took around 20 min to fall below 30 °C, from 37 °C to <30 °C it took around 12 min. Thus, the actual recovery time was shorter than 1 h. Nevertheless, the cells were recovering under those conditions, which was shown at the transcriptional level. The comparison of the transcriptome/translatome with the proteome indicated that there are proteins that exhibit increased stability under stress as the downregulation at the transcriptional level resulted in no change of the protein levels whereas others became more instable and transcriptional upregulation was essential to maintain the soluble protein levels. It was shown for about 30 - 50 % of those proteins that increased aggregation and degradation under stress are balanced by translation. Aggregation processes gain importance at elevated temperatures while they are almost negligible under mild heat stress. The analysis of the ubiquitination levels revealed that under mild and severe heat stress many more proteins are ubiquitinated than under non-stress conditions. Hence, even though proteasomal degradation was found to be upregulated, this system seemed to be exhausted or at its limit under heat stress. During recovery, the overload of ubiquitinated proteins was efficiently cleared. Under sublethal cell stress, protein degradation was not upregulated anymore. MS analysis of the ubiquitome after 30 min heat stress was not very insightful in comparison to the other MS data. Possibly the ubiquitin pulldown should have been performed at earlier time points as ubiquitination precedes degradation. As increased ubiquitination does not necessarily mean that proteasomal degradation is upregulated, the experimental setup was changed to inhibiting the proteasome with bortezomib. This analysis indicated that besides proteasomal degradation also other proteases, possibly comparable to the heat shock proteases found in *E. coli* (e.g.

Lon or FtsH) (Meyer and Baker, 2011), are involved in the degradation of the more instable proteins under stress. The proteome data of cells treated with CHX or bortezomib had to be normalized on the histone signal, to correct for the normalization in MaxQuant, which masks the global shift induced by the inhibitors. Importantly, the normalization of the other proteome data hardly changed the resulting plots. Unfortunately, in the different MS measurements not always exactly the same proteins could be identified which strongly decreases the amount of proteins, which could be compared. Furthermore, the corridor of $-0.3 < \log_2 fc < 0.3$ for the definition of *unchanged* is very conservative and leads to a small protein number. As exactly those proteins should be investigated in more detail, different thresholds for *unchanged* were tested, whereas 0.6 seemed to be the best trade-off between the amount of proteins that fall into the *unchanged* group and the risk that an up- or downregulation of $2^{0.6}$-fold might already be significant. Furthermore it should be noted, that applying such static thresholds is presumably not the best approach. A gene, that is upregulated 2.1-fold, which results in a protein change of 1.4 fold up ($\log_2 fc < 0.6$) is most possibly less affected by aggregation and degradation than a gene that is 5-fold upregulated and the protein level is really unchanged. Thus, in case of doubt, single genes/proteins should be classified separately and the overall percentages might be biased by such borderline cases. Of note, applying a bigger threshold ($\log_2 fc < 0.6$) did not strongly elevate the percentage of proteins, for which the constant levels could be explained be upregulated degradation or aggregation (37 °C: 35 %; 42 °C: 58 %).

The proteins were also analyzed based on their biophysical properties to come up with determinants that, in the future, might allow predicting what happens to single proteins under stress. The half-life, cpc, pI, instability index and content of IDRs were the most meaningful attributes. At 37 °C and 42 °C, high cpc values were correlating with *increased stability*, which makes sense as a lot of protein molecules need to be degraded or aggregating to observe a two-fold change in the soluble proteome. Hence, this does not necessarily mean that those proteins are more stable, they are simply very abundant. To be able to state that they are more stable, absolute quantifications would be needed. A correlation of high cpcs and stability was also observed in other studies, nevertheless, the cpc was also not considered to be a good predictor for stability in those studies (Jarzab et al., 2020, Leuenberger et al., 2017). Accordingly, changed proteins tend to exhibit smaller cpcs, but much less significantly than it was observed for the high abundance proteins. The instability indices that can be found in the database correlate well with the behavior observed at 37 °C. The upregulated and more stable proteins show low instability values (which means high stability), whereas the downregulated and less stable proteins exhibit high values. At 42 °C, the stabilities seem to change and the correlation with the values determined for non-stress conditions became less good. According to the presented data, an elevated pI correlates with less stability whereas a high half-life at 25 °C was linked to more stable and upregulated proteins, which makes sense. In addition, a

high half-life also correlates with pellet-enrichment. The amount of those long-lived proteins might be less dynamic due to less protein turnover. As it was recently shown that proteins tend to be expressed at their solubility limits (Ciryam et al., 2015, Tartaglia et al., 2007) and heat stress possibly reduces those limits, this could explain the pellet-enrichment of the proteins with high half-lives. Notably, this observation fits to data published for *C. elegans* (Vecchi et al., 2020). Furthermore, pellet-enriched proteins were enriched in proteins that carry IDRs (predicted) by 10 - 13 % in comparison to the overall measured proteins. For *C. elegans* proteins, a relative increase of 14.2 % was observed and in other species as well, an increased content of IDRs was shown to correlate with decreased stability (Vecchi et al., 2020, Jarzab et al., 2020). Additionally, it was stated that a high copy number results in lower aggregation propensity (Vecchi et al., 2020, Tartaglia et al., 2007, Walther et al., 2015). According to fold changes, the data presented in this thesis also tend to support this hypothesis, but this might be again simply due to the relative evaluation as mentioned above. Correlations of abundance and relative changes should be supported by absolute proteome data, which were not measured in this thesis. Interestingly, under severe stress, IDRs appeared to be favorable for stability. Especially the lack of IDRs seemed to have negative effects on stability. Usually, the solubility of proteins is closely linked to the folded native state. As the IDRs are already hardly structured (but still soluble) under non-stress conditions, their solubility might be less affected by an increase of the temperature. It was also observed in other studies that proteins, which were enriched in IDRs tended to be less aggregation prone (Galea et al., 2009, Tsuboyama et al., 2020, Jarzab et al., 2020). Those proteins often carry numerous charged residues and might be post-translationally modified which could also increase their solubility (Jarzab et al., 2020, Tsuboyama et al., 2020).

As mentioned in the beginning, the model of the heat shock response obtained in this work, was that growth and metabolism are maintained as long as possible (Figure 58A). Hence, the response to mild and severe heat shock is *productive*. It was shown that stress-dependent aggregation and degradation processes are balanced by transcription and translation to maintain the active protein pool. In addition, chaperones are strongly upregulated (Figure 58B). Those stress-protective proteins most likely stabilize the proteome under stress and thus contribute to the overall small proteomic changes with apparent stability increases for many proteins, as well. At 46 °C, aggregation is the dominating process and the cells stop growth. The main goal of the response to sublethal stress is to overcome the stress alive without further growth or metabolism. Thus, the cells enter a rather *dormant* stage under sublethal stress.
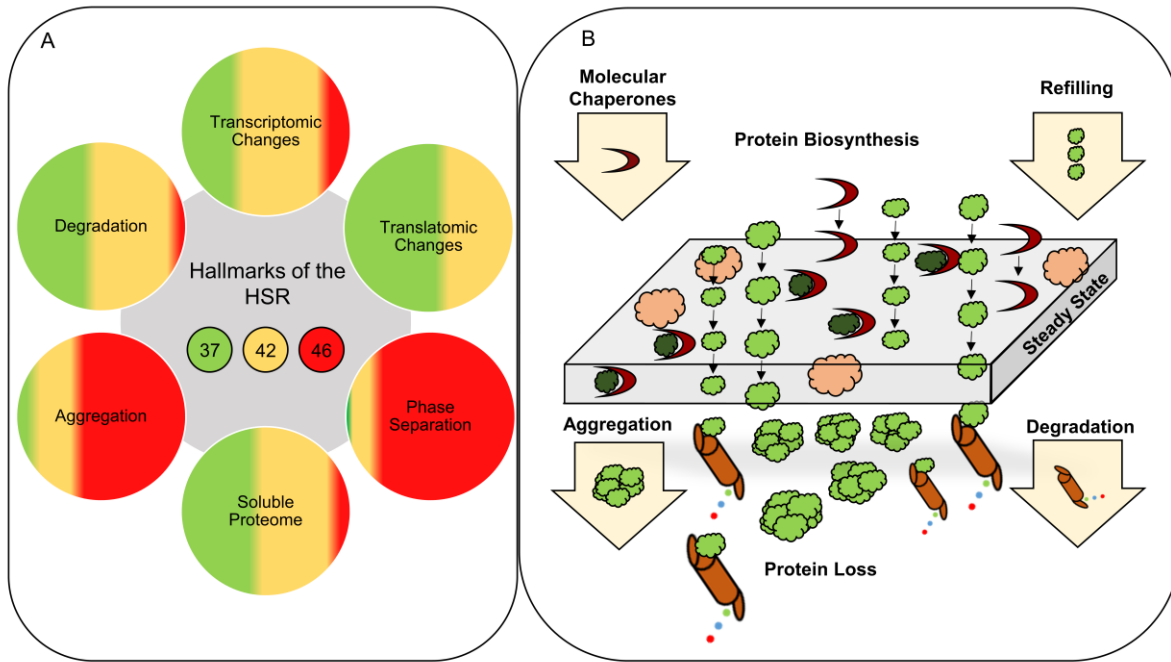
Figure 58: Overview of the HSR of S. cerevisiae. *A) Scheme of the Regulated Anti STress Answer (RASTA). Changes at the different levels are reflected by the sizes of the areas within the circles. Changes at 37 °C are indicated in green, at 42 °C in yellow and at 46 °C in red. B) Protein biosynthesis allows the upregulation of stress-protective factors (chaperones) and the maintenance of the active protein pool (steady state). This is necessary as instable proteins were found to aggregate and to be degraded under stress. Figure part B can also be found as the graphical abstract of the associated publication (Mühlhofer et al., 2019).*

4.3 Transcriptional regulation of the HSR in *S. cerevisiae*

The impact of the three transcription factors Hsf1, Msn2 and Msn4, which are thought to be the main TFs that orchestrate the HSR in yeast, was analyzed by the combination of *MSN2/4* deletion and the depletion of Hsf1 with the anchor-away system (Solís et al., 2016, Verghese et al., 2012). It could be shown that deletion of *MSN2/4* or depletion of Hsf1 lead to a dulled HSR whereas the overall changes still correlate very well with the changes observed in the WT. Absence of Msn2/4 mostly leads to less upregulation of enzymes involved in sugar metabolism. Thus, *glycolysis* and *trehalose biosynthesis* seem to be the main targets that are positively regulated under heat stress by Msn2/4. Cluster analysis further indicated that *phospholipid metabolic processes* are upregulated by Msn2/4 under stress, which indicates that stress-induced adjustments in the membrane are regulated by Msn2/4, as well. As expected, the targets of Hsf1 are more stress-specific and almost exclusively comprise chaperones, which, of course, play a very important role in the HSR. Furthermore, cells that lack Hsf1 do not adapt to mild heat stress as it was observed for the other strains. It seems that the stress-induced reprogramming is less efficient in the Hsf1-depleted strain and that the cells have to maintain their stress-responsive program at 37 °C. Of note, there is no alternative way for the upregulation of Hsf1-dependent genes. Their levels remain reduced also after

173

30 min at 37 °C. In addition to gene repression, the absence of the transcription factors leads to derepression of many genes. After 30 min at 42 °C for example, Msn2/4 and Hsf1 seem to be involved in the transcriptional repression of up to 600 genes under heat stress. Those genes mostly are clustered into *RNA processing* and are closely linked to *translation*. Further cluster analyses also indicated that the TFs reduce *cell cycle progression*, hence *growth*. Interestingly, the TFs exhibit a quite big set of overlapping targets, which only are changed in the absence of all TFs. This indicates a redundancy in their function as already suggested earlier but challenged by other studies (Boy-Marcotte et al., 1999, Treger et al., 1998). Therefore, only the lack of all TFs leads to a strongly reduced response in comparison to the WT. Nevertheless, there are also targets that are specific for Msn2/4 or Hsf1. Those are already changed in the mutants lacking either Msn2/4 or Hsf1. Additionally, in those mutants some genes are changed that are not affected in the strain where all TFs are absent. From this observation, it is concluded that some genes might be contrarily regulated by Msn2/4 and Hsf1. After 30 min at 37 °C, this effect was especially strong with cells depleted of Hsf1, as in those cells no adaption was observed. Obviously, the Hsf1 feedback loop plays a very important role for the kinetics of the transcriptional HSR. Furthermore, the deletion of *MSN2/4* alone led to the repression of more than 100 genes that were not repressed in the strain without all three TFs after 30 min at 42 °C. Those genes are responsible for *cell cycle progression* and seemingly repressed by Hsf1 as the effect was gone after the additional depletion of Hsf1. Thus, Hsf1 inhibits further growth under stress in this mutant strain. From this, it can be concluded that the functions of Msn2/4 and Hsf1 are not necessarily contrary. It rather appears that in the absence of Msn2/4, the action spectrum of Hsf1 is expanded to stop growth under those unfavorable conditions. Those results underline the importance of Hsf1 and its feedback loop for the control of the HSR in yeast. Overall, the transcriptome data of the mutant lacking all three TFs strongly suggest that the central HSR is switched off and that the cells shift away from the productive response to the formation of stress-resistant spores. Stress-induced sporulation is obviously independent of Hsf1 and Msn2/4. Presumably, in this case the stress is sensed by the cell wall integrity pathway (CWI), which can induce sporulation (Piccirillo et al., 2015). It should be noted, that in the shown analyses, WT cells kept at 25 °C were taken as a control and the fold changes calculated based on their transcriptome. Importantly, deletion of the transcription factors also changes the transcriptome at 25 °C. Even though the changes are not comparable to the changes that are induced by heat shock, the transcriptomes differ. If always the same genotype was used as a base, the pictures were less extreme. If for example the changes in the Hsf1-depleted strain in comparison to the WT were compared, the levels of the HDGs that are constitutively expressed were of course also reduced at 25 °C. Interestingly, in comparison to the Hsf1-depleted strain at 25 °C, the HDGs were upregulated again under stress even to a similar extent (concerning the relative fold change) as it was observed for the WT. Most

possibly this is due to a non-perfect depletion and extremely low transcript copy numbers under non-stress after the depletion of Hsf1. If Hsf1 becomes activated the effect of the leakiness of the system presumably becomes more visible. It could also indicate that other factors are involved. Nevertheless, their role would be secondary and much weaker than the role of Hsf1. A relatively new method to search for new transcription factors is called assay for transposase accessible chromatin (ATAC-seq). This method allows the analysis of the accessibility of genomic DNA and thus changes in the transcriptional activity can be monitored. For the analysis of TFs especially changes in the promoter regions were of interest. In the scope of this thesis, the method could be established and principally seemed to work. A well-suited quality control of the transposition reaction is to analyze if a histone pattern is visible in the data. As the DNA is tightly packed around the histones, in those regions fragments of around 147 bp should be enriched, whereas in between, the fragments should be smaller as many insertions will take place. This pattern was visible in the generated dataset. Nevertheless, first data evaluation revealed that the changes observed under stress, seem to be rather small. Interestingly, besides Hsf1 and Msn2/4, also the CWI transcription factors Swi4/Swi6 and Rlm1 exhibited very low p-values. Especially Rlm1, which targets stress-responsive genes, was an extraordinary significant hit. Thus, the CWI seems to be indeed involved in the regulation of the HSR in yeast. This supports the hypothesis that under stress the CWI might induce sporulation in the absence of Hsf1 and Msn2/4. In addition, the well-characterized TF Gcn4, which is activated by the ISR, was found amongst the enriched TFs after prolonged stress. Translation of *GCN4* transcripts is favored under stress and not repressed by the ISR (Hinnebusch, 2005, Costa-Mattioli and Walter, 2020). Thus, it also makes sense that Gcn4 comes up as a secondary transcription factor, as it has to be translated first, whereas Hsf1 and Msn2/4 are expressed constitutively and represent the first responders. This is only preliminary data and the evaluation method has not been ultimately fixed yet. Thus, the ongoing bioinformatic evaluation might reveal more significant changes in the near future. Overall, the approach looks promising and as the method technically seems to work, it might also be applied to the strain lacking all three transcription factors as soon as a robust evaluation method has been established.

5 Outlook

Hsp26

Phosphomimetic substitutions of all described Hsp26 phosphorylation sites were analyzed *in vitro* and phosphorylation was shown to modulate the activity of the chaperone, especially at temperatures below heat stress. As the *all-phospho* mutant only forms monomers or dimers, it would be interesting to find out the switch from the oligomer to the smaller species by sequentially back-mutating the single sites and different combinations of the point-mutations.

In vivo the results were less clear. The sensitive microscopy experiments have been performed with heat-stressed cells, which is presumably not optimal to study the phosphomimetic mutants. Hence, in the future it should be tried to induce proteotoxic stress at 25 °C in combination with the luciferase reporter, which seems to be the most promising approach. Nevertheless the stress-inductor must not be too toxic, to avoid aggregation of the instable luciferase independent of the presence of Hsp26. To understand the function of Hsp26 phosphorylation *in vivo* it would also be important to find out more about the conditions that induce phosphorylation of the chaperone. The previous phospho-proteomic studies were not specifically designed to answer this question. Therefore, different stresses should be tested and phospho-proteomics performed. In those analyses, also recovery samples should be included as phosphorylation might also influence the dissolution of Hsp26 – substrate complexes. In addition, the MS analysis might help to understand the regulatory kinase cascade as well as the sensor that induces phosphorylation of Hsp26 in yeast. If more is known about the conditions that lead to Hsp26 phosphorylation *in vivo*, further, more directed studies could be designed to analyze the function of Hsp26 phosphorylation.

To understand the chaperone activity of Hsp26 in more detail, NMR could be used complementary to cryo-EM to gain more insight into the flexible parts of the protein. Especially the *all-phospho* mutant might be well suited for NMR analysis, as it does not form big oligomers. More details of the MD would be of special interest as it is essential for the chaperone activity of Hsp26 (Haslbeck et al., 2004b). Based on the H/DX results another promising experiment might be to delete aa 32 - 61 and to check the activity and size of the remaining protein. Possibly the thermosensor part of the protein can even be narrowed down to this peptide stretch. In addition, crosslinking MS experiments should be performed to validate the interaction of the MD and the loop in the ACD, which was indicated in the H/DX MS measurement.

Global analysis of the HSR

This project offers a multitude of possibilities to go on further. It was shown that a major part of the regulation serves to counteract increased protein aggregation and degradation. In addition, it would be very interesting to find out more about the features that make proteins instable to be able to predict the behavior of proteins under stress *in vivo*. This was already started but might be refined by integrating protein stability data obtained in other studies (Leuenberger et al., 2017, Jarzab et al., 2020).

It would also be interesting to follow translation at 42 °C over a longer time scale. Growth experiments indicated that cell growth was not completely stopped at this temperature, which means that translation should also be resumed with time. It would be interesting to see if also at 42 °C stress adaption is possible. The role of phase separation in the regulation of the HSR should also be revised and refined. The results presented here support the view that transcriptional regulation is the main process that activates the HSR under mild and severe heat stress. Nevertheless, phase separation processes might be involved in the activation of Hsf1 by sequestering Hsp70 into the formed condensates.

Furthermore, a few uncharacterized proteins were found to be upregulated in the MS studies. As the amount of upregulated proteins was not extraordinarily high, it can be assumed that protein upregulation has a meaning. Therefore, it should be tried to characterize those proteins *in vitro*. Possibly new heat shock proteins are amongst them.

Of course, it would also be interesting to convert this established workflow to mammalian cell culture to analyze to what extent the observations are conferrable to higher eukaryotes.

Transcriptional regulation of the HSR

Here, it was shown that cells lacking Hsf1 and Msn2/4 cannot initiate the common HSR anymore. Thus, the primary goal to switch off the HSR was achieved. Nevertheless, there is still a response taking place that should be analyzed in more detail. This response is most likely initiated by the cell wall integrity pathway. As a further genomic manipulating of the anchor away strain with deleted *MSN2* and *4* is challenging, this topic might be addressed using ATAC-seq. The method was established in this thesis, but an appropriate evaluation strategy is still under development. The data obtained with the WT so far already pinpoint Rlm1 and Swi4/6, the transcription factors associated to the CWI pathway.

It would also be interesting to analyze the proteome of cells that do not exhibit the common HSR. Without the stress-protective chaperones, a proteostasis collapse is expected much

earlier. Refilling reactions might still be initiated but will possibly be much less successful than in the WT. Thus, in the soluble proteome more downregulation should be visible in this strain.

Furthermore, it would be worth to check translation in this strain. The data indicated that translation is less repressed in the absence of the stress-responsive transcription factors. On the other hand, a fast collapse of the proteostasis network should lead to an equally fast translational arrest. In parallel, one could check how successful the cells are in the formation of spores, thus checking whether this program really rescues the cells or whether the rescue program fails.

6 Appendix

6.1 H/DX Peptide coverage
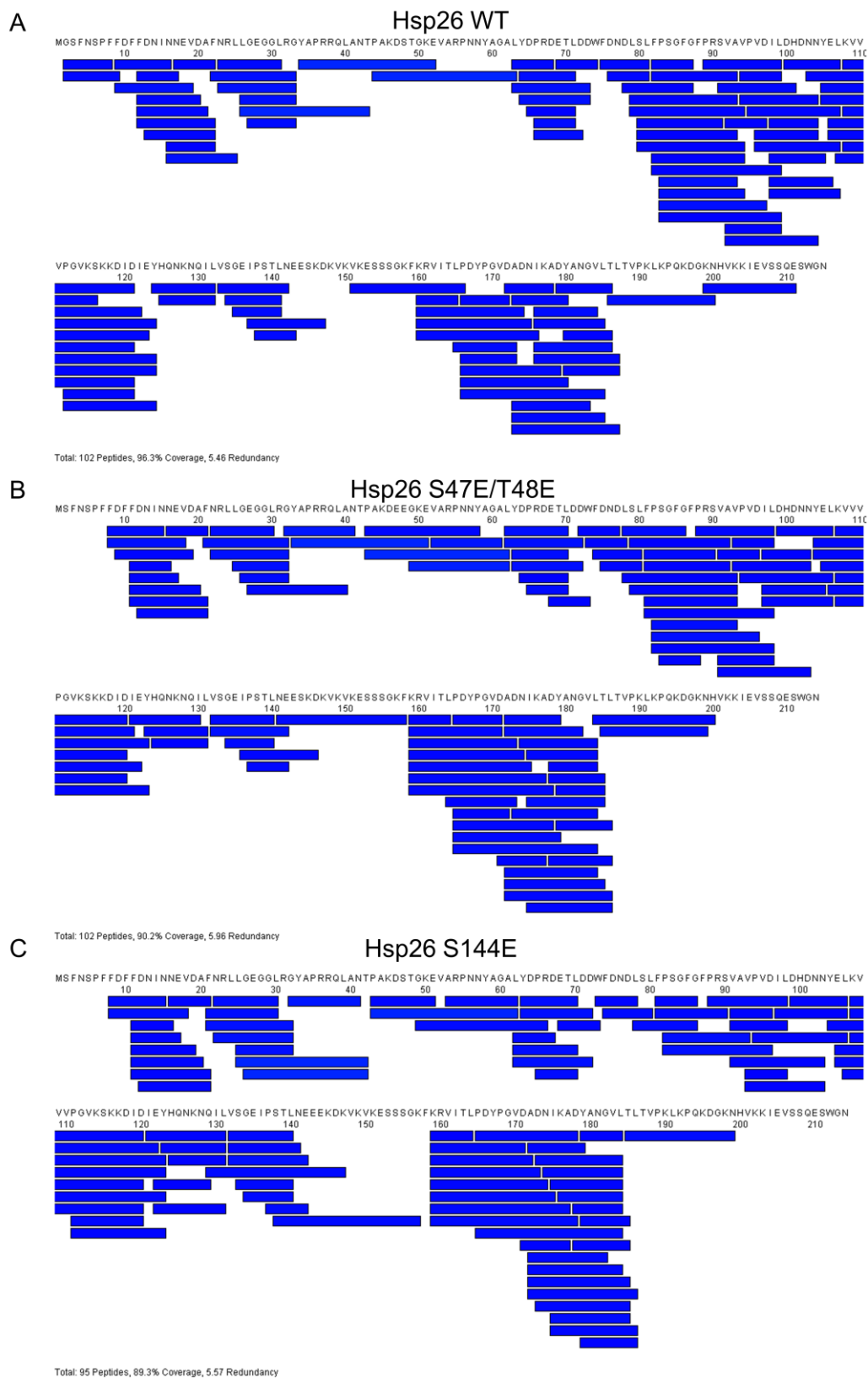
Figure S1: Peptide coverage of the H/DX measurements. *A) Hsp26 WT. B) Hsp26 S47E/T48E. C) Hsp26 S144E. The figure belongs to figure 24.*

6.2 Data availability

The MS data shown in the corresponding publication have been deposited to the ProteomeXChange Consortium via the PRIDE partner repository (Perez-Riverol et al., 2019) and can be accessed with the dataset identifier: PXD014189.

The proteome samples in which the proteasome was inhibited with bortezomib can be accessed with the identifier: PXD016125.

The microarray data have been deposited in NCBI's Gene Expression Omnibus (Edgar et al., 2002) and can be accessed with: GSE132186

(https://www.ncbi.nlm.nih.gov/geo/query/acc.cgi?acc=GSE132186).

Sequencing data shown in the corresponding publication are deposited at the SRA database. SRA database: PRJNA548255 (https://www.ncbi.nlm.nih.gov/sra/PRJNA548255).

7 Abbreviations

(s)Hsp	(small) heat shock protein
A	adenine
aa	amino acid
AA	anchor away
ABC	ammonium bicarbonate
ACD	α-crystallin domain
ACN	acetonitrile
AGC	automatic gain control
Amp	ampicillin
ATAC	assay for transposase accessible chromatin
ATP	adenosintriphosphate
AUC	analytical ultracentrifugation
AZC	azetidine-2-carboxilic acid
BCA	bicinchoninic acid
bp	base pairs
BSA	bovine serum albumin
C	cysteine
ca.	circa
CD	circular dichroism
CE	control element
ChIP	chromatin immunoprecipitation
COMPASS	complex of proteins associated with Set1
cpc	copies per cell
CSM	complete supplement mixture
CTA	C-terminal transactivation domain
CTR	C-terminal region
CWI	cell wall integrity
Da	Dalton
DBD	DNA binding domain
DNA	deoxyribonucleic acid
dNTP	deoxynucleotide triphosphate
DOX	doxycycline
DTT	dithiothreitol
E	glutamate
FA	formic acid
fc	fold change
FDR	false discovery rate
g	g-force
G418	geneticin
GFP	green fluorescent protein
GO	gene ontology
H/DX	hydrogen deuterium exchange
HA	hemagglutinin
HCl	hydrochloric acid
HDG	Hsf1 dependent gene
HEPES	2-(4-(2-hydroxyethyl)piperazin-1-yl)ethane sulfonic acid

HF	high fidelity
HPLC	high performance liquid chromatography
HSE	heat shock element
HSR	heat shock response
IAA	iodoacetamide
IDR	intrinsically disordered region
INQ	intranuclear quality control
IPOD	intracellular protein deposit
IPSL	3-(2-iodoacetamido)-proxyl
IPTG	isopropyl β-d-1-thiogalactopyranoside
ISR	integrated stress response
JUNQ	juxtanuclear quality control
K	Kelvin
Kan	kanamycin
KCl	potassium chloride
KO	knock-out
LB_0	lysogeny broth
LFQ	label-free quantification
LMW	low molecular weight
MALS	multi angle light scattering
MD	middle domain
MDH	malate dehydrogenase
MS	mass spectrometry
M_W	molecular weight
NaCl	sodium chloride
NaOAc	sodium acetate
NaOH	sodium hydroxide
NAT	nourseothricin
NBD	nucleotide binding domain
NC	nitrocellulose
NLS	nuclear localization sequence
nt	nucleotide
NTA	N-terminal transactivation domain
NTR	N-terminal region
OD	optical density
PB	processing body
PBS (T)	phosphate buffered saline (with tween)
PCR	polymerase chain reaction
pI	isoelectric point
PRE	paramagnetic relaxation enhancement
qRT	quantitative real time
RI	refractive index
RNA	ribonucleic acid
RP	ribosome profiling
RPF	ribosome protected fragment
rpm	rounds per minute
rRNA	ribosomal RNA

RT	room temperature
S	serine
S (AUC)	Svedberg
SBD	substrate binding domain
s.d.	standard deviation
SDS-PAGE	sodium dodecyl sulfate polyacrylamide gel electrophoresis
SEC	size exclusion chromatography
SEM	scanning electron microscopy
seq	sequencing
SG	stress granule
SGD	saccharomyces genome database
STRE	stress response element
TCEP	tris(2-carboxyethyl)phosphine
TE	translation efficiency
TEM	transmission electron microscopy
TFA	trifluoroacetic acid
Tris	Tris(hydroxymethyl)-aminomethane
UTR	untranslated region
UV	ultra violet
WT	wild type
YPD	yeast extract peptone dextrose
Δ	deletion

8 Literature

ABBAS-TERKI, T., DONZE, O., BRIAND, P. A. & PICARD, D. 2001. Hsp104 interacts with Hsp90 cochaperones in respiring yeast. *Mol Cell Biol,* 21**,** 7569-75.

AKERFELT, M., MORIMOTO, R. I. & SISTONEN, L. 2010. Heat shock factors: integrators of cell stress, development and lifespan. *Nature reviews. Molecular cell biology,* 11**,** 545-555.

ALBERTI, S. 2012. Molecular mechanisms of spatial protein quality control. *Prion,* 6**,** 437-442.

ALBUQUERQUE, C. P., SMOLKA, M. B., PAYNE, S. H., BAFNA, V., ENG, J. & ZHOU, H. 2008. A multidimensional chromatography technology for in-depth phosphoproteome analysis. *Molecular & Cellular Proteomics,* 7**,** 1389-1396.

AMORÓS, M. & ESTRUCH, F. 2001. Hsf1p and Msn2/4p cooperate in the expression of Saccharomyces cerevisiae genes HSP26 and HSP104 in a gene- and stress type-dependent manner. *Molecular Microbiology,* 39**,** 1523-1532.

ANFINSEN, C. B. 1973. Principles that govern the folding of protein chains. *Science,* 181**,** 223-30.

ANFINSEN, C. B., HABER, E., SELA, M. & WHITE, F. H., JR. 1961. The kinetics of formation of native ribonuclease during oxidation of the reduced polypeptide chain. *Proceedings of the National Academy of Sciences of the United States of America,* 47**,** 1309-1314.

ANFINSEN, C. B. & SCHERAGA, H. A. 1975. Experimental and Theoretical Aspects of Protein Folding. *In:* ANFINSEN, C. B., EDSALL, J. T. & RICHARDS, F. M. (eds.) *Advances in Protein Chemistry.* Academic Press.

APETRI, A. C. & HORWICH, A. L. 2008. Chaperonin chamber accelerates protein folding through passive action of preventing aggregation. *Proceedings of the National Academy of Sciences,* 105**,** 17351-17355.

ARRIGO, A.-P. 2013. Human small heat shock proteins: protein interactomes of homo-and hetero-oligomeric complexes: an update. *FEBS letters,* 587**,** 1959-1969.

ARRIGO, A.-P. & GIBERT, B. 2012. HspB1 dynamic phospho-oligomeric structure dependent interactome as cancer therapeutic target. *Current molecular medicine,* 12**,** 1151-1163.

ASHBURNER, M., BALL, C. A., BLAKE, J. A., BOTSTEIN, D., BUTLER, H., CHERRY, J. M., DAVIS, A. P., DOLINSKI, K., DWIGHT, S. S., EPPIG, J. T., HARRIS, M. A., HILL, D. P., ISSEL-TARVER, L., KASARSKIS, A., LEWIS, S., MATESE, J. C., RICHARDSON, J. E., RINGWALD, M., RUBIN, G. M. & SHERLOCK, G. 2000. Gene ontology: tool for the unification of biology. The Gene Ontology Consortium. *Nat Genet,* 25**,** 25-9.

ASHBURNER, M. & BONNER, J. J. 1979. The induction of gene activity in drosophila by heat shock. *Cell,* 17**,** 241-254.

BAETZ, K., MOFFAT, J., HAYNES, J., CHANG, M. & ANDREWS, B. 2001. Transcriptional coregulation by the cell integrity mitogen-activated protein kinase Slt2 and the cell cycle regulator Swi4. *Molecular and cellular biology,* 21**,** 6515-6528.

BAGNERIS, C., BATEMAN, O. A., NAYLOR, C. E., CRONIN, N., BOELENS, W., KEEP, N. H. & SLINGSBY, C. 2009. Crystal structures of α-crystallin domain dimers of αB-crystallin and Hsp20. *Journal of molecular biology,* 392**,** 1242-1252.

BALAKRISHNAN, R., PARK, J., KARRA, K., HITZ, B. C., BINKLEY, G., HONG, E. L., SULLIVAN, J., MICKLEM, G. & CHERRY, J. M. 2012. YeastMine--an integrated data warehouse for Saccharomyces cerevisiae data as a multipurpose tool-kit. *Database : the journal of biological databases and curation,* 2012**,** bar062-bar062.

BALER, R., WELCH, W. J. & VOELLMY, R. 1992. Heat shock gene regulation by nascent polypeptides and denatured proteins: hsp70 as a potential autoregulatory factor. *The Journal of cell biology,* 117**,** 1151-1159.

BARANOVA, E., WEEKS, S., BEELEN, S., BUKACH, O., GUSEV, N. & STRELKOV, S. 2011. Three-dimensional structure of α-crystallin domain dimers of human small heat shock proteins HSPB1 and HSPB6. *Journal of molecular biology,* 411**,** 110-122.

BASHA, E., JONES, C., BLACKWELL, A. E., CHENG, G., WATERS, E. R., SAMSEL, K. A., SIDDIQUE, M., PETT, V., WYSOCKI, V. & VIERLING, E. 2013. An unusual dimeric small heat shock protein provides

insight into the mechanism of this class of chaperones. *Journal of molecular biology,* 425**,** 1683-1696.

BASHA, E., LEE, G. J., DEMELER, B. & VIERLING, E. 2004. Chaperone activity of cytosolic small heat shock proteins from wheat. *European Journal of Biochemistry,* 271**,** 1426-1436.

BASHA, E., O'NEILL, H. & VIERLING, E. 2012. Small heat shock proteins and α-crystallins: dynamic proteins with flexible functions. *Trends in biochemical sciences,* 37**,** 106-117.

BECK, T. & HALL, M. N. 1999. The TOR signalling pathway controls nuclear localization of nutrient-regulated transcription factors. *Nature,* 402**,** 689-692.

BENESCH, J. L. P., AQUILINA, J. A., BALDWIN, A. J., REKAS, A., STENGEL, F., LINDNER, R. A., BASHA, E., DEVLIN, G. L., HORWITZ, J., VIERLING, E., CARVER, J. A. & ROBINSON, C. V. 2010. The quaternary organization and dynamics of the molecular chaperone HSP26 are thermally regulated. *Chemistry & biology,* 17**,** 1008-1017.

BENJAMINI, Y. & HOCHBERG, Y. 1995. Controlling the False Discovery Rate: A Practical and Powerful Approach to Multiple Testing. 57**,** 289-300.

BEPPERLING, A., ALTE, F., KRIEHUBER, T., BRAUN, N., WEINKAUF, S., GROLL, M., HASLBECK, M. & BUCHNER, J. 2012. Alternative bacterial two-component small heat shock protein systems. *Proceedings of the National Academy of Sciences,* 109**,** 20407-20412.

BERRY, D. B. & GASCH, A. P. 2008. Stress-activated genomic expression changes serve a preparative role for impending stress in yeast. *Molecular biology of the cell,* 19**,** 4580-4587.

BOCZEK, E. E., REEFSCHLÄGER, L. G., DEHLING, M., STRULLER, T. J., HÄUSLER, E., SEIDL, A., KAILA, V. R. I. & BUCHNER, J. 2015. Conformational processing of oncogenic v-Src kinase by the molecular chaperone Hsp90. *Proceedings of the National Academy of Sciences,* 112**,** E3189-E3198.

BODENMILLER, B., WANKA, S., KRAFT, C., URBAN, J., CAMPBELL, D., PEDRIOLI, P. G., GERRITS, B., PICOTTI, P., LAM, H., VITEK, O., BRUSNIAK, M.-Y., ROSCHITZKI, B., ZHANG, C., SHOKAT, K. M., SCHLAPBACH, R., COLMAN-LERNER, A., NOLAN, G. P., NESVIZHSKII, A. I., PETER, M., LOEWITH, R., VON MERING, C. & AEBERSOLD, R. 2010. Phosphoproteomic Analysis Reveals Interconnected System-Wide Responses to Perturbations of Kinases and Phosphatases in Yeast. *Science Signaling,* 3**,** rs4-rs4.

BONNER, J., BALLOU, C. & FACKENTHAL, D. L. 1994. Interactions between DNA-bound trimers of the yeast heat shock factor. *Molecular and cellular biology,* 14**,** 501-508.

BONNER, J. J., HEYWARD, S. & FACKENTHAL, D. L. 1992. Temperature-dependent regulation of a heterologous transcriptional activation domain fused to yeast heat shock transcription factor. *Molecular and cellular biology,* 12**,** 1021-1030.

BORKOVICH, K. A., FARRELLY, F. W., FINKELSTEIN, D. B., TAULIEN, J. & LINDQUIST, S. 1989. hsp82 is an essential protein that is required in higher concentrations for growth of cells at higher temperatures. *Molecular and Cellular Biology,* 9**,** 3919-3930.

BOSCH, T. C., KRYLOW, S. M., BODE, H. R. & STEELE, R. E. 1988. Thermotolerance and synthesis of heat shock proteins: these responses are present in Hydra attenuata but absent in Hydra oligactis. *Proceedings of the National Academy of Sciences,* 85**,** 7927-7931.

BOSE, S., DUTKO, J. A. & ZITOMER, R. S. 2005. Genetic Factors That Regulate the Attenuation of the General Stress Response of Yeast. *Genetics,* 169**,** 1215-1226.

BOWIE, J. U., LUTHY, R. & EISENBERG, D. 1991. A method to identify protein sequences that fold into a known three-dimensional structure. *Science,* 253**,** 164-70.

BOY-MARCOTTE, E., GARMENDIA, C., GARREAU, H., LALLET, S., MALLET, L. & JACQUET, M. 2006. The transcriptional activation region of Msn2p, in Saccharomyces cerevisiae, is regulated by stress but is insensitive to the cAMP signalling pathway. *Molecular Genetics and Genomics,* 275**,** 277-287.

BOY-MARCOTTE, E., LAGNIEL, G., PERROT, M., BUSSEREAU, F., BOUDSOCQ, A., JACQUET, M. & LABARRE, J. 1999. The heat shock response in yeast: differential regulations and contributions of the Msn2p/Msn4p and Hsf1p regulons. *Molecular Microbiology,* 33**,** 274-283.

BOY-MARCOTTE, E., PERROT, M., BUSSEREAU, F., BOUCHERIE, H. & JACQUET, M. 1998. Msn2p and Msn4p control a large number of genes induced at the diauxic transition which are repressed by cyclic AMP inSaccharomyces cerevisiae. *Journal of bacteriology,* 180**,** 1044-1052.

BRAUN, N., ZACHARIAS, M., PESCHEK, J., KASTENMÜLLER, A., ZOU, J., HANZLIK, M., HASLBECK, M., RAPPSILBER, J., BUCHNER, J. & WEINKAUF, S. 2011. Multiple molecular architectures of the eye lens chaperone αB-crystallin elucidated by a triple hybrid approach. *Proceedings of the National Academy of Sciences,* 108**,** 20491-20496.

BROWN, G. C. 1991. Total cell protein concentration as an evolutionary constraint on the metabolic control distribution in cells. *Journal of Theoretical Biology,* 153**,** 195-203.

BROWN, P. H. & SCHUCK, P. 2006. Macromolecular size-and-shape distributions by sedimentation velocity analytical ultracentrifugation. *Biophys J,* 90**,** 4651-61.

BRYNGELSON, J. D., ONUCHIC, J. N., SOCCI, N. D. & WOLYNES, P. G. 1995. Funnels, pathways, and the energy landscape of protein folding: a synthesis. *Proteins,* 21**,** 167-95.

BUCHAN, J. R. & PARKER, R. 2009. Eukaryotic Stress Granules: The Ins and Outs of Translation. *Molecular Cell,* 36**,** 932-941.

BUCHAN, J. R., YOON, J.-H. & PARKER, R. 2011. Stress-specific composition, assembly and kinetics of stress granules in Saccharomyces cerevisiae. *Journal of cell science,* 124**,** 228-239.

BUCHNER, J. 1999. Hsp90 & Co.–a holding for folding. *Trends in biochemical sciences,* 24**,** 136-141.

BUDZYNSKI, M. A., PUUSTINEN, M. C., JOUTSEN, J. & SISTONEN, L. 2015. Uncoupling Stress-Inducible Phosphorylation of Heat Shock Factor 1 from Its Activation. *Mol Cell Biol,* 35**,** 2530-40.

BUENROSTRO, J. D., GIRESI, P. G., ZABA, L. C., CHANG, H. Y. & GREENLEAF, W. J. 2013. Transposition of native chromatin for fast and sensitive epigenomic profiling of open chromatin, DNA-binding proteins and nucleosome position. *Nature Methods,* 10**,** 1213-1218.

BUENROSTRO, J. D., WU, B., CHANG, H. Y. & GREENLEAF, W. J. 2015. ATAC-seq: A Method for Assaying Chromatin Accessibility Genome-Wide. *Current protocols in molecular biology,* 109**,** 21.29.1-21.29.9.

BUKACH, O. V., SEIT-NEBI, A. S., MARSTON, S. B. & GUSEV, N. B. 2004. Some properties of human small heat shock protein Hsp20 (HspB6). *European Journal of Biochemistry,* 271**,** 291-302.

BUKAU, B., HESTERKAMP, T. & LUIRINK, J. 1996. Growing up in a dangerous environment: a network of multiple targeting and folding pathways for nascent polypeptides in the cytosol. *Trends in Cell Biology,* 6**,** 480-486.

BULMAN, A. L. & NELSON, H. C. M. 2005. Role of trehalose and heat in the structure of the C-terminal activation domain of the heat shock transcription factor. *Proteins: Structure, Function, and Bioinformatics,* 58**,** 826-835.

BULT, C. J., WHITE, O., OLSEN, G. J., ZHOU, L., FLEISCHMANN, R. D., SUTTON, G. G., BLAKE, J. A., FITZGERALD, L. M., CLAYTON, R. A., GOCAYNE, J. D., KERLAVAGE, A. R., DOUGHERTY, B. A., TOMB, J.-F., ADAMS, M. D., REICH, C. I., OVERBEEK, R., KIRKNESS, E. F., WEINSTOCK, K. G., MERRICK, J. M., GLODEK, A., SCOTT, J. L., GEOGHAGEN, N. S. M., WEIDMAN, J. F., FUHRMANN, J. L., NGUYEN, D., UTTERBACK, T. R., KELLEY, J. M., PETERSON, J. D., SADOW, P. W., HANNA, M. C., COTTON, M. D., ROBERTS, K. M., HURST, M. A., KAINE, B. P., BORODOVSKY, M., KLENK, H.-P., FRASER, C. M., SMITH, H. O., WOESE, C. R. & VENTER, J. C. 1996. Complete Genome Sequence of the Methanogenic Archaeon, Methanococcus jannaschii. *Science,* 273**,** 1058-1073.

CAO, A., HU, D. & LAI, L. 2004. Formation of amyloid fibrils from fully reduced hen egg white lysozyme. *Protein science : a publication of the Protein Society,* 13**,** 319-324.

CARRA, S., ALBERTI, S., ARRIGO, P. A., BENESCH, J. L., BENJAMIN, I. J., BOELENS, W., BARTELT-KIRBACH, B., BRUNDEL, B. J. J. M., BUCHNER, J., BUKAU, B., CARVER, J. A., ECROYD, H., EMANUELSSON, C., FINET, S., GOLENHOFEN, N., GOLOUBINOFF, P., GUSEV, N., HASLBECK, M., HIGHTOWER, L. E., KAMPINGA, H. H., KLEVIT, R. E., LIBEREK, K., MCHAOURAB, H. S., MCMENIMEN, K. A., POLETTI, A., QUINLAN, R., STRELKOV, S. V., TOTH, M. E., VIERLING, E. & TANGUAY, R. M. 2017. The growing world of small heat shock proteins: from structure to functions. *Cell stress & chaperones,* 22**,** 601-611.

CASHIKAR, A. G., DUENNWALD, M. & LINDQUIST, S. L. 2005. A chaperone pathway in protein disaggregation. Hsp26 alters the nature of protein aggregates to facilitate reactivation by Hsp104. *J Biol Chem,* 280**,** 23869-75.

CASPERS, G. J., LEUNISSEN, J. A. & DE JONG, W. W. 1995. The expanding small heat-shock protein family, and structure predictions of the conserved "alpha-crystallin domain". *J Mol Evol,* 40**,** 238-48.

CAUSTON, H. C., REN, B., KOH, S. S., HARBISON, C. T., KANIN, E., JENNINGS, E. G., LEE, T. I., TRUE, H. L., LANDER, E. S. & YOUNG, R. A. 2001. Remodeling of Yeast Genome Expression in Response to Environmental Changes. *Molecular Biology of the Cell,* 12**,** 323-337.

CHEN, J., FEIGE, M. J., FRANZMANN, T. M., BEPPERLING, A. & BUCHNER, J. 2010a. Regions Outside the α-Crystallin Domain of the Small Heat Shock Protein Hsp26 Are Required for Its Dimerization. *Journal of Molecular Biology,* 398**,** 122-131.

CHEN, S.-H., ALBUQUERQUE, C. P., LIANG, J., SUHANDYNATA, R. T. & ZHOU, H. 2010b. A proteome-wide analysis of kinase-substrate network in the DNA damage response. *Journal of Biological Chemistry,* 285**,** 12803-12812.

CHEREJI, R. V., RAMACHANDRAN, S., BRYSON, T. D. & HENIKOFF, S. 2018. Precise genome-wide mapping of single nucleosomes and linkers in vivo. *Genome Biology,* 19**,** 19.

CHERKASOV, V., GROUSL, T., THEER, P., VAINSHTEIN, Y., GLÄßER, C., MONGIS, C., KRAMER, G., STOECKLIN, G., KNOP, M., MOGK, A. & BUKAU, B. 2015. Systemic control of protein synthesis through sequestration of translation and ribosome biogenesis factors during severe heat stress. 589**,** 3654-3664.

CHO, B.-R. & HAHN, J.-S. 2017. CK2-dependent phosphorylation positively regulates stress-induced activation of Msn2 in Saccharomyces cerevisiae. *Biochimica et Biophysica Acta (BBA) - Gene Regulatory Mechanisms,* 1860**,** 695-704.

CIRYAM, P., KUNDRA, R., MORIMOTO, R. I., DOBSON, C. M. & VENDRUSCOLO, M. 2015. Supersaturation is a major driving force for protein aggregation in neurodegenerative diseases. *Trends in pharmacological sciences,* 36**,** 72-77.

CLARK, M. S. & PECK, L. S. 2009. HSP70 heat shock proteins and environmental stress in Antarctic marine organisms: a mini-review. *Marine genomics,* 1**,** 11-18.

CLARKE, A. 2014. The thermal limits to life on Earth. *International Journal of Astrobiology,* 13**,** 141-154.

COHEN, E., BIESCHKE, J., PERCIAVALLE, R. M., KELLY, J. W. & DILLIN, A. 2006. Opposing activities protect against age-onset proteotoxicity. *Science,* 313**,** 1604-10.

COLLART, M. A. & OLIVIERO, S. 1993. Preparation of Yeast RNA. 23**,** 13.12.1-13.12.5.

CONLIN, L. K. & NELSON, H. C. M. 2007. The Natural Osmolyte Trehalose Is a Positive Regulator of the Heat-Induced Activity of Yeast Heat Shock Transcription Factor. 27**,** 1505-1515.

COSTA-MATTIOLI, M. & WALTER, P. 2020. The integrated stress response: From mechanism to disease. *Science,* 368**,** eaat5314.

COX, J., HEIN, M. Y., LUBER, C. A., PARON, I., NAGARAJ, N. & MANN, M. 2014. Accurate proteome-wide label-free quantification by delayed normalization and maximal peptide ratio extraction, termed MaxLFQ. *Molecular & cellular proteomics : MCP,* 13**,** 2513-2526.

COX, J. & MANN, M. 2008. MaxQuant enables high peptide identification rates, individualized p.p.b.-range mass accuracies and proteome-wide protein quantification. *Nature Biotechnology,* 26**,** 1367.

COX, J. & MANN, M. 2012. 1D and 2D annotation enrichment: a statistical method integrating quantitative proteomics with complementary high-throughput data. *BMC bioinformatics,* 13 Suppl 16**,** S12-S12.

CRAIG, E. A. & GROSS, C. A. 1991. Is hsp70 the cellular thermometer? *Trends in Biochemical Sciences,* 16**,** 135-140.

CRAIG, E. A. & JACOBSEN, K. 1985. Mutations in cognate genes of Saccharomyces cerevisiae hsp70 result in reduced growth rates at low temperatures. *Molecular and cellular biology,* 5**,** 3517-3524.

CRAWFORD, R. A. & PAVITT, G. D. 2019. Translational regulation in response to stress in Saccharomyces cerevisiae. *Yeast,* 36**,** 5-21.

CROWE, J. H. 2007. Trehalose as a "chemical chaperone". *Molecular aspects of the stress response: chaperones, membranes and networks.* Springer.

DE JONG, W. W., LEUNISSEN, J. A. & VOORTER, C. 1993. Evolution of the alpha-crystallin/small heat-shock protein family. *Molecular biology and evolution,* 10**,** 103-126.

DE VIRGILIO, C., HOTTIGER, T., DOMINGUEZ, J., BOLLER, T. & WIEMKEN, A. 1994. The role of trehalose synthesis for the acquisition of thermotolerance in yeast: I. Genetic evidence that trehalose is a thermoprotectant. *European Journal of Biochemistry,* 219**,** 179-186.

DE WEVER, V., REITER, W., BALLARINI, A., AMMERER, G. & BROCARD, C. 2005. A dual role for PP1 in shaping the Msn2-dependent transcriptional response to glucose starvation. *The EMBO Journal,* 24**,** 4115-4123.

DELBECQ, S. P., JEHLE, S. & KLEVIT, R. 2012. Binding determinants of the small heat shock protein, αB-crystallin: recognition of the 'IxI' motif. *The EMBO Journal,* 31**,** 4587-4594.

DELBECQ, S. P. & KLEVIT, R. E. 2013. One size does not fit all: the oligomeric states of αB crystallin. *FEBS letters,* 587**,** 1073-1080.

DERISI, J. L., IYER, V. R. & BROWN, P. O. 1997. Exploring the metabolic and genetic control of gene expression on a genomic scale. *Science,* 278**,** 680-686.

DEVER, T. E., FENG, L., WEK, R. C., CIGAN, A. M., DONAHUE, T. F. & HINNEBUSCH, A. G. 1992. Phosphorylation of initiation factor 2α by protein kinase GCN2 mediates gene-specific translational control of GCN4 in yeast. *Cell,* 68**,** 585-596.

DEVER, T. E., KINZY, T. G. & PAVITT, G. D. 2016. Mechanism and Regulation of Protein Synthesis in Saccharomyces cerevisiae. *Genetics,* 203**,** 65-107.

DILL, K. A., OZKAN, S. B., SHELL, M. S. & WEIKL, T. R. 2008. The protein folding problem. *Annual review of biophysics,* 37**,** 289-316.

DISSMEYER, N. & SCHNITTGER, A. 2011. Use of phospho-site substitutions to analyze the biological relevance of phosphorylation events in regulatory networks. *Methods Mol Biol,* 779**,** 93-138.

DOUGLAS, P. M., SUMMERS, D. W. & CYR, D. M. 2009. Molecular chaperones antagonize proteotoxicity by differentially modulating protein aggregation pathways. *Prion,* 3**,** 51-8.

DOYLE, S. M. & WICKNER, S. 2009. Hsp104 and ClpB: protein disaggregating machines. *Trends in biochemical sciences,* 34**,** 40-48.

DREES, B. L., GROTKOPP, E. K. & NELSON, H. C. 1997. The GCN4 leucine zipper can functionally substitute for the heat shock transcription factor's trimerization domain. *Journal of molecular biology,* 273**,** 61-74.

DURCHSCHLAG, E., REITER, W., AMMERER, G. & SCHULLER, C. 2004. Nuclear localization destabilizes the stress-regulated transcription factor Msn2. *J Biol Chem,* 279**,** 55425-32.

EDEN, E., NAVON, R., STEINFELD, I., LIPSON, D. & YAKHINI, Z. 2009. GOrilla: a tool for discovery and visualization of enriched GO terms in ranked gene lists. *BMC Bioinformatics,* 10**,** 48.

EDGAR, R., DOMRACHEV, M. & LASH, A. E. 2002. Gene Expression Omnibus: NCBI gene expression and hybridization array data repository. *Nucleic Acids Res,* 30**,** 207-10.

EISEN, M. B., SPELLMAN, P. T., BROWN, P. O. & BOTSTEIN, D. 1998. Cluster analysis and display of genome-wide expression patterns. *Proc Natl Acad Sci U S A,* 95**,** 14863-8.

ESCUSA-TORET, S., VONK, W. I. M. & FRYDMAN, J. 2013. Spatial sequestration of misfolded proteins by a dynamic chaperone pathway enhances cellular fitness during stress. *Nature Cell Biology,* 15**,** 1231.

ESPOSITO, A. M. & KINZY, T. G. 2014. In vivo [35S]-methionine incorporation. *Methods Enzymol,* 536**,** 55-64.

ESTRUCH, F. 2000. Stress-controlled transcription factors, stress-induced genes and stress tolerance in budding yeast. *FEMS microbiology reviews,* 24**,** 469-486.

ESTRUCH, F. & CARLSON, M. 1993. Two homologous zinc finger genes identified by multicopy suppression in a SNF1 protein kinase mutant of Saccharomyces cerevisiae. *Molecular and cellular biology,* 13**,** 3872-3881.

FAIRBANKS, G., STECK, T. L. & WALLACH, D. F. 1971. Electrophoretic analysis of the major polypeptides of the human erythrocyte membrane. *Biochemistry,* 10**,** 2606-17.

FEIGE, M. J., GROSCURTH, S., MARCINOWSKI, M., SHIMIZU, Y., KESSLER, H., HENDERSHOT, L. M. & BUCHNER, J. 2009. An unfolded CH1 domain controls the assembly and secretion of IgG antibodies. *Molecular cell,* 34**,** 569-579.

FERSHT, A. R. 1997. Nucleation mechanisms in protein folding. *Current opinion in structural biology,* 7**,** 3-9.

FICARRO, S. B., MCCLELAND, M. L., STUKENBERG, P. T., BURKE, D. J., ROSS, M. M., SHABANOWITZ, J., HUNT, D. F. & WHITE, F. M. 2002. Phosphoproteome analysis by mass spectrometry and its application to Saccharomyces cerevisiae. *Nature Biotechnology,* 20**,** 301-305.

FLECKENSTEIN, T., KASTENMÜLLER, A., STEIN, M. L., PETERS, C., DAAKE, M., KRAUSE, M., WEINFURTNER, D., HASLBECK, M., WEINKAUF, S., GROLL, M. & BUCHNER, J. 2015. The Chaperone Activity of the Developmental Small Heat Shock Protein Sip1 Is Regulated by pH-Dependent Conformational Changes. *Mol Cell,* 58**,** 1067-78.

FLEISCHER, T. C., WEAVER, C. M., MCAFEE, K. J., JENNINGS, J. L. & LINK, A. J. 2006. Systematic identification and functional screens of uncharacterized proteins associated with eukaryotic ribosomal complexes. *Genes Dev,* 20**,** 1294-307.

FOURNIER, M. L., PAULSON, A., PAVELKA, N., MOSLEY, A. L., GAUDENZ, K., BRADFORD, W. D., GLYNN, E., LI, H., SARDIU, M. E., FLEHARTY, B., SEIDEL, C., FLORENS, L. & WASHBURN, M. P. 2010. Delayed correlation of mRNA and protein expression in rapamycin-treated cells and a role for Ggc1 in cellular sensitivity to rapamycin. *Mol Cell Proteomics,* 9**,** 271-84.

FRANKS, T. M. & LYKKE-ANDERSEN, J. 2007. TTP and BRF proteins nucleate processing body formation to silence mRNAs with AU-rich elements. *Genes & development,* 21**,** 719-735.

FRANZMANN, T. M., MENHORN, P., WALTER, S. & BUCHNER, J. 2008. Activation of the Chaperone Hsp26 Is Controlled by the Rearrangement of Its Thermosensor Domain. *Molecular Cell,* 29**,** 207-216.

FRANZMANN, T. M., WÜHR, M., RICHTER, K., WALTER, S. & BUCHNER, J. 2005. The activation mechanism of Hsp26 does not require dissociation of the oligomer. *J Mol Biol,* 350**,** 1083-93.

FREEMAN, B. C., MYERS, M., SCHUMACHER, R. & MORIMOTO, R. I. 1995. Identification of a regulatory motif in Hsp70 that affects ATPase activity, substrate binding and interaction with HDJ-1. *The EMBO journal,* 14**,** 2281-2292.

FRIEDRICH, K. L., GIESE, K. C., BUAN, N. R. & VIERLING, E. 2004. Interactions between small heat shock protein subunits and substrate in small heat shock protein-substrate complexes. *J Biol Chem,* 279**,** 1080-9.

FRUEH, D. P. 2014. Practical aspects of NMR signal assignment in larger and challenging proteins. *Prog Nucl Magn Reson Spectrosc,* 78**,** 47-75.

FRYDMAN, J., NIMMESGERN, E., ERDJUMENT-BROMAGE, H., WALL, J., TEMPST, P. & HARTL, F. 1992. Function in protein folding of TRiC, a cytosolic ring complex containing TCP-1 and structurally related subunits. *The EMBO journal,* 11**,** 4767-4778.

FUJIWARA, K., ISHIHAMA, Y., NAKAHIGASHI, K., SOGA, T. & TAGUCHI, H. 2010. A systematic survey of in vivo obligate chaperonin-dependent substrates. *The EMBO journal,* 29**,** 1552-1564.

GALEA, C. A., HIGH, A. A., OBENAUER, J. C., MISHRA, A., PARK, C.-G., PUNTA, M., SCHLESSINGER, A., MA, J., ROST, B., SLAUGHTER, C. A. & KRIWACKI, R. W. 2009. Large-scale analysis of thermostable, mammalian proteins provides insights into the intrinsically disordered proteome. *Journal of proteome research,* 8**,** 211-226.

GALLINA, I., COLDING, C., HENRIKSEN, P., BELI, P., NAKAMURA, K., OFFMAN, J., MATHIASEN, D. P., SILVA, S., HOFFMANN, E. & GROTH, A. 2015. Cmr1/WDR76 defines a nuclear genotoxic stress body linking genome integrity and protein quality control. *Nature communications,* 6**,** 1-16.

GAO, Z., PUTNAM, A. A., BOWERS, H. A., GUENTHER, U.-P., YE, X., KINDSFATHER, A., HILLIKER, A. K. & JANKOWSKY, E. 2016. Coupling between the DEAD-box RNA helicases Ded1p and eIF4A. *eLife,* 5**,** e16408.

GARÍ, E., PIEDRAFITA, L., ALDEA, M. & HERRERO, E. 1997. A set of vectors with a tetracycline-regulatable promoter system for modulated gene expression in Saccharomyces cerevisiae. *Yeast,* 13**,** 837-848.

GARREAU, H., HASAN, R. N., RENAULT, G., ESTRUCH, F., BOY-MARCOTTE, E. & JACQUET, M. 2000. Hyperphosphorylation of Msn2p and Msn4p in response to heat shock and the diauxic shift is inhibited by cAMP in Saccharomyces cerevisiae. *Microbiology,* 146**,** 2113-2120.

GASCH, A. P., SPELLMAN, P. T., KAO, C. M., CARMEL-HAREL, O., EISEN, M. B., STORZ, G., BOTSTEIN, D. & BROWN, P. O. 2000. Genomic Expression Programs in the Response of Yeast Cells to Environmental Changes. *Molecular Biology of the Cell,* 11**,** 4241-4257.

GATES, S. N., YOKOM, A. L., LIN, J., JACKREL, M. E., RIZO, A. N., KENDSERSKY, N. M., BUELL, C. E., SWEENY, E. A., MACK, K. L., CHUANG, E., TORRENTE, M. P., SU, M., SHORTER, J. & SOUTHWORTH, D. R. 2017. Ratchet-like polypeptide translocation mechanism of the AAA+ disaggregase Hsp104. *Science,* 357**,** 273-279.

GAUTSCHI, M., LILIE, H., FÜNFSCHILLING, U., MUN, A., ROSS, S., LITHGOW, T., RÜCKNAGEL, P. & ROSPERT, S. 2001. RAC, a stable ribosome-associated complex in yeast formed by the DnaK-DnaJ homologs Ssz1p and zuotin. *Proceedings of the National Academy of Sciences,* 98**,** 3762-3767.

GERASHCHENKO, M. V. & GLADYSHEV, V. N. 2014. Translation inhibitors cause abnormalities in ribosome profiling experiments. *Nucleic Acids Research,* 42**,** e134-e134.

GERASHCHENKO, M. V., LOBANOV, A. V. & GLADYSHEV, V. N. 2012. Genome-wide ribosome profiling reveals complex translational regulation in response to oxidative stress. 109**,** 17394-17399.

GERSHENSON, A. & GIERASCH, L. M. 2011. Protein folding in the cell: challenges and progress. *Current opinion in structural biology,* 21**,** 32-41.

GHAEMMAGHAMI, S., HUH, W.-K., BOWER, K., HOWSON, R. W., BELLE, A., DEPHOURE, N., O'SHEA, E. K. & WEISSMAN, J. S. 2003. Global analysis of protein expression in yeast. *Nature,* 425**,** 737.

GIARDINA, C. & LIS, J. T. 1995. Dynamic protein-DNA architecture of a yeast heat shock promoter. *Molecular and cellular biology,* 15**,** 2737-2744.

GIESE, K. C. & VIERLING, E. 2002. Changes in oligomerization are essential for the chaperone activity of a small heat shock protein in vivo and in vitro. *J Biol Chem,* 277**,** 46310-8.

GILL, S. C. & VON HIPPEL, P. H. 1989. Calculation of protein extinction coefficients from amino acid sequence data. *Anal Biochem,* 182**,** 319-26.

GORNER, W., DURCHSCHLAG, E., MARTINEZ-PASTOR, M. T., ESTRUCH, F., AMMERER, G., HAMILTON, B., RUIS, H. & SCHULLER, C. 1998. Nuclear localization of the C2H2 zinc finger protein Msn2p is regulated by stress and protein kinase A activity. *Genes Dev,* 12**,** 586-97.

GÖRNER, W., DURCHSCHLAG, E., WOLF, J., BROWN, E. L., AMMERER, G., RUIS, H. & SCHÜLLER, C. 2002. Acute glucose starvation activates the nuclear localization signal of a stress-specific yeast transcription factor. *The EMBO Journal,* 21**,** 135-144.

GÖRNER, W., SCHÜLLER, C. & RUIS, H. 1999. Being at the Right Place at the Right Time: The Role of Nuclear Transport in Dynamic Transcriptional Regulation in Yeast. *Biological Chemistry.*

GRAGEROV, A. I., MARTIN, E. S., KRUPENKO, M. A., KASHLEV, M. V. & NIKIFOROV, V. G. 1991. Protein aggregation and inclusion body formation in Escherichia coli rpoH mutant defective in heat shock protein induction. *FEBS Letters,* 291**,** 222-224.

GRALLERT, H. & BUCHNER, J. 2001. A structural view of the GroE chaperone cycle. *Journal of structural biology,* 135**,** 95-103.

GREENFIELD, N. J. 2006. Using circular dichroism spectra to estimate protein secondary structure. *Nature protocols,* 1**,** 2876-2890.

GROLL, M., BERKERS, C. R., PLOEGH, H. L. & OVAA, H. 2006. Crystal Structure of the Boronic Acid-Based Proteasome Inhibitor Bortezomib in Complex with the Yeast 20S Proteasome. *Structure,* 14**,** 451-456.

GROUSL, T., IVANOV, P., FRÝDLOVÁ, I., VASICOVÁ, P., JANDA, F., VOJTOVÁ, J., MALıNSKÁ, K. & MALCOVÁ, I. 2009. Nová ková, L., Janosková, D., et al.(2009). Robust heat shock induces

eIF2alpha-phosphorylation-independent assembly of stress granules containing eIF3 and 40S ribosomal subunits in budding yeast, Saccharomyces cerevisiae. *J. Cell Sci,* 122, **2078-2088.**

GROUSL, T., UNGELENK, S., MILLER, S., HO, C.-T., KHOKHRINA, M., MAYER, M. P., BUKAU, B. & MOGK, A. 2018. A prion-like domain in Hsp42 drives chaperone-facilitated aggregation of misfolded proteins. 217, **1269-1285.**

GUPTA, R., KASTURI, P., BRACHER, A., LOEW, C., ZHENG, M., VILLELLA, A., GARZA, D., HARTL, F. U. & RAYCHAUDHURI, S. 2011. Firefly luciferase mutants as sensors of proteome stress. *Nat Methods,* 8, **879-84.**

HAHN, J.-S., HU, Z., THIELE, D. J. & IYER, V. R. 2004. Genome-wide analysis of the biology of stress responses through heat shock transcription factor. *Molecular and cellular biology,* 24, **5249-5256.**

HAHN, J. S. & THIELE, D. J. 2004. Activation of the Saccharomyces cerevisiae heat shock transcription factor under glucose starvation conditions by Snf1 protein kinase. *J Biol Chem,* 279, **5169-76.**

HAINZL, O., LAPINA, M. C., BUCHNER, J. & RICHTER, K. 2009. The charged linker region is an important regulator of Hsp90 function. *Journal of Biological Chemistry,* 284, **22559-22567.**

HANAZONO, Y., TAKEDA, K., OKA, T., ABE, T., TOMONARI, T., AKIYAMA, N., AIKAWA, Y., YOHDA, M. & MIKI, K. 2013. Nonequivalence observed for the 16-meric structure of a small heat shock protein, SpHsp16. 0, from Schizosaccharomyces pombe. *Structure,* 21, **220-228.**

HARRIS, S. F., SHIAU, A. K. & AGARD, D. A. 2004. The crystal structure of the carboxy-terminal dimerization domain of htpG, the Escherichia coli Hsp90, reveals a potential substrate binding site. *Structure,* 12, **1087-1097.**

HARTL, F. U., BRACHER, A. & HAYER-HARTL, M. 2011. Molecular chaperones in protein folding and proteostasis. *Nature,* 475, **324.**

HARTL, F. U. & HAYER-HARTL, M. 2002. Molecular chaperones in the cytosol: from nascent chain to folded protein. *Science,* 295, **1852-1858.**

HARUKI, H., NISHIKAWA, J. & LAEMMLI, U. K. 2008. The anchor-away technique: rapid, conditional establishment of yeast mutant phenotypes. *Mol Cell,* 31, **925-32.**

HASAN, R., LEROY, C., ISNARD, A. D., LABARRE, J., BOY-MARCOTTE, E. & TOLEDANO, M. B. 2002. The control of the yeast H2O2 response by the Msn2/4 transcription factors. *Molecular microbiology,* 45, **233-241.**

HASHIKAWA, N., YAMAMOTO, N. & SAKURAI, H. 2007. Different mechanisms are involved in the transcriptional activation by yeast heat shock transcription factor through two different types of heat shock elements. *Journal of Biological Chemistry,* 282, **10333-10340.**

HASLBECK, M., BRAUN, N., STROMER, T., RICHTER, B., MODEL, N., WEINKAUF, S. & BUCHNER, J. 2004a. Hsp42 is the general small heat shock protein in the cytosol of Saccharomyces cerevisiae. *Embo j,* 23, **638-49.**

HASLBECK, M., FRANZMANN, T., WEINFURTNER, D. & BUCHNER, J. 2005a. Some like it hot: the structure and function of small heat-shock proteins. *Nature Structural & Molecular Biology,* 12, **842-846.**

HASLBECK, M., IGNATIOU, A., SAIBIL, H., HELMICH, S., FRENZL, E., STROMER, T. & BUCHNER, J. 2004b. A domain in the N-terminal part of Hsp26 is essential for chaperone function and oligomerization. *Journal of molecular biology,* 343, **445-455.**

HASLBECK, M., MIESS, A., STROMER, T., WALTER, S. & BUCHNER, J. 2005b. Disassembling protein aggregates in the yeast cytosol The cooperation of Hsp26 with Ssa1 and Hsp104. *Journal of Biological Chemistry,* 280, **23861-23868.**

HASLBECK, M. & VIERLING, E. 2015. A First Line of Stress Defense: Small Heat Shock Proteins and Their Function in Protein Homeostasis. *Journal of Molecular Biology,* 427, **1537-1548.**

HASLBECK, M., WALKE, S., STROMER, T., EHRNSPERGER, M., WHITE, H. E., CHEN, S., SAIBIL, H. R. & BUCHNER, J. 1999. Hsp26: a temperature-regulated chaperone. *The EMBO journal,* 18, **6744-6751.**

HASLBECK, M., WEINKAUF, S. & BUCHNER, J. 2015. The Big Book on Small Heat Shock Proteins.

HASLBECK, M., WEINKAUF, S. & BUCHNER, J. 2019. Small heat shock proteins: Simplicity meets complexity. *Journal of Biological Chemistry,* 294**,** 2121-2132.

HATTENDORF, D. A. & LINDQUIST, S. L. 2002. Cooperative kinetics of both Hsp104 ATPase domains and interdomain communication revealed by AAA sensor-1 mutants. *The EMBO journal,* 21**,** 12-21.

HE, X.-J., MULFORD, K. E. & FASSLER, J. S. 2009. Oxidative Stress Function of the Saccharomyces cerevisiae Skn7 Receiver Domain. *Eukaryotic Cell,* 8**,** 768-778.

HEIRBAUT, M., STRELKOV, S. V. & WEEKS, S. D. 2015. Everything but the ACD, Functional Conservation of the Non-conserved Terminal Regions in sHSPs. *The Big Book on Small Heat Shock Proteins.* Springer.

HELBIG, A. O., ROSATI, S., PIJNAPPEL, P. W. W. M., VAN BREUKELEN, B., TIMMERS, M. H. T. H., MOHAMMED, S., SLIJPER, M. & HECK, A. J. R. 2010. Perturbation of the yeast N-acetyltransferase NatB induces elevation of protein phosphorylation levels. *BMC Genomics,* 11**,** 685.

HELM, S. & BAGINSKY, S. 2018. MSE for Label-Free Absolute Protein Quantification in Complex Proteomes. *Methods Mol Biol,* 1696**,** 235-247.

HESSLING, M., RICHTER, K. & BUCHNER, J. 2009. Dissection of the ATP-induced conformational cycle of the molecular chaperone Hsp90. *Nature Structural & Molecular Biology,* 16**,** 287-293.

HILL, S. M., HANZÉN, S. & NYSTRÖM, T. 2017. Restricted access: spatial sequestration of damaged proteins during stress and aging. *EMBO reports,* 18**,** 377-391.

HINNEBUSCH, A. G. 2005. TRANSLATIONAL REGULATION OF GCN4 AND THE GENERAL AMINO ACID CONTROL OF YEAST. *Annual Review of Microbiology,* 59**,** 407-450.

HIPP, M. S., KASTURI, P. & HARTL, F. U. 2019. The proteostasis network and its decline in ageing. *Nature Reviews Molecular Cell Biology,* 20**,** 421-435.

HIRATA, Y., ANDOH, T., ASAHARA, T. & KIKUCHI, A. 2003. Yeast Glycogen Synthase Kinase-3 Activates Msn2p-dependent Transcription of Stress Responsive Genes. *Molecular Biology of the Cell,* 14**,** 302-312.

HO, C.-T., GROUSL, T., SHATZ, O., JAWED, A., RUGER-HERREROS, C., SEMMELINK, M., ZAHN, R., RICHTER, K., BUKAU, B. & MOGK, A. 2019. Cellular sequestrases maintain basal Hsp70 capacity ensuring balanced proteostasis. *Nature Communications,* 10**,** 4851.

HOHMANN, S. 2002. Osmotic stress signaling and osmoadaptation in yeasts. *Microbiol Mol Biol Rev,* 66**,** 300-72.

HØJ, A. & JAKOBSEN, B. 1994. A short element required for turning off heat shock transcription factor: evidence that phosphorylation enhances deactivation. *The EMBO journal,* 13**,** 2617-2624.

HOLCIK, M. & SONENBERG, N. 2005. Translational control in stress and apoptosis. *Nature reviews Molecular cell biology,* 6**,** 318-327.

HOLT, L. J., TUCH, B. B., VILLÉN, J., JOHNSON, A. D., GYGI, S. P. & MORGAN, D. O. 2009. Global Analysis of Cdk1 Substrate Phosphorylation Sites Provides Insights into Evolution. *Science,* 325**,** 1682-1686.

HONDELE, M., SACHDEV, R., HEINRICH, S., WANG, J., VALLOTTON, P., FONTOURA, B. M. A. & WEIS, K. 2019. DEAD-box ATPases are global regulators of phase-separated organelles. *Nature,* 573**,** 144-148.

HORWICH, A. L., FARR, G. W. & FENTON, W. A. 2006. GroEL– GroES-mediated protein folding. *Chemical reviews,* 106**,** 1917-1930.

HORWITZ, J. 1992. Alpha-crystallin can function as a molecular chaperone. *Proceedings of the National Academy of Sciences,* 89**,** 10449-10453.

HORWITZ, J. 2003. Alpha-crystallin. *Experimental eye research,* 76**,** 145-153.

HOTTIGER, T., DE VIRGILIO, C., HALL, M. N., BOLLER, T. & WIEMKEN, A. 1994. The role of trehalose synthesis for the acquisition of thermotolerance in yeast: II. Physiological concentrations of trehalose increase the thermal stability of proteins in vitro. *European Journal of Biochemistry,* 219, 187-193.

HOYLE, N. P., CASTELLI, L. M., CAMPBELL, S. G., HOLMES, L. E. & ASHE, M. P. 2007. Stress-dependent relocalization of translationally primed mRNPs to cytoplasmic granules that are kinetically and spatially distinct from P-bodies. *The Journal of cell biology,* 179**,** 65-74.

HUANG DA, W., SHERMAN, B. T. & LEMPICKI, R. A. 2009. Systematic and integrative analysis of large gene lists using DAVID bioinformatics resources. *Nat Protoc,* 4**,** 44-57.

HUBER, A., BODENMILLER, B., UOTILA, A., STAHL, M., WANKA, S., GERRITS, B., AEBERSOLD, R. & LOEWITH, R. 2009. Characterization of the rapamycin-sensitive phosphoproteome reveals that Sch9 is a central coordinator of protein synthesis. *Genes & development,* 23**,** 1929-1943.

HUSSMANN, J. A., PATCHETT, S., JOHNSON, A., SAWYER, S. & PRESS, W. H. 2015. Understanding Biases in Ribosome Profiling Experiments Reveals Signatures of Translation Dynamics in Yeast. *PLOS Genetics,* 11**,** e1005732.

HVIDT, A. & NIELSEN, S. O. 1966. Hydrogen Exchange in Proteins. *In:* ANFINSEN, C. B., ANSON, M. L., EDSALL, J. T. & RICHARDS, F. M. (eds.) *Advances in Protein Chemistry.* Academic Press.

IKNER, A. & SHIOZAKI, K. 2005. Yeast signaling pathways in the oxidative stress response. *Mutat Res,* 569**,** 13-27.

INGOLIA, N. T., GHAEMMAGHAMI, S., NEWMAN, J. R. S. & WEISSMAN, J. S. 2009. Genome-Wide Analysis in Vivo of Translation with Nucleotide Resolution Using Ribosome Profiling. 324**,** 218-223.

INGOLIA, NICHOLAS T., LAREAU, LIANA F. & WEISSMAN, JONATHAN S. 2011. Ribosome Profiling of Mouse Embryonic Stem Cells Reveals the Complexity and Dynamics of Mammalian Proteomes. *Cell,* 147**,** 789-802.

ISERMAN, C., DESROCHES ALTAMIRANO, C., JEGERS, C., FRIEDRICH, U., ZARIN, T., FRITSCH, A. W., MITTASCH, M., DOMINGUES, A., HERSEMANN, L., JAHNEL, M., RICHTER, D., GUENTHER, U.-P., HENTZE, M. W., MOSES, A. M., HYMAN, A. A., KRAMER, G., KREYSING, M., FRANZMANN, T. M. & ALBERTI, S. 2020. Condensation of Ded1p Promotes a Translational Switch from Housekeeping to Stress Protein Production. *Cell,* 181**,** 818-831.e19.

ITO, H., OKAMOTO, K., NAKAYAMA, H., ISOBE, T. & KATO, K. 1997. Phosphorylation of αB-Crystallin in Response to Various Types of Stress. *Journal of Biological Chemistry,* 272**,** 29934-29941.

JAKOB, U., GAESTEL, M., ENGEL, K. & BUCHNER, J. 1993. Small heat shock proteins are molecular chaperones. *J Biol Chem,* 268**,** 1517-20.

JAKOBSEN, B. K. & PELHAM, H. 1991. A conserved heptapeptide restrains the activity of the yeast heat shock transcription factor. *The EMBO journal,* 10**,** 369-375.

JAMES, P., PFUND, C. & CRAIG, E. A. 1997. Functional specificity among Hsp70 molecular chaperones. *Science,* 275**,** 387-389.

JANKE, C., MAGIERA, M. M., RATHFELDER, N., TAXIS, C., REBER, S., MAEKAWA, H., MORENO-BORCHART, A., DOENGES, G., SCHWOB, E., SCHIEBEL, E. & KNOP, M. 2004. A versatile toolbox for PCR-based tagging of yeast genes: new fluorescent proteins, more markers and promoter substitution cassettes. *Yeast,* 21**,** 947-62.

JARNUCZAK, A. F., ALBORNOZ, M. G., EYERS, C. E., GRANT, C. M. & HUBBARD, S. J. 2018. A quantitative and temporal map of proteostasis during heat shock in Saccharomyces cerevisiae. *Molecular Omics,* 14**,** 37-52.

JARZAB, A., KURZAWA, N., HOPF, T., MOERCH, M., ZECHA, J., LEIJTEN, N., BIAN, Y., MUSIOL, E., MASCHBERGER, M. & STOEHR, G. 2020. Meltome atlas—thermal proteome stability across the tree of life. *Nature Methods***,** 1-9.

JEHLE, S., VAN ROSSUM, B., STOUT, J. R., NOGUCHI, S. M., FALBER, K., REHBEIN, K., OSCHKINAT, H., KLEVIT, R. E. & RAJAGOPAL, P. 2009. αB-crystallin: a hybrid solid-state/solution-state NMR investigation reveals structural aspects of the heterogeneous oligomer. *Journal of molecular biology,* 385**,** 1481-1497.

JOHNSON 1988. Secondary Structure of Proteins Through Circular Dichroism Spectroscopy. *Annual Review of Biophysics and Biophysical Chemistry,* 17**,** 145-166.

JONES, D. T. & KANDATHIL, S. M. 2018. High precision in protein contact prediction using fully convolutional neural networks and minimal sequence features. *Bioinformatics,* 34**,** 3308-3315.

JONES, D. T., TAYLOR, W. R. & THORNTON, J. M. 1992. A new approach to protein fold recognition. *Nature,* 358**,** 86-9.

JURETSCHKE, J., MENSSEN, R., SICKMANN, A. & WOLF, D. H. 2010. The Hsp70 chaperone Ssa1 is essential for catabolite induced degradation of the gluconeogenic enzyme fructose-1, 6-bisphosphatase. *Biochemical and biophysical research communications,* 397**,** 447-452.

KABIR, M. A., UDDIN, W., NARAYANAN, A., REDDY, P. K., JAIRAJPURI, M. A., SHERMAN, F. & AHMAD, Z. 2011. Functional Subunits of Eukaryotic Chaperonin CCT/TRiC in Protein Folding. *Journal of amino acids,* 2011**,** 843206-843206.

KAGANOVICH, D., KOPITO, R. & FRYDMAN, J. 2008. Misfolded proteins partition between two distinct quality control compartments. *Nature,* 454**,** 1088-95.

KAIMAL, J. M., KANDASAMY, G., GASSER, F. & ANDRÉASSON, C. 2017. Coordinated Hsp110 and Hsp104 Activities Power Protein Disaggregation in Saccharomyces cerevisiae. *Molecular and Cellular Biology,* 37**,** e00027-17.

KAISER, C. J. O., PETERS, C., SCHMID, P. W. N., STAVROPOULOU, M., ZOU, J., DAHIYA, V., MYMRIKOV, E. V., ROCKEL, B., ASAMI, S., HASLBECK, M., RAPPSILBER, J., REIF, B., ZACHARIAS, M., BUCHNER, J. & WEINKAUF, S. 2019. The structure and oxidation of the eye lens chaperone αA-crystallin. *Nature Structural & Molecular Biology,* 26**,** 1141-1150.

KALLI, A., SMITH, G. T., SWEREDOSKI, M. J. & HESS, S. 2013. Evaluation and optimization of mass spectrometric settings during data-dependent acquisition mode: focus on LTQ-Orbitrap mass analyzers. *Journal of proteome research,* 12**,** 3071-3086.

KAMPINGA, H. H. & CRAIG, E. A. 2010. The HSP70 chaperone machinery: J proteins as drivers of functional specificity. *Nature reviews Molecular cell biology,* 11**,** 579-592.

KANDROR, O., BRETSCHNEIDER, N., KREYDIN, E., CAVALIERI, D. & GOLDBERG, A. L. 2004. Yeast adapt to near-freezing temperatures by STRE/Msn2, 4-dependent induction of trehalose synthesis and certain molecular chaperones. *Molecular cell,* 13**,** 771-781.

KANSHIN, E., KUBINIOK, P., THATTIKOTA, Y., D'AMOURS, D. & THIBAULT, P. 2015. Phosphoproteome dynamics of Saccharomyces cerevisiae under heat shock and cold stress. *Molecular systems biology,* 11**,** 813-813.

KAPPÉ, G., AQUILINA, J. A., WUNDERINK, L., KAMPS, B., ROBINSON, C. V., GARATE, T., BOELENS, W. C. & DE JONG, W. W. 2004. Tsp36, a tapeworm small heat-shock protein with a duplicated α-crystallin domain, forms dimers and tetramers with good chaperone-like activity. *Proteins: Structure, Function, and Bioinformatics,* 57**,** 109-117.

KAPPÉ, G., FRANCK, E., VERSCHUURE, P., BOELENS, W. C., LEUNISSEN, J. A. & DE JONG, W. W. 2003. The human genome encodes 10 α-crystallin–related small heat shock proteins: HspB1–10. *Cell stress & chaperones,* 8**,** 53.

KAPPÉ, G., LEUNISSEN, J. A. & DE JONG, W. W. 2002. Evolution and diversity of prokaryotic small heat shock proteins. *Small stress proteins.* Springer.

KARPLUS, M. 1997. The Levinthal paradox: yesterday and today. *Folding and design,* 2**,** S69-S75.

KARPLUS, M. & WEAVER, D. L. 1979. Diffusion–collision model for protein folding. *Biopolymers: Original Research on Biomolecules,* 18**,** 1421-1437.

KARPOVA, T. S., MCNALLY, J. G., MOLTZ, S. L. & COOPER, J. A. 1998. Assembly and function of the actin cytoskeleton of yeast: relationships between cables and patches. *The Journal of cell biology,* 142**,** 1501-1517.

KATO, K., ITO, H., KAMEI, K., INAGUMA, Y., IWAMOTO, I. & SAGA, S. 1998. Phosphorylation of αB-crystallin in Mitotic Cells and Identification of Enzymatic Activities Responsible for Phosphorylation. *Journal of Biological Chemistry,* 273**,** 28346-28354.

KEDERSHA, N., STOECKLIN, G., AYODELE, M., YACONO, P., LYKKE-ANDERSEN, J., FRITZLER, M. J., SCHEUNER, D., KAUFMAN, R. J., GOLAN, D. E. & ANDERSON, P. 2005. Stress granules and processing bodies are dynamically linked sites of mRNP remodeling. *J Cell Biol,* 169**,** 871-84.

KEILHAUER, E. C., HEIN, M. Y. & MANN, M. 2015. Accurate protein complex retrieval by affinity enrichment mass spectrometry (AE-MS) rather than affinity purification mass spectrometry (AP-MS). *Molecular & cellular proteomics : MCP,* 14**,** 120-135.

KELLEY, L. A., MEZULIS, S., YATES, C. M., WASS, M. N. & STERNBERG, M. J. E. 2015. The Phyre2 web portal for protein modeling, prediction and analysis. *Nature Protocols,* 10**,** 845-858.

KELLEY, P. M. & SCHLESINGER, M. J. 1978. The effect of amino acid analogues and heat shock on gene expression in chicken embryo fibroblasts. *Cell,* 15**,** 1277-86.

KIEFHABER, T., RUDOLPH, R., KOHLER, H.-H. & BUCHNER, J. 1991. Protein Aggregation in vitro and in vivo: A Quantitative Model of the Kinetic Competition between Folding and Aggregation. *Bio/Technology,* 9**,** 825-829.

KIM, K. K., KIM, R. & KIM, S.-H. 1998a. Crystal structure of a small heat-shock protein. *Nature,* 394**,** 595-599.

KIM, S., SCHILKE, B., CRAIG, E. A. & HORWICH, A. L. 1998b. Folding in vivo of a newly translated yeast cytosolic enzyme is mediated by the SSA class of cytosolic yeast Hsp70 proteins. *Proceedings of the National Academy of Sciences,* 95**,** 12860-12865.

KLEIN, M., SWINNEN, S., THEVELEIN, J. M. & NEVOIGT, E. 2017. Glycerol metabolism and transport in yeast and fungi: established knowledge and ambiguities. *Environ Microbiol,* 19**,** 878-893.

KNOWLES, T. P. J., VENDRUSCOLO, M. & DOBSON, C. M. 2014. The amyloid state and its association with protein misfolding diseases. *Nature Reviews Molecular Cell Biology,* 15**,** 384-396.

KOBAYASHI, N. & MCENTEE, K. 1990. Evidence for a heat shock transcription factor-independent mechanism for heat shock induction of transcription in Saccharomyces cerevisiae. *Proceedings of the National Academy of Sciences,* 87**,** 6550-6554.

KOBAYASHI, N. & MCENTEE, K. 1993. Identification of cis and trans components of a novel heat shock stress regulatory pathway in Saccharomyces cerevisiae. *Molecular and cellular biology,* 13**,** 248-256.

KOKINA, A., KIBILDS, J. & LIEPINS, J. 2014. Adenine auxotrophy – be aware: some effects of adenine auxotrophy in Saccharomyces cerevisiae strain W303-1A. *FEMS Yeast Research,* 14**,** 697-707.

KONERMANN, L., PAN, J. & LIU, Y. H. 2011. Hydrogen exchange mass spectrometry for studying protein structure and dynamics. *Chem Soc Rev,* 40**,** 1224-34.

KRAKOWIAK, J., ZHENG, X., PATEL, N., FEDER, Z. A., ANANDHAKUMAR, J., VALERIUS, K., GROSS, D. S., KHALIL, A. S. & PINCUS, D. 2018. Hsf1 and Hsp70 constitute a two-component feedback loop that regulates the yeast heat shock response. *eLife,* 7**,** e31668.

KRAMER, G., BOEHRINGER, D., BAN, N. & BUKAU, B. 2009. The ribosome as a platform for co-translational processing, folding and targeting of newly synthesized proteins. *Nature Structural & Molecular Biology,* 16**,** 589-597.

KRIEHUBER, T., RATTEI, T., WEINMAIER, T., BEPPERLING, A., HASLBECK, M. & BUCHNER, J. 2010. Independent evolution of the core domain and its flanking sequences in small heat shock proteins. *The FASEB Journal,* 24**,** 3633-3642.

KROSCHWALD, S., MUNDER, M. C., MAHARANA, S., FRANZMANN, T. M., RICHTER, D., RUER, M., HYMAN, A. A. & ALBERTI, S. 2018. Different Material States of Pub1 Condensates Define Distinct Modes of Stress Adaptation and Recovery. *Cell Rep,* 23**,** 3327-3339.

KUHLMAN, B. & BRADLEY, P. 2019. Advances in protein structure prediction and design. *Nature Reviews Molecular Cell Biology,* 20**,** 681-697.

KULAK, N. A., PICHLER, G., PARON, I., NAGARAJ, N. & MANN, M. 2014. Minimal, encapsulated proteomic-sample processing applied to copy-number estimation in eukaryotic cells. *Nature Methods,* 11**,** 319.

LACKNER, D. H., SCHMIDT, M. W., WU, S., WOLF, D. A. & BÄHLER, J. J. G. B. 2012. Regulation of transcriptome, translation, and proteome in response to environmental stress in fission yeast. 13**,** R25.

LACROUTE, F. 1973. RNA and protein elongation rates in Saccharomyces cerevisiae. *Molecular and General Genetics MGG,* 125**,** 319-327.

LAEMMLI, U. K. 1970. Cleavage of Structural Proteins during the Assembly of the Head of Bacteriophage T4. *Nature,* 227**,** 680-685.

LALLET, S., GARREAU, H., POISIER, C., BOY-MARCOTTE, E. & JACQUET, M. 2004. Heat shock-induced degradation of Msn2p, a Saccharomyces cerevisiae transcription factor, occurs in the nucleus. *Molecular Genetics and Genomics,* 272**,** 353-362.

LEE, D. H. & GOLDBERG, A. L. 2010. Hsp104 is essential for the selective degradation in yeast of polyglutamine expanded ataxin-1 but not most misfolded proteins generally. *Biochemical and biophysical research communications,* 391**,** 1056-1061.

LEE, G. J., POKALA, N. & VIERLING, E. 1995. Structure and in Vitro Molecular Chaperone Activity of Cytosolic Small Heat Shock Proteins from Pea. *Journal of Biological Chemistry,* 270**,** 10432-10438.

LEE, G. J., ROSEMAN, A. M., SAIBIL, H. R. & VIERLING, E. 1997. A small heat shock protein stably binds heat-denatured model substrates and can maintain a substrate in a folding-competent state. *The EMBO journal,* 16**,** 659-671.

LEE, M. V., TOPPER, S. E., HUBLER, S. L., HOSE, J., WENGER, C. D., COON, J. J. & GASCH, A. P. 2011. A dynamic model of proteome changes reveals new roles for transcript alteration in yeast. 7**,** 514.

LEE, P., CHO, B. R., JOO, H. S. & HAHN, J. S. 2008. Yeast Yak1 kinase, a bridge between PKA and stress-responsive transcription factors, Hsf1 and Msn2/Msn4. *Molecular microbiology,* 70**,** 882-895.

LEMAUX, P. G., HERENDEEN, S. L., BLOCH, P. L. & NEIDHARDT, F. C. 1978. Transient rates of synthesis of individual polypeptides in E. coli following temperature shifts. *Cell,* 13**,** 427-434.

LENSSEN, E., JAMES, N., PEDRUZZI, I., DUBOULOZ, F., CAMERONI, E., BISIG, R., MAILLET, L., WERNER, M., ROOSEN, J., PETROVIC, K., WINDERICKX, J., COLLART, M. A. & DE VIRGILIO, C. 2005. The Ccr4-Not Complex Independently Controls both Msn2-Dependent Transcriptional Activation—via a Newly Identified Glc7/Bud14 Type I Protein Phosphatase Module—and TFIID Promoter Distribution. *Molecular and Cellular Biology,* 25**,** 488-498.

LESK, A. M. & ROSE, G. D. 1981. Folding units in globular proteins. *Proceedings of the National Academy of Sciences,* 78**,** 4304-4308.

LEUENBERGER, P., GANSCHA, S., KAHRAMAN, A., CAPPELLETTI, V., BOERSEMA, P. J., VON MERING, C., CLAASSEN, M. & PICOTTI, P. 2017. Cell-wide analysis of protein thermal unfolding reveals determinants of thermostability. *Science,* 355**,** eaai7825.

LEVIN, D. E. 2011. Regulation of cell wall biogenesis in Saccharomyces cerevisiae: the cell wall integrity signaling pathway. *Genetics,* 189**,** 1145-1175.

LEVINTHAL, C. 1969. How to fold graciously. *Mossbauer spectroscopy in biological systems,* 67**,** 22-24.

LINDQUIST, S. 1980. Varying patterns of protein synthesis in Drosophila during heat shock: implications for regulation. *Developmental biology,* 77**,** 463-479.

LINDQUIST, S. 1986. The heat-shock response. *Annual review of biochemistry,* 55**,** 1151-1191.

LINDQUIST, S. & CRAIG, E. A. 1988. The heat-shock proteins. *Annu Rev Genet,* 22**,** 631-77.

LINDQUIST, S. & KIM, G. 1996. Heat-shock protein 104 expression is sufficient for thermotolerance in yeast. *Proceedings of the National Academy of Sciences,* 93**,** 5301-5306.

LIS, J. & WU, C. 1993. Protein traffic on the heat shock promoter: parking, stalling, and trucking along. *Cell,* 74**,** 1-4.

LITTLEFIELD, O. & NELSON, H. C. M. 1999. A new use for the 'wing' of the 'winged' helix-turn-helix motif in the HSF–DNA cocrystal. *Nature Structural Biology,* 6**,** 464-470.

LIU, I. C., CHIU, S. W., LEE, H. Y. & LEU, J. Y. 2012. The histone deacetylase Hos2 forms an Hsp42-dependent cytoplasmic granule in quiescent yeast cells. *Mol Biol Cell,* 23**,** 1231-42.

LIU, Y., BEYER, A. & AEBERSOLD, R. 2016. On the Dependency of Cellular Protein Levels on mRNA Abundance. *Cell,* 165**,** 535-550.

MA, C., HASLBECK, M., BABUJEE, L., JAHN, O. & REUMANN, S. 2006. Identification and characterization of a stress-inducible and a constitutive small heat-shock protein targeted to the matrix of plant peroxisomes. *Plant physiology,* 141**,** 47-60.

MACE, K., KRAKOWIAK, J., EL-SAMAD, H. & PINCUS, D. 2020. Multi-kinase control of environmental stress responsive transcription. *PLOS ONE,* 15**,** e0230246.

MACKAY, R. G., HELSEN, C. W., TKACH, J. M. & GLOVER, J. R. 2008. The C-terminal Extension of Saccharomyces cerevisiae Hsp104 Plays a Role in Oligomer Assembly. *Biochemistry,* 47**,** 1918-1927.

MACKENZIE, R. J., LAWLESS, C., HOLMAN, S. W., LANTHALER, K., BEYNON, R. J., GRANT, C. M., HUBBARD, S. J. & EYERS, C. E. 2016. Absolute protein quantification of the yeast chaperome under conditions of heat shock. *PROTEOMICS,* 16**,** 2128-2140.

MACKERETH, C. D., MADL, T., BONNAL, S., SIMON, B., ZANIER, K., GASCH, A., RYBIN, V., VALCÁRCEL, J. & SATTLER, M. 2011. Multi-domain conformational selection underlies pre-mRNA splicing regulation by U2AF. *Nature,* 475**,** 408-411.

MACOSSAY-CASTILLO, M., MARVELLI, G., GUHAROY, M., JAIN, A., KIHARA, D., TOMPA, P. & WODAK, S. J. 2019. The Balancing Act of Intrinsically Disordered Proteins: Enabling Functional Diversity while Minimizing Promiscuity. *Journal of Molecular Biology,* 431**,** 1650-1670.

MAHAT, DIG B., SALAMANCA, H. H., DUARTE, FABIANA M., DANKO, CHARLES G. & LIS, JOHN T. 2016. Mammalian Heat Shock Response and Mechanisms Underlying Its Genome-wide Transcriptional Regulation. *Molecular Cell,* 62**,** 63-78.

MAINZ, A., PESCHEK, J., STAVROPOULOU, M., BACK, K. C., BARDIAUX, B., ASAMI, S., PRADE, E., PETERS, C., WEINKAUF, S. & BUCHNER, J. 2015. The chaperone αB-crystallin uses different interfaces to capture an amorphous and an amyloid client. *Nature structural & molecular biology,* 22**,** 898-905.

MALINOVSKA, L., KROSCHWALD, S., MUNDER, M. C., RICHTER, D. & ALBERTI, S. 2012. Molecular chaperones and stress-inducible protein-sorting factors coordinate the spatiotemporal distribution of protein aggregates. *Mol Biol Cell,* 23**,** 3041-56.

MARSHALL, R. S., MCLOUGHLIN, F. & VIERSTRA, R. D. 2016. Autophagic turnover of inactive 26S proteasomes in yeast is directed by the ubiquitin receptor Cue5 and the Hsp42 chaperone. *Cell reports,* 16**,** 1717-1732.

MARTÍNEZ-PASTOR, M. T., MARCHLER, G., SCHÜLLER, C., MARCHLER-BAUER, A., RUIS, H. & ESTRUCH, F. 1996. The Saccharomyces cerevisiae zinc finger proteins Msn2p and Msn4p are required for transcriptional induction through the stress response element (STRE). *The EMBO journal,* 15**,** 2227-2235.

MASSON, G. R., BURKE, J. E., AHN, N. G., ANAND, G. S., BORCHERS, C., BRIER, S., BOU-ASSAF, G. M., ENGEN, J. R., ENGLANDER, S. W., FABER, J., GARLISH, R., GRIFFIN, P. R., GROSS, M. L., GUTTMAN, M., HAMURO, Y., HECK, A. J. R., HOUDE, D., IACOB, R. E., JØRGENSEN, T. J. D., KALTASHOV, I. A., KLINMAN, J. P., KONERMANN, L., MAN, P., MAYNE, L., PASCAL, B. D., REICHMANN, D., SKEHEL, M., SNIJDER, J., STRUTZENBERG, T. S., UNDERBAKKE, E. S., WAGNER, C., WALES, T. E., WALTERS, B. T., WEIS, D. D., WILSON, D. J., WINTRODE, P. L., ZHANG, Z., ZHENG, J., SCHRIEMER, D. C. & RAND, K. D. 2019. Recommendations for performing, interpreting and reporting hydrogen deuterium exchange mass spectrometry (HDX-MS) experiments. *Nature Methods,* 16**,** 595-602.

MASTRONARDE, D. N. 2005. Automated electron microscope tomography using robust prediction of specimen movements. *Journal of Structural Biology,* 152**,** 36-51.

MAYER, M. & BUKAU, B. 2005. Hsp70 chaperones: cellular functions and molecular mechanism. *Cellular and molecular life sciences,* 62**,** 670.

MAYER, M. P. 2010. Gymnastics of Molecular Chaperones. *Molecular Cell,* 39**,** 321-331.

MAYER, M. P. 2013. Hsp70 chaperone dynamics and molecular mechanism. *Trends in Biochemical Sciences,* 38**,** 507-514.

MCALISTER, L. & FINKELSTEIN, D. B. 1980. Heat shock proteins and thermal resistance in yeast. *Biochem Biophys Res Commun,* 93**,** 819-24.

MCCLELLAN, A. J. & BRODSKY, J. L. 2000. Mutation of the ATP-binding pocket of SSA1 indicates that a functional interaction between Ssa1p and Ydj1p is required for post-translational translocation into the yeast endoplasmic reticulum. *Genetics,* 156**,** 501-512.

MCCLELLAN, A. J., XIA, Y., DEUTSCHBAUER, A. M., DAVIS, R. W., GERSTEIN, M. & FRYDMAN, J. 2007. Diverse cellular functions of the Hsp90 molecular chaperone uncovered using systems approaches. *Cell,* 131**,** 121-135.

MCDANIEL, D., CAPLAN, A., LEE, M., ADAMS, C., FISHEL, B., GROSS, D. & GARRARD, W. 1989. Basal-level expression of the yeast HSP82 gene requires a heat shock regulatory element. *Molecular and cellular biology,* 9**,** 4789-4798.

MCHAOURAB, H. S., DODSON, E. K. & KOTEICHE, H. A. 2002. Mechanism of chaperone function in small heat shock proteins. Two-mode binding of the excited states of T4 lysozyme mutants by alphaA-crystallin. *J Biol Chem,* 277**,** 40557-66.

MCHAOURAB, H. S., GODAR, J. A. & STEWART, P. L. 2009. Structure and mechanism of protein stability sensors: chaperone activity of small heat shock proteins. *Biochemistry,* 48**,** 3828-3837.

MENG, Q., LI, B. X. & XIAO, X. 2018. Toward Developing Chemical Modulators of Hsp60 as Potential Therapeutics. *Frontiers in molecular biosciences,* 5**,** 35-35.

MEYER, A. S. & BAKER, T. A. 2011. Proteolysis in the Escherichia coli heat shock response: a player at many levels. *Current opinion in microbiology,* 14**,** 194-199.

MICSONAI, A., WIEN, F., BULYÁKI, É., KUN, J., MOUSSONG, É., LEE, Y.-H., GOTO, Y., RÉFRÉGIERS, M. & KARDOS, J. 2018. BeStSel: a web server for accurate protein secondary structure prediction and fold recognition from the circular dichroism spectra. *Nucleic acids research,* 46**,** W315-W322.

MILLER, M. J., XUONG, N. H. & GEIDUSCHEK, E. P. 1979. A response of protein synthesis to temperature shift in the yeast Saccharomyces cerevisiae. *Proceedings of the National Academy of Sciences of the United States of America,* 76**,** 5222-5225.

MILLER, S. B., HO, C. T., WINKLER, J., KHOKHRINA, M., NEUNER, A., MOHAMED, M. Y., GUILBRIDE, D. L., RICHTER, K., LISBY, M., SCHIEBEL, E., MOGK, A. & BUKAU, B. 2015a. Compartment-specific aggregases direct distinct nuclear and cytoplasmic aggregate deposition. e201489524.

MILLER, S. B. M., MOGK, A. & BUKAU, B. 2015b. Spatially Organized Aggregation of Misfolded Proteins as Cellular Stress Defense Strategy. *Journal of Molecular Biology,* 427**,** 1564-1574.

MISSELWITZ, B., STAECK, O. & RAPOPORT, T. A. 1998. J proteins catalytically activate Hsp70 molecules to trap a wide range of peptide sequences. *Molecular cell,* 2**,** 593-603.

MOGK, A., SCHLIEKER, C., FRIEDRICH, K. L., SCHÖNFELD, H.-J., VIERLING, E. & BUKAU, B. 2003. Refolding of Substrates Bound to Small Hsps Relies on a Disaggregation Reaction Mediated Most Efficiently by ClpB/DnaK. *Journal of Biological Chemistry,* 278**,** 31033-31042.

MORANO, K. A., GRANT, C. M. & MOYE-ROWLEY, W. S. 2012. The Response to Heat Shock and Oxidative Stress in Saccharomyces cerevisiae. 190**,** 1157-1195.

MORANO, K. A., SANTORO, N., KOCH, K. A. & THIELE, D. J. 1999. A trans-activation domain in yeast heat shock transcription factor is essential for cell cycle progression during stress. *Molecular and cellular biology,* 19**,** 402-411.

MORIMOTO, R. 1993. Cells in stress: transcriptional activation of heat shock genes. *Science,* 259**,** 1409-1410.

MORIMOTO, R. I. 1998. Regulation of the heat shock transcriptional response: cross talk between a family of heat shock factors, molecular chaperones, and negative regulators. *Genes Dev,* 12**,** 3788-96.

MORROW, G., INAGUMA, Y., KATO, K. & TANGUAY, R. M. 2000. The small heat shock protein Hsp22 of Drosophila melanogaster is a mitochondrial protein displaying oligomeric organization. *Journal of Biological Chemistry,* 275**,** 31204-31210.

MÜHLHOFER, M., BERCHTOLD, E., STRATIL, C. G., CSABA, G., KUNOLD, E., BACH, N. C., SIEBER, S. A., HASLBECK, M., ZIMMER, R. & BUCHNER, J. 2019. The Heat Shock Response in Yeast Maintains Protein Homeostasis by Chaperoning and Replenishing Proteins. *Cell Rep,* 29**,** 4593-4607.e8.

MYERS, J. K. & OAS, T. G. 2001. Preorganized secondary structure as an important determinant of fast protein folding. *Nature structural biology,* 8**,** 552-558.

MYMRIKOV, E. V., DAAKE, M., RICHTER, B., HASLBECK, M. & BUCHNER, J. 2017. The Chaperone Activity and Substrate Spectrum of Human Small Heat Shock Proteins. *Journal of Biological Chemistry,* 292**,** 672-684.

MYMRIKOV, E. V., RIEDL, M., PETERS, C., WEINKAUF, S., HASLBECK, M. & BUCHNER, J. 2019. Regulation of small heat shock proteins by hetero-oligomer formation. *Journal of Biological Chemistry*.

NARBERHAUS, F. 2002. α-Crystallin-type heat shock proteins: socializing minichaperones in the context of a multichaperone network. *Microbiol. Mol. Biol. Rev.,* 66**,** 64-93.

NELSON, R. J., HESCHL, M. & CRAIG, E. A. 1992. Isolation and characterization of extragenic suppressors of mutations in the SSA hsp70 genes of Saccharomyces cerevisiae. *Genetics,* 131**,** 277-285.

NEUDEGGER, T., VERGHESE, J., HAYER-HARTL, M., HARTL, F. U. & BRACHER, A. 2016. Structure of human heat-shock transcription factor 1 in complex with DNA. *Nature Structural & Molecular Biology,* 23**,** 140-146.

NIETO-SOTELO, J., WIEDERRECHT, G., OKUDA, A. & PARKER, C. S. 1990. The yeast heat shock transcription factor contains a transcriptional activation domain whose activity is repressed under nonshock conditions. *Cell,* 62**,** 807-817.

NILLEGODA, N. B., KIRSTEIN, J., SZLACHCIC, A., BERYNSKYY, M., STANK, A., STENGEL, F., ARNSBURG, K., GAO, X., SCIOR, A. & AEBERSOLD, R. 2015. Crucial HSP70 co-chaperone complex unlocks metazoan protein disaggregation. *Nature,* 524**,** 247-251.

NILLEGODA, N. B., WENTINK, A. S. & BUKAU, B. 2018. Protein disaggregation in multicellular organisms. *Trends in biochemical sciences,* 43**,** 285-300.

ORLANDI, I., CAVADINI, P., POPOLO, L. & VAI, M. 1996. Cloning, sequencing and regulation of a cDNA encoding a small heat-shock protein from Schizosaccharomyces pombe. *Biochimica et Biophysica Acta (BBA)-Gene Structure and Expression,* 1307**,** 129-131.

OZGUR, S., CHEKULAEVA, M. & STOECKLIN, G. 2010. Human Pat1b connects deadenylation with mRNA decapping and controls the assembly of processing bodies. *Molecular and cellular biology,* 30**,** 4308-4323.

PACE, C. N., VAJDOS, F., FEE, L., GRIMSLEY, G. & GRAY, T. 1995. How to measure and predict the molar absorption coefficient of a protein. *Protein Sci,* 4**,** 2411-23.

PASTA, S. Y., RAMAN, B., RAMAKRISHNA, T. & RAO, C. M. 2004. The IXI/V motif in the C-terminal extension of alpha-crystallins: alternative interactions and oligomeric assemblies. *Mol Vis,* 10**,** 655-662.

PATRIARCA, E. J. & MARESCA, B. 1990. Acquired thermotolerance following heat shock protein synthesis prevents impairment of mitochondrial ATPase activity at elevated temperatures in Saccharomyces cerevisiae. *Exp Cell Res,* 190**,** 57-64.

PATTARAMANON, N., SANGHA, N. & GAFNI, A. 2007. The carboxy-terminal domain of heat-shock factor 1 is largely unfolded but can be induced to collapse into a compact, partially structured state. *Biochemistry,* 46**,** 3405-3415.

PAULING, L., COREY, R. B. & BRANSON, H. R. 1951. The structure of proteins: two hydrogen-bonded helical configurations of the polypeptide chain. *Proceedings of the National Academy of Sciences,* 37**,** 205-211.

PEFFER, S., GONÇALVES, D. & MORANO, K. A. 2019. Regulation of the Hsf1-dependent transcriptome via conserved bipartite contacts with Hsp70 promotes survival in yeast. *Journal of Biological Chemistry*.

PEISKER, K., CHIABUDINI, M. & ROSPERT, S. 2010. The ribosome-bound Hsp70 homolog Ssb of Saccharomyces cerevisiae. *Biochimica et Biophysica Acta (BBA) - Molecular Cell Research,* 1803**,** 662-672.

PELECHANO, V., WEI, W. & STEINMETZ, LARS M. 2015. Widespread Co-translational RNA Decay Reveals Ribosome Dynamics. *Cell,* 161**,** 1400-1412.

PEREZ-RIVEROL, Y., CSORDAS, A., BAI, J., BERNAL-LLINARES, M., HEWAPATHIRANA, S., KUNDU, D. J., INUGANTI, A., GRISS, J., MAYER, G., EISENACHER, M., PEREZ, E., USZKOREIT, J., PFEUFFER, J., SACHSENBERG, T., YILMAZ, S., TIWARY, S., COX, J., AUDAIN, E., WALZER, M., JARNUCZAK, A. F., TERNENT, T., BRAZMA, A. & VIZCAINO, J. A. 2019. The PRIDE database and related tools and

resources in 2019: improving support for quantification data. *Nucleic Acids Res,* 47**,** D442-d450.

PERSEUSDIGITALLIBRARY. Available: http://141.61.102.106:8080/share.cgi?ssid=0qF9uFn#0qF9uFn/OrganismSpecific:s [Accessed 05/06/2019].

PESCHEK, J., BRAUN, N., FRANZMANN, T. M., GEORGALIS, Y., HASLBECK, M., WEINKAUF, S. & BUCHNER, J. 2009. The eye lens chaperone α-crystallin forms defined globular assemblies. *Proceedings of the National Academy of Sciences,* 106**,** 13272-13277.

PESCHEK, J., BRAUN, N., ROHRBERG, J., BACK, K. C., KRIEHUBER, T., KASTENMÜLLER, A., WEINKAUF, S. & BUCHNER, J. 2013. Regulated structural transitions unleash the chaperone activity of αB-crystallin. *Proceedings of the National Academy of Sciences,* 110**,** E3780-E3789.

PETERS, L. Z., KARMON, O., DAVID-KADOCH, G., HAZAN, R., YU, T., GLICKMAN, M. H. & BEN-AROYA, S. 2015. The protein quality control machinery regulates its misassembled proteasome subunits. *PLoS genetics,* 11.

PETKO, L. & LINDQUIST, S. 1986. Hsp26 is not required for growth at high temperatures, nor for thermotolerance, spore development, or germination. *Cell,* 45**,** 885-894.

PFUND, C., HUANG, P., LOPEZ-HOYO, N. & CRAIG, E. A. 2001. Divergent functional properties of the ribosome-associated molecular chaperone Ssb compared with other Hsp70s. *Molecular biology of the cell,* 12**,** 3773-3782.

PICARD, D. 2002. Heat-shock protein 90, a chaperone for folding and regulation. *Cellular and Molecular Life Sciences CMLS,* 59**,** 1640-1648.

PICCIRILLO, S., MORALES, R., WHITE, M. G., SMITH, K., KAPROS, T. & HONIGBERG, S. M. 2015. Cell Differentiation and Spatial Organization in Yeast Colonies: Role of Cell-Wall Integrity Pathway. *Genetics,* 201**,** 1427-1438.

PLESSET, J., PALM, C. & MCLAUGHLIN, C. S. 1982. Induction of heat shock proteins and thermotolerance by ethanol in Saccharomycescerevisiae. *Biochemical and Biophysical Research Communications,* 108**,** 1340-1345.

PRAEKELT, U. M. & MEACOCK, P. A. 1990. HSP12, a new small heat shock gene of Saccharomyces cerevisiae: analysis of structure, regulation and function. *Mol Gen Genet,* 223**,** 97-106.

PRATT, W. B. & TOFT, D. O. 2003. Regulation of signaling protein function and trafficking by the hsp90/hsp70-based chaperone machinery. *Experimental biology and medicine,* 228**,** 111-133.

PREISS, T., BARON-BENHAMOU, J., ANSORGE, W. & HENTZE, M. W. 2003. Homodirectional changes in transcriptome composition and mRNA translation induced by rapamycin and heat shock. *Nature Structural & Molecular Biology,* 10**,** 1039-1047.

PREISS, T. & HENTZE, M. W. 1998. Dual function of the messenger RNA cap structure in poly(A)-tail-promoted translation in yeast. *Nature,* 392**,** 516-520.

PRÉVÔT, D., DARLIX, J.-L. & OHLMANN, T. 2003. Conducting the initiation of protein synthesis: the role of eIF4G. *Biology of the Cell,* 95**,** 141-156.

PRODROMOU, C., ROE, S. M., O'BRIEN, R., LADBURY, J. E., PIPER, P. W. & PEARL, L. H. 1997. Identification and structural characterization of the ATP/ADP-binding site in the Hsp90 molecular chaperone. *Cell,* 90**,** 65-75.

PUNJANI, A., RUBINSTEIN, J. L., FLEET, D. J. & BRUBAKER, M. A. 2017. cryoSPARC: algorithms for rapid unsupervised cryo-EM structure determination. *Nature Methods,* 14**,** 290-296.

PURDIE, N. 1996. Circular Dichroism and the Conformational Analysis of Biomolecules Edited by Gerald D. Fasman (Brandeis University). Plenum Press: New York. 1996. x + 738 pp. $125.00. ISBN 0-306-45142-5. *Journal of the American Chemical Society,* 118**,** 12871-12871.

RABINDRAN, S. K., HAROUN, R. I., CLOS, J., WISNIEWSKI, J. & WU, C. 1993. Regulation of heat shock factor trimer formation: role of a conserved leucine zipper. *Science,* 259**,** 230-234.

RAPPSILBER, J., MANN, M. & ISHIHAMA, Y. 2007. Protocol for micro-purification, enrichment, pre-fractionation and storage of peptides for proteomics using StageTips. *Nat Protoc,* 2**,** 1896-906.

RATAJCZAK, E., ZIĘTKIEWICZ, S. & LIBEREK, K. 2009. Distinct activities of Escherichia coli small heat shock proteins IbpA and IbpB promote efficient protein disaggregation. *Journal of molecular biology,* 386**,** 178-189.

RAUCH, J. N., TSE, E., FREILICH, R., MOK, S.-A., MAKLEY, L. N., SOUTHWORTH, D. R. & GESTWICKI, J. E. 2017. BAG3 is a modular, scaffolding protein that physically links heat shock protein 70 (Hsp70) to the small heat shock proteins. *Journal of molecular biology,* 429**,** 128-141.

RAYCHAUDHURI, S., LOEW, C., KORNER, R., PINKERT, S., THEIS, M., HAYER-HARTL, M., BUCHHOLZ, F. & HARTL, F. U. 2014. Interplay of acetyltransferase EP300 and the proteasome system in regulating heat shock transcription factor 1. *Cell,* 156**,** 975-85.

RHOADS, R. E. & LAMPHEAR, B. J. 1995. Cap-Independent Translation of Heat Shock Messenger RNAs. *In:* SARNOW, P. (ed.) *Cap-Independent Translation.* Berlin, Heidelberg: Springer Berlin Heidelberg.

RIBACK, J. A., KATANSKI, C. D., KEAR-SCOTT, J. L., PILIPENKO, E. V., ROJEK, A. E., SOSNICK, T. R. & DRUMMOND, D. A. 2017. Stress-Triggered Phase Separation Is an Adaptive, Evolutionarily Tuned Response. *Cell,* 168**,** 1028-1040.e19.

RICHTER, K., HASLBECK, M. & BUCHNER, J. 2010. The heat shock response: life on the verge of death. *Mol Cell,* 40**,** 253-66.

RICHTER, K., MUSCHLER, P., HAINZL, O., REINSTEIN, J. & BUCHNER, J. 2003. Sti1 Is a Non-competitive Inhibitor of the Hsp90 ATPase: BINDING PREVENTS THE N-TERMINAL DIMERIZATION REACTION DURING THE ATPASE CYCLE. *Journal of Biological Chemistry,* 278**,** 10328-10333.

RITOSSA, F. 1962. A new puffing pattern induced by temperature shock and DNP in drosophila. *Experientia,* 18**,** 571-573.

ROTHE, S., PRAKASH, A. & TYEDMERS, J. 2018. The Insoluble Protein Deposit (IPOD) in Yeast. *Frontiers in Molecular Neuroscience,* 11.

ROWLEY, A., JOHNSTON, G. C., BUTLER, B., WERNER-WASHBURNE, M. & SINGER, R. A. 1993. Heat shock-mediated cell cycle blockage and G1 cyclin expression in the yeast Saccharomyces cerevisiae. *Molecular and cellular biology,* 13**,** 1034-1041.

SADEH, A., MOVSHOVICH, N., VOLOKH, M., GHEBER, L. & AHARONI, A. 2011. Fine-tuning of the Msn2/4-mediated yeast stress responses as revealed by systematic deletion of Msn2/4 partners. *Molecular biology of the cell,* 22**,** 3127-3138.

SAKURAI, H. & TAKEMORI, Y. 2007. Interaction between Heat Shock Transcription Factors (HSFs) and divergent binding sequences binding specificities of yeast HSFs and human HSF1. *Journal of Biological Chemistry,* 282**,** 13334-13341.

SAMANT, R. S., LIVINGSTON, C. M., SONTAG, E. M. & FRYDMAN, J. 2018. Distinct proteostasis circuits cooperate in nuclear and cytoplasmic protein quality control. *Nature,* 563**,** 407-411.

SANCHEZ, Y. & LINDQUIST, S. L. 1990. HSP104 required for induced thermotolerance. *Science,* 248**,** 1112-5.

SANTHANAM, A., HARTLEY, A., DÜVEL, K., BROACH, J. R. & GARRETT, S. 2004. PP2A Phosphatase Activity Is Required for Stress and Tor Kinase Regulation of Yeast Stress Response Factor Msn2p. *Eukaryotic Cell,* 3**,** 1261-1271.

SANTORO, N., JOHANSSON, N. & THIELE, D. J. 1998. Heat shock element architecture is an important determinant in the temperature and transactivation domain requirements for heat shock transcription factor. *Molecular and cellular biology,* 18**,** 6340-6352.

SANZ, A. B., GARCÍA, R., RODRÍGUEZ-PEÑA, J. M. & ARROYO, J. 2017. The CWI Pathway: Regulation of the Transcriptional Adaptive Response to Cell Wall Stress in Yeast. *Journal of fungi (Basel, Switzerland),* 4**,** 1.

SATYANARAYANA, C., SCHRÖDER-KÖHNE, S., CRAIG, E. A., SCHU, P. V. & HORST, M. 2000. Cytosolic Hsp70s are involved in the transport of aminopeptidase 1 from the cytoplasm into the vacuole. *FEBS letters,* 470**,** 232-238.

SCHAFFRATH, R. & STARK, M. J. R. 2014. Decoding the biosynthesis and function of diphthamide, an enigmatic modification of translation elongation factor 2 (EF2). *Microbial cell (Graz, Austria),* 1**,** 203-205.

SCHEP, A. N., BUENROSTRO, J. D., DENNY, S. K., SCHWARTZ, K., SHERLOCK, G. & GREENLEAF, W. J. 2015. Structured nucleosome fingerprints enable high-resolution mapping of chromatin architecture within regulatory regions. *Genome research,* 25**,** 1757-1770.

SCHERES, S. H. W. 2012a. A Bayesian View on Cryo-EM Structure Determination. *J Mol Biol,* 415**,** 406-418.

SCHERES, S. H. W. 2012b. RELION: Implementation of a Bayesian approach to cryo-EM structure determination. *J Struct Biol,* 180**,** 519-530.

SCHINDELIN, J., ARGANDA-CARRERAS, I., FRISE, E., KAYNIG, V., LONGAIR, M., PIETZSCH, T., PREIBISCH, S., RUEDEN, C., SAALFELD, S., SCHMID, B., TINEVEZ, J.-Y., WHITE, D. J., HARTENSTEIN, V., ELICEIRI, K., TOMANCAK, P. & CARDONA, A. 2012. Fiji: an open-source platform for biological-image analysis. *Nature Methods,* 9**,** 676.

SCHIRMER, E. C., GLOVER, J. R., SINGER, M. A. & LINDQUIST, S. 1996. HSP100/Clp proteins: a common mechanism explains diverse functions. *Trends in Biochemical Sciences,* 21**,** 289-296.

SCHIRMER, E. C., QUEITSCH, C., KOWAL, A. S., PARSELL, D. A. & LINDQUIST, S. 1998. The ATPase activity of Hsp104, effects of environmental conditions and mutations. *Journal of Biological Chemistry,* 273**,** 15546-15552.

SCHMITT, A. P. & MCENTEE, K. 1996. Msn2p, a zinc finger DNA-binding protein, is the transcriptional activator of the multistress response in Saccharomyces cerevisiae. *Proceedings of the National Academy of Sciences,* 93**,** 5777-5782.

SCHOPF, F. H., BIEBL, M. M. & BUCHNER, J. 2017. The HSP90 chaperone machinery. *Nature Reviews Molecular Cell Biology,* 18**,** 345-360.

SCHOPF, F. H., HUBER, E. M., DODT, C., LOPEZ, A., BIEBL, M. M., RUTZ, D. A., MÜHLHOFER, M., RICHTER, G., MADL, T., SATTLER, M., GROLL, M. & BUCHNER, J. 2019. The Co-chaperone Cns1 and the Recruiter Protein Hgh1 Link Hsp90 to Translation Elongation via Chaperoning Elongation Factor 2. *Molecular Cell*.

SCHREIBER, T. B., MÄUSBACHER, N., SOROKA, J., WANDINGER, S. K., BUCHNER, J. & DAUB, H. 2012. Global analysis of phosphoproteome regulation by the Ser/Thr phosphatase Ppt1 in Saccharomyces cerevisiae. *Journal of proteome research,* 11**,** 2397-2408.

SCHUCK, P. 2000. Size-distribution analysis of macromolecules by sedimentation velocity ultracentrifugation and lamm equation modeling. *Biophys J,* 78**,** 1606-19.

SEN, N. D., ZHOU, F., INGOLIA, N. T. & HINNEBUSCH, A. G. 2015. Genome-wide analysis of translational efficiency reveals distinct but overlapping functions of yeast DEAD-box RNA helicases Ded1 and eIF4A. 25**,** 1196-1205.

SHALGI, R., HURT, J. A., KRYKBAEVA, I., TAIPALE, M., LINDQUIST, S. & BURGE, C. B. 2013. Widespread regulation of translation by elongation pausing in heat shock. *Mol Cell,* 49**,** 439-52.

SHARMA, D. & MASISON, D. C. 2011. Single methyl group determines prion propagation and protein degradation activities of yeast heat shock protein (Hsp)-70 chaperones Ssa1p and Ssa2p. *Proceedings of the National Academy of Sciences,* 108**,** 13665-13670.

SHARMA, S., CHAKRABORTY, K., MÜLLER, B. K., ASTOLA, N., TANG, Y.-C., LAMB, D. C., HAYER-HARTL, M. & HARTL, F. U. 2008. Monitoring Protein Conformation along the Pathway of Chaperonin-Assisted Folding. *Cell,* 133**,** 142-153.

SHENTON, D., SMIRNOVA, J. B., SELLEY, J. N., CARROLL, K., HUBBARD, S. J., PAVITT, G. D., ASHE, M. P. & GRANT, C. M. 2006. Global Translational Responses to Oxidative Stress Impact upon Multiple Levels of Protein Synthesis. *Journal of Biological Chemistry,* 281**,** 29011-29021.

SHIROKIKH, N. E. & SPIRIN, A. S. 2008. Poly(A) leader of eukaryotic mRNA bypasses the dependence of translation on initiation factors. *Proceedings of the National Academy of Sciences,* 105**,** 10738-10743.

SHOICHET, B. K., BAASE, W. A., KUROKI, R. & MATTHEWS, B. W. 1995. A relationship between protein stability and protein function. *Proceedings of the National Academy of Sciences,* 92**,** 452-456.

SHORTER, J. & SOUTHWORTH, D. R. 2019. Spiraling in Control: Structures and Mechanisms of the Hsp104 Disaggregase. *Cold Spring Harbor perspectives in biology,* 11**,** a034033.

SHULGA, N., ROBERTS, P., GU, Z., SPITZ, L., TABB, M. M., NOMURA, M. & GOLDFARB, D. S. 1996. In vivo nuclear transport kinetics in Saccharomyces cerevisiae: a role for heat shock protein 70 during targeting and translocation. *The Journal of Cell Biology,* 135**,** 329-339.

SIDDIQUE, M., GERNHARD, S., VON KOSKULL-DÖRING, P., VIERLING, E. & SCHARF, K.-D. 2008. The plant sHSP superfamily: five new members in Arabidopsis thaliana with unexpected properties. *Cell Stress and Chaperones,* 13**,** 183-197.

SIEGERS, K., WALDMANN, T., LEROUX, M. R., GREIN, K., SHEVCHENKO, A., SCHIEBEL, E. & HARTL, F. U. 1999. Compartmentation of protein folding in vivo: sequestration of non-native polypeptide by the chaperonin–GimC system. *The EMBO journal,* 18**,** 75-84.

SILBERG, J. J., TAPLEY, T. L., HOFF, K. G. & VICKERY, L. E. 2004. Regulation of the HscA ATPase reaction cycle by the co-chaperone HscB and the iron-sulfur cluster assembly protein IscU. *Journal of Biological Chemistry,* 279**,** 53924-53931.

SIMMONS, S. O., FAN, C.-Y. & RAMABHADRAN, R. 2009. Cellular stress response pathway system as a sentinel ensemble in toxicological screening. *Toxicological sciences,* 111**,** 202-225.

SIMONS, K. T., BONNEAU, R., RUCZINSKI, I. & BAKER, D. 1999. Ab initio protein structure prediction of CASP III targets using ROSETTA. *Proteins: Structure, Function, and Bioinformatics,* 37**,** 171-176.

SINGER, M. A. & LINDQUIST, S. 1998. Multiple effects of trehalose on protein folding in vitro and in vivo. *Molecular cell,* 1**,** 639-648.

SLINGSBY, C., WISTOW, G. J. & CLARK, A. R. 2013. Evolution of crystallins for a role in the vertebrate eye lens. *Protein Science,* 22**,** 367-380.

SLUCHANKO, N. N., BEELEN, S., KULIKOVA, A. A., WEEKS, S. D., ANTSON, A. A., GUSEV, N. B. & STRELKOV, S. V. 2017. Structural Basis for the Interaction of a Human Small Heat Shock Protein with the 14-3-3 Universal Signaling Regulator. *Structure (London, England : 1993),* 25**,** 305-316.

SMITH, P. K., KROHN, R. I., HERMANSON, G. T., MALLIA, A. K., GARTNER, F. H., PROVENZANO, M. D., FUJIMOTO, E. K., GOEKE, N. M., OLSON, B. J. & KLENK, D. C. 1985. Measurement of protein using bicinchoninic acid. *Anal Biochem,* 150**,** 76-85.

SMOLKA, M. B., ALBUQUERQUE, C. P., CHEN, S.-H. & ZHOU, H. 2007. Proteome-wide identification of in vivo targets of DNA damage checkpoint kinases. *Proceedings of the National Academy of Sciences,* 104**,** 10364-10369.

SOLÍS, ERIC J., PANDEY, JAI P., ZHENG, X., JIN, DEXTER X., GUPTA, PIYUSH B., AIROLDI, EDOARDO M., PINCUS, D. & DENIC, V. 2016. Defining the Essential Function of Yeast Hsf1 Reveals a Compact Transcriptional Program for Maintaining Eukaryotic Proteostasis. *Molecular Cell,* 63**,** 60-71.

SONTAG, E. M., SAMANT, R. S. & FRYDMAN, J. 2017. Mechanisms and functions of spatial protein quality control. *Annual review of biochemistry,* 86**,** 97-122.

SONTAG, E. M., VONK, W. I. & FRYDMAN, J. 2014. Sorting out the trash: the spatial nature of eukaryotic protein quality control. *Current opinion in cell biology,* 26**,** 139-146.

SORGER, P. K. 1990. Yeast heat shock factor contains separable transient and sustained response transcriptional activators. *Cell,* 62**,** 793-805.

SORGER, P. K., LEWIS, M. J. & PELHAM, H. R. 1987. Heat shock factor is regulated differently in yeast and HeLa cells. *Nature,* 329**,** 81-84.

SORGER, P. K. & PELHAM, H. 1987. Purification and characterization of a heat-shock element binding protein from yeast. *The EMBO journal,* 6**,** 3035-3041.

SORGER, P. K. & PELHAM, H. R. 1988. Yeast heat shock factor is an essential DNA-binding protein that exhibits temperature-dependent phosphorylation. *Cell,* 54**,** 855-864.

SOUFI, B., KELSTRUP, C. D., STOEHR, G., FRÖHLICH, F., WALTHER, T. C. & OLSEN, J. V. 2009. Global analysis of the yeast osmotic stress response by quantitative proteomics. *Molecular BioSystems,* 5**,** 1337-1346.

SPECHT, S., MILLER, S. B. M., MOGK, A. & BUKAU, B. 2011. Hsp42 is required for sequestration of protein aggregates into deposition sites in Saccharomyces cerevisiae. *The Journal of cell biology,* 195**,** 617-629.

SPECTOR, D., GOLDMANN, R. & LEINWAND, L. 1998. Preparative methods for scanning electron microscopy. *Cells. Cold Spring Harbor Laboratory Press, Cold Spring Harbor, New York*, 122.1-123.27.

STAMLER, R., KAPPÉ, G., BOELENS, W. & SLINGSBY, C. 2005. Wrapping the α-Crystallin Domain Fold in a Chaperone Assembly. *Journal of Molecular Biology,* 353, 68-79.

STOECKLIN, G. & KEDERSHA, N. 2013. Relationship of GW/P-bodies with stress granules. *Advances in experimental medicine and biology,* 768, 197-211.

STRATIL, C. G. 2015. *The Small Heat Shock Proteins and the Heat Stress Response of Baker's Yeast.* Dr. rer. nat., TUM.

STROMER, T., EHRNSPERGER, M., GAESTEL, M. & BUCHNER, J. 2003. Analysis of the Interaction of Small Heat Shock Proteins with Unfolding Proteins. *Journal of Biological Chemistry,* 278, 18015-18021.

STROMER, T., FISCHER, E., RICHTER, K., HASLBECK, M. & BUCHNER, J. 2004. Analysis of the Regulation of the Molecular Chaperone Hsp26 by Temperature-induced Dissociation: THE N-TERMINAL DOMAIN IS IMPORTANT FOR OLIGOMER ASSEMBLY AND THE BINDING OF UNFOLDING PROTEINS. *Journal of Biological Chemistry,* 279, 11222-11228.

SUN, Y. & MACRAE, T. H. 2005. The small heat shock proteins and their role in human disease. *The FEBS journal,* 272, 2613-2627.

SUSEK, R. & LINDQUIST, S. 1989. hsp26 of Saccharomyces cerevisiae is related to the superfamily of small heat shock proteins but is without a demonstrable function. *Molecular and cellular biology,* 9, 5265-5271.

SWEENY, E. A., TARIQ, A., GURPINAR, E., GO, M. S., SOCHOR, M. A., KAN, Z.-Y., MAYNE, L., ENGLANDER, S. W. & SHORTER, J. 2019. Structural and mechanistic insights into Hsp104 function revealed by synchrotron x-ray footprinting. *Journal of Biological Chemistry*.

SWINEHART, D. F. 1962. The Beer-Lambert Law. *Journal of Chemical Education,* 39, 333.

TAMAI, K. T., LIU, X., SILAR, P., SOSINOWSKI, T. & THIELE, D. J. 1994. Heat shock transcription factor activates yeast metallothionein gene expression in response to heat and glucose starvation via distinct signalling pathways. *Molecular and cellular biology,* 14, 8155-8165.

TAPIA, H., YOUNG, L., FOX, D., BERTOZZI, C. R. & KOSHLAND, D. 2015. Increasing intracellular trehalose is sufficient to confer desiccation tolerance to Saccharomyces cerevisiae. *Proceedings of the National Academy of Sciences,* 112, 6122-6127.

TAPLEY, T. L., FRANZMANN, T. M., CHAKRABORTY, S., JAKOB, U. & BARDWELL, J. C. 2010. Protein refolding by pH-triggered chaperone binding and release. *Proceedings of the national Academy of Sciences,* 107, 1071-1076.

TARTAGLIA, G. G., PECHMANN, S., DOBSON, C. M. & VENDRUSCOLO, M. 2007. Life on the edge: a link between gene expression levels and aggregation rates of human proteins. *Trends Biochem Sci,* 32, 204-6.

TISSIÉRES, A., MITCHELL, H. K. & TRACY, U. M. 1974. Protein synthesis in salivary glands of Drosophila melanogaster: Relation to chromosome puffs. *Journal of Molecular Biology,* 84, 389-398.

TOIVOLA, D. M., STRNAD, P., HABTEZION, A. & OMARY, M. B. 2010. Intermediate filaments take the heat as stress proteins. *Trends in Cell Biology,* 20, 79-91.

TREGER, J. M., SCHMITT, A. P., SIMON, J. R. & MCENTEE, K. 1998. Transcriptional factor mutations reveal regulatory complexities of heat shock and newly identified stress genes in Saccharomyces cerevisiae. *Journal of Biological Chemistry,* 273, 26875-26879.

TREWEEK, T. M., ECROYD, H., WILLIAMS, D. M., MEEHAN, S., CARVER, J. A. & WALKER, M. J. 2007. Site-directed mutations in the C-terminal extension of human αB-crystallin affect chaperone function and block amyloid fibril formation. *PLoS One,* 2.

TROTT, A. & MORANO, K. A. 2003. The yeast response to heat shock. *In:* HOHMANN, S. & MAGER, W. H. (eds.) *Yeast Stress Responses.* Berlin, Heidelberg: Springer Berlin Heidelberg.

TSUBOYAMA, K., OSAKI, T., MATSUURA-SUZUKI, E., KOZUKA-HATA, H., OKADA, Y., OYAMA, M., IKEUCHI, Y., IWASAKI, S. & TOMARI, Y. 2020. A widespread family of heat-resistant obscure

(Hero) proteins protect against protein instability and aggregation. *PLOS Biology,* 18**,** e3000632.

TYANOVA, S., TEMU, T., SINITCYN, P., CARLSON, A., HEIN, M. Y., GEIGER, T., MANN, M. & COX, J. 2016. The Perseus computational platform for comprehensive analysis of (prote)omics data. *Nat Methods,* 13**,** 731-40.

UNGELENK, S., MOAYED, F., HO, C. T., GROUSL, T., SCHARF, A., MASHAGHI, A., TANS, S., MAYER, M. P., MOGK, A. & BUKAU, B. 2016. Small heat shock proteins sequester misfolding proteins in near-native conformation for cellular protection and efficient refolding. *Nat Commun,* 7**,** 13673.

VAINBERG, I. E., LEWIS, S. A., ROMMELAERE, H., AMPE, C., VANDEKERCKHOVE, J., KLEIN, H. L. & COWAN, N. J. 1998. Prefoldin, a chaperone that delivers unfolded proteins to cytosolic chaperonin. *Cell,* 93**,** 863-73.

VALPUESTA, J. M., MARTíN-BENITO, J., GÓMEZ-PUERTAS, P., CARRASCOSA, J. L. & WILLISON, K. R. 2002. Structure and function of a protein folding machine: the eukaryotic cytosolic chaperonin CCT. *FEBS letters,* 529**,** 11-16.

VAN DIJK, E., COUGOT, N., MEYER, S., BABAJKO, S., WAHLE, E. & SERAPHIN, B. 2002. Human Dcp2: a catalytically active mRNA decapping enzyme located in specific cytoplasmic structures. *Embo j,* 21**,** 6915-24.

VAN MONTFORT, R., SLINGSBY, C. & VIERLING, E. 2001a. Structure and function of the small heat shock protein/α-crystallin family of molecular chaperones. *Advances in protein chemistry,* 59**,** 105-156.

VAN MONTFORT, R. L., BASHA, E., FRIEDRICH, K. L., SLINGSBY, C. & VIERLING, E. 2001b. Crystal structure and assembly of a eukaryotic small heat shock protein. *Nature structural biology,* 8**,** 1025-1030.

VECCHI, G., SORMANNI, P., MANNINI, B., VANDELLI, A., TARTAGLIA, G. G., DOBSON, C. M., HARTL, F. U. & VENDRUSCOLO, M. 2020. Proteome-wide observation of the phenomenon of life on the edge of solubility. *Proceedings of the National Academy of Sciences,* 117**,** 1015-1020.

VEINGER, L., DIAMANT, S., BUCHNER, J. & GOLOUBINOFF, P. 1998. The Small Heat-shock Protein IbpB from Escherichia coli Stabilizes Stress-denatured Proteins for Subsequent Refolding by a Multichaperone Network. *Journal of Biological Chemistry,* 273**,** 11032-11037.

VERGHESE, J., ABRAMS, J., WANG, Y. & MORANO, K. A. 2012. Biology of the Heat Shock Response and Protein Chaperones: Budding Yeast (Saccharomyces cerevisiae) as a Model System. *Microbiology and Molecular Biology Reviews,* 76**,** 115-158.

VERNA, J., LODDER, A., LEE, K., VAGTS, A. & BALLESTER, R. 1997. A family of genes required for maintenance of cell wall integrity and for the stress response in Saccharomyces cerevisiae. *Proceedings of the National Academy of Sciences,* 94**,** 13804-13809.

VIGH, L., NAKAMOTO, H., LANDRY, J., GOMEZ-MUNOZ, A., HARWOOD, J. L. & HORVATH, I. 2007. Membrane regulation of the stress response from prokaryotic models to mammalian cells. *Annals of the New York Academy of Sciences,* 1113**,** 40-51.

VIITANEN, P. V., GATENBY, A. A. & LORIMER, G. H. 1992. Purified chaperonin 60 (groEL) interacts with the nonnative states of a multitude of Escherichia coli proteins. *Protein Science,* 1**,** 363-369.

VOELLMY, R. & BOELLMANN, F. 2007. Chaperone regulation of the heat shock protein response. *Molecular Aspects of the Stress Response: Chaperones, Membranes and Networks.* Springer.

VOGEL, J. L., PARSELL, D. A. & LINDQUIST, S. 1995. Heat-shock proteins Hsp104 and Hsp70 reactivate mRNA splicing after heat inactivation. *Current Biology,* 5**,** 306-317.

VOGEL, M., BUKAU, B. & MAYER, M. P. 2006a. Allosteric regulation of Hsp70 chaperones by a proline switch. *Molecular cell,* 21**,** 359-367.

VOGEL, M., MAYER, M. P. & BUKAU, B. 2006b. Allosteric regulation of Hsp70 chaperones involves a conserved interdomain linker. *Journal of Biological Chemistry,* 281**,** 38705-38711.

WALLACE, EDWARD W. J., KEAR-SCOTT, JAMIE L., PILIPENKO, EVGENY V., SCHWARTZ, MICHAEL H., LASKOWSKI, PAWEL R., ROJEK, ALEXANDRA E., KATANSKI, CHRISTOPHER D., RIBACK, JOSHUA A., DION, MICHAEL F., FRANKS, ALEXANDER M., AIROLDI, EDOARDO M., PAN, T.,

BUDNIK, BOGDAN A. & DRUMMOND, D. A. 2015. Reversible, Specific, Active Aggregates of Endogenous Proteins Assemble upon Heat Stress. *Cell,* 162**,** 1286-1298.

WALTER, S. & BUCHNER, J. 2002. Molecular chaperones—cellular machines for protein folding. *Angewandte Chemie International Edition,* 41**,** 1098-1113.

WALTHER, D. M., KASTURI, P., ZHENG, M., PINKERT, S., VECCHI, G., CIRYAM, P., MORIMOTO, R. I., DOBSON, C. M., VENDRUSCOLO, M., MANN, M. & HARTL, F. U. 2015. Widespread Proteome Remodeling and Aggregation in Aging C. elegans. *Cell,* 161**,** 919-32.

WATANABE, Y., TAKAESU, G., HAGIWARA, M., IRIE, K. & MATSUMOTO, K. 1997. Characterization of a serum response factor-like protein in Saccharomyces cerevisiae, Rlm1, which has transcriptional activity regulated by the Mpk1 (Slt2) mitogen-activated protein kinase pathway. *Molecular and cellular biology,* 17**,** 2615-2623.

WATERS, E. R. 2013. The evolution, function, structure, and expression of the plant sHSPs. *Journal of experimental botany,* 64**,** 391-403.

WATERS, E. R. & VIERLING, E. 1999. Chloroplast small heat shock proteins: evidence for atypical evolution of an organelle-localized protein. *Proceedings of the National Academy of Sciences,* 96**,** 14394-14399.

WATSON, K. & CAVICCHIOLI, R. 1983. Acquisition of ethanol tolerance in yeast cells by heat shock. *Biotechnology Letters,* 5**,** 683-688.

WAUDBY, C. A., DOBSON, C. M. & CHRISTODOULOU, J. 2019. Nature and Regulation of Protein Folding on the Ribosome. *Trends in Biochemical Sciences,* 44**,** 914-926.

WAYNE, N. & BOLON, D. N. 2007. Dimerization of Hsp90 is required for in Vivo Function design and analysis of monomers and dimers. *Journal of Biological Chemistry,* 282**,** 35386-35395.

WELCH, W. J. & SUHAN, J. P. 1985. Morphological study of the mammalian stress response: characterization of changes in cytoplasmic organelles, cytoskeleton, and nucleoli, and appearance of intranuclear actin filaments in rat fibroblasts after heat-shock treatment. *J Cell Biol,* 101**,** 1198-211.

WELKER, S., RUDOLPH, B., FRENZEL, E., HAGN, F., LIEBISCH, G., SCHMITZ, G., SCHEURING, J., KERTH, A., BLUME, A., WEINKAUF, S., HASLBECK, M., KESSLER, H. & BUCHNER, J. 2010. Hsp12 Is an Intrinsically Unstructured Stress Protein that Folds upon Membrane Association and Modulates Membrane Function. *Molecular Cell,* 39**,** 507-520.

WENDLER, P., SHORTER, J., SNEAD, D., PLISSON, C., CLARE, D. K., LINDQUIST, S. & SAIBIL, H. R. 2009. Motor Mechanism for Protein Threading through Hsp104. *Molecular Cell,* 34**,** 81-92.

WERA, S., SCHRIJVER, E. D., GEYSKENS, I., NWAKA, S. & THEVELEIN, J. M. 1999. Opposite roles of trehalase activity in heat-shock recovery and heat-shock survival in Saccharomyces cerevisiae. *Biochemical Journal,* 343**,** 621-626.

WERNER-WASHBURNE, M., STONE, D. E. & CRAIG, E. A. 1987. Complex interactions among members of an essential subfamily of hsp70 genes in Saccharomyces cerevisiae. *Molecular and cellular biology,* 7**,** 2568-2577.

WESSEL, D. & FLUGGE, U. I. 1984. A method for the quantitative recovery of protein in dilute solution in the presence of detergents and lipids. *Anal Biochem,* 138**,** 141-3.

WHITE, H. E., ORLOVA, E. V., CHEN, S., WANG, L., IGNATIOU, A., GOWEN, B., STROMER, T., FRANZMANN, T. M., HASLBECK, M., BUCHNER, J. & SAIBIL, H. R. 2006. Multiple Distinct Assemblies Reveal Conformational Flexibility in the Small Heat Shock Protein Hsp26. *Structure,* 14**,** 1197-1204.

WIESER, R., ADAM, G., WAGNER, A., SCHÜLLER, C., MARCHLER, G., RUIS, H., KRAWIEC, Z. & BILINSKI, T. 1991. Heat shock factor-independent heat control of transcription of the CTT1 gene encoding the cytosolic catalase T of Saccharomyces cerevisiae. *Journal of Biological Chemistry,* 266**,** 12406-12411.

WILFINGER, W. W., MACKEY, K. & CHOMCZYNSKI, P. 1997. Effect of pH and ionic strength on the spectrophotometric assessment of nucleic acid purity. *Biotechniques,* 22**,** 474-6, 478-81.

WILKINS, M. R., GASTEIGER, E., BAIROCH, A., SANCHEZ, J. C., WILLIAMS, K. L., APPEL, R. D. & HOCHSTRASSER, D. F. 1999. Protein identification and analysis tools in the ExPASy server. *Methods Mol Biol,* 112**,** 531-52.

WILLIAMS, D. L., PITTMAN, T. L., DESHOTEL, M., OBY-ROBINSON, S., SMITH, I. & HUSSON, R. 2007. Molecular basis of the defective heat stress response in Mycobacterium leprae. *Journal of bacteriology,* 189**,** 8818-8827.

WIŚNIEWSKI, J. R., HEIN, M. Y., COX, J. & MANN, M. 2014. A "proteomic ruler" for protein copy number and concentration estimation without spike-in standards. *Molecular & cellular proteomics : MCP,* 13**,** 3497-3506.

WIŚNIEWSKI, J. R., ZOUGMAN, A., NAGARAJ, N. & MANN, M. 2009. Universal sample preparation method for proteome analysis. *Nature Methods,* 6**,** 359.

WOTTON, D., FREEMAN, K. & SHORE, D. 1996. Multimerization of Hsp42p, a novel heat shock protein of Saccharomyces cerevisiae, is dependent on a conserved carboxyl-terminal sequence. *Journal of Biological Chemistry,* 271**,** 2717-2723.

WU, D., VONK, J. J., SALLES, F., VONK, D., HASLBECK, M., MELKI, R., BERGINK, S. & KAMPINGA, H. H. 2019. The N terminus of the small heat shock protein HSPB7 drives its polyQ aggregation-suppressing activity. *J Biol Chem,* 294**,** 9985-9994.

XIA, X., MACKAY, V., YAO, X., WU, J., MIURA, F., ITO, T. & MORRIS, D. R. 2011. Translation initiation: a regulatory role for poly(A) tracts in front of the AUG codon in Saccharomyces cerevisiae. *Genetics,* 189**,** 469-478.

YAM, A. Y., XIA, Y., LIN, H.-T. J., BURLINGAME, A., GERSTEIN, M. & FRYDMAN, J. 2008. Defining the TRiC/CCT interactome links chaperonin function to stabilization of newly made proteins with complex topologies. *Nature Structural & Molecular Biology,* 15**,** 1255-1262.

YAMAMOTO, N., TAKEMORI, Y., SAKURAI, M., SUGIYAMA, K. & SAKURAI, H. 2009. Differential recognition of heat shock elements by members of the heat shock transcription factor family. *The FEBS journal,* 276**,** 1962-1974.

YANG, J. S., CHEN, W. W., SKOLNICK, J. & SHAKHNOVICH, E. I. 2007. All-atom ab initio folding of a diverse set of proteins. *Structure,* 15**,** 53-63.

YOO, H., TRIANDAFILLOU, C. & DRUMMOND, D. A. 2019. Cellular sensing by phase separation: Using the process, not just the products. *J Biol Chem,* 294**,** 7151-7159.

YOST, H. J. & LINDQUIST, S. 1991. Heat shock proteins affect RNA processing during the heat shock response of Saccharomyces cerevisiae. *Molecular and cellular biology,* 11**,** 1062-1068.

ZABORSKE, J. M., NARASIMHAN, J., JIANG, L., WEK, S. A., DITTMAR, K. A., FREIMOSER, F., PAN, T. & WEK, R. C. 2009. Genome-wide Analysis of tRNA Charging and Activation of the eIF2 Kinase Gcn2p. *Journal of Biological Chemistry,* 284**,** 25254-25267.

ZEUTHEN, E. 1971. Synchrony in Tetrahymena by heat shocks spaced a normal cell generation apart. *Experimental cell research,* 68**,** 49-60.

ZHANG, K. 2016. Gctf: Real-time CTF determination and correction. *Journal of structural biology,* 193**,** 1-12.

ZHENG, S. Q., PALOVCAK, E., ARMACHE, J.-P., VERBA, K. A., CHENG, Y. & AGARD, D. A. 2017. MotionCor2: anisotropic correction of beam-induced motion for improved cryo-electron microscopy. *Nature methods,* 14**,** 331-332.

ZHENG, X., KRAKOWIAK, J., PATEL, N., BEYZAVI, A., EZIKE, J., KHALIL, A. S. & PINCUS, D. 2016. Dynamic control of Hsf1 during heat shock by a chaperone switch and phosphorylation. *eLife,* 5**,** e18638.

ZHU, X., ZHAO, X., BURKHOLDER, W. F., GRAGEROV, A., OGATA, C. M., GOTTESMAN, M. E. & HENDRICKSON, W. A. 1996. Structural analysis of substrate binding by the molecular chaperone DnaK. *Science,* 272**,** 1606-1614.

ZU, T., VERNA, J. & BALLESTER, R. 2001. Mutations in WSC genes for putative stress receptors result in sensitivity to multiple stress conditions and impairment of Rlm1-dependent gene expression in Saccharomyces cerevisiae. *Molecular Genetics and Genomics,* 266**,** 142-155.

9 Publications

MÜHLHOFER, M., BERCHTOLD, E., STRATIL, C. G., CSABA, G., KUNOLD, E., BACH, N. C., SIEBER, S. A., HASLBECK, M., ZIMMER, R. & BUCHNER, J. 2019. The Heat Shock Response in Yeast Maintains Protein Homeostasis by Chaperoning and Replenishing Proteins. *Cell Rep,* 29**,** 4593-4607.e8.

SCHOPF, F. H., HUBER, E. M., DODT, C., LOPEZ, A., BIEBL, M. M., RUTZ, D. A., MÜHLHOFER, M., RICHTER, G., MADL, T., SATTLER, M., GROLL, M. & BUCHNER, J. 2019. The Co-chaperone Cns1 and the Recruiter Protein Hgh1 Link Hsp90 to Translation Elongation via Chaperoning Elongation Factor 2. *Molecular Cell.*

10 Danksagung

Mein erster Dank gilt meinem Doktorvater Johannes Buchner für die Möglichkeit an einem sowohl spannenden, als auch sehr vielseitigen Projekt zu arbeiten. Ich möchte mich für die stete Unterstützung bedanken, die vielen Freiheiten, sowie das Vertrauen, mich auch neue Methoden ausprobieren zu lassen. Ein weiterer Dank gilt Martin Haslbeck, von dem ich bereits während des Studiums viel lernen durfte und der mir auch während der Doktorarbeit immer mit Rat und Tat zu Seite stand.

Ein herzlicher Dank geht natürlich an die Studienstiftung des deutschen Volkes für die finanzielle und ideelle Unterstützung dieser Doktorarbeit.

Ein ganz besonderer Dank geht an Frau Rubinstein dafür, dass man immer mit einem Lächeln empfangen wird und dass sie stets den Überblick über unsere bürokratischen Verpflichtungen behält. Ich danke Florian, Anja und besonders Laura und Bettina für ihre Unterstützung im Labor. Außerdem danke ich Katja Bäuml für viele MS Messungen und Marie-Lena Jokisch für Volllängen MS Messungen. Ein weiterer großer Dank geht an Evi Berchtold und Gergely Csaba aus Ralf Zimmers Gruppe für bioinformatische Analysen. Beate Rockel und Carsten Peters aus der Gruppe von Sevil Weinkauf danke ich für TEM und Cryo-EM Messungen, sowie Hyun Seo Kang aus Michael Sattlers Gruppe für die NMR Messungen. Nina Bach aus Stephan Siebers Gruppe danke ich für die Unterstützung bei der Planung von MS Experimenten, sowie für Ratschläge zur Auswertung. Stefan Krebs aus Helmut Blums Gruppe möchte ich für die Sequenzierungen, sowie für seine Ratschläge zur Vorbereitung entsprechender Libraries danken. Bei Florian Schopf und Maximilian Biebl bedanke ich mich für die Hilfe bei Radioaktivexperimenten und bei Pamina Kazman für AUC und TEM Messungen. Zuletzt will ich mich auch bei allen meinen Praktikanten, HiWis und Bachloranden für ihre Hilfe bedanken. Ein weiterer großer Dank geht an Sarah Reschke für die RNA Sequenzierungen der Hsf1 anchor-away Experimente.

Ich danke allen Kollegen herzlich für die sehr gute Zusammenarbeit, besonders natürlich den Kollegen, die mich während der ganzen Doktorarbeit begleiteten. Danke, Pamina, Jannis und Mareike, für viele sehr gute berufliche, als auch private Gespräche. Insgesamt danke an alle meine ehemaligen und aktuellen Bürokollegen für eine sehr angenehme Arbeitsatmosphäre.

Der größte Dank geht an meine Familie. An Maria und Quirin, die besten Mitbewohner, die man sich wünschen kann und an Quirin für viele gemeinsame und erholsame (zumindest manchmal;)) Bergtouren. Rahel, an dich geht ein ganz besonderer Dank. Dafür, dass du mich jeden Stress vergessen lässt und für die tolle Begleitung durch die Corona-bescherte Schreibzeit, einfach für alles! Zu guter Letzt noch ein ganz großer Dank an meine Eltern für ihre ständige und einzigartige Unterstützung in allen Phasen meines Lebens.

11 Eidesstattliche Erklärung

Hiermit erkläre ich, Moritz Mühlhofer, dass ich die vorliegende Arbeit selbständig verfasst habe und keine weiteren, außer den angegebenen Quellen und Hilfsmitteln, verwendet habe. Diese Arbeit wurde bisher keiner Prüfungskommission vorgelegt. Teile der Arbeit wurden bzw. werden in wissenschaftlichen Journalen veröffentlicht.

I, Moritz Mühlhofer, hereby declare that this thesis was written by me independently and that only the stated resources and references were used. This work has not been submitted to any audit commission so far. Parts of the work already have been or will be published in scientific journals.

_____

Moritz Mühlhofer